

University of New Mexico

UNM Digital Repository

Earth and Planetary Sciences ETDs

Electronic Theses and Dissertations

Summer 7-13-2020

Triple Oxygen Isotope Composition of Carbonates

Jordan A.G. Wostbrock

University of New Mexico - Main Campus

Follow this and additional works at: https://digitalrepository.unm.edu/eps_etds



Part of the [Geochemistry Commons](#), and the [Geology Commons](#)

Recommended Citation

Wostbrock, Jordan A.G.. "Triple Oxygen Isotope Composition of Carbonates." (2020).
https://digitalrepository.unm.edu/eps_etds/274

This Dissertation is brought to you for free and open access by the Electronic Theses and Dissertations at UNM Digital Repository. It has been accepted for inclusion in Earth and Planetary Sciences ETDs by an authorized administrator of UNM Digital Repository. For more information, please contact amywinter@unm.edu, lsloane@salud.unm.edu, sarahrk@unm.edu.

Jordan Anne Gibbons Wostbrock

Candidate

Earth and Planetary Sciences

Department

This dissertation is approved, and it is acceptable in quality and form for publication:

Approved by the Dissertation Committee:

Zachary Sharp, Chairperson

Maya Elrick

Peter Fawcett

Viorel Atudorei

Peter Swart

**TRIPLE OXYGEN ISOTOPE COMPOSITION OF
CARBONATES**

by

JORDAN ANNE GIBBONS WOSTBROCK

M.S, Earth and Planetary Sciences, University of New Mexico, 2014
B.S, Environmental Sciences, Westfield State University, 2010

DISSERTATION

Submitted in Partial Fulfillment of the
Requirements for the Degree of

**Doctor of Philosophy in
Earth and Planetary Sciences**

The University of New Mexico

Albuquerque, New Mexico

July 2020

ACKNOWLEDGEMENTS

While completing a PhD might appear as a huge personal achievement, it is by no means a lonely one. It took an amazing community to help me through this process and I would like to thank everyone who helped me along the way.

Zach – It is difficult to put into words the gratitude I have for the many roles you have served as an advisor. Thank you for your patience and generosity in advice, planning, research, everything about a mass spec, lab use, etc. If I were to put into words just one of the many important things you have taught me, I would say you have taught me to be very comfortable with what I do not know. Whether it is standing over a broken mass spec or staring at unexplainable data, it isn't that the problem doesn't make sense, it is just that we don't understand it yet.

Karen, Chris, and Jim – Thank you for teaching me so much about lab maintenance and repair.

Viorel and Laura – Thank you for the open lab use and always making room for my random sporadic samples. I know, “can I just throw a couple on the back of that tray” adds up to a lot of samples over four years and I thank you for all of your help.

My co-authors, committee members, and all the faculty at UNM – Thank you for your generosity in supplying samples and your patience answering all my, sometimes quite basic, questions. I tend to be a pop in, don't make an appointment type of person and I thank everyone for their willingness to meet and UNM's general open-door policy. It makes for such a great research atmosphere between graduate students and faculty.

Thank you, Cori and James for the crash course about cephalopods. Also, thank you Peter Swart for being willing to jump onto my committee with short notice and serve as an outside committee member.

All the graduate students and lab mates current and former – You all make grad school better. Thanks for all the happy, sad, and for no reason at all beers and get togethers. Thanks to Tony and Erick for listening to all my presentations that really haven't changed that much over four years, but you keep showing up. Thanks to Jeff and Oleg, the first years of grad school were awesome with you guys and kept me motivated to keep pursuing my PhD. Thanks to Lauren Wheeler for so many dog walks and conversations. The list can go on and on but a few more names to thank are Marisa, Margaret, Cato, etc. etc.

Friends and family near and far – Thank you reminding me that there is a whole big world outside this small academic bubble. You keep me grounded.

Lastly, I would be completely remiss if I didn't thank the other half of my team – Neal. Thank you for packing up and moving with me to NM to pursue my career and supporting me the whole way. You have made this process infinitely easier with your unwavering support.

TRIPLE OXGEN ISOTOPE COMPOSITIONS OF CARBONATES

by

Jordan Anne Gibbons Wostbrock

B.S, Environmental Sciences, Westfield State University, 2010
M.S, Earth and Planetary Sciences, University of New Mexico, 2014
PhD, Earth and Planetary Sciences University of New Mexico, 2020

ABSTRACT

This dissertation presents a method of analyzing the triple oxygen isotope compositions of carbonates, presents an empirical calibration of the carbonate-water equilibrium fractionation line, presents a triple oxygen isotope equipped fluid-rock mixing model for carbonates to see-through diagenesis, and applies all these findings to ancient carbonate samples. Using modern carbonates and associate water, the following equations are calculated to describe equilibrium triple oxygen isotope fractionation of carbonates:

$$1000\ln\alpha^{18}\text{O}_{\text{cc-wt}} = \frac{2.84(\pm 0.02) \times 10^6}{T^2} - 2.96(\pm 0.19) \quad 1),$$

$$\theta_{\text{cc-wt}} = \frac{-1.39(\pm 0.01)}{T} + 0.5305 \quad 2).$$

Using these fractionation equations provides an extremely useful tool to determine whether a carbonate sample is altered or preserves its original isotopic composition. In samples that are altered, a fluid-rock mixing model is used to see-through the diagenesis. Applying these tools to ancient carbonate rocks shows that many samples thought to be pristine are altered and are confusing paleoenvironmental interpretations. This work shows that seawater temperature and isotopic composition is unchanged over the Phanerozoic, an important consideration when reconstruction paleoenvironments.

TABLE OF CONTENTS

LIST OF FIGURES	x
LIST OF TABLES	xiii
PREFACE.....	xiv
1. INTRODUCTION.....	1
2. AN INTERNALLY CONSISTENT TRIPLE OXYGEN ISOTOPE CALIBRATION OF STANDARDS FOR SILICATES, CARBONATES AND AIR RELATIVE TO VSMOW2 AND SLAP2.....	5
2.1 Introduction	5
2.2 Isotope Systematics	9
2.3 Methods	10
<i>2.3.1 Waters</i>	<i>10</i>
<i>2.3.2 Silicates</i>	<i>11</i>
<i>2.3.3 Carbonates.....</i>	<i>11</i>
<i>2.3.4 CO₂ gas</i>	<i>12</i>
<i>2.3.5 Oxygen gas purification and O₂ analysis.....</i>	<i>12</i>
<i>2.3.6 Air</i>	<i>13</i>
2.4 Results/Discussion	14
<i>2.4.1 Water standards</i>	<i>14</i>
<i>2.4.2 Calcite standards</i>	<i>17</i>
<i>2.4.3 CO₂ from calcite</i>	<i>21</i>
<i>2.4.4 Silicate standards.....</i>	<i>22</i>
<i>2.4.5 Air</i>	<i>25</i>

2.5 Conclusion.....	26
2.6 Acknowledgements.....	27
3. CALIBRATION OF CARBONATE-WATER TRIPLE OXYGEN ISOTOPE FRACTIONATION: SEEING THROUGH DIAGENESIS IN ANCIENT CARBONATES.....	28
3.1 Introduction	28
3.2 Methods	32
3.2.1 <i>Inorganic precipitation</i>	32
3.2.2 <i>Natural Carbonates</i>	34
3.2.3 <i>Isotopic analyses</i>	35
3.3 Results	39
3.4 Discussion.....	41
3.4.1 <i>Calcite-water oxygen isotope fractionation using $\delta^{18}O$ values of modern carbonates.....</i>	41
3.4.2 <i>Calcite-water triple oxygen isotope fractionation using modern calcite.....</i>	49
3.4.2.1 <i>θ-T dependence</i>	49
3.4.2.2 <i>Triple oxygen isotope fractionation.....</i>	51
3.4.3 Application to ancient carbonates	53
3.4.3.1 <i>Triple oxygen isotope compositions of ancient carbonates and implications on ancient seawater.....</i>	56
3.4.3.2 <i>Triple oxygen isotopes and carbonate diagenesis</i>	58
3.5 Conclusions	61
3.6 Acknowledgements.....	62
4. SEEING THROUGH DIAGENESIS IN PHANEROZOIC CARBONATE ROCKS	63
4.1 Introduction	63

4.2 Sample information	65
4.2.1 <i>Carbonate concretions from the late Cretaceous Western Interior Seaway</i> ...	65
4.2.1.1 <i>Geologic setting</i>	65
4.2.1.2 <i>Sample preparation</i>	68
4.2.2 <i>Early Triassic ammonites</i>	68
4.2.2.1 <i>Geologic setting</i>	68
4.2.2.2 <i>Sample preparation</i>	70
4.2.3 <i>Early Triassic bulk rock</i>	70
4.2.3.1 <i>Geologic setting</i>	70
4.2.3.2 <i>Sample preparation</i>	71
4.2.4 <i>Rugose coral from Hirnantian glaciation (late Ordovician)</i>	71
4.2.4.1 <i>Geologic setting</i>	71
4.2.4.2 <i>Sample preparation</i>	72
4.3 Oxygen isotope systematics	73
4.4 Oxygen isotope analysis	75
4.5 Results and discussion	76
4.5.1 <i>Carbonate concretions from the Western Interior Seaway</i>	77
4.5.2 <i>Early Triassic ammonites</i>	84
4.5.3 <i>Early Triassic bulk rock</i>	86
4.5.4 <i>Hirnantian glaciation (late Ordovician) carbonate samples</i>	87
4.6 Conclusions	91
4.7 Acknowledgements	92
5. TRIPLE OXYGEN ISOTOPES IN THE SILICA–WATER AND CARBONATE–WATER SYSTEM	93
5.1 Introduction	93

5.2 Mineral–water oxygen isotope thermometers	94
5.2.1 $^{18}\text{O}/^{16}\text{O}$ fractionation	94
5.2.2 Triple oxygen isotope fractionation	98
5.2.3 Equilibrium triple oxygen isotope fractionation – the $\Delta^{17}\text{O} - \delta^{48}\text{O}$ plot.....	100
5.2.4 Changing ocean composition in the past	102
5.2.5 Diagenetic trends	103
5.3 Silica–water fractionation.....	108
5.3.1 Calibration of the triple oxygen isotope thermometer	108
5.3.2 Silica in the terrestrial environment	110
5.4 Triple oxygen isotope measurements of carbonates.....	112
5.4.1 Triple oxygen isotope analysis of carbonates	112
5.4.2 Triple oxygen isotope fractionation in the calcite (aragonite) – water system	114
5.4.3 Applications to natural calcite samples	117
5.5 Application to diagenesis in silica and carbonate samples	119
5.5.1 Ancient silica and diagenesis	121
5.5.2 Ancient calcite and diagenesis	128
5.6 Triple oxygen isotopes of quartz and coexisting calcite.....	130
5.7 Conclusions	134
5.8 Acknowledgements.....	134
6. CONCLUSIONS	135
APPENDICES	137
Appendix A. Mass spec linearity and pressure effect	138
Appendix B. Residual gas analysis after carbonate fluorination.....	139

Appendix C. Published triple oxygen isotope values of silicates	140
Appendix D. Published triple oxygen isotope values of air	141
Appendix E. Photos of samples from Chapter 3	142
Appendix F. Raw data of marine samples from Chapter 3.....	143
Appendix G. Raw data of synthesized samples and Devils Hole from Chapter 3	144
Appendix H. Raw data of ancient calcite from Chapter 3	145
Appendix I. Fractionation associated with fluorination of carbonates in a Ni-tube	146
Appendix J. $1000\ln\alpha^{18}\text{O}_{\text{cc-wt}}$ values used to derive calcite-water fractionation line	148
Appendix K. Literature compilation of $1000\ln\alpha$ values for calcite–water	149
REFERENCES.....	153

LIST OF FIGURES

Figure 1.1 - Different interpretations of the secular trend seen in the $\delta^{18}\text{O}$ values of carbonates over the Phanerozoic (500 Ma).....	2
Figure 2.1- Separation of Ar and O ₂ in our chilled GC column during an Air sample injection.....	14
Figure 2.2 - Triple oxygen isotope composition of SLAP2.....	15
Figure 2.3 - Memory effect of switching from VSMOW2 samples to SLAP2 samples for analysis. The first three injections of SLAP gave high $\delta^{18}\text{O}$ values.....	17
Figure 2.4 - $\Delta^{17}\text{O}$ vs. the difference between the $\delta^{18}\text{O}_{\text{measured}}$ and the $\delta^{18}\text{O}_{\text{accepted}}$ value ($\delta^{18}\text{O}_{\text{measured}} - \delta^{18}\text{O}_{\text{accepted}}$)	20
Figure 2.5 - $\Delta^{17}\text{O}$ and $\delta^{18}\text{O}$ values of air from individual analyses of this study and previous work.....	25
Figure 3.1 - SEM images of synthesized calcite.....	46
Figure 3.2 - TEM and diffraction pattern of vaterite crystal.....	47
Figure 3.3 - Measured $\delta^{18}\text{O}$ calcite-water fractionations compared to a range of literature calibrations.....	48
Figure 3.4 - The θ - T relationship of samples from this study and of published relationships.....	50
Figure 3.5 - Triple oxygen isotope fractionation curves for calcite-water and aragonite-water.....	52
Figure 3.6 - Application of the triple oxygen isotope equilibrium curve to ancient carbonates	55
Figure 4.1 - A) Map of sample location and reconstruction of the Western Interior Seaway during the Late Campanian. B) Ammonite biozones of the Lower Maastrichtian and Upper Campanian Western Interior Seaway.....	65
Figure 4.2 - Images of the samples from the Western Interior Seaway.....	67
Figure 4.3 - A) Sample location map for early Triassic samples. B) Reconstruction of the southwestern U.S from 245 to 248 Ma (Blakey, 2013). C) Pictures of ammonite fossils used in this study.....	69
Figure 4.4 - A) Images of the samples from the Laframboise member, Anticosti Island, eastern Canada. B) Reconstructed global map of 450 Ma (Blakey, 2016).....	72

Figure 4.5 - The $\delta^{13}\text{C}$ values vs. the $\delta^{18}\text{O}$ values of the calcite phases from the carbonate concretions of the Late Cretaceous Western Interior Seaway.	78
Figure 4.6 - Triple oxygen isotope values of calcite phases in carbonate concretions from the late Cretaceous Western Interior Seaway	79
Figure 4.7 – Testing the fluid-rock mixing model sensitivity to alteration fluid oxygen isotope composition and summary of ocean temperature reconstruction.....	81
Figure 4.8 - Triple oxygen isotope values of early Smithian (A) and late Spathian (B) ammonite fossils	84
Figure 4.9 - Triple oxygen isotope values of bulk rock from the Early Triassic.....	86
Figure 4.10 - Triple oxygen isotope values of host rock and rugose coral from the Laframboise member, Anticosti Island, Canada.....	88
Figure 5.1 - Quartz-water and calcite-water oxygen isotope fractionation	96
Figure 5.2 - $\Delta^{17}\text{O}$ - $\delta^{18}\text{O}$ plot for silica-water.....	100
Figure 5.3 - $\Delta^{17}\text{O}$ - $\delta^{18}\text{O}$ plot of changing seawater composition in relation to changing the ratio of high to low temperature alteration.....	102
Figure 5.4 - Alteration trajectories in $\Delta^{17}\text{O}$ - $\delta^{18}\text{O}$ space	105
Figure 5.5 - Alteration trajectories for a rock starting with a $\delta^{18}\text{O}$ - $\Delta^{17}\text{O}$ of δr_{init}	106
Figure 5.6 - Generalized fields for sedimentary silica.....	107
Figure 5.7 - Comparison of the quartz-water fractionation equation with low temperature diatom data.....	109
Figure 5.8 - Measured θ values for natural samples and best fit for a θ vs. $1/T$ relationship	110
Figure 5.9 - Triple isotope compositions of low-T terrestrial silica samples	111
Figure 5.10 - The $\Delta\Delta^{17}\text{O}_{\text{carb-wt}}$ as a function of temperature from published studies	115
Figure 5.11 - The $\Delta^{17}\text{O}$ values vs. the $\delta^{18}\text{O}$ values of ancient carbonates	118
Figure 5.12 - Published $\Delta^{17}\text{O}$ and $\delta^{18}\text{O}$ values of ancient chert.....	123
Figure 5.13 - Various seawater triple oxygen isotope compositions can describe published $\Delta^{17}\text{O}$ and $\delta^{18}\text{O}$ values of ancient chert	125

Figure 5.14 - Back-calculated initial triple oxygen isotope compositions of altered brachiopod and ammonite samples	129
Figure 5.15 - $\Delta^{17}\text{O}$ - $\delta^{18}\text{O}$ plot for quartz and calcite and the equilibrium $\theta_{\text{qz-cc}}$ values from 0 to 70 °C.	131
Figure 5.16 - Isotopic compositions of authigenic euhedral quartz crystals hosted in carbonates	132
Figure 5.17 - Possible reaction sequence for chert from France.....	133

LIST OF TABLES

Table 2.1 - Individual and average VSMOW2-SLAP2 data of this study.....	16
Table 2.2 - Compilation of published triple oxygen isotope values of SLAP2 on the VSMOW2 scale	16
Table 2.3 - Triple oxygen isotope data for carbonate standards and CO ₂ extracted by phosphoric acid digestion at 25°C	19
Table 2.4 - $\delta^{17}\text{O}$ and $\delta^{18}\text{O}$ values of IAEA carbonate standards	21
Table 2.5 - Triple oxygen isotope data for silicate standards	23
Table 2.6 - Triple oxygen isotope data for individual air analyses.....	25
Table 3.1 – Sample descriptions	36
Table 3.2 - The oxygen isotope compositions of the synthesized carbonates and Devils Hole with corresponding water.....	42
Table 3.3 - Oxygen isotope composition of modern carbonate and aragonite	44
Table 3.4 - Isotopic compositions of ancient brachiopods from the Phanerozoic	57
Table 4.1 - Raw data from late Cretaceous Western Interior Seaway carbonate concretions	82
Table 4.2 - Raw data from the early Triassic sample suite.....	85
Table 4.3 - Raw data from the Hirnantian glaciation (late Ordovician) sample suite	90

PREFACE

The purpose of this preface is to acknowledge appropriate funding sources and outline the roles co-authors and collaborators performed in each chapter, pursuant to requirements of the Department of Earth and Planetary Sciences at the University of New Mexico. Jordan A.G. Wostbrock is the primary author of and conducted greater than or equal to 51% of the work in each chapter of this dissertation. Two National Science Foundation (NSF) grants funded all the research found within this dissertation: 1) An NSF Graduate Research Fellowship Program (DGE-1418062), and 2) An NSF EAR titled, “Terrestrial applications of the triple oxygen isotope geothermometer” (EAR-1551226; PI – Zachary Sharp).

Chapter 2 has been published in the journal, *Chemical Geology* (DOI: 10.1016/j.chemgeo.2019.119432) with coauthors Erick J. Cano and Zachary D. Sharp. Jordan A.G. Wostbrock analyzed all water, carbonate, and CO₂ samples, consolidated and interpreted all data, and wrote the manuscript. Erick J. Cano analyzed the majority of the silicate samples and provided edits to the manuscript. Zachary Sharp managed the research, analyzed some of the Air samples (Jordan Wostbrock analyzed some as well) and provided edits and advice on the manuscript.

Chapter 3 has been submitted to the journal, *Geochimica Cosmochimica Acta*, with coauthors Uwe Brand, Tyler B. Coplen, Peter K. Swart, Sandra J. Carlson, Adrian Brearley, and Zachary D. Sharp. Jordan Wostbrock analyzed and interpreted all the data and wrote the manuscript. Uwe Brand provided modern (except *L. Ery*) and ancient brachiopod samples and edited the manuscript. Tyler B. Coplen provided carbonate and water samples from Devils Hole and edited the manuscript. Peter K. Swart provided

marine aragonite samples and edited the manuscript. Sandra J. Carlson provided the *L. Ery* brachiopod and edited the manuscript. Adrian Brearley analyzed the precipitated calcite on the TEM, identified the vaterite polymorph, assisted in writing the methods section about the TEM use, formatted the diffraction pattern in Fig. 3.2, and edited the manuscript. Zachary D. Sharp managed the research and provided help and guidance on every aspect as well as edited the manuscript.

Chapter 4 is unpublished work. Cori Myers and James D. Witts provided the late Cretaceous carbonate concretions from their collections. Viorel Atudorei provided the early Triassic ammonites and bulk rock from EPS collections. Maya Elrick provided the late Ordovician rugose coral and bulk rock from her collections.

Chapter 5 has been submitted as a review paper to *Reviews in Mineralogy and Geochemistry*, “Triple Oxygen Isotopes on Earth” volume. Jordan Wostbrock is the primary author and wrote at least 51% of the manuscript. Zachary D. Sharp is co-author and wrote the remaining 49%.

1. INTRODUCTION

The field of carbonate stable isotope geochemistry began over 60 years ago with the idea that the oxygen isotopic composition of carbonates may preserve the temperature of the ocean and track the evolution of ocean surface temperatures. In the standard calcite-water fractionation equation (see Chapter 3, equation 3.2 and 3.3) there are two unknown variables – temperature and oxygen isotope composition of the water. Over 60 years since Urey et al. (1951) and Epstein et al. (1951) published the first calcite-water ocean paleotemperature records, scientists are still trying to develop new techniques to apply to ancient carbonates to solve these two variables while minimizing assumptions concerning the oxygen isotope composition of the ocean, the oxygen isotope equilibrium status of the carbonate, and that the carbonate sample is free from diagenesis. Various methods that obtain temperature data without assuming the oxygen isotope composition of the water have been developed with moderate success, such as trace element analysis, mineral-mineral thermometry, and Ca/Mg ratios (Moberly Jr., 1968; Weber, 1974). Carbonate clumped-isotope thermometry measures carbonate ions that contain both ^{13}C and ^{18}O . The abundance of ions that contain ^{13}C and ^{18}O is related to temperature and is reported as Δ_{47} – the difference between the measured abundance and the expected abundance based on stochastic distribution (Ghosh et al., 2006; Schauble et al., 2006; Eiler, 2007). Carbonate clumped-isotope thermometry, which is independent of the isotopic composition of the water, has been considerably successful. However, research is ongoing about the preservation of clumped isotope values due to potential thermal resetting which can alter the Δ_{47} values but not the $\delta^{18}\text{O}$ values (Henkes et al., 2014; Winkelstern and Lohmann, 2016; Stolper et al., 2018).

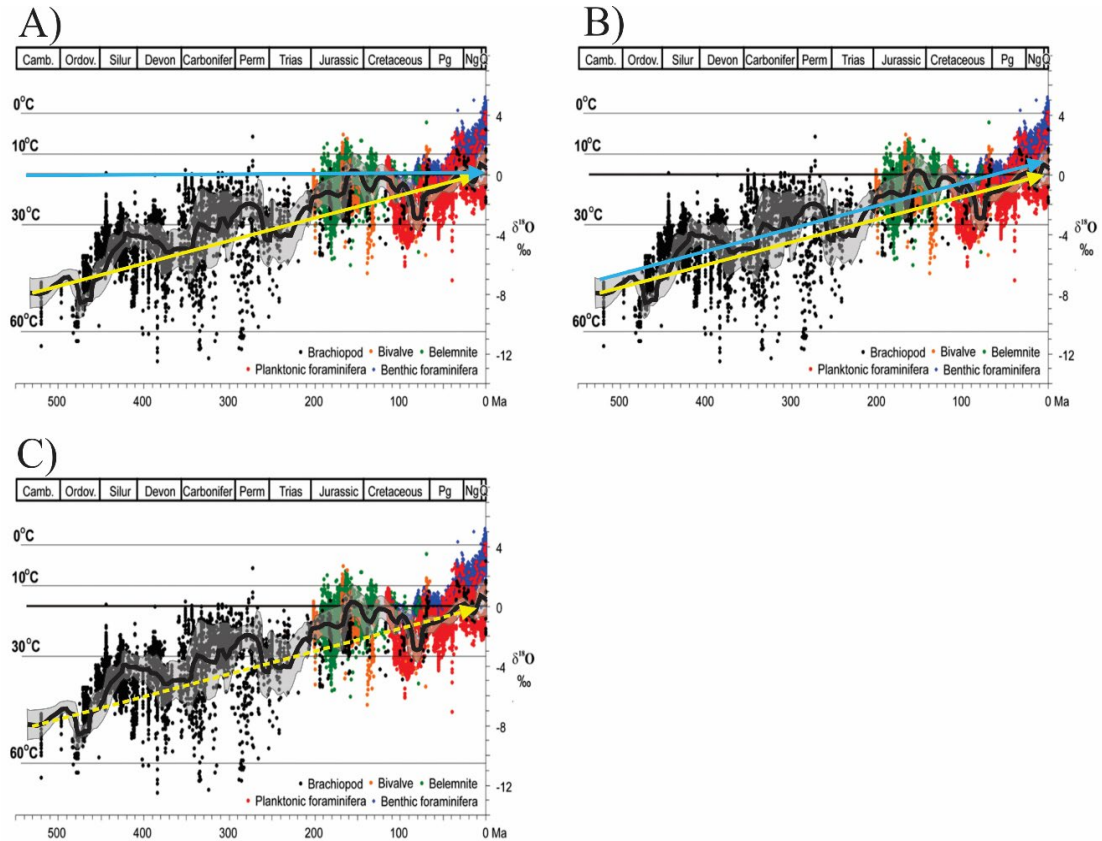


Figure 1.1 - Different interpretations of the secular trend seen in the $\delta^{18}\text{O}$ values of carbonates over the Phanerozoic (500 Ma). Data and graphs are from Veizer and Prokoph (2015). The thick black line represents a running average and the gray band is the 68 % confidence interval (Veizer et al., 1999). A) The secular trend is a primary $\delta^{18}\text{O}$ signal and represents a 40 °C increase in seawater temperature over 500 Ma. The ocean (blue line) $\delta^{18}\text{O}$ value remains constant while the carbonate $\delta^{18}\text{O}$ average value increases (yellow line). B) The secular trend is a primary $\delta^{18}\text{O}$ signal in the carbonate record but reflects a changing $\delta^{18}\text{O}$ value of seawater. Both the ocean (blue line) and carbonate (yellow line) $\delta^{18}\text{O}$ average values increase. C) The secular trend is a diagenetic signal where older samples are more altered than younger samples (dotted yellow line).

The $\delta^{18}\text{O}$ values of carbonates tend to increase over time where older carbonates have lower $\delta^{18}\text{O}$ values than modern carbonates (Degens and Epstein, 1962; Keith and Weber, 1964; Veizer and Hoefs, 1976; Popp et al., 1986; Lohmann and Walker, 1989). Multiple ideas are used to explain this secular change and were first suggested by (Degens and Epstein, 1962; Figure 1). One idea is that the increase in carbonate $\delta^{18}\text{O}$ values over the last 500 Ma (or more) purely reflects the temperature of the ocean and the ocean was warmer in the past and is cooling toward the modern. Most studies that

support this idea look at older rocks than the Phanerozoic and take the evidence that the ocean $\delta^{18}\text{O}$ value has been buffered in deeper time to infer that the ocean continued to be buffered to 0 during the Phanerozoic (Knauth and Epstein, 1976; Knauth and Lowe, 1978; Muehlenbachs, 1986; Figure 1A). The second idea is that the temperature of the ocean has been constant through time and the carbonate $\delta^{18}\text{O}$ record reflects a change in the $\delta^{18}\text{O}$ value of seawater Figure 1B (Perry, 1967; Perry and Tan, 1972; Popp et al., 1986; Lohmann and Walker, 1989; Walker and Lohmann, 1989; Veizer et al., 1997; Wallmann, 2001; Kasting et al., 2006; Jaffrés et al., 2007; Kanzaki, 2020). The third idea to explain the secular trend is that the $\delta^{18}\text{O}$ values are altered and no longer preserve the initial $\delta^{18}\text{O}$ composition during formation (Gao and Land, 1991; Brand, 2004). Therefore, the signal is overprinted with older carbonates having more of a diagenetic signal than younger carbonates (Figure 1C).

In this dissertation, a novel technique is used to measure the triple oxygen isotope (combined $^{17}\text{O}/^{16}\text{O}$ and $^{18}\text{O}/^{16}\text{O}$ ratios) composition of carbonates to address some of the basic assumptions described above. The triple oxygen isotope system provides two independent water–temperature equations, one for the $^{17}\text{O}/^{16}\text{O}$ ratio ($\delta^{17}\text{O}$) and one for the $^{18}\text{O}/^{16}\text{O}$ ratio ($\delta^{18}\text{O}$). Therefore, the two unknown variables, temperature and oxygen isotopic composition of the water, can be determined independently. Since this is a new technique, the method had to be tested and standardized against a suite of international standards (Chapter 2) before being used as a tool to answer geologic questions. After the method was shown to work, an empirical calcite–water triple oxygen isotope fractionation line was developed using modern calcite that formed in water with a known water oxygen isotope composition (Chapter 3). A major advantage that triple oxygen

isotope measurements have over other multiple element systems is that all three isotopes of oxygen have the same diagenetic potential thereby creating a unique solution per analyzed value to be in equilibrium with water. These key characteristics allow for the isotopic composition of the water to be calculated and clearly differentiates between samples that form in equilibrium vs. out of equilibrium of the fluid (Chapter 3; Wostbrock et al., 2020a). During diagenesis, triple oxygen isotope values change in a predictable manner. A simple fluid-rock interaction model can reconstruct the diagenetic fluid to ‘see through’ post-depositional diagenesis and estimate the ‘pristine’ triple oxygen isotope composition of the carbonate (Chapters 3-5). The final chapter is a review chapter that includes the research to date on both silicate– and carbonate– water fractionation (Chapter 5). This chapter uses the fluid-rock mixing model presented in Chapters 3 and 4 to look at how diagenesis may have affected the chert and carbonate record. Overall, this dissertation lays the ground work for future application of triple oxygen isotope compositions of carbonates to answer, hopefully, important geologic, climatologic, and paleoenvironmental questions.

2. AN INTERNALLY CONSISTENT TRIPLE OXYGEN ISOTOPE CALIBRATION OF STANDARDS FOR SILICATES, CARBONATES AND AIR RELATIVE TO VSMOW2 AND SLAP2

2.1 Introduction

The International Atomic Energy Agency (IAEA) working group recognized the necessity of having well-characterized stable isotope standards to allow all laboratories to be calibrated to the same scale. In the case of oxygen, samples are ultimately related to Vienna Standard Mean Ocean Water (VSMOW, now VSMOW2), defined as having a $\delta^{18}\text{O}$ value of 0‰ (Gonfiantini, 1978). To correct for possible instrumental compression of stable isotope analyses made over a wide range of isotopic compositions, a second light water standard with a $\delta^{18}\text{O}$ value of -55.5‰, called Standard Light Antarctic Precipitation (SLAP, now SLAP2), is used to correct for different laboratory ‘stretching factors’. Original batches of VSMOW and SLAP are extinguished, and another batch of standards are currently distributed under the names VSMOW2 and SLAP2 with essentially identical $\delta^{18}\text{O}$ and δD (hydrogen isotope ratio) values as their original counterpart. A second oxygen scale is related to Peedee Belemnite (PDB or VPDB for Vienna Peedee Belemnite), defined relative to the carbonate standard NBS 19 (where NBS is National Bureau of Standards) with a $\delta^{18}\text{O}$ value of -2.20‰ on the VPDB scale. The carbonate standard is ultimately related to VSMOW2 by laboratories that have quantitatively extracted total oxygen from carbonates by fluorination and O_2 of water by fluorination or $\text{CO}_2\text{-H}_2\text{O}$ equilibration (Sharma and Clayton, 1965; Kim and O’Neil, 1997; Kim et al., 2007a). The VSMOW2 and VPDB scales are related by the equation by Friedman and O’Neil (1977) corrected in Coplen et al. (1983):

$$\delta^{18}\text{O}_{VSMOW} = 1.03091 \times \delta^{18}\text{O}_{VPDB} + 30.91 \quad 2.1).$$

All laboratories are now able to report their oxygen isotope data relative to VSMOW2 by calibrating their secondary standards to widely available IAEA reference materials.

There has been a recent interest in measuring the $^{17}\text{O}/^{16}\text{O}$ ratio of terrestrial materials with high precision (Pack and Herwartz, 2014). A number of studies have calibrated silicate materials relative to VSMOW or VSMOW2 by fluorinating both the solids and VSMOW or VSMOW2 in the same extraction system (Kusakabe and Matsuhisa, 2008; Tanaka and Nakamura, 2013; Pack et al., 2016; Sharp et al., 2016). There is some disagreement as to the accepted $\delta^{17}\text{O}$ values of these standards, but more importantly, there is no direct calibration to VSMOW2 for the $\delta^{17}\text{O}$ values of carbonates. In this work, silicate and carbonate standards are calibrated to VSMOW2 by directly fluorinating water, silicates and carbonates using the same extraction line. The $\delta^{17}\text{O}$ and $\delta^{18}\text{O}$ values of air are measured on the same extraction line. The work provides $\delta^{17}\text{O}$ values of IAEA carbonate reference materials and calibrates new silicate standards that can be requested from the Center for Stable Isotopes (CSI) at the University of New Mexico (see csi.unm.edu for details).

Inter-calibration of water, carbonates, and silicates is complicated due to the different methods traditionally used for their analysis. The $\delta^{18}\text{O}$ values of silicates are measured directly on O_2 gas quantitatively extracted from the sample by fluorination in nickel bombs (Clayton and Mayeda, 1963) or by laser fluorination (Sharp, 1990). Waters and carbonates, on the other hand, are commonly measured indirectly. Waters are generally analyzed using the CO_2 equilibration method originally developed by Cohn and Urey (1938) or, rarely, directly using the fluorination method of O'Neil and Epstein (1966) or the CoF_3 method by Baker et al. (2002) and modified by Barkan and Luz

(2005). Carbonates are analyzed as CO₂ using the phosphoric acid digestion method developed by McCrea (1950). Only 2/3 of the oxygen is liberated during phosphoric acid digestion and the $\delta^{18}\text{O}$ value of the CO₂ gas is not the same as that of the original sample. A correction factor (α value) must be applied in order to relate the sample back to the VSMOW2 scale. In order to determine the appropriate α value, waters and carbonates have been analyzed quantitatively using fluorination methods to extract 100% of the oxygen (Sharma and Clayton, 1965; O'Neil and Epstein, 1966). Even after a sizeable number of studies aimed at determining the phosphoric acid digestion fractionation factor (α_{ACID}), variations of up to 0.5‰ for the carbonate-CO₂ and H₂O-CO₂ fractionation factor still exist (Compston and Epstein, 1958; Staschewski, 1964; Sharma and Clayton, 1965; Majzoub, 1966; O'Neil and Epstein, 1966; Bottinga and Craig, 1969; O'Neil et al., 1969; Matsuhisa et al., 1971; Blattner, 1973; O'Neil et al., 1975; Kim and O'Neil, 1997; Kim et al., 2007a). These uncertainties translate into similar uncertainties for the conversion from the VPDB to VSMOW scale (Craig, 1957, 1961; Friedman and O'Neil, 1977; Coplen et al., 1983).

Calibration of the $\delta^{17}\text{O}$ values of reference materials is much more limited. Several studies have fluorinated waters and silicates (Kusakabe and Matsuhisa, 2008; Tanaka and Nakamura, 2013; Pack and Herwartz, 2014; Pack et al., 2016; Sharp et al., 2016) in order to determine the $\delta^{17}\text{O}$ value on the VSMOW-SLAP scale. In studies where water was also fluorinated, published $\delta^{18}\text{O}$ and $\Delta^{17}\text{O}$ (defined below, Eq. 2.4) values of San Carlos olivine vary by 0.36 and 0.168, respectively (Kusakabe and Matsuhisa, 2008; Tanaka and Nakamura, 2013; Pack et al., 2016; Sharp et al., 2016). The problem is further compounded due to variability in the $\delta^{18}\text{O}$ values of different aliquots of San

Carlos olivine (Starkey et al., 2016). There are several published $\delta^{18}\text{O}$ and $\Delta^{17}\text{O}$ values of air (Barkan and Luz, 2003; Barkan and Luz, 2011; Yeung et al., 2012; Young et al., 2014; Pack et al., 2017) ranging between 23.4-24.15 and -0.363 and -0.453 ‰, respectively (Note, Young et al. (2014) published $\Delta^{17}\text{O}$ values of air are in respect to San Carlos olivine and not directly to VSMOW). Since the troposphere is expected to be homogenous, the variations are probably related to slight differences in analytical technique and calibration.

To date, no direct calibration of the $\Delta^{17}\text{O}$ values of carbonates have been made using the method of fluorination. Barkan et al. (2015; 2019) and Passey et al. (2014) presented triple oxygen isotope values of CO_2 of common standards NBS 18, NBS 19 and IAEA-603 for CO_2 released using phosphoric acid digestion at 25°C and 90°C, respectively. The authors used different methods for analyzing for triple oxygen isotope values as well as different temperatures of acid digestion. Barkan et al. (2015; 2019) determined the $\delta^{17}\text{O}$ value using a $\text{CO}_2\text{-O}_2$ equilibration method modelled after Mahata et al. (2013). Passey et al. (2014) used methanation to convert the CO_2 to H_2O and then fluorinated the H_2O using the CoF_3 method of Barkan and Luz (2005). Although helpful for standardizing laboratories making these measurements, the standards reported are for CO_2 only and not the total carbonate value.

Having a wide suite of $\delta^{18}\text{O}$ values of silicates, carbonates, and air that have been analyzed on the same mass spectrometer using the same reference gas and inlet systems and that are calibrated to VSMOW2-SLAP2 should reduce the interlaboratory errors discussed earlier. Laboratories can calibrate and stretch their own working reference gas to the sample values and report all values relative to the VSMOW2-SLAP2 scale.

Common silicate standards (NBS 28, University of Wisconsin-Gore Mountain Garnet 2 (UWG), and San Carlos Olivine (SCO)) are presented as a complete dataset to any laboratory making triple oxygen isotope measurements to calibrate their reference gas to the VSMOW2-SLAP2 scale. All labs conducting oxygen isotope analyses for either $\delta^{18}\text{O}$ or paired $\delta^{17}\text{O}$ - $\delta^{18}\text{O}$ measurements, can use these standards to calibrate their reference gas on the VSMOW2-SLAP2 scale. The carbonate triple oxygen isotope composition of NBS 18, NBS 19, and IAEA-603 measured by total fluorination are presented so laboratories measuring the triple oxygen isotope composition of CO_2 evolved by phosphoric acid digestion can correct directly to the oxygen isotope values of the total carbonate.

2.2 Isotope Systematics

The isotopic abundance ratio is reported in standard δ -notation (McKinney et al., 1950) and defined as:

$$\delta^x\text{O} = \left(\frac{{}^xR_{\text{sample}}}{{}^xR_{\text{VSMOW}}} - 1 \right) \times 1000 \quad 2.2),$$

${}^xR = {}^x\text{O}/{}^{16}\text{O}$ and x is either mass 17 or 18. In this study, all samples are reported in linearized notation relative to the VSMOW2-SLAP2 scale. Linear notation is used to remove curvature effects that exist when comparing $\delta^{18}\text{O}$ and $\delta^{17}\text{O}$ values across a large scale and is defined as (Hulston and Thode, 1965; Miller, 2002):

$$\delta'^x\text{O} = 1000 \ln \left(\frac{\delta^x\text{O}}{1000} + 1 \right) \quad 2.3),$$

where x refers to ${}^{17}\text{O}$ or ${}^{18}\text{O}$. By combining and rewriting the equilibrium fractionation equation with δ' notation, the mass-dependent equilibrium fractionation between two

phases can be written as $1000 \ln \alpha_{a-b} = \delta^x O_a - \delta^x O_b$ (where x is either mass 17 or 18 and $\alpha = {}^{17}R/{}^{18}R$). Deviations of $\delta^{17}O$ from a reference slope are expressed as $\Delta^{17}O$, given by,

$$\Delta^{17}O = \delta^{17}O - \lambda_{RL} \times \delta^{18}O + \gamma \quad 2.4),$$

where λ_{RL} is the reference slope and γ is the y-intercept (for this study $\gamma=0$). In this work, a λ_{RL} value of 0.528 is used to keep in line with the original literature reporting triple oxygen isotope standards and align geological papers with the broader triple oxygen isotope community (Meijer and Li, 1998; Passey et al., 2014; Sharp et al., 2018; Barkan et al., 2019).

While λ is used to describe the slope of the best fit, θ is used to describe processes controlled by thermodynamic equilibrium, defined for the triple oxygen isotope system as:

$$\theta_{a-b} = \frac{\delta^{17}O_a - \delta^{17}O_b}{\delta^{18}O_a - \delta^{18}O_b} \quad 2.5),$$

where a and b are any two phases.

2.3 Methods

All samples (except air) were fluorinated using BrF_5 as the fluorinating agent. The fluorination procedures for waters, silicates and carbonates are slightly different, but the post-fluorination O_2 purification and analysis were identical for all methods and all samples were measured on the same mass spectrometer relative to the same working gas.

2.3.1 Waters

Waters were fluorinated using a modification of the procedure outlined in O'Neil and Epstein (1966). 1.8 μ l of water were injected through a Valco® 1/8" septum injector nut with support and low bleed septum using a 2 μ l Hamilton© series 7000 Gastight®

syringe into an evacuated glass U-trap. The H₂O was cryogenically transferred into a ¼" Ni U-trap bounded on either side by a Swagelok SS-4H welded bellows valve. 500-550 μmoles of BrF₅ were then frozen into the U-trap. The volume was isolated and the entire region (including the bellows valve block) was heated for 5 minutes using a heat gun. The reaction products were expanded into the laser fluorination chamber for further purification. Precision of analyses is 0.091 and 0.164 ‰ for δ¹⁷O and δ¹⁸O respectively and 0.006 for Δ¹⁷O values. The higher precision for Δ¹⁷O is due to the fact that small uncertainties in the δ¹⁷O and δ¹⁸O are correlated (Wostbrock et al., 2018).

2.3.2 *Silicates*

Silicates were reacted using the standard laser fluorination procedure of Sharp (1990). Two mg sized samples were loaded onto a Ni sample block with individual holes for up to 44 samples. The block was evacuated in the heated reaction chamber using a turbomolecular pump for 24 hours while being heated by an external halogen heat lamp. Samples were then prefluorinated for about one hour at room temperature to remove any adsorbed water or other contaminants. Samples were heated with a 50 W CO₂ laser in the presence of 100 torr BrF₅ (~500 μmoles) until the sample was completely fluorinated. Purification of the O₂ gas is described below.

2.3.3 *Carbonates*

Carbonates were quantitatively fluorinated at high temperatures using the conventional 'Ni bomb' method, similar to a method used by Sharma and Clayton (1965). The procedure involves loading 5-6 mg of carbonate into Ni tubes and heating under vacuum at ~100°C for 12 hours to remove any adsorbed H₂O. A 30-times excess of BrF₅ (30x more gas than stoichiometrically necessary for complete reaction) is then

added as an oxidizing reagent and the tubes are heated to 750 °C for 4 days to ensure complete fluorination. The bombs are frozen with liquid nitrogen and O₂ is quantitatively released into the laser fluorination chamber/cleanup line. The bombs are then isolated, warmed and refrozen to release any remaining O₂ that might have been trapped in the residual BrF_x ice. A Pfeiffer PrismPlus quadrupole mass spectrometer was used to test the presence of unreacted COF₂.

2.3.4 CO₂ gas

The CO₂ released via phosphoric acid digestion at 25°C from the 3 standards was also fluorinated using the same method as the carbonates. To release the CO₂, 8-10 mg of carbonate were loaded into glass tubes along with a smaller tube containing 3 ml of 102% phosphoric acid (McCrea, 1950). Samples were degassed for 12 hours and then placed in a water bath for 1 hour to equilibrate to 25°C. The phosphoric acid was then reacted with the carbonate for ~15 hours in the water bath. The released CO₂ was purified using cryogenic traps to remove H₂O and non-condensable gases and transferred cryogenically into Ni tubes for fluorination. The same Ni tubes were used for both CO₂ and carbonate fluorination. After BrF₅ was added to the Ni tube, the tubes were heated to 750 °C for 4 days. Released O₂ was transferred into the mass spectrometer following the exact same purification process as the O₂ released from carbonate fluorination.

2.3.5 Oxygen gas purification and O₂ analysis

Following fluorination of a sample, the O₂ gas was passed over two traps cooled with liquid nitrogen and then through a warmed (~100°C) NaCl trap to remove traces of F₂. The gas passed through an additional cold trap and was adsorbed onto a 5Å mol. sieve cooled to liquid nitrogen temperature. The sample gas was transferred through a 6', 1/8"

diameter, 5x mol sieve gas chromatograph in a He stream set at a constant flow of 6.0 ml/min at room temperature and collected on a second mol sieve trap at the inlet of the mass spectrometer (The high purity He was first passed through a large U-trap filled with activated 5Å mol sieve cooled to liquid nitrogen temperatures for further purification and removal of any trace O₂). Excess He was pumped away, and the O₂ was expanded into a Thermo-Finnegan MAT 253+ mass spectrometer at the Center for Stable Isotopes at the University of New Mexico specifically configured for O₂ gas. The oxygen was measured using long integration (26 sec) with 30 iterations per analysis and measured against the same O₂ reference gas. The instrument was checked for any pressure effects described by Yeung et al. (2018) and no pressure effect was found so no correction was applied. The test involved measuring two different gases ($\Delta\delta^{18}\text{O}\approx 25\text{‰}$) at 3V, 5V, and 10V intensities on mass 32 and the resulting $\Delta^{17}\text{O}$ value varied by 0.002‰, and $\delta^{18}\text{O}$ value varied by less than 0.04‰ (Appendix A). Nevertheless, every attempt was made to run our samples at a constant intensity of 5.5 V on mass 32, corresponding to a pressure of ~55 mbar in the bellows and 6.8×10^{-8} mbar in the source.

2.3.6 Air

For air analyses, 3 ml of outside Albuquerque air was injected into a vacuum line, frozen into a 4-way valve with a liquid nitrogen trap filled with 5Å mol sieve. Purified He was used to carry the sample through a 4-meter 1/8" packed 5x mol sieve column cooled with a mixture of dry ice-ethanol (-80°C) with a He flow rate of 12.8 ml/min. The O₂ was collected on a second mol sieve liquid nitrogen trap and excess He was pumped away before being expanded into the mass spectrometer. Argon and O₂ separation were complete (Figure 2.1) with ~10 seconds between argon and the beginning of the O₂ peak.

The Ar concentration remaining in the O₂ sample gas was ~0.05% based on relative peak intensities for masses 32 and 40.

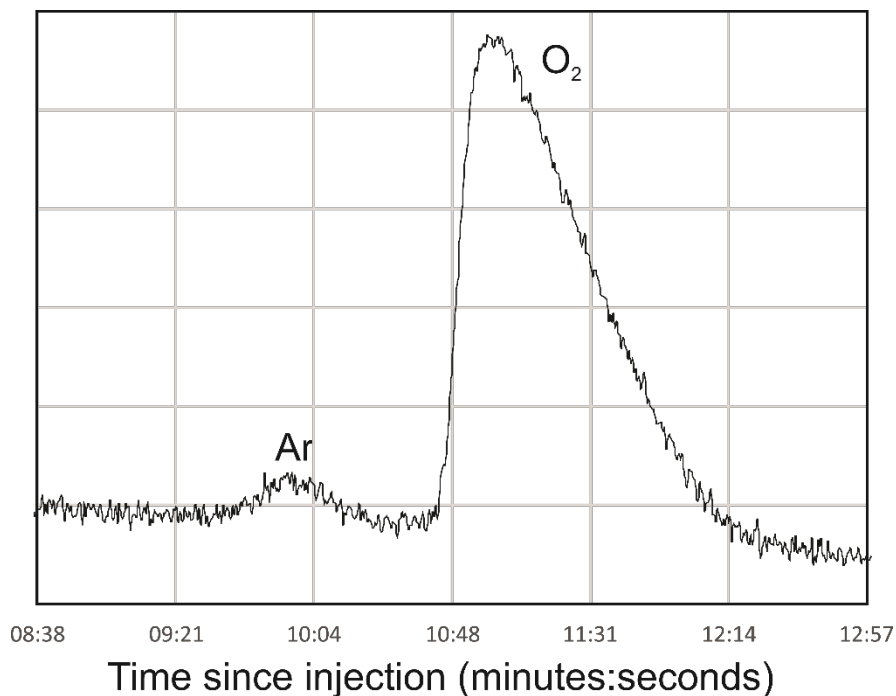


Figure 2.1- Separation of Ar and O₂ in our chilled GC column during an Air sample injection.

2.4 Results/Discussion

All results are reported in Tables 2.1, 2.3, 2.5, and 2.6.

2.4.1 Water standards

All data are reported normalized to VSMOW2 with oxygen isotope values $\equiv 0$. Our analyses for VSMOW2 have the following uncertainty (1σ , $n = 8$): $\delta^{18}\text{O} \pm 0.16\text{‰}$, $\delta^{17}\text{O} \pm 0.09\text{‰}$, $\Delta^{17}\text{O} \pm 0.006\text{‰}$. (Table 2.1). The average oxygen isotope values of SLAP2 are $\delta^{17}\text{O} = -29.74 \pm 0.10\text{‰}$, $\delta^{18}\text{O} = -55.55 \pm 0.19\text{‰}$ and $\Delta^{17}\text{O} = -0.015 \pm 0.005\text{‰}$ ($n=5$), nearly identical to the accepted value for $\delta^{18}\text{O} = -55.5\text{‰}$ (Gonfiantini, 1978), but with a $\Delta^{17}\text{O}$ value slightly less than the recommended value of 0.00‰ (Schoenemann et al., 2013). It should be pointed out that the measured $\Delta^{17}\text{O}$ value of SLAP2 by Schoenemann et al. (2013) is -0.005‰ . The $\Delta^{17}\text{O}$ value of 0 is an artificial one that is

taken for convenience only. A clear trend exists where lower published $\delta^{18}\text{O}$ values correspond to lower $\Delta^{17}\text{O}$ values (Figure 2.2). In studies where VSMOW2 and SLAP2

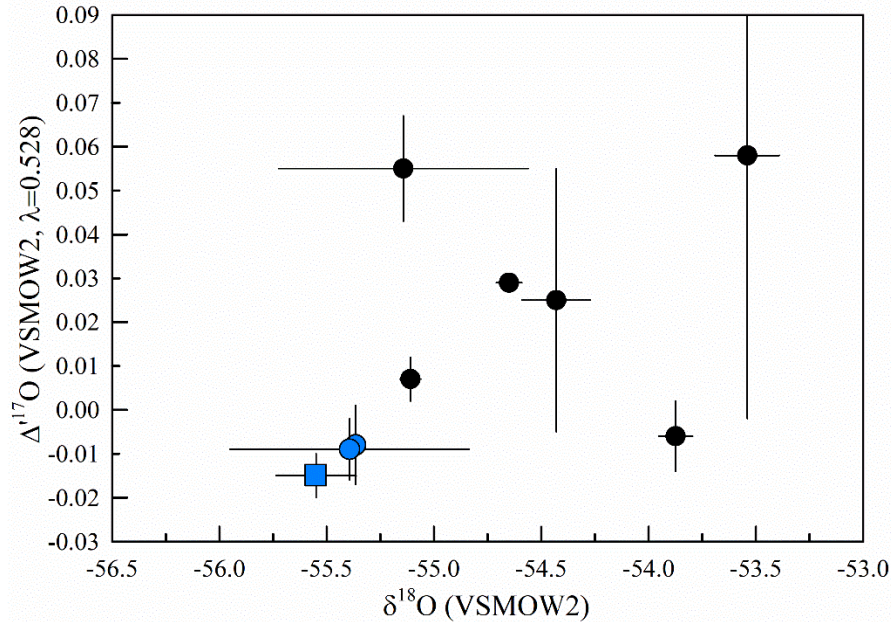


Figure 2.2 - Triple oxygen isotope composition of SLAP2. A literature compilation (Table 2; circles) of $\Delta^{17}\text{O}$ values shows a relationship with $\delta^{18}\text{O}$ values for SLAP2 where higher $\delta^{18}\text{O}$ values result in higher $\Delta^{17}\text{O}$ values. This study (blue square) is the closest $\delta^{18}\text{O}$ value to IAEA. Studies with $\delta^{18}\text{O}$ values close to the IAEA accepted value of -55.5 (blue circles) were used to define SLAP2 values. Studies not used to define SLAP2 values are represented as black circles.

are analyzed for triple oxygen isotope analyses, most $\delta^{18}\text{O}$ values are higher than the IAEA value of -55.5‰ (Table 2.2). Measurement of SLAP2 is notoriously difficult due to a persistent memory effect. Our memory effect was minimal after 4 iterations (Figure 2.3). Other studies may not have completely erased the memory effect or suffer from an unidentified compression factor. Given that the lowest $\delta^{18}\text{O}$ values of SLAP are most likely to be the closest to reality, the corresponding $\Delta^{17}\text{O}$ values should also be closest to the true value. Even small traces of meteoric/atmospheric water in the fluorination line will result in higher measured SLAP $\delta^{18}\text{O}$ and $\Delta^{17}\text{O}$ values. Traces of NF_3 in the sample gas also increase the measured $\Delta^{17}\text{O}$ values. A GC column is used in this study to completely eliminate any traces of NF_3 . The three lowest published $\delta^{18}\text{O}$ and $\Delta^{17}\text{O}$

Table 2.1 - Individual and average VSMOW2-SLAP2 data of this study reported in ‰ notation. All data have been normalized to VSMOW2 having a $\delta^{17}\text{O} = \delta^{18}\text{O} = 0.000\text{‰}$.

Sample	$\delta^{17}\text{O}$	$\delta^{18}\text{O}$	$\delta^{17}\text{O}$	$\delta^{18}\text{O}$	$\Delta^{17}\text{O}$ ($\lambda=0.528$)
VSMOW2_1	-0.085	-0.163	-0.085	-0.163	0.001
VSMOW2_2	-0.116	-0.204	-0.116	-0.204	-0.008
VSMOW2_3	-0.017	-0.027	-0.017	-0.027	-0.002
VSMOW2_4	0.108	0.194	0.108	0.194	0.006
VSMOW2_5	0.102	0.194	0.102	0.194	0.000
VSMOW2_6	-0.097	-0.169	-0.097	-0.169	-0.008
VSMOW2_7	0.063	0.105	0.063	0.105	0.008
VSMOW2_8	0.040	0.070	0.040	0.070	0.003
Average	0.000	0.000	0.000	0.000	0.000
St. Dev ($\pm 1\sigma$)	0.091	0.164	0.091	0.164	0.006
SLAP2_1*	-28.205	-52.689	-28.611	-54.128	-0.031
SLAP2_2*	-28.504	-53.244	-28.918	-54.714	-0.029
SLAP2_3*	-29.452	-54.991	-29.895	-56.561	-0.031
SLAP2_4	-29.850	-55.761	-30.305	-57.376	-0.010
SLAP2_5	-29.633	-55.355	-30.081	-56.946	-0.013
SLAP2_6	-29.792	-55.651	-30.245	-57.259	-0.012
SLAP2_7	-29.637	-55.349	-30.085	-56.939	-0.021
SLAP2_8	-29.792	-55.635	-30.245	-57.242	-0.021
Average	-29.741	-55.550	-30.192	-57.153	-0.015
St. Dev ($\pm 1\sigma$)	0.100	0.187	0.103	0.198	0.005

*denotes samples of observed consecutive memory effect after earlier VSMOW2 injections and are not included in averages or standard deviation.

Table 2.2 - Compilation of published triple oxygen isotope values of SLAP2 on the VSMOW2 scale, all values are reported in ‰.

	$\delta^{17}\text{O}$	$\delta^{18}\text{O}$	$\delta^{17}\text{O}$	$\delta^{18}\text{O}$	$\Delta^{17}\text{O}$ ($\lambda=0.528$)
Jabeen and Kusakabe (1997)	-28.58 (± 0.13)	-53.54 (± 0.15)	-28.996	-55.027	0.058 (± 0.06)
Barkan and Luz (2005)	-29.48 (± 0.03)	-55.11 (± 0.05)	-29.923	-56.687	0.007 (± 0.005)
Kusakabe and Matsuhisa (2008)	-29.21 (± 0.07)	-54.65 (± 0.06)	-29.645	-56.200	0.029 ^a
Lin et al. (2010) ^b	-29.10 (± 0.10)	-54.43 (± 0.16)	-29.529	-55.972	0.025 (± 0.030)
Schoenemann et al. (2013)	-28.822 (± 0.04)	-53.874 (± 0.08)	-29.245	-55.380	-0.006 (± 0.008)
Pack et al. (2016) - GZG	-29.451 (± 0.314)	-55.143 (± 0.582)	-29.893	-56.722	0.055 (± 0.012)
Pack et al. (2016) - ISEI	-29.633 (± 0.028)	-55.366 (± 0.044)	-30.089	-56.958	-0.008 (± 0.009)
Sharp et al. (2016)	-29.650 (± 0.296)	-55.394 (± 0.556)	-30.099	-56.987	-0.009 (± 0.007)
This study	-29.741 (± 0.100)	-55.550 (± 0.187)	-30.192	-57.153	-0.015 (± 0.005)

Bolded studies are 3 lowest SLAP values which averages $\delta^{18}\text{O} = -55.438 \pm 0.099$ and $\Delta^{17}\text{O} = -0.011 \pm 0.004$

^a - standard deviation unreported in publication

^b - SLAP2 corrected to VSMOW2

values are shown as the bolded samples in Table 2.2. The $\Delta^{17}\text{O}$ values of these three studies average -0.011‰ (± 0.003), corresponding to a $\delta^{17}\text{O}$ and $\delta^{18}\text{O}$ value of SLAP2 = -29.7093‰ and -55.5‰ relative to $\delta^{17}\text{O}$ and $\delta^{18}\text{O}$ value of VSMOW $\equiv 0$. The average values of the three studies that gave the nearly-correct $\delta^{18}\text{O}$ values may more accurately reflect the true $\Delta^{17}\text{O}$ values of SLAP2. The effect of using a $\Delta^{17}\text{O}$ value of -0.011‰ (or -0.015‰) for SLAP rather than 0.00‰ is negligible for all but extremely light or heavy $\delta^{18}\text{O}$ values. The difference between the two calibrations for a carbonate with a $\delta^{18}\text{O}$ value of 30‰ is only 0.006‰ so that either reference gives the same $\Delta^{17}\text{O}$ values, within error, for most natural materials.

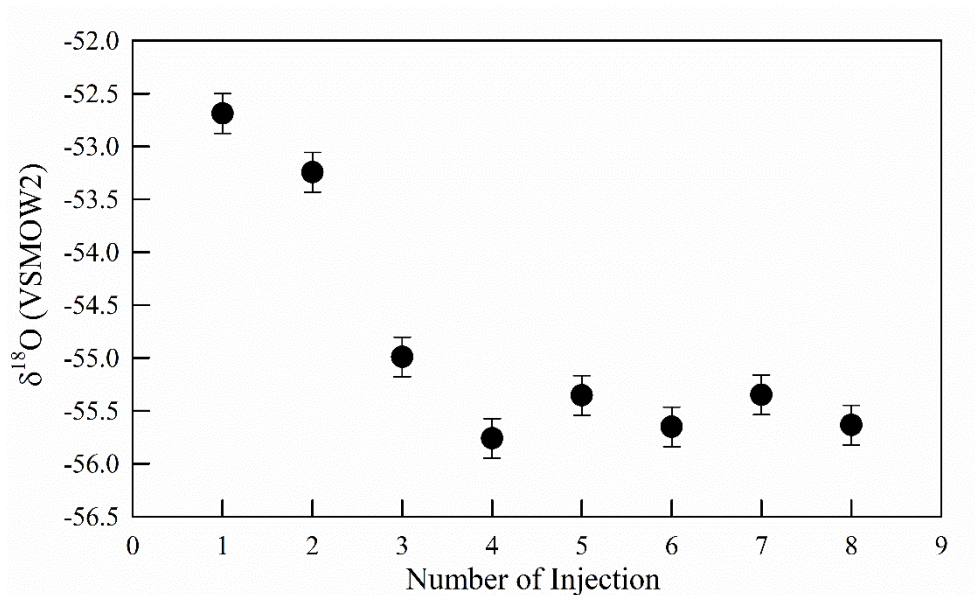


Figure 2.3 - Memory effect of switching from VSMOW2 samples to SLAP2 samples for analysis. The first three injections of SLAP gave high $\delta^{18}\text{O}$ values.

2.4.2 Calcite standards

Three methods have been used to quantitatively extract oxygen from carbonates (Sharma and Clayton, 1965). The first involves low temperature fluorination at 125°C to produce CO_2 and O_2 ; the latter is then combusted to CO_2 and all CO_2 is recombined for the total $\delta^{18}\text{O}$ analysis. This procedure is not applicable for triple isotope analyses as the

ultimate product, CO₂, is not easily measured for ¹⁷O/¹⁶O ratio (see however, Adnew et al., 2019). The second is complete fluorination in nickel bombs run at temperatures in excess of 700°C. Sharma and Clayton (1965) found that the δ¹⁸O value from this method were 0.5‰ lower than for the low-T fluorination method. They hypothesized that the lower δ¹⁸O values are due to the presence of COF₂ that produced an ion beam at mass 47 (COF⁺), which was collected along with mass 44 in the large cup of their double-collector mass spectrometer. The third method involves thermal decarbonation in a vacuum producing CO₂ followed by fluorination of the remaining oxide. The oxygen is reacted with carbon to form CO₂ and the two extracted CO₂ gases are combined for the total δ¹⁸O value. Sharma and Clayton (1965) did not use this method for calcite, but interestingly obtained the same result using decarbonation-fluorination and total fluorination (methods 2 and 3) for most other divalent cation carbonates. All other studies (Kim and O'Neil, 1997; Das Sharma et al., 2002; Kim et al., 2007a) used the third technique for δ¹⁸O determinations of calcite.

NBS 18, NBS 19 (and NBS 19a), and IAEA-603 carbonate standards were measured using high temperature fluorination at 750°C (Table 2.3). Unreacted COF₂ (mass 66) was tested for by analyzing the reaction products left in the nickel tubes after O₂ removal using a Pfeiffer PrismPlus Quadrupole. There was a very small peak at mass 47 (COF⁺), but almost undetectable COF₂ at mass 66 (Appendix B). Therefore, the reaction is extremely close to completion and total O₂ content of the carbonates are measured.

The δ¹⁸O values measured using the high temperature fluorination method in this study have a variability as high as 1‰ (1σ) and a standard error of 0.5‰, making the data

Table 2.3 - Triple oxygen isotope data for carbonate standards and CO₂ extracted by phosphoric acid digestion at 25°C. The measured $\Delta^{17}\text{O}$ value and accepted $\delta^{18}\text{O}$ value of the standards were used to calculate the $\delta^{17}\text{O}$ value relative to the accepted $\delta^{18}\text{O}$ value (corr data). The θ and α values are for CO₂-calcite. All samples are reported in ‰ relative to VSMOW2-SLAP2.

Sample	Type	$\delta^{17}\text{O}$	$\delta^{18}\text{O}$	$\delta^{17}\text{O}$	$\delta^{18}\text{O}$	$\Delta^{17}\text{O}$ ($\lambda=0.528$)	$\delta^{17}\text{O}_{\text{corr}}^{\text{a}}$	$\delta^{18}\text{O}_{\text{corr}}^{\text{b}}$	$\delta^{17}\text{O}_{\text{corr}}^{\text{c}}$	$\delta^{18}\text{O}_{\text{corr}}$
NBS18 1	calcite	3.795	7.286	3.787	7.260	-0.046	3.749	7.200	3.742	7.174
NBS18 2	calcite	3.484	6.692	3.478	6.670	-0.043	3.752	7.200	3.745	7.174
NBS18 3	calcite	3.772	7.273	3.765	7.247	-0.062	3.733	7.200	3.726	7.174
NBS18 4	calcite	3.539	6.793	3.532	6.770	-0.042	3.753	7.200	3.746	7.174
	Average	3.647	7.011	3.641	6.986	-0.048	3.747	7.200	3.740	7.174
	$\pm 1\sigma$	0.159	0.313	0.158	0.311	0.009	0.010	0.010	--	--
	St. err^d	0.079	0.156	0.079	0.155	0.005	0.005	0.005	--	--
NBS18 1	CO ₂	9.049	17.400	9.008	17.250	-0.100	9.114	17.524	9.072	17.372
		$\theta=0.52294, ^{17}\alpha=1.00538, ^{18}\alpha=1.01032$					$\theta_{\text{corr}}=0.52291, ^{17}\alpha_{\text{corr}}=1.00535, ^{18}\alpha_{\text{corr}}=1.01025$			
NBS19 1	calcite	15.139	29.055	15.026	28.641	-0.097	14.928	28.650	14.818	28.247
NBS19 2	calcite	14.888	28.560	14.778	28.160	-0.090	14.935	28.650	14.825	28.247
NBS19 3	calcite	15.014	28.827	14.903	28.419	-0.103	14.922	28.650	14.812	28.247
NBS19 4	calcite	14.894	28.622	14.784	28.220	-0.116	14.909	28.650	14.799	28.247
NBS19 5	calcite	14.761	28.341	14.653	27.947	-0.103	14.922	28.650	14.812	28.247
NBS19A 1	calcite	14.510	27.830	14.406	27.450	-0.088	14.937	28.650	14.827	28.247
NBS19A 2	calcite	12.891	24.744	12.809	24.443	-0.097	14.928	28.650	14.818	28.247
NBS19A 3	calcite	13.775	26.462	13.681	26.118	-0.109	14.915	28.650	14.805	28.247
NBS19A 4	calcite	14.992	28.803	14.880	28.396	-0.112	14.912	28.650	14.802	28.247
	Average	14.541	27.916	14.436	27.533	-0.102	14.923	28.650	14.813	28.247
	$\pm 1\sigma$	0.741	1.423	0.730	1.385	0.010	0.010	--	0.010	--
	St. err	0.247	0.474	0.243	0.462	0.003	0.003	--	0.003	--
NBS19A 1	CO ₂	19.188	36.955	19.006	36.288	-0.154	20.349	39.194	20.145	38.445
NBS19A 2	CO ₂	19.749	38.030	19.556	37.325	-0.151	20.352	39.194	20.148	38.445
NBS19A 3	CO ₂	19.709	37.964	19.517	37.261	-0.157	20.346	39.194	20.142	38.445
NBS19A 4	CO ₂	19.817	38.175	19.624	37.464	-0.158	20.346	39.194	20.141	38.445
	Average	19.616	37.781	19.426	37.085	-0.155	20.348	39.194	20.144	38.445
	$\pm 1\sigma$	0.289	0.558	0.283	0.538	0.003	0.003	--	0.003	--
	St. err	0.144	0.279	0.142	0.269	0.001	0.001	--	0.001	--
		$\theta=0.52241, ^{17}\alpha=1.00500, ^{18}\alpha=1.00960$					$\theta_{\text{corr}}=0.52276, ^{17}\alpha_{\text{corr}}=1.00535, ^{18}\alpha_{\text{corr}}=1.01025$			
IAEA603 1	calcite	15.266	29.307	15.151	28.885	-0.101	14.830	28.47	14.722	28.072
IAEA603 2	calcite	14.213	27.263	14.113	26.898	-0.090	14.841	28.47	14.732	28.072
IAEA603 3	calcite	14.746	28.322	14.638	27.928	-0.108	14.823	28.47	14.714	28.072
IAEA603 4	calcite	14.674	28.179	14.567	27.789	-0.105	14.826	28.47	14.717	28.072
IAEA603 5	calcite	13.442	25.797	13.352	25.470	-0.096	14.835	28.47	14.726	28.072
IAEA603 6	calcite	14.497	27.832	14.393	27.452	-0.102	14.829	28.47	14.720	28.072
	Average	14.473	27.783	14.369	27.404	-0.100	14.831	28.470	14.722	28.072
	$\pm 1\sigma$	0.612	1.182	0.604	1.150	0.007	0.007	--	0.007	--
	St. err	0.250	0.483	0.247	0.470	0.003	0.003	--	0.003	--
IAEA603 1	CO ₂	19.446	37.417	19.260	36.734	-0.136	20.273	39.012	20.071	38.270
IAEA603 2	CO ₂	19.358	37.245	19.173	36.568	-0.135	20.275	39.012	20.072	38.270
IAEA603 3	CO ₂	19.709	37.964	19.517	37.261	-0.157	20.252	39.012	20.050	38.270
IAEA603 4	CO ₂	19.817	38.175	19.624	37.464	-0.158	20.251	39.012	20.049	38.270
IAEA603 5	CO ₂	19.847	38.215	19.653	37.503	-0.149	20.260	39.012	20.058	38.270
	Average	19.635	37.803	19.445	37.106	-0.147	20.262	39.012	20.060	38.270
	$\pm 1\sigma$	0.221	0.446	0.217	0.429	0.011	0.011	--	0.011	--
	St. err	0.099	0.199	0.097	0.192	0.005	0.005	--	0.005	--
		$\theta=0.52319, ^{17}\alpha=1.00509, ^{18}\alpha=1.00975$					$\theta_{\text{corr}}=0.52342, ^{17}\alpha_{\text{corr}}=1.00535, ^{18}\alpha_{\text{corr}}=1.01025$			

^a – corrected using Eq. 2.3

^b – IAEA accepted values

^c – corrected using Eq. 2.4

^d – St. err = Stdev/ \sqrt{n} , where n is number of analyses

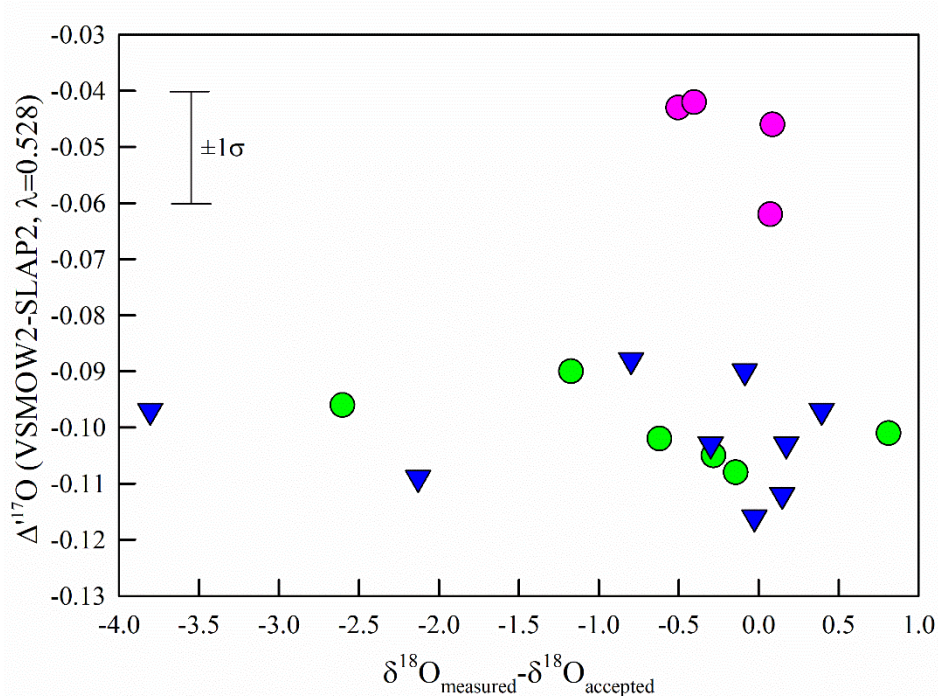


Figure 2.4 - $\Delta^{17}\text{O}$ vs. the difference between the $\delta^{18}\text{O}_{\text{measured}}$ and the $\delta^{18}\text{O}_{\text{accepted}}$ value ($\delta^{18}\text{O}_{\text{measured}} - \delta^{18}\text{O}_{\text{accepted}}$). Regardless of the measured $\delta^{18}\text{O}$ value, the $\Delta^{17}\text{O}$ values are within our reported error and do not correlate with $\delta^{18}\text{O}$ value. NBS18 (magenta), NBS19/NBS19A (blue) and IAEA603 (green).

unsuitable for accurate determinations of the $\delta^{18}\text{O}$ value (Table 2.3). However, $\delta^{18}\text{O}$ and $\delta^{17}\text{O}$ covary with a $\lambda = 0.528$, so that the $\Delta^{17}\text{O}$ value is constant with a standard deviation of 0.01‰ or less. There is no trend for the $\Delta^{17}\text{O}$ value vs the $\delta^{18}\text{O}$ value, giving us high confidence on the accuracy of the $\Delta^{17}\text{O}$ value. (Figure 2.4). The $\Delta^{17}\text{O}$ values of the sedimentary carbonates are consistent with low temperatures of formation with seawater whereas the carbonatite (NBS 18) has a higher $\Delta^{17}\text{O}$ typical of mantle origin (Sharp et al., 2018). Our $\Delta^{17}\text{O}_{\text{NBS 19}} - \Delta^{17}\text{O}_{\text{NBS-18}}$ value (the $\Delta\Delta^{17}\text{O}_{\text{NBS-19 - NBS-18}}$ value) is -0.054 ‰, in agreement with the expected differences for a low temperature calcite (NBS 19) and an igneous carbonatite (NBS 18). Other published values for this difference are -0.037 (Passey et al., 2014) and -0.019 (Barkan et al., 2019), both measured on CO_2

extracted from carbonate at 90 and 25 °C, respectively. The $\Delta\Delta^{17}\text{O}_{\text{NBS-19} - \text{NBS-18}}$ value should be constant, regardless of extraction procedure.

The IAEA recommended $\delta^{18}\text{O}$ values and the calculated $\delta^{17}\text{O}$ values from our data are in Table 2.4. The corrected $\delta^{17}\text{O}$ are determined from the measured $\Delta^{17}\text{O}$ values and the accepted $\delta^{18}\text{O}$ value using equation 2.4 ($\delta^{17}\text{O} = \Delta^{17}\text{O}_{(\text{avg})} + 0.528 \times \delta^{18}\text{O}_{\text{IAEA value}}$).

Table 2.4 - $\delta^{17}\text{O}$ and $\delta^{18}\text{O}$ values of IAEA carbonate standards. $\delta^{18}\text{O}$ values are accepted IAEA values. $\delta^{17}\text{O}$ values are calculated from the measured $\Delta^{17}\text{O}$ values using Eqs. 2.3 and 2.4.

Sample	$\delta^{17}\text{O}$	$\delta^{18}\text{O}$	$\Delta^{17}\text{O} (\pm 1\sigma)$ ($\lambda = 0.528$)
NBS 18*	3.636	6.99	-0.048 (± 0.009)
NBS 18**	3.747	7.20	-0.048 (± 0.009)
NBS19, 19a**	14.923	28.65	-0.102 (± 0.010)
IAEA603*	14.831	28.47	-0.100 (± 0.007)

*Value given by IAEA data sheet:

https://nucleus.iaea.org/rpst/ReferenceProducts/ReferenceMaterials/Stable_Isotopes/13C18and7Li/NBS_18.htm

**Value of IUPAC technical report (Brand et al., 2014; Coplen et al., 1983)

2.4.3 CO_2 from calcite

The $\delta^{17}\text{O}$ and $\delta^{18}\text{O}$ values of CO_2 extracted from calcite using phosphoric acid digestion at 25°C are determined in a similar manner to calcite. The $\delta^{18}\text{O}$ value of the CO_2 extracted using phosphoric acid digestion was measured before fluorination. The $\Delta^{17}\text{O}$ values determined from the measured $\delta^{17}\text{O}$ and $\delta^{18}\text{O}$ are constant for all analyses, so the average $\Delta^{17}\text{O}$ values are used to back-calculate the $\delta^{17}\text{O}$ value from the $\delta^{18}\text{O}$ value determined conventionally. These data are reported in Table 2.3. The calculated θ_{ACID} value for CO_2 -calcite extracted by phosphoric acid digestion at 25 °C is 0.5230 ± 0.0003 , where $\theta = \ln \alpha^{17}\text{O}_{\text{CO}_2\text{-calcite(ACID)}} / \ln \alpha^{18}\text{O}_{\text{CO}_2\text{-calcite(ACID)}}$, corresponding to an $^{18}\alpha_{\text{CO}_2\text{-calcite(ACID)}}$ value of 1.01025 and an $^{17}\alpha_{\text{CO}_2\text{-calcite(ACID)}}$ value of $1.0053 \pm 3.55 \times 10^{-6}$ (note that the error of the corrected $^{17}\alpha_{\text{CO}_2\text{-calcite(ACID)}}$ is influenced by the error on $\Delta^{17}\text{O}$ values).

Laboratories that make triple oxygen isotope measurements of carbonates commonly measure the CO₂ liberated via phosphoric acid digestion (Passey et al., 2014; Barkan et al., 2015; Barkan et al., 2019; Passey and Ji, 2019) using the methods described in the introduction. Laboratories can now use one of the reported carbonate standards and the measured θ_{ACID} (0.5230 ± 0.0003 , Table 2.3) value presented here to correct for the fractionation that occurs for $\delta^{17}\text{O}$ during phosphoric acid digestion.

2.4.4 Silicate standards

Three commonly used silicate standards (San Carlos Olivine, NBS 28, and UW-Gore Mountain Garnet-2) were analyzed, as well as a laboratory inhouse quartz standard (NM-Q, Table 2.5). Estimated yield was based on measured weight of each sample and the pressure in the bellows of the mass spectrometer. Analyses with low yields were removed from the dataset. Lower yields generally corresponded to higher $\delta^{18}\text{O}$ and lower $\Delta^{17}\text{O}$ values. The average $\delta^{18}\text{O}$ and $\Delta^{17}\text{O}$ values of the silicate standards changed by less than 0.05 and 0.002 ‰, respectively, after data removal.

Five previous publications calibrated silicate standards relative to a gas that was calibrated to VSMOW-SLAP using the same fluorination line (Kusakabe and Matsuhisa, 2008; Ahn et al., 2012; Tanaka and Nakamura, 2013; Pack et al., 2016; Sharp et al., 2016). Four other papers have published various silicate standard using either oxygen gas calibrated to reference gas that is calibrated to VSMOW2-SLAP2 (Pack and Herwartz, 2014), oxygen gas calibrated to a combination of UWG-2, NBS 28 and San Carlos Olivine (Starkey et al., 2016), oxygen gas calibrated in respect to San Carlos Olivine with an assumed $\Delta^{17}\text{O}$ value of 0.0 (Young et al., 2014), or have run only SMOW to calibrate the reference gas (Franchi et al., 1999). The average $\delta^{18}\text{O}$ and $\Delta^{17}\text{O}$

Table 2.5 - Triple oxygen isotope data for silicate standards. All samples are reported in ‰ relative to the VSMOW2-SLAP2 scale.

Sample	Weight (mg)	$\delta^{17}\text{O}$	$\delta^{18}\text{O}$	$\delta^{17}\text{O}$	$\delta^{18}\text{O}$	$\Delta^{17}\text{O}$ ($\lambda=0.528$)
UWG 1	2.7	2.909	5.645	2.904	5.629	-0.068
UWG 2	2.5	2.964	5.768	2.960	5.752	-0.077
UWG 3	2.5	2.961	5.769	2.956	5.752	-0.081
UWG 4	3.4	2.913	5.649	2.909	5.633	-0.066
UWG 5	2.1	2.912	5.651	2.908	5.635	-0.068
UWG 6	2.4	3.047	5.922	3.043	5.905	-0.075
UWG 7	2.2	2.948	5.728	2.943	5.712	-0.073
UWG 8	2.3	2.884	5.598	2.880	5.582	-0.067
UWG 9	2.1	2.851	5.534	2.847	5.519	-0.067
	Average	2.932	5.696	2.928	5.680	-0.071
	$\pm 1\sigma$	0.057	0.115	0.056	0.114	0.005
NBS28 1	1.4	4.951	9.518	4.939	9.473	-0.063
NBS28 2	1.0	4.947	9.500	4.935	9.455	-0.057
NBS28 3	1.5	4.923	9.450	4.910	9.405	-0.056
NBS28 4	1.5	4.976	9.555	4.964	9.510	-0.057
NBS28 5	1.3	4.961	9.537	4.948	9.491	-0.063
NBS28 6	1.3	5.071	9.735	5.058	9.688	-0.057
NBS28 7	1.2	5.079	9.743	5.066	9.696	-0.053
NBS28 8	1.2	5.046	9.702	5.033	9.656	-0.065
NBS28 9	1.2	4.990	9.576	4.978	9.530	-0.054
NBS28 10	1.2	5.050	9.706	5.037	9.659	-0.063
NBS28 11	1.5	4.934	9.474	4.922	9.430	-0.057
NBS28 12	1.4	4.944	9.494	4.932	9.449	-0.057
NBS28 13	1.3	4.951	9.516	4.939	9.471	-0.062
	Average	4.986	9.577	4.974	9.532	-0.059
	$\pm 1\sigma$	0.055	0.106	0.055	0.105	0.004
NM-SCO-1	2.2	2.746	5.336	2.742	5.321	-0.067
NM-SCO 2	2.3	2.749	5.338	2.746	5.324	-0.065
NM-SCO 3	2.1	2.660	5.148	2.657	5.134	-0.054
NM-SCO 4	2.0	2.805	5.424	2.801	5.410	-0.055
NM-SCO 5	1.6	2.742	5.326	2.738	5.312	-0.067
NM-SCO 6	1.7	2.806	5.428	2.802	5.413	-0.056
NM-SCO 7	2.4	2.721	5.264	2.717	5.250	-0.055
NM-SCO-8	1.8	2.765	5.373	2.761	5.359	-0.068
NM-SCO 9	1.8	2.688	5.209	2.684	5.196	-0.059
NM-SCO 10	1.4	2.738	5.298	2.734	5.284	-0.055
NM-SCO 11	1.7	2.763	5.357	2.759	5.343	-0.062
NM-SCO 12	2.2	2.668	5.165	2.665	5.152	-0.055
NM-SCO 13	2.1	2.667	5.155	2.664	5.142	-0.051
NM-SCO 14	2.3	2.652	5.136	2.648	5.123	-0.057
NM-SCO-15	1.9	2.730	5.279	2.726	5.265	-0.054
NM-SCO 16	2.2	2.652	5.125	2.649	5.112	-0.050
NM-SCO 17	2.1	2.714	5.259	2.710	5.246	-0.060
NM-SCO 18	2.2	2.687	5.213	2.684	5.199	-0.062
	Average	2.720	5.268	2.716	5.255	-0.058
	$\pm 1\sigma$	0.048	0.096	0.048	0.095	0.005
NM-Q 1	1.3	9.405	18.032	9.362	17.871	-0.075
NM-Q 2	1.4	9.350	17.945	9.306	17.786	-0.085
NM-Q 3	1.3	9.458	18.158	9.414	17.995	-0.087
NM-Q 4	1.4	9.521	18.260	9.476	18.096	-0.078
NM-Q 5	1.5	9.359	17.957	9.315	17.798	-0.082
	Average	9.419	18.070	9.375	17.909	-0.081
	$\pm 1\sigma$	0.072	0.136	0.071	0.133	0.005

values of previous studies for San Carlos olivine are 5.19 ± 0.20 and -0.014 ± 0.056 ‰, respectively. It has been demonstrated that not all San Carlos olivine has the same $\delta^{18}\text{O}$ (Starkey et al., 2016) which may explain some of the spread. Removal of studies reporting $\delta^{18}\text{O}$ value of <5.0 ‰, yields an average of 5.27 ± 0.129 and -0.010 ± 0.057 ‰ for $\delta^{18}\text{O}$ and $\Delta^{17}\text{O}$ values, respectively. Our average $\delta^{18}\text{O}$ and $\Delta^{17}\text{O}$ values are 5.268 ± 0.096 ‰ and -0.058 ± 0.005 ‰. San Carlos Olivine was analyzed over two analytical sessions separated by 2 months. The average $\Delta^{17}\text{O}$ values between the two analytical sessions varied by 0.005‰. Our NBS 28 $\delta^{18}\text{O}$ value of 9.577 ± 0.105 ‰ and is indistinguishable from the IAEA reported value of 9.6‰. The $\Delta^{17}\text{O}$ value is -0.059 ± 0.004 ‰. Lastly, the UWG-2 garnet has a $\Delta^{17}\text{O}$ value of -0.071 ± 0.005 ‰ and a $\delta^{18}\text{O}$ value of 5.696 ± 0.115 ‰, slightly lower but within error of the reported interlaboratory average of 5.78‰ (commonly rounded to 5.8‰) and the University of Wisconsin laboratory's average of 5.74‰ (Valley et al., 1995). Our and previously measured values are shown in Figure 2.5 and Appendix C.

A clean size-fractionated mineral separate of a large aliquot of San Carlos olivine was made. No obvious heterogeneity in different aliquots have been found. This standard is available (NM-SCO) to other laboratories to ensure that all laboratory calibrations of San Carlos olivine are made on samples with the same isotopic composition. This will minimize the problem of sample-to-sample heterogeneity (Starkey et al., 2016) and allow laboratories that do not fluorinate waters to calibrate their silicate data to the VSMOW2-SLAP2 scale. Our average NM-Q values for $\delta^{18}\text{O}$ and $\Delta^{17}\text{O}$ values are 18.070 ± 0.136 ‰ and -0.081 ± 0.005 ‰, respectively. Common silicate standards are all <10 ‰. Using a silicate sample that is heavier than most samples analyzed will allow laboratories to now

calibrate their mass spectrometer without the need to analyze water. This is an essential way to improve interlaboratory calibration. Interested parties should go to www.csi.unm.edu to request an aliquot of NM-SCO or NM-Q. The silicate standard, NBS 28, is available for purchase from the IAEA.

Table 2.6 - Triple oxygen isotope data for individual air analyses. All samples are reported in ‰ relative to the VSMOW2-SLAP2 scale.

Sample	$\delta^{17}\text{O}$	$\delta^{18}\text{O}$	$\delta^{17}\text{O}$	$\delta^{18}\text{O}$	$\Delta^{17}\text{O}$ ($\lambda=0.528$)
Air 1	12.283	24.212	12.208	23.923	-0.424
Air 2	12.136	23.958	12.063	23.676	-0.437
Air 3	12.132	23.978	12.059	23.695	-0.452
Air 4	12.136	23.987	12.063	23.704	-0.453
Air 5	12.205	24.095	12.131	23.809	-0.440
Average	12.178	24.046	12.105	23.761	-0.441
$\pm 1\sigma$	0.066	0.107	0.065	0.104	0.012

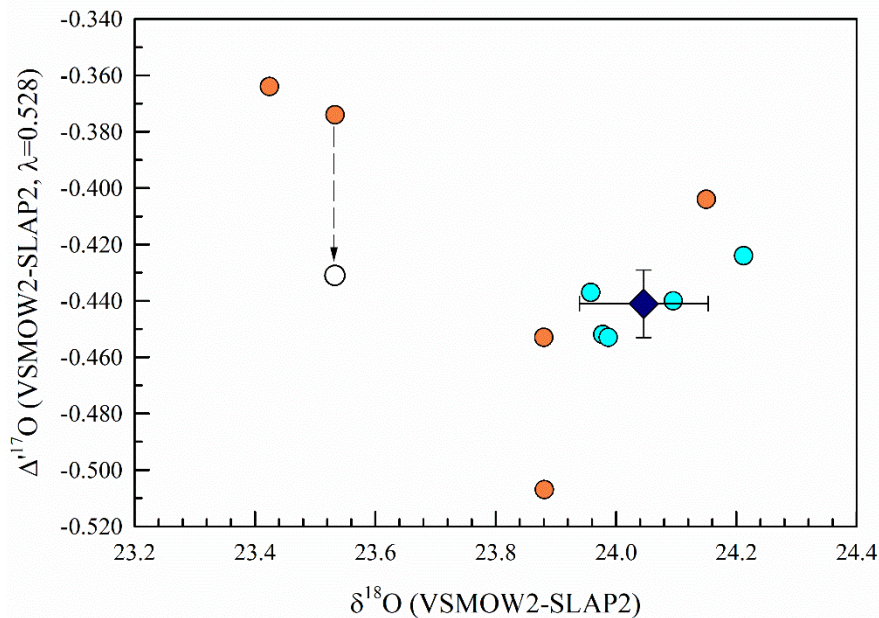


Figure 2.5 - $\Delta^{17}\text{O}$ and $\delta^{18}\text{O}$ values of air from individual analyses of this study (light blue circles) and the average (dark blue diamond, with error bars) and previous work (orange circles). Data from Barkan and Luz (2005); Barkan and Luz (2011), Pack et al. (2017), Yeung et al. (2012), and Young et al. (2014). Note, Young et al. (2014) reported data relative to San Carlos olivine $\Delta^{17}\text{O}$ value of 0.0‰. When corrected to the $\Delta^{17}\text{O}$ value of San Carlos olivine reported in this paper, the data in Young et al. (2014) becomes a lower $\Delta^{17}\text{O}$ value (arrow and open circle).

2.4.5 Air

Air O_2 is, in theory, an attractive standard for triple oxygen isotope analysis. It is homogeneous and is readily available. The difficulty with using air as a standard is that

the O₂ must be purified of Ar (Barkan and Luz, 2003) which requires passing the air sample through a long, chilled GC column. Five samples of outside air near Northrop Hall, University of New Mexico were analyzed using cryogenic GC purification. Average $\delta^{17}\text{O}$, $\delta^{18}\text{O}$, and $\Delta^{17}\text{O}$ values are 12.178 ± 0.066 , 24.046 ± 0.107 , and -0.441 ± 0.012 ‰, respectively (Table 2.6). Ar/O₂ ratios averaged 0.0005, sufficiently low enough to not affect the $\Delta^{17}\text{O}$ value (Barkan and Luz, 2003).

Our results agree with the average of published values in laboratories where VSMOW2 and SLAP2 were also measured (Figure 2.6; Appendix D). The data from Young et al. (2014) and Yeung et al. (2012) are significantly lighter in $\delta^{18}\text{O}$ and heavier in $\Delta^{17}\text{O}$ than the other calibrations, but are calibrated only to their San Carlos olivine standard, likely explaining the discrepancy. When correcting the data from Young et al. (2014) to the San Carlos olivine reported in this study, the $\Delta^{17}\text{O}$ value is -0.436 ‰, within error of our reported $\Delta^{17}\text{O}$ value of air. Assuming that air is homogenous, then laboratories that can separate O₂ and Ar using a GC column are encouraged to use air as a high $\delta^{18}\text{O}$ value reference.

2.5 Conclusion

In this communication triple oxygen isotope data for standard carbonate, silicate and air samples all calibrated to VSMOW2 and SLAP2 were presented. All analyses were made on the same Thermo Finnigan 253 Plus mass spectrometer using the same inlet system and reference gas. Most of the samples are available from the IAEA website. An aliquot of our San Carlos olivine standard and quartz standard (NM-SCO and NM-Q) can be requested from csi.unm.edu. The calibration presented here will allow laboratories measuring carbonates for triple oxygen isotope ratios to be calibrated directly to waters

and silicates. This internally consistent data set, tied to VSMOW2 and SLAP2, should lead to improved intercalibration for triple oxygen isotope analyses.

2.6 Acknowledgements

We would like to thank Sergey Assonov from the IAEA for the generous supply of carbonate, quartz, and water samples. We acknowledge the constructive reviews from Andreas Pack and an anonymous reviewer that helped improve the manuscript. We recognize the support from NSF GRFP grant DGE-1418062, NSF EAR 1551226, and NSF EAR 1747703.

3. CALIBRATION OF CARBONATE-WATER TRIPLE OXYGEN ISOTOPE FRACTIONATION: SEEING THROUGH DIAGENESIS IN ANCIENT CARBONATES

3.1 Introduction

In 1947, Harold Urey published a paper suggesting that the oxygen isotope composition of oxides could provide formation temperature information in geological samples (Urey, 1947). Four years later, three papers published calcite-water “isotopic temperature scales” (McCrea, 1950; Epstein et al., 1951; Urey et al., 1951). These seminal papers led to numerous works aimed at the reconstruction of ocean sea surface temperatures (Lowenstam and Epstein, 1954; Emiliani, 1955; Shackleton, 1967; Douglas and Savin, 1971; Douglas and Savin, 1973; Savin et al., 1975; Shackleton and Kennett, 1975; Savin, 1977; Zachos et al., 1994). Many studies have since published refined calcite-water oxygen isotope fractionation equations (Appendix K) using either biogenic calcite (such as shells/tests), abiogenic calcite (such as speleothems in caves) or synthesized calcite in a benchtop laboratory setting. There is disagreement regarding which calcite precipitation scenario best represents thermodynamic equilibrium calcite-water precipitation and which is most applicable to natural samples (Coplen, 2007; Tremaine et al., 2011; Brand et al., 2019; Daëron et al., 2019). Regarding the use of carbonates as a paleothermometer, Urey (1947) cautioned that it is unknown whether animals deposit carbonate in oxygen isotope equilibrium with the water in which they are living and whether carbonate exchanges oxygen with water after burial (Lowenstam, 1961; Brand and Veizer, 1981). Over 70 years after that publication, geochemists are still trying to understand the relationship between the oxygen isotope compositions of carbonate secreting organisms and the temperature at which it formed.

Analyzing an additional isotope of oxygen (oxygen-17) allows us to better evaluate equilibrium precipitation. Triple oxygen isotope measurements are combined $\delta^{17}\text{O}$ - $\delta^{18}\text{O}$ values, where $\delta^x\text{O} = R_p^x / R_{\text{std}}^x - 1$ and x is either mass number 17 or 18 and R_p^x is the isotope ratio $R(^i\text{E} / ^j\text{E})_p$ where i is the mass number of the heavy isotope (17 or 18), j is the mass number of the light isotope (16), and E is the symbol of the element, O, in substance P (Kim et al., 2015). Here, all equations will report in per mil notation, where $\delta^x\text{O} = [(R_p^x / R_{\text{std}}^x) - 1] \times 1000$ (cf. McKinney et al., 1950). Triple isotope measurements commonly are used in mass-independent oxygen isotope studies such as sulfur oxidation effects (Bao et al., 2000) or analysis of meteorites (Thiemens and Heidenreich, 1983; Clayton, 1993). Triple oxygen isotope values are expressed in terms of $\Delta^{17}\text{O}$, or the deviation of $\delta^{17}\text{O}$ from a reference slope defined as:

$$\Delta^{17}\text{O} = \delta^{17}\text{O} - \lambda \times \delta^{18}\text{O} + \gamma \quad 3.1),$$

where λ is the reference slope, γ is the y-intercept, and the common δ -notation in per mil is linearized and expressed as δ' -notation ($\delta^x\text{O} = 1000 \ln[\delta^x\text{O}/1000 + 1]$). Linearization of the δ -notation is used because of a slight curve in the reference slope of terrestrial materials when comparing δ values across a large range of values (Hulston and Thode, 1965; Miller, 2002). This study uses $\lambda=0.528$ and $\gamma=0$ (Meijer and Li, 1998; Luz and Barkan, 2010).

Equilibrium fractionation between any two phases is given as

$$\alpha_{\text{A-B}}^x = R_{\text{A}}^x / R_{\text{B}}^x \quad 3.2),$$

where R_{A}^x and R_{B}^x are the isotope ratios of phases A and B. In δ' -notation, this is

$$1000 \ln \alpha_{\text{A-B}}^x = \delta^x\text{O}_{\text{A}} - \delta^x\text{O}_{\text{B}} \quad 3.3).$$

For equilibrium triple oxygen isotope fractionation, Eq. 3.2 can be used to describe the $\alpha^{17}\text{O}_{\text{A-B}}$ as:

$$\alpha^{17}\text{O}_{\text{A-B}} = (\alpha^{18}\text{O}_{\text{A-B}})^{\theta} \quad 3.4)$$

and

$$\theta = \frac{\delta^{17}\text{O}_{\text{A}} - \delta^{17}\text{O}_{\text{B}}}{\delta^{18}\text{O}_{\text{A}} - \delta^{18}\text{O}_{\text{B}}} \quad 3.5).$$

From theoretical models, the θ values for equilibrium processes are temperature dependent and range from about 0.52 to the theoretical high limit of 0.5305 (Cao and Liu, 2011; Hayles et al., 2018).

High precision triple oxygen isotope measurements ($\Delta^{17}\text{O}$ values with precision better than 0.01 ‰ 1σ) have been applied to a variety of terrestrial materials to examine equilibrium, mass-dependent fractionation (Pack and Herwartz, 2014; Passey et al., 2014; Barkan et al., 2015; Sharp et al., 2016; Wostbrock et al., 2018; Barkan et al., 2019; Bergel et al., 2020; Voarintsoa et al., 2020) and address a variety of geologic questions (Herwartz et al., 2015; Herwartz et al., 2017; Bindeman et al., 2018; Gázquez et al., 2018; Sengupta and Pack, 2018; Zakharov and Bindeman, 2019; Sutherland et al., 2020). The number of studies using triple oxygen isotope compositions of carbonates has increased in recent years due to the development of methods capable of analyzing the $\delta^{17}\text{O}$ value of CO_2 liberated by phosphoric acid digestion (Barkan and Luz, 2012; Mahata et al., 2013; Passey et al., 2014). Determination of the $\delta^{17}\text{O}$ and $\delta^{18}\text{O}$ values of carbonate standards and/or the CO_2 released from phosphoric acid digestion of carbonate standards have been presented in multiple studies (Passey et al., 2014; Barkan et al., 2015; Barkan et al., 2019; Passey and Ji, 2019; Fosu et al., 2020; Wostbrock et al., 2020b).

Evaporation, relative humidity, and paleo-hydrology as a whole has been studied using the triple oxygen isotope compositions of lake (Passey and Ji, 2019) and cave (Sha et al., 2020) carbonates. Empirical equilibrium fractionation for the triple oxygen isotope composition of carbonate-water was presented using freshwater aragonitic mollusks (Bergel et al., 2020) and synthetic mixtures of aragonite and calcite (Voarintsoa et al., 2020). Kinetic effects governing the $\Delta^{17}\text{O}$ values of carbonates were evaluated from measurements of natural calcite and aragonite samples (Fosu et al., 2020). The abovementioned studies analyzed the CO_2 released from phosphoric acid digestion of the carbonate and not the total oxygen isotope composition of the carbonate. A triple oxygen isotope equilibrium fractionation line derived from the total oxygen component of the carbonate and coexisting water removes the uncertainties associated with calcite- CO_2 and water- CO_2 fractionation factors and allows for a direct comparison to theoretically modelled relationships between temperature and triple oxygen isotope compositions.

Here, triple oxygen isotope calcite-water fractionation equations are presented for synthetic calcite, abiogenic calcite from Devils Hole, biogenic marine calcite, and both abiogenic and biogenic (hereafter referred to as a/biogenic) marine aragonite (Table 3.1). The addition of bovine carbonic anhydrase to the solution when precipitating carbonate in a laboratory setting has been shown to drive the reaction towards isotopic equilibrium (Uchikawa and Zeebe, 2012; Watkins et al., 2013). This chapter explores how the addition of bovine carbonic anhydrase affects the triple oxygen isotope composition of synthesized carbonates at temperatures between 5 and 40 °C. It also explores the disagreement between the $\delta^{18}\text{O}$ carbonate-water fractionation of naturally occurring biogenic and abiogenic carbonates by analyzing a suite of marine biogenic carbonates

and Devils Hole carbonate and water (Coplen, 2007). After deriving a triple oxygen isotope equilibrium fractionation line for the carbonate-water system, ancient carbonates from the Phanerozoic are examined to explore how the $\delta^{18}\text{O}$ value of seawater may have changed over the last 500 million years.

3.2 Methods

3.2.1 Inorganic precipitation

Two sets of inorganic calcite, one with the addition of bovine carbonic anhydrase (Uchikawa and Zeebe, 2012; Watkins et al., 2013) and one without, were synthesized at the Center of Stable Isotopes (CSI) at the University of New Mexico. Calcite was precipitated in deionized water at 5, 20, and 40 °C following the method of Kim and O'Neil (1997). Bovine carbonic anhydrase is assumed to be active over this temperature range based on a study of a similar range in temperature and the effect on catalytic reactions using human carbonic anhydrase (Sanyal and Maren, 1981). Two 1000 mL Erlenmeyer flasks were each filled with 1000 mL of distilled water and connected in series via rubber stoppers and tubing with the second (downstream) flask equipped with a fine frit at the bottom of the flask to induce small bubbles during sparging. Purified carbon dioxide was filtered into the flask located on a stirrer plate for about 5-10 minutes until pH was 4.0 or lower. After the desired pH was reached, 2.1 g of sodium bicarbonate and 2.8 g of calcium chloride was added sequentially, waiting for the first to dissolve before adding the second, resulting in a 25 mM solution. For the catalyzed set of samples, 8.5-10 mg of bovine carbonic anhydrase was added after dissolution of the NaHCO_3 and CaCl_2 . The flask with solution was then placed in a thermostatic water bath for 1.5 hr to allow the fluid to thermally equilibrate to a specific temperature (either 5, 20, or 40 °C). After temperature equilibration, the solution was slowly sparged with nitrogen gas by

bubbling through the first flask and then the second. The purpose of the first flask was to saturate the N₂ gas with water vapor having an isotopic composition equivalent to that of the second flask, thereby minimizing any changes to the oxygen isotope value of the water during synthesis. Nitrogen gas was slowly introduced to the flask with the NaHCO₃ and CaCl₂ solution with 1-3 bubbles every 30 seconds. This created a slow precipitation with the first visible crystals occurring about 3 days after the experiment began and with the entire experiment occurring over 5-7 days, depending on temperature. The pH of the water at the end of the experiments never exceeded 8.4. Due to the slow sparging, low pH, and 25 mM solution, it is assumed that all dissolved ions had sufficient time (72 h) to isotopically equilibrate before precipitation. Beck et al. (2005) found 24 hours to be sufficient for isotopic equilibration of dissolved ions at 15 °C in a 25 mM solution. No obvious evaporation occurred during the experiments, documented by no liquid level change in the flasks. After precipitation, about 30 mL of water was collected from the flask with the NaHCO₃ and CaCl₂ solution and stored in a refrigerator for stable isotope analysis. The remaining water was vacuum filtered to collect the precipitated calcite. Rubber policeman were used to scrape residual precipitates from glass walls and tubing. Filters with the precipitates were dried in a 60 °C oven for 12 hours, and subsequently weighed and stored until analysis.

Examination of each sample to determine crystal morphology was performed at 15.0 kV with a TESCAN Vega3 SEM. Images were acquired using the integrated backscatter electron detector at 1000x and 500x resolution, depending on the crystal size. The integrated TESCAN Essence EDSTM was used to determine any contamination.

The 5 °C sample precipitated without carbonic anhydrase was examined under TEM due to a unique doughnut-shaped feature seen on the SEM image (Figures 3.1A and 3.2A). The samples were prepared for TEM analysis by dropping a suspension of carbonate crystallites in acetone onto a copper TEM grid coated with a lacey carbon film and allowing the acetone to evaporate. Due to residual carbon contamination after X-ray analysis, another round of imaging occurred by sprinkling a small amount of carbonate directly onto the copper TEM grid. Transmission electron microscope studies were performed at 200 kV using a JEOL 2010F FEG FASTEM TEM/STEM equipped with a GATAN GIF 2000 energy filtered spectrometer in the Department of Earth and Planetary Sciences (EPS) at the University of New Mexico (UNM). A variety of TEM techniques were utilized, including bright-field imaging, electron diffraction, and high-angle annular dark field scanning transmission electron microscopy.

3.2.2 Natural Carbonates

Triple oxygen isotope analyses were made on eight well studied calcite and aragonite samples (Table 3.1; Appendix E) to create an empirical triple oxygen isotope calcite-water fractionation curve applicable to natural samples. Holocene-aged, abiogenic calcite (sample DHC2-8 from Coplen, 2007) and modern water from Devils Hole, NV, were analyzed to compare differences in the calcite-water oxygen isotope fractionation between biogenic and abiogenic samples. Four modern (calcite) brachiopods and a variety of aragonite samples from Florida and the Bahamas were also analyzed (see Table 3.1 for detailed descriptions). The temperature at which the samples formed and the $\delta^{18}\text{O}$ value of the water were determined in previous studies (Leder et al., 1996; Rosenheim et al., 2005; Swart et al., 2005; Brand et al., 2013; Kercher, 2014; Brand et al., 2019).

Measured temperatures ranged from 0 – 30 °C while $\delta^{18}\text{O}$ values of the water ranged from -1.2 to +1.5 ‰ (VSMOW). Since the actual water was no longer available, $\delta^{18}\text{O}$ values (which were all close to 0 vs. VSMOW) were obtained through either publications or communications (see Table 3.1). A $\Delta^{17}\text{O}$ value of -0.005 ‰ (Luz and Barkan, 2010) was inferred for all marine samples.

Each carbonate sample was cleaned following the procedure of Zaky et al. (2015) for cleaning brachiopods for Rare Earth Element (REEs) analysis. Consolidated samples were manually scraped under a microscope to remove any organic material coating the sample. The sample was then reacted with 10 % hydrochloric acid (HCl) for 15-30 seconds for aggressive organic matter removal, rinsed with water, and then manually scrapped again until the sample no longer had any visual organic material adhered to the outside of the sample. The sample was then crushed and reacted with 30 % hydrogen peroxide until reaction ceased. The sample was rinsed three times with deionized water and then reacted with ~5 % sodium hypochlorite. Samples were again rinsed three times with deionized water, dried in an oven at 60 °C, and stored for future analysis. Some samples arrived for analysis already powdered so the manual organic matter removal and HCl cleaning steps were either done by source material providers or not performed (Table 3.1).

3.2.3 Isotopic analyses

Between 0.3 and 0.4 mg of carbonate were reacted with >100 % phosphoric acid (determined by density being above 1.8 mg/mL) in vials at 50 °C and analyzed for their $\delta^{18}\text{O}$ values. A Thermo-Finnegan Gas Bench II autosampler was used to transfer the released CO_2 into a Thermo-Finnegan Delta Plus XL mass spectrometer in continuous

Table 3.1 – Sample descriptions

Sample	Description
Calcite.5	Synthesized calcite at 5 °C without carbonic anhydrase. Associated water is Water.5
Calcite.20	Synthesized calcite at 20 °C without carbonic anhydrase. Associated water is Water.20
Calcite.40	Synthesized calcite at 40 °C without carbonic anhydrase. Associated water is Water.40
Calcite.CA.5	Synthesized calcite at 5 °C with carbonic anhydrase. Associated water is Water.CA.5
Calcite.CA.20	Synthesized calcite at 20 °C with carbonic anhydrase. Associated water is Water.CA.20
Calcite.CA.40	Synthesized calcite at 40 °C with carbonic anhydrase. Associated water is Water.CA.40
Calcite.DH	Holocene aged, subaqueous carbonate slab (DHC2-8) from Devils Hole, NV. Associated water is was sampled in 2000 and presented in Coplen (2007), labelled in this study as Water.DH.
Palau	<i>Thecidellina congregata</i> brachiopod. ~5 mm long valve composed of calcite from the Palau Islands. Water data from Brand et al. (2013, 2019). $\delta^{18}\text{O}_{\text{water}} = -0.1\text{‰}$, Temp: 29.5 °C
L.Ery	<i>Laqueus erythraeus</i> brachiopod. Low-Mg calcite composition from Monterey Bay, CA from 160 m depth. Water data from Kercher (2014) M.S thesis. $\delta^{18}\text{O}_{\text{water}} = -0.08\text{‰}$, Temp: 9 (± 1) °C
Signy	<i>Liothyrella uva</i> brachiopod. Valve comprised of low-Mg calcite from Signy Island, Antarctica. Water data from Brand et al. (2013, 2019). $\delta^{18}\text{O}_{\text{water}} = -1.2\text{‰}$, Temp: -2 °C
Rothera	<i>Liothyrella uva</i> brachiopod. Valve comprised of low-Mg calcite found near Rothera Research Station, Antarctica. Water data from Brand et al. (2013, 2019). $\delta^{18}\text{O}_{\text{water}} = -0.87\text{‰}$, Temp: -0.4 °C
Reef	Sediment off Alina's Reef in Biscayne National Park comprised of mostly aragonite shell fragments and small snail and bivalve shells. Sample was picked by hand under a microscope to select fragments with low organic matter (by color, assuming a whiter color has less organic matter than a browner color). Due to the size of the sediment, manual scraping and HCl cleaning were avoided. Water data from Leder et al. (1996). $\delta^{18}\text{O}_{\text{water}} = 1.1\text{‰}$, Temp: 26 °C
Ooid	Sediment comprised of 1-2 mm ooids made of aragonite from the Great Bahama Bank. Sample was picked by hand under a microscope to select ooids with low organic matter (by color, assuming a whiter color has less organic matter than a browner color). Due to the size of the sediment, manual scraping and HCl cleaning were avoided. Water data from Swart et al. (2009). $\delta^{18}\text{O}_{\text{water}} = 1.5\text{‰}$, Temp: 25 °C
GBB	Fine, abiogenic and biogenic mix sediment from the Great Bahama Bank. Sediment is fine in texture, manual scraping and HCl cleaning were avoided. Water data from Swart et al. (2009). $\delta^{18}\text{O}_{\text{water}} = 1.5\text{‰}$, Temp: 25 °C
Sclero	<i>Ceratoporella nicholsoni</i> sclerosponge. Sclerosponge comprised of aragonite from Exuma Sounds, FL, found at 136 m depth. Water data from Rosenheim et al. (2005). $\delta^{18}\text{O}_{\text{water}} = 1.25\text{‰}$, Temp: 25 °C.
CM3a	Brachiopod fragment comprised of low-Mg calcite from the Mid Ordovician found in Carlington, Ontario. Sample supplied by Uwe Brand and presented in Brand (2004).
IR70c	Brachiopod fragment comprised of low-Mg calcite from the Silurian (Wenlock) found in western New York State. Sample supplied by Uwe Brand and presented in Brand (2004).
NB428	<i>Athyris spiriferoides</i> brachiopod comprised of calcite from the Mid Devonian found in Eighteen Mile Cr, western New York State. Sample supplied by Uwe Brand and presented in Bates and Brand (1991).
AC332	Unidentified spiriferid brachiopod fragment comprised of low-Mg calcite from the Late Pennsylvanian found in Arrow Canyon, NV. Sample supplied by Uwe Brand and presented in Brand et al. (2012).
C539	<i>Chatwinothyris</i> sp. brachiopod comprised of low-Mg calcite from the Mid Maastrichtian found near Maastricht, Netherlands. Sample supplied by Uwe Brand from unpublished collection.
PDB	Belemnite of an unknown species comprised of calcite from the Mid Cretaceous found in the Peedee Formation, specific locale unknown.

flow mode. Measured values were corrected to Carrara marble, an inhouse standard at the University of New Mexico's Center for Stable Isotopes. The inhouse standard has been calibrated to IAEA reference samples NBS 19 (28.65 ‰) and NBS 18 (7.2 ‰) (Brand et al., 2014). Aragonite samples are corrected using the oxygen isotope fractionation factor

1.00967 (Kim et al., 2007b). Average standard deviation is about 0.1 ‰ and values are reported relative to VSMOW by converting the $\delta^{18}\text{O}$ values from VPDB to VSMOW using the equation $\delta^{18}\text{O}_{\text{VSMOW}} = 1.03092 \times \delta^{18}\text{O}_{\text{PDB}} + 30.92$ (Kim et al., 2015).

The conventional fluorination method of Sharma and Clayton (1965), modified by Wostbrock et al. (2020b) Wostbrock et al. (2020), was used for determining the triple oxygen isotope values of carbonate samples. Five to six milligrams of powdered carbonate were loaded into nickel reaction vessels and degassed at ~ 100 °C for 12 hours to remove any adsorbed H_2O . After degassing, a 30-fold stoichiometric excess of BrF_5 was frozen into each vessel and allowed to react at 750 °C for 4 days.

The $\delta^{18}\text{O}$ values were determined using phosphoric acid digestion (Wostbrock et al., 2020). Fluorination was only used to determine the $\Delta^{17}\text{O}$ values. The $\delta^{17}\text{O}$ value was calculated by rearranging Eq. 3.1 ($\delta^{17}\text{O} = \Delta^{17}\text{O} + 0.528 \times \delta^{18}\text{O}$). As described in Wostbrock et al. (2020), carbonate fluorination results in $\delta^{18}\text{O}$ values that are generally about 1 to 1.5 ‰ lower than values obtained via phosphoric acid digestion. However, any fractionation occurring during the reaction follows a slope (λ) approximating 0.528 (± 0.003) (see Section 3.3 and Appendix I for a thorough discussion). Therefore, the measured $\Delta^{17}\text{O}$ is constant (relative to $\lambda = 0.528$) within analytical error and the $\delta^{17}\text{O}$ value can be extrapolated relative to the $\delta^{18}\text{O}$ value determined using phosphoric acid digestion. It should be noted that this type of correction where the $\delta^{18}\text{O}$ value is obtained from one procedure and the $\Delta^{17}\text{O}$ value is obtained from a different procedure is used in other triple isotope systems. The triple oxygen isotope values of sulfates (Bao and Thiemens, 2000; Cowie and Johnston, 2016) and CO_2 (Brenninkmeijer and Röckmann, 1998; Barkan et al., 2019) are generally determined in this fashion.

The triple oxygen isotope composition of water was measured using the water fluorination technique of O'Neil and Epstein (1966) modified by Wostbrock et al. (2020b). A 2 μL Hamilton© series 7000 Gastright® syringe filled with 1.8 μL of water is injected through a Restek® low bleed septum. Water is frozen into a ¼" Ni-200 U-trap and 500-550 μmol of BrF_5 is added to the U-trap. The U-trap is isolated from the rest of the fluorination line and heated for five minutes using a heat gun. This heating procedure quantitatively converts H_2O to O_2 and HF .

The O_2 released from fluorination of both calcite and water is purified following identical procedures using the same purification line. The O_2 is passed through two liquid nitrogen (LN_2) traps, then through a 100 °C NaCl trap to eliminate any trace F_2 gas. Any F_2 gas that is present reacts with NaCl to produce NaF and Cl_2 gas, which is trapped in a third LN_2 trap. The O_2 gas is quantitatively adsorbed on a 5 Å mol sieve cooled with LN_2 . The O_2 gas is then transferred through a 5x mol sieve gas chromatographic column in a 6 mL/min ultrahigh purity helium flow to separate any trace NF_3 or N_2 contamination. The O_2 gas is collected on a second mol sieve at the inlet of a Thermo-Finnegan MAT 253+ mass spectrometer at the CSI. The O_2 gas is measured in dual-inlet mode with a 26 sec integration time with an additional 20 sec delay time per changeover, and 30 iterations per analysis. The O_2 from both calcite and water is measured against the same inhouse O_2 reference gas calibrated to the VSMOW-SLAP scale (Wostbrock et al., 2020b). The difference between the $\delta^{18}\text{O}$ values of VSMOW and SLAP measured in our laboratory is 55.5 ‰, so no stretching factor needs to be applied to our analyses. Yeung et al. (2018) found that some mass spectrometers have a baseline pressure effect that can influence $\Delta^{17}\text{O}$ values, especially when the $\delta^{18}\text{O}$ value of the sample gas is very different (>10 ‰

difference) from the $\delta^{18}\text{O}$ value of the reference gas. Two O_2 standard gases were measured that differ in $\delta^{18}\text{O}$ and $\Delta^{17}\text{O}$ values by 25 ‰ and 0.3 ‰, respectively, at different pressures (3V, 5V, and 10V). The resulting standard deviation over the full pressure range for $\delta^{18}\text{O}$ and $\Delta^{17}\text{O}$ values are 0.02 ‰ and 0.002 ‰, respectively. This is well within the analytical uncertainty reported in this study and no pressure correction was applied to our study (see Wostbrock et al., 2020 – Supplementary materials for further discussion). Precision for water analyses are 0.089, 0.165, and 0.007 ‰ for $\delta^{17}\text{O}$, $\delta^{18}\text{O}$, and $\Delta^{17}\text{O}$, respectively (error is reported standard deviation of the mean and given to three decimal places to reduce rounding errors in the $\Delta^{17}\text{O}$ calculation). Precision for carbonate analyses by fluorination are 0.171, 0.329, and 0.005 ‰ for $\delta^{17}\text{O}$, $\delta^{18}\text{O}$, and $\Delta^{17}\text{O}$, respectively, based on the standard deviation of repeated analyses of samples. To account for variation in fractionation during the fluorination reaction, a more conservative error of 0.010 ‰ is reported for $\Delta^{17}\text{O}$ values of the carbonates (see Section 3.3 and Appendix I for detailed information).

3.3 Results

The primary goal of this study is to determine the oxygen isotope calcite-water fractionation (hereafter referred to as the $1000\ln\alpha_{\text{cc-wt}}$ value) as a function of temperature for both $\delta^{18}\text{O}$ and $\delta^{17}\text{O}$ measurements. Comparing calcite synthesized with and without a carbonic anhydrase (CA) catalyst, marine a/biogenic carbonates, and slowly formed abiogenic calcite (Devils Hole) can determine if formation processes affect the oxygen isotope fractionation and compare our observations and results to published calcite-water oxygen isotope fractionation values. Using the triple oxygen isotope fractionation curve

determined herein, ancient carbonate samples are evaluated for diagenesis in order to reconstruct environments where the carbonate formed.

All results are listed in Tables 3.1-3.4, Figures 3.1-3.6, and Appendices E-K. Raw triple oxygen isotope data obtained from fluorination is presented in Appendices F, G, and H. As mentioned earlier, fluorination generally yields lower $\delta^{18}\text{O}$ values than those obtained from phosphoric acid digestion. The average difference between the measured $\delta^{18}\text{O}$ value and the “accepted” $\delta^{18}\text{O}$ value (obtained through conventional phosphoric acid digestion) is -1.14‰ with a standard deviation of $\pm 0.30\text{‰}$. Although the measured $\delta^{18}\text{O}$ values are lower than the accepted $\delta^{18}\text{O}$ values, the standard deviation is also low, meaning there is not sufficient variability in the data to precisely calculate the λ associated with potential fractionation during fluorination. However, λ was estimated using one sample from this study (5 °C calcite precipitates without a catalyst) that has a larger spread in $\delta^{18}\text{O}$ values and two carbonate standards (NBS 19 and IAEA 603) presented in Wostbrock et al. (2020). Fractionation occurs during fluorination following a slope ranging from 0.5249 to 0.5305, with an average slope of 0.5275 (± 0.0028). This corresponds to an added error in the accuracy of our measurement of 0.0056‰ . Combining the analytical error ($\pm 0.005\text{‰}$) with the variation in the fractionation during fluorination (using Root Sum Squares (RSS)), the total reported uncertainty for Ni-vessel fluorination of carbonates is $\pm 0.008\text{‰}$. Since only three slope of the reaction was calculated, more variation may potentially exist in the reactions vessels and, therefore, a total error of $\pm 0.010\text{‰}$ is reported for this study.

3.4 Discussion

3.4.1 Calcite-water oxygen isotope fractionation using $\delta^{18}\text{O}$ values of modern carbonates

The θ - T relationship for carbonate-water requires a knowledge of the $\delta^{18}\text{O}$ and $\delta^{17}\text{O}$ fractionation over a range of temperatures. For $\delta^{18}\text{O}$, our $1000\ln\alpha_{\text{cc-wt}}$ equation is calculated using the difference in the $\delta^{18}\text{O}$ values of carbonate and water for their respective temperatures of formation. Data from both the laboratory synthesis experiments and the biogenic and abiogenic empirical results from natural samples were included. For laboratory experiments, crystallization temperatures and the $\delta^{18}\text{O}$ values of the water and the calcite were measured (Table 3.2). For the Devils Hole sample, modern temperatures and water were measured, but the calcite that was analyzed formed in the Holocene (>4.5 ka; Tables 3.1 & 3.2; Coplen, 2007). It is assumed that the ambient conditions and isotopic composition of the water during calcite formation were the same as modern. The temperature and $\delta^{18}\text{O}$ values of the marine samples were determined previously (Tables 3.1 & 3.3). The $\Delta^{17}\text{O}$ value of marine water was assumed to be -0.005‰ (Luz and Barkan, 2010). All data were considered in our temperature-fractionation equation. Although previous studies suggest that the oxygen isotope fractionation between aragonite and water is slightly larger than for calcite-water (Grossman and Ku, 1986; Kim et al., 2007a; Guo and Zhou, 2019), our aragonite-water data plot on our best fit line and are therefore included. Similar calcite-water and aragonite-water fractionations were seen in Voarintsoa et al. (2020).

Table 3.2 - The oxygen isotope compositions of the synthesized carbonates and Devils Hole with corresponding water. All values are reported in ‰ and relative to VSMOW unless otherwise noted.

Sample		$\delta^{17}\text{O}$	$\delta^{17}\text{O}^a$	$\delta^{18}\text{O}^a$	$\delta^{18}\text{O}$	$\Delta^{17}\text{O}$ ($\lambda=0.528$)	1000ln α^{17b}	1000ln α^{18b}	$\Delta\Delta^{17}\text{O}$ cc-wt ^b	θ
No Carbonic Anhydrase - Temp: 5 °C										
$\delta^{18}\text{O}_{\text{calcite}} = -9.5 \text{ ‰ (VPDB)}$										
Water.5.1		-7.132	-7.158	-13.492	-13.584	0.014				
Water.5.2		-7.223	-7.249	-13.675	-13.769	0.021				
		Avg. -7.178	-7.204	-13.583	-13.677	0.018				
		±1σ 0.064		0.129		0.005				
Calcite.5.1		11.035	10.975	21.126	20.906	-0.064	18.178	34.582	-0.081	0.5256
Calcite.5.2		11.033	10.973	21.126	20.906	-0.065	18.176	34.582	-0.083	0.5256
Calcite.5.3		11.042	10.982	21.126	20.906	-0.057	18.185	34.582	-0.074	0.5258
Calcite.5.4		11.042	10.981	21.126	20.906	-0.057	18.185	34.582	-0.075	0.5258
Calcite.5.5		11.033	10.973	21.126	20.906	-0.065	18.176	34.582	-0.083	0.5256
Calcite.5.6		11.029	10.969	21.126	20.906	-0.069	18.172	34.582	-0.087	0.5255
		Avg. 11.036	10.975	21.126	20.906	-0.063	18.179	34.582	-0.081	0.5257
		±1σ				0.005^a				0.0001
No Carbonic Anhydrase - Temp: 20 °C										
$\delta^{18}\text{O}_{\text{calcite}} = -13.0 \text{ ‰ (VPDB)}$										
Water.20.1	20	-7.195	-7.221	-13.615	-13.709	0.017				
Water.20.2		-6.844	-6.868	-12.970	-13.055	0.025				
		Avg. -7.020	-7.045	-13.293	-13.382	0.021				
		±1σ 0.248		0.456		0.006				
Calcite.20.1	20	9.158	9.116	17.518	17.366	-0.053	16.161	30.748	-0.074	0.5256
Calcite.20.2		9.160	9.118	17.518	17.366	-0.051	16.163	30.748	-0.072	0.5256
		Avg. 9.159	9.117	17.518	17.366	-0.052	16.162	30.748	-0.066	0.5256
		±1σ				0.001				4.83x10⁻⁵
No Carbonic Anhydrase - Temp: 40 °C										
$\delta^{18}\text{O}_{\text{calcite}} = -17.0 \text{ ‰ (VPDB)}$										
Water.40.1	40	-7.138	-7.164	-13.511	-13.603	0.018				
Water.40.2		-6.966	-6.990	-13.174	-13.262	0.012				
Water.40.3		-6.918	-6.942	-13.117	-13.204	0.030				
		Avg. -7.007	-7.032	-13.268	-13.356	0.020				
		±1σ 0.116		0.212		0.009				
Calcite.40.1	40	7.124	7.099	13.601	13.509	-0.034	14.131	26.866	-0.054	0.5260
Calcite.40.2		7.117	7.092	13.601	13.509	-0.041	14.124	26.866	-0.061	0.5257
Calcite.40.3		7.103	7.078	13.601	13.509	-0.055	14.120	26.866	-0.075	0.5252
Calcite.40.4		7.123	7.097	13.601	13.509	-0.035	14.129	26.866	-0.056	0.5259
Calcite.40.5		7.131	7.106	13.601	13.509	-0.027	14.138	26.866	-0.047	0.5262
Calcite.40.6		7.125	7.100	13.601	13.509	-0.033	14.132	26.866	-0.053	0.5260
Calcite.40.7		7.108	7.083	13.601	13.509	-0.050	14.115	26.866	-0.070	0.5254
Calcite.40.8		7.123	7.097	13.601	13.509	-0.035	14.129	26.866	-0.056	0.5259
Calcite.40.9		7.119	7.094	13.601	13.509	-0.039	14.126	26.866	-0.059	0.5258
		Avg. 7.119	7.094	13.601	13.509	-0.039	14.126	26.866	-0.059	0.5258
		±1σ				0.009				0.0003
With Carbonic Anhydrase - Temp: 5 °C										
$\delta^{18}\text{O}_{\text{calcite}} = -10.0 \text{ ‰ (VPDB)}$										
Water.CA.5.1	5	-6.772	-6.795	-12.845	-12.928	0.031				
Water.CA.5.2		-6.986	-7.011	-13.205	-13.293	0.008				
Water.CA.5.3		-6.927	-6.951	-13.124	-13.211	0.024				
Water.CA.5.4		-7.106	-7.131	-13.428	-13.519	0.007				
		Avg. -6.948	-6.972	-13.150	-13.238	0.018				
		±1σ 0.139		0.241		0.012				

Table 3.2 (Cont.)

Sample	$\delta^{17}\text{O}$	$\delta^{17}\text{O}^a$	$\delta^{18}\text{O}^a$	$\delta^{18}\text{O}$	$\Delta^{17}\text{O}$ ($\lambda=0.528$)	$1000\ln\alpha^{17b}$	$1000\ln\alpha^{18b}$	$\Delta\Delta^{17}\text{O}$ <i>cc-wr</i> ^b	θ	Sample
Calcite.CA.5.1	5	10.783	10.725	20.611	20.401	-0.047	17.697	33.639	-0.065	0.5261
Calcite.CA.5.2		10.770	10.713	20.611	20.401	-0.059	17.685	33.639	-0.077	0.5257
Calcite.CA.5.3		10.774	10.716	20.611	20.401	-0.056	17.688	33.639	-0.073	0.5258
Calcite.CA.5.4		10.777	10.720	20.611	20.401	-0.052	17.692	33.639	-0.070	0.5259
	Avg.	10.776	10.719	20.611	20.401	-0.053	17.691	33.639	-0.071	0.5259
	$\pm 1\sigma$					0.005				0.0002
With Carbonic Anhydrase - Temp: 20 °C										
$\delta^{18}\text{O}_{\text{calcite}} = -13.2 \text{‰ (VPDB)}$										
Water.CA.20.1	20	-7.131	-7.157	-13.482	-13.574	0.010				
Water.CA.20.2		-6.924	-6.948	-13.079	-13.165	0.003				
Water.CA.20.3		-7.014	-7.039	-13.272	-13.361	0.016				
	Avg.	-7.023	-7.048	-13.278	-13.367	0.010				
	$\pm 1\sigma$	0.104		0.202		0.007				
Calcite.CA.20.1	20	9.054	9.013	17.312	17.164	-0.049	16.061	30.531	-0.059	0.5261
Calcite.CA.20.2		9.053	9.012	17.312	17.164	-0.050	16.060	30.531	-0.060	0.5260
Calcite.CA.20.3		9.053	9.012	17.312	17.164	-0.051	16.060	30.531	-0.060	0.5260
Calcite.CA.20.4		9.052	9.012	17.312	17.164	-0.051	16.060	30.531	-0.060	0.5260
Calcite.CA.20.5		9.046	9.006	17.312	17.164	-0.057	16.054	30.531	-0.066	0.5258
	Avg.	9.052	9.011	17.312	17.164	-0.051	16.059	30.531	-0.061	0.5260
	$\pm 1\sigma$					0.003				0.0001
With Carbonic Anhydrase - Temp: 40 °C										
$\delta^{18}\text{O}_{\text{calcite}} = -16.8 \text{‰ (VPDB)}$										
Water.CA.40.1	40	-6.949	-6.973	-13.137	-13.224	0.009				
Water.CA.40.2		-6.865	-6.889	-13.001	-13.086	0.020				
	Avg.	-6.907	-6.931	-13.069	-13.155	0.015				
	$\pm 1\sigma$	0.059		0.096		0.008				
Calcite.CA.40.1	40	7.004	6.980	13.394	13.305	-0.045	13.911	26.460	-0.060	0.5257
Calcite.CA.40.2		7.006	6.982	13.394	13.305	-0.043	13.913	26.460	-0.058	0.5258
Calcite.CA.40.3		7.004	6.979	13.394	13.305	-0.046	13.910	26.460	-0.061	0.5257
Calcite.CA.40.4		7.013	6.989	13.394	13.305	-0.036	13.920	26.460	-0.051	0.5261
	Avg.	7.007	6.982	13.394	13.305	-0.043	13.913	26.460	-0.058	0.5258
	$\pm 1\sigma$					0.004				0.0002
Devils Hole – Temp: 33.7 °C										
$\delta^{18}\text{O}_{\text{calcite}} = -15.8 \text{‰ (VPDB)}$										
Water.DH.1		-7.028	-7.053	-13.312	-13.401	0.023				
Water.DH.2		-7.106	-7.131	-13.465	-13.556	0.027				
	Avg.	-7.067	-7.092	-13.388	-13.479	0.025				
	$\pm 1\sigma$	0.054		0.108		0.003				
Calcite.DH.1		7.646	7.617	14.621	14.515	-0.047	14.709	27.994	-0.072	0.5254
Calcite.DH.2		7.662	7.632	14.621	14.515	-0.032	14.724	27.994	-0.056	0.5260
Calcite.DH.3		7.645	7.616	14.621	14.515	-0.048	14.708	27.994	-0.073	0.5254
Calcite.DH.4		7.648	7.619	14.621	14.515	-0.045	14.711	27.994	-0.069	0.5255
Calcite.DH.5		7.648	7.619	14.621	14.515	-0.045	14.711	27.994	-0.070	0.5255
	Avg.	7.650	7.621	14.621	14.515	-0.043	14.713	27.994	-0.068	0.5256
	$\pm 1\sigma$					0.007				0.0002

^a-All calcite data are corrected to the $\delta^{18}\text{O}$ value from conventional methods. The $\delta^{17}\text{O}$ value is calculated using the equation $\delta^{17}\text{O} = \Delta^{17}\text{O} + 0.528\delta^{18}\text{O}$ (Eq. 3.1). Therefore, the error is driven by the $\Delta^{17}\text{O}$ precision. See Appendices F-I.

^b-The average oxygen isotopic value of the corresponding water is used in the calculations.

Table 3.3 - Oxygen isotope composition of modern carbonate and aragonite. All values are reported in ‰ and relative to VSMOW unless otherwise noted. See Table 3.1 and Appendix E for in depth sample descriptions and pictures. The $\Delta^{17}\text{O}$ values of all water samples is assumed to be -0.005 ‰. Temperature and $\delta^{18}\text{O}_{\text{water}}$ is compiled from the literature (Bates and Brand, 1991; Leder et al., 1996; Brand, 2004; Rosenheim et al., 2005; Swart et al., 2005; Brand et al., 2012; Kercher, 2014).

Sample	$\delta^{17}\text{O}$	$\delta^{17}\text{O}^a$	$\delta^{18}\text{O}^a$	$\delta^{18}\text{O}$	$\Delta^{17}\text{O}$ ($\lambda=0.528$)	1000ln α^{17}	1000ln α^{18}	$\Delta\Delta^{17}\text{O}$ cc-wt	θ
<i>Thecidellina congregata brachiopod - Calcite</i>									
Locale: Palau Islands, $\delta^{18}\text{O}_{\text{calcite}} = -2.1$ ‰ (VPDB)									
$\delta^{18}\text{O}_{\text{water}} = -0.1$ ‰, Temp: 29.5 °C									
Palau-1	14.990	14.878	28.724	28.319	-0.074	14.936	28.419	-0.069	0.5256
Palau-2	14.996	14.884	28.724	28.319	-0.068	14.942	28.419	-0.063	0.5258
Palau-3	15.002	14.890	28.724	28.319	-0.062	14.948	28.419	-0.057	0.5260
Avg.	14.996	14.879	28.724	28.319	-0.068	14.942	28.419	-0.063	0.5258
$\pm 1\sigma$				0.006					0.0002
<i>Laqueus erythraeus brachiopod - Calcite</i>									
Locale: Monterey Bay, CA, $\delta^{18}\text{O}_{\text{calcite}} = +1.7$ ‰ (VPDB)									
$\delta^{18}\text{O}_{\text{water}} = -0.08$ ‰, Temp: 9 (± 1) °C									
L.Ery-1	17.034	16.891	32.679	32.156	-0.088	16.938	32.236	-0.083	0.5254
L.Ery-2	17.043	16.899	32.679	32.156	-0.080	16.946	32.236	-0.075	0.5257
L.Ery-3	17.053	16.909	32.679	32.156	-0.070	16.956	32.236	-0.065	0.5260
Avg.	17.043	16.900	32.679	32.156	-0.079	16.947	32.236	-0.074	0.5257
$\pm 1\sigma$				0.009					0.0003
<i>Liothyrella uva brachiopod - Calcite</i>									
Locale: Rothera, Antarctica, $\delta^{18}\text{O}_{\text{calcite}} = +3.0$ ‰ (VPDB)									
$\delta^{18}\text{O}_{\text{water}} = -0.87$ ‰, Temp: -0.4 (± 0.0) °C									
Rothera-1	17.736	17.581	34.044	33.477	-0.095	18.044	34.345	-0.090	0.5254
Rothera-2	17.739	17.584	34.044	33.477	-0.092	18.047	34.345	-0.087	0.5255
Rothera-3	17.744	17.589	34.044	33.477	-0.087	18.052	34.345	-0.082	0.5256
Rothera-4	17.741	17.585	34.044	33.477	-0.091	18.048	34.345	-0.086	0.5255
Rothera-5	17.737	17.581	34.044	33.477	-0.095	18.044	34.345	-0.090	0.5254
Avg.	17.740	17.584	34.044	33.477	-0.092	18.047	34.345	-0.087	0.5255
$\pm 1\sigma$				0.003					0.0001
<i>Liothyrella uva brachiopod - Calcite</i>									
Locale: Signy Island, Antarctica, $\delta^{18}\text{O}_{\text{calcite}} = +3.8$ ‰ (VPDB)									
$\delta^{18}\text{O}_{\text{water}} = -1.21$ ‰, Temp: -2 °C									
Signy-1	18.158	17.995	34.847	34.254	-0.091	18.636	35.459	-0.086	0.5256
Signy-2	18.145	17.983	34.847	34.254	-0.103	18.624	35.459	-0.098	0.5252
Signy-3	18.154	17.991	34.847	34.254	-0.095	18.633	35.459	-0.090	0.5255
Signy-4	18.141	17.978	34.847	34.254	-0.108	18.620	35.459	-0.103	0.5251
Signy-5	18.151	17.989	34.847	34.254	-0.097	18.630	35.459	-0.092	0.5254
Signy-6	18.155	17.992	34.847	34.254	-0.094	18.633	35.459	-0.089	0.5255
Signy-7	18.150	17.988	34.847	34.254	-0.098	18.629	35.459	-0.093	0.5254
Signy-8	18.149	17.986	34.847	34.254	-0.100	18.628	35.459	-0.095	0.5253
Avg.	18.150	17.988	34.847	34.254	-0.098	18.629	35.459	-0.093	0.5254
$\pm 1\sigma$				0.005					0.0002
<i>Florida Reef Sediment - Aragonite</i>									
Locale: Florida, $\delta^{18}\text{O}_{\text{calcite}} = -1.1$ ‰ (VPDB)									
$\delta^{18}\text{O}_{\text{water}} = +1.1$ ‰, Temp: 26 °C									
Reef-1	15.539	15.420	29.762	29.328	-0.065	14.844	28.228	-0.060	0.5259
Reef-2	15.514	15.395	29.762	29.328	-0.090	14.820	28.228	-0.085	0.5250
Reef-3	15.529	15.409	29.762	29.328	-0.076	14.834	28.228	-0.071	0.5255
Reef-4	15.522	15.403	29.762	29.328	-0.082	14.828	28.228	-0.077	0.5253
Reef-5	15.515	15.396	29.762	29.328	-0.089	14.820	28.228	-0.084	0.5250
Avg.	15.524	15.405	29.762	29.328	-0.080	14.829	28.228	-0.075	0.5253
$\pm 1\sigma$				0.010					0.0004

Table 3.3 (Cont.)

Sample	$\delta^{17}\text{O}$	$\delta^{17}\text{O}^a$	$\delta^{18}\text{O}^a$	$\delta^{18}\text{O}$	$\Delta^{17}\text{O}$ ($\lambda=0.528$)	$1000\ln\alpha^{17}$	$1000\ln\alpha^{18}$	$\Delta\Delta^{17}\text{O}$ cc-wt	θ
Ooid Sediment – Aragonite									
Locale: Great Bahama Bank, $\delta^{18}\text{O}_{\text{calcite}} = 0.0 \text{‰}$ (VPDB)									
$\delta^{18}\text{O}_{\text{water}} = +1.5 \text{‰}$, Temp: 25 °C									
Ooid-1	16.104	15.976	30.889	30.422	-0.087	15.189	28.923	-0.082	0.5252
Ooid-2	16.108	15.980	30.889	30.422	-0.083	15.193	28.923	-0.078	0.5253
Ooid-3	16.108	15.980	30.889	30.422	-0.082	15.194	28.923	-0.077	0.5253
Avg.	16.107	15.979	30.889	30.422	-0.084	15.192	28.923	-0.079	0.5253
$\pm 1\sigma$					0.002				0.0001
Great Bahama Bank Sediment – Aragonite									
Locale: Great Bahama Bank, $\delta^{18}\text{O}_{\text{calcite}} = 0.0 \text{‰}$ (VPDB)									
$\delta^{18}\text{O}_{\text{water}} = +1.5 \text{‰}$, Temp: 25 °C									
GBB-1	16.117	15.988	30.904	30.436	-0.082	15.202	28.937	-0.077	0.5253
GBB-2	16.117	15.988	30.904	30.436	-0.082	15.202	28.937	-0.077	0.5253
GBB-3	16.132	16.003	30.904	30.436	-0.067	15.217	28.937	-0.062	0.5258
GBB-4	16.129	16.000	30.904	30.436	-0.070	15.214	28.937	-0.065	0.5258
Avg.	16.123	15.995	30.904	30.436	-0.075	15.208	28.937	-0.070	0.5256
$\pm 1\sigma$					0.008				0.0003
Ceratoporella nicholsoni sclerosponge – Aragonite									
Locale: Exuma Sound, FL, $\delta^{18}\text{O}_{\text{calcite}} = +0.2 \text{‰}$ (VPDB)									
$\delta^{18}\text{O}_{\text{water}} = +1.25 \text{‰}$, Temp: 25 °C									
Sclero-1	16.234	16.104	31.136	30.661	-0.085	15.449	29.412	-0.080	0.5253
Sclero-2	16.240	16.110	31.136	30.661	-0.079	15.455	29.412	-0.074	0.5255
Sclero-3	16.230	16.100	31.136	30.661	-0.089	15.445	29.412	-0.084	0.5251
Avg.	16.235	16.105	31.136	30.661	-0.084	15.450	29.412	-0.079	0.5253
$\pm 1\sigma$					0.005				0.0002

^a-All calcite data are corrected to the $\delta^{18}\text{O}$ value from conventional methods. The $\delta^{17}\text{O}$ value is calculated using the equation $\delta^{17}\text{O} = \Delta^{17}\text{O} + 0.528\delta^{18}\text{O}$ (Eq. 3.1). Therefore, the error is driven by the $\Delta^{17}\text{O}$ precision. See Appendices F-I for all raw data.

The SEM and TEM imaging showed that the 5 °C calcite sample precipitated without CA had a large fraction of vaterite crystals (Figure 3.1 & Figure 3.2). Vaterite, a polymorph of CaCO_3 , has a fractionation factor enriched by $\sim 0.5 \text{‰}$ relative to calcite (Tarutani et al., 1969; Kim and O'Neil, 1997; Kluge and John, 2015). Separation of calcite crystals from the vaterite crystals was not possible due to their small size (5 μm). Therefore, the calcite-water oxygen isotope fractionation experimental data for the calcite samples without carbonic anhydrase precipitated at 5 °C from is excluded from further consideration. The SEM imaging only showed vaterite crystals present in the 5 °C without CA experimental runs, whereas samples of all other experimental runs were pure calcite (Figure 3.1).

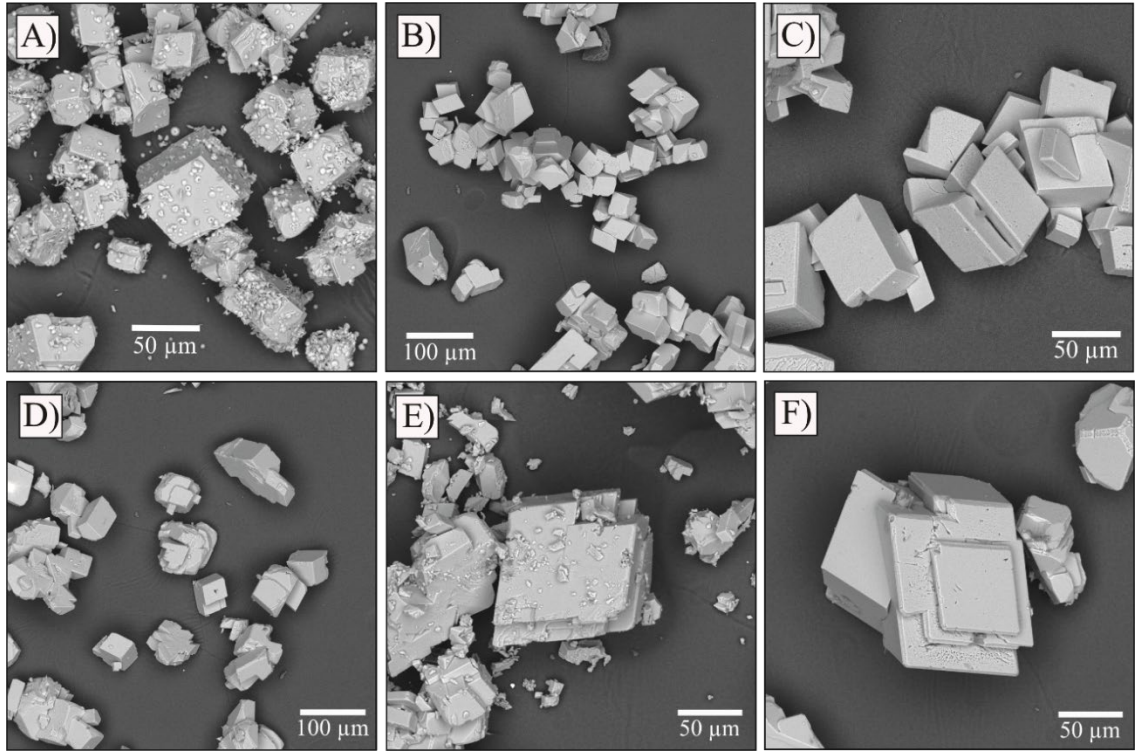


Figure 3.1 - SEM images of synthesized calcite: Samples in A–C were precipitated without carbonic anhydrase at 5, 20, and 40 °C, respectively, and samples in D–F were precipitated with carbonic anhydrase at 5, 20, and 40 °C, respectively. The small doughnut shapes in A) are vaterite crystals (see Fig. 3.2). The smaller pieces seen in E) were not vaterite but smaller calcite crystals. Based on crystal morphology, the majority of crystals appear to be calcite.

No difference was found in the $1000\ln\alpha_{cc-wt}$ values between each carbonate-water pair including the synthetic calcite precipitated with and without carbonic anhydrase, marine α /biogenic calcite or aragonite, or abiogenic calcite from Devils Hole (when the 5 °C without CA sample containing vaterite is removed). Based on the results of this study, there is no difference in the $1000\ln\alpha^{18O}$ values between calcite-water and aragonite-water at 25 °C (all aragonite samples in this study precipitated at 25 °C). The δ^{18O} - T equilibrium fractionation line was calculated by combining all datasets (calcite with CA, calcite without CA (excluding 5 °C runs), marine biogenic calcite, and marine α /biogenic aragonite) and the high temperature experimental data from O'Neil et al. (1969) which yielded the following δ^{18O} - T equilibrium fractionation equation:

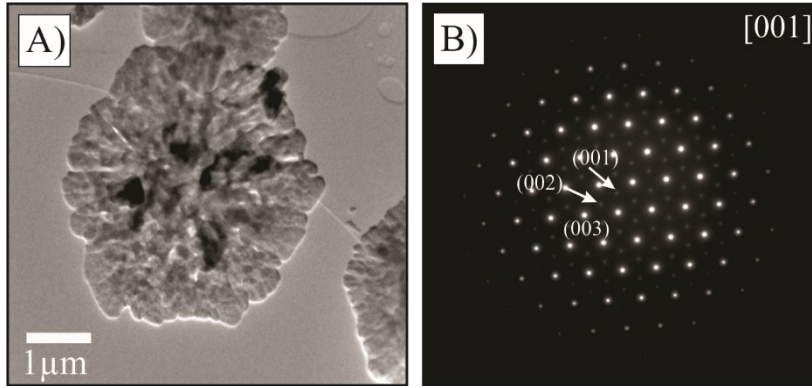


Figure 3.2 - TEM and diffraction pattern of vaterite crystal. A) Brightfield TEM image of vaterite crystal co-precipitated at 5 °C without carbonic anhydrase. B) Electron diffraction pattern of [001] zone axis from a vaterite crystal from the same sample showing strong (300)-type diffraction maxima and weak (100) and (200) diffraction maxima (white arrows) that are all absent in calcite.

$$1000\ln\alpha^{18}\text{O}_{\text{cc-wt}} = \frac{2.84(\pm 0.02) \times 10^6}{T^2} - 2.96(\pm 0.19) \quad R^2=0.999 \quad (3.6),$$

where T is temperature in Kelvin and standard error of the temperature coefficients are in parentheses (Fig. 3.3; Appendix J). The variables in the Eq. 3.6 are highly correlated with a Pearson correlation coefficient of 0.999 and p -value of 2.36×10^{-6} . The values from O'Neil et al. (1969) are corrected to reflect the commonly accepted $\alpha_{\text{CO}_2\text{-wt}}$ of 1.0412 (Friedman and O'Neil, 1977; Kim et al., 2015). It is worth noting that the fractionation equation can take many different forms. This study chose $1000\ln\alpha_{\text{cc-wt}} = a/T^2 + c$ in order to minimize residuals in the best fit while also combining the two datasets (this study and O'Neil et al. (1969)) to be applicable over a wider range of temperatures (up to 700 °C). Ideally, the data would be fit to the equation $1000\ln\alpha_{\text{cc-wt}} = a/T^2 + b/T$ to eliminate crossovers at higher temperatures (Criss, 1991) and force the $1000\ln\alpha_{\text{cc-wt}}$ to approach zero as T approaches ∞ . However, fitting the data using the latter equation resulted in higher residuals (6.01) and standard error on (0.548) than the former equation format (3.89 and 0.441 for residuals and standard error, respectively).

A $1000\ln\alpha^{18}\text{O}_{\text{cc-wt}}$ value of $29.0 (\pm 0.2)$ at $25\text{ }^\circ\text{C}$ determined in Eq. 3.6 is in excellent agreement with the value of 29.19 from experiments by Voarintsoa et al (2020). Our $1000\ln\alpha^{18}\text{O}_{\text{cc-wt}}$ value sits between those of Coplen (2007) of 29.8 using very slow growing calcite from Devils Hole, NV, and 28.0 based on synthetic calcite presented in Kim and O’Neil (1997) (Figure 3.3). Although there are many other calcite-water fractionation equations in the literature, for the sake of brevity, these results are only compared to the most cited $1000\ln\alpha_{\text{cc-wt}}$ equations (see Appendix K for a more detailed list). The results are on the high end of the published calcite-water oxygen isotope fractionation factors, suggesting that the synthetic calcite precipitated close to equilibrium in a laboratory setting (Figure 3.3). Therefore, the slow, compared to other published experiments, precipitation times of 5-7 days promoted precipitation close to equilibrium regardless if carbonic anhydrase was used as a catalyst.

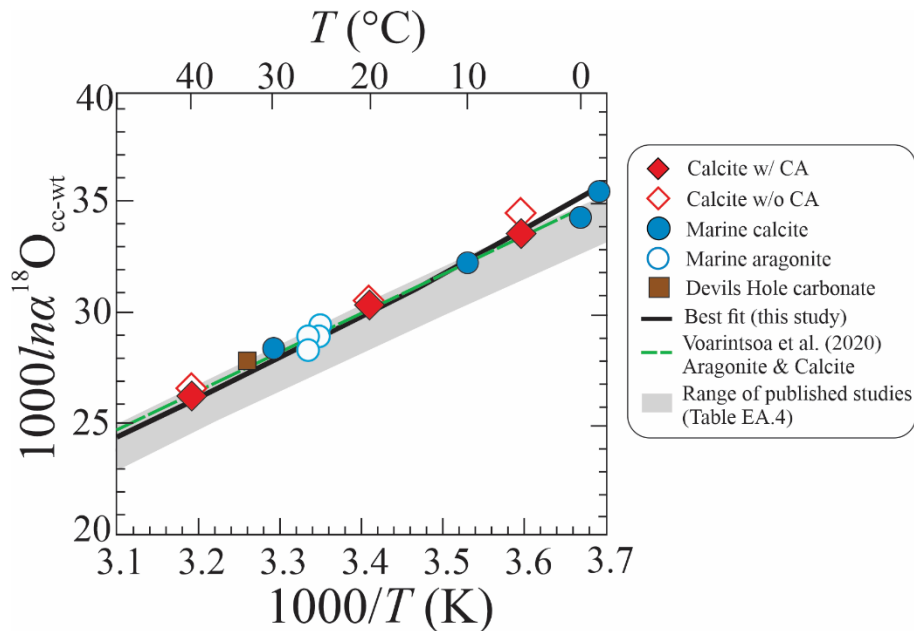


Figure 3.3 - Measured calcite-water fractionations compared to a range of literature calibrations (gray band, data in Appendix K). The $\delta^{18}\text{O}-T$ relationship (black line; Eq. 6) was calculated by combining the synthetic samples precipitated with carbonic anhydrase (solid red diamonds), marine biogenic calcite (solid blue circles), Devils Hole calcite, marine a/biogenic aragonite (empty blue circles), and the synthetic samples precipitated without carbonic anhydrase (excluding the $5\text{ }^\circ\text{C}$ experiment, empty red diamonds). We also included the high temperature calcite-water experiments from O’Neil et al. (1969) in the best fit (Eq.6) calculation (see Appendix J for further details). We compare our results (black line) with a recently published $\delta^{18}\text{O}-T$ relationship from Voarintsoa et al. (2020, green dashed line).

3.4.2 Calcite-water triple oxygen isotope fractionation using modern calcite

3.4.2.1 θ - T dependence

The θ values at a given temperature are calculated from the $\delta^{17}\text{O}$ and $\delta^{18}\text{O}$ values of the carbonate and water using Eq. 5 and are reproducible with an average error of ± 0.0002 , derived from the average standard deviation of replicated samples (Tables 3.2 and 3.3). There was no statistical difference between the θ values of the calcite samples (marine calcite, synthetic calcite precipitated with catalyst, synthetic calcite precipitated without catalyst). However, there was a statistical difference between the θ values of the aragonite samples and the calcite samples (Tukey's post-hoc analysis $p < 0.05$). Therefore, two θ - T relationships were calculated, one with the combined calcite samples and one with the aragonite samples. The best fit of each data set was calculated using a simple regression between $1/T$ and θ , with a y-intercept of 0.5305, the theoretical high temperature limit at $T = \infty$. Note, the aragonite data are a two-point fit – the θ values at ~ 25 °C and the θ value at infinite temperature. The best fit (with standard error of the temperature coefficients in parentheses) for the calcite samples is:

$$\theta_{\text{cc-wt}} = \frac{-1.39(\pm 0.02)}{T} + 0.5305 \quad (R^2=0.997) \quad 3.7),$$

and the best fit for the aragonite samples is:

$$\theta_{\text{ara-wt}} = \frac{-1.43(\pm 0.01)}{T} + 0.5305 \quad (R^2=0.997) \quad 3.8).$$

Using Eq. 3.7 and Eq. 3.8, the difference in θ between 0 and 50 °C is 0.0008 and 0.0009, respectively, corresponding to a change in θ of 0.00002/°C, identical to the predicted

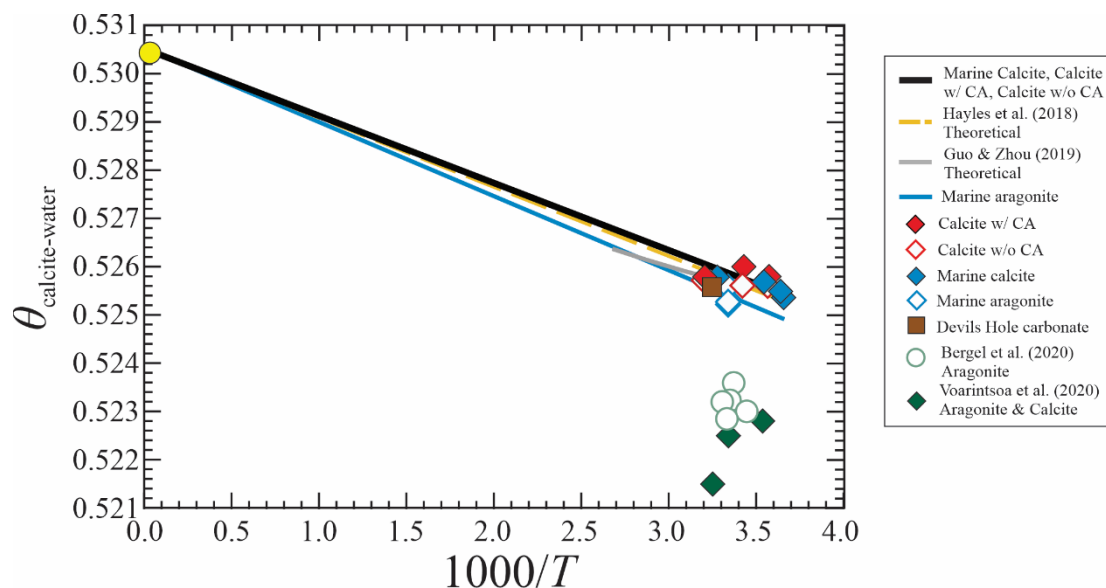


Figure 3.4 - The θ - T relationship of samples from this study and of published relationships. Points are averages of the θ values of multiple analyses for visual clarity and error is smaller than the symbols, but best fits were calculated using all analyses. The θ values of the marine calcite samples (blue diamonds), catalyzed carbonic anhydrase samples (red diamonds), and uncatalyzed carbonic anhydrase samples (open blue diamonds) were combined to calculate the best fit (black line). The marine aragonite (open blue diamonds) tend to have lower θ values than any of the other sample sets from this study and were not included in the best fit calculation. Both the best fits of the calcite samples and aragonite samples are within error of the 0-50 °C theoretical calculations from Guo and Zhou (2019, gray line) and the theoretical calculation over all temperatures from Hayles et al. (2018, yellow dashed line). Bergel et al. (2020, light green empty circles) and Voarintsoa et al. (2020, dark green diamonds) reported no significant θ - T relationships and their θ values are significantly lower than those of this study ($p < 0.05$, Tukey's post-hoc analysis). The θ value of the Devils Hole carbonate (brown square) is similar to that of the other ~30 °C calcite samples from this study.

change in θ /°C of Hayles et al. (2018) and slightly higher than the 0.00001/°C predicted in Guo and Zhou (2019).

The θ value of abiogenic calcite precipitated in water at 33.7 °C from Devils Hole agrees with the θ - T relationship of the marine biogenic calcite, suggesting there is no difference in the triple oxygen isotope fractionation between biogenic and abiogenic carbonate. Although we hypothesized that the synthetic calcite with CA may most-closely represent thermodynamic equilibrium, we found no differences between synthetic, biogenic, or abiogenic calcites and do not see any potential disequilibrium effects from the θ values of different materials. It is not unlikely that some disequilibrium

may exist in most naturally occurring carbonates (Brand et al., 2003; Bajnai et al., 2018; Daëron et al., 2019), but such disequilibrium did not manifest in either the $1000\ln\alpha^{18}\text{O}_{\text{cc-wt}}$ or the θ value of the different materials.

The θ - T relationship of calcite-water is in agreement with theoretical predictions of Hayles et al. (2018) and Guo and Zhou (2019) ($p>0.05$ using ANOVA with Tukey post-hoc analysis, Fig. .4) when comparing over the temperature range of 0-50 °C. The θ value for aragonite-water at 25 °C is 0.0004 less than that of calcite-water (0.5254 vs. 0.5258, respectively). Guo and Zhou (2019) calculated that the θ value at 25 °C for aragonite-water is slightly higher than that of calcite-water (0.5257 vs. 0.5256, respectively).

There is a large disagreement between the θ - T relationships of this paper and the empirical data of Voarintsoa et al. (2020) and Bergel et al. (2020) (Figure 3.4). Their $\theta_{\text{CO}_2\text{-H}_2\text{O}}$ data were converted to $\theta_{\text{CC-H}_2\text{O}}$ using published $\theta_{\text{CO}_2\text{-CC}}$ values (Guo and Zhou, 2019; Wostbrock et al., 2020b). We cannot explain the disparity, but both Voarintsoa et al. (2020) and Bergel et al. (2020) measured the CO_2 released via phosphoric acid digestion of the carbonate and then determined the triple oxygen isotope values of the CO_2 by equilibration with O_2 following the procedure of Barkan et al. (2015) and analyzing the O_2 on their mass spectrometer. It is known that there are non-equilibrium oxygen isotope fractionation effects that occur during the equilibration of CO_2 and O_2 in the presence of a hot platinum catalyst (Fosu et al., 2020) which deserves further study.

3.4.2.2 Triple oxygen isotope fractionation

Using the relationship that $1000\ln\alpha^{17}\text{O}_{\text{cc-wt}} = \theta(1000\ln\alpha^{18}\text{O}_{\text{cc-wt}})$ (Eq. 3.4), the $1000\ln\alpha^{17}\text{O}_{\text{cc-wt}}$ for calcite-water is:

$$1000\ln\alpha^{17}\text{O}_{\text{cc-wt}} = \left(\frac{2.84(\pm 0.02) \times 10^6}{T^2} - 2.69(\pm 0.19) \right) \left(\frac{-1.39(\pm 0.01)}{T} + 0.5305 \right) \quad 3.9).$$

The $\Delta^{17}\text{O}_{\text{cc}} - \Delta^{17}\text{O}_{\text{wt}}$ fractionation equation is given by:

$$\Delta^{17}\text{O}_{\text{cc}} - \Delta^{17}\text{O}_{\text{wt}} = \left(\frac{2.84(\pm 0.02) \times 10^6}{T^2} - 2.69(\pm 0.19) \right) \left(\frac{-1.39(\pm 0.01)}{T} + 0.5305 - \lambda \right) \quad 3.10,$$

where λ is the reference slope, taken herein as 0.528.

The $1000 \ln \alpha^{17}\text{O}_{\text{ara-wt}}$ for aragonite-water is:

$$1000 \ln \alpha^{17}\text{O}_{\text{ara-wt}} = \left(\frac{2.84(\pm 0.02) \times 10^6}{T^2} - 2.96(\pm 0.19) \right) \left(\frac{-1.53(\pm 0.02)}{T} + 0.5305 \right) \quad 3.11.$$

The $\Delta^{17}\text{O}_{\text{ara}} - \Delta^{17}\text{O}_{\text{wt}}$ aragonite-water fractionation equation is given by:

$$\Delta^{17}\text{O}_{\text{ara}} - \Delta^{17}\text{O}_{\text{wt}} = \left(\frac{2.84(\pm 0.02) \times 10^6}{T^2} - 2.96(\pm 0.19) \right) \left(\frac{-1.53(\pm 0.02)}{T} + 0.5305 - \lambda \right) \quad 3.12.$$

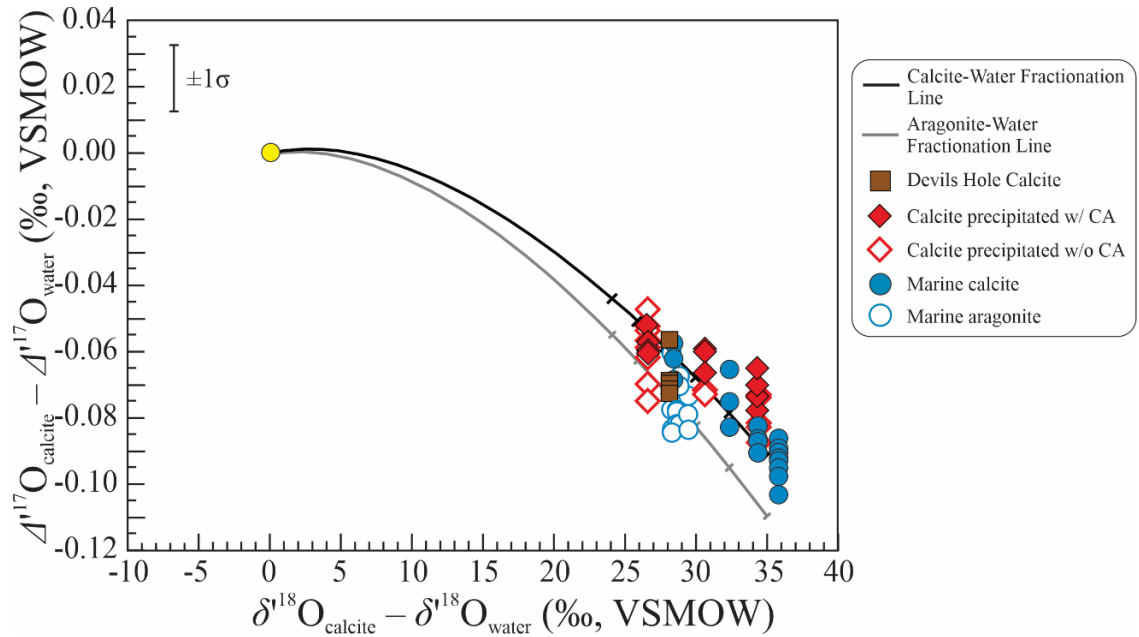


Figure 3.5 - Triple oxygen isotope fractionation curves for calcite-water (black line) and aragonite-water (gray line). Hash marks on each fractionation line denotes temperatures ranging from 0 – 50 °C. Triple oxygen isotope fractionation approaches zero with increasing temperature (yellow circle). The calcite-water fractionation line (black line) was calculated using Eq. 3.10 and includes the marine calcite (blue diamonds), synthetic calcite precipitated with catalyst (red diamonds), and synthetic calcite precipitated without catalyst (open red diamonds). The aragonite-water fractionation line (gray line) was calculated with Eq. 3.12 and includes the marine aragonite samples (open blue circles). The fractionation curve of the calcite plots higher than the aragonite-water fractionation curve. The Devils Hole carbonate samples (brown squares) have an average triple oxygen isotope value that suggests similar fractionation as the other calcite samples.

The $\Delta^{17}\text{O}_{\text{carb}} - \Delta^{17}\text{O}_{\text{water}}$ (or $\Delta\Delta^{17}\text{O}_{\text{carb-wt}}$) vs $\delta^{18}\text{O}_{\text{carb}} - \delta^{18}\text{O}_{\text{wt}}$ relationship is shown in Figure 3.5. For oxygen isotope studies of aragonite, it would be more reasonable to use the $1000\ln\alpha^{17}\text{O}_{\text{ara-wt}}$ derived using the marine aragonite (Eq. 3.11). Since we are ultimately interested in using the triple oxygen isotope method for paleoclimatic reconstruction with brachiopod shells initially precipitated as calcite, we will use Eq. 3.9 (derived from the calcite samples) when considering our ancient carbonate samples.

3.4.3 Application to ancient carbonates

It has long been recognized that there is a secular decrease in the $\delta^{18}\text{O}$ values of marine carbonates with age through the Phanerozoic (Degens and Epstein, 1962; Keith and Weber, 1964; Veizer and Hoefs, 1976; Popp et al., 1986; Lohmann and Walker, 1989; Veizer et al., 1997). The explanation for this secular trend is still elusive, but generally falls into one of three hypotheses (Degens and Epstein, 1962). The first suggests that the oxygen isotope value of the ocean has changed over this time period from about -5‰ at the beginning of the Phanerozoic to zero today (Perry, 1967; Perry and Tan, 1972; Popp et al., 1986; Lohmann and Walker, 1989; Walker and Lohmann, 1989; Veizer et al., 1997; Wallmann, 2001; Kasting et al., 2006; Jaffrés et al., 2007; Veizer and Prokoph, 2015; Kanzaki, 2020). The second is that the secular trend reflects a decrease in ocean temperature toward modern. However, this idea of a ‘hot ocean’ is generally reserved for samples much older than the Phanerozoic (Knauth and Epstein, 1976; Knauth and Lowe, 1978; Muehlenbachs, 1986; Muehlenbachs, 1998). The third idea is that the secular trend is a function of diagenesis, with older samples having undergone a larger degree of alteration, in spite of best efforts to screen out

diagenetically-altered samples using various chemical tests (Gao and Land, 1991; Brand, 2004).

The addition of $\delta^{17}\text{O}$ measurements will increase the robustness of $\delta^{18}\text{O}$ measurements because of the additional constraint to the temperature-fractionation equation and/or the oxygen isotope composition of the water in which the carbonate precipitated. Under the three scenarios described earlier for the secular increase of $\delta^{18}\text{O}$ values, trends in $\delta^{17}\text{O}$ and $\delta^{18}\text{O}$ values of the carbonate can be predicted (Fig. 3.6A). If the triple oxygen isotope composition of seawater changed through the Phanerozoic, then the triple oxygen isotope values of the carbonates would plot above the modern triple oxygen isotope equilibrium line, following the seawater alteration model of Sengupta and Pack (2018; Fig. 3.6A). In the Sengupta and Pack (2018) model, the ratio of high to low temperature alteration controls the $\delta^{18}\text{O}$ and $\Delta^{17}\text{O}$ values of seawater. Higher proportions of continental weathering and low temperature off-axis alteration (relative to modern) would lower the $\delta^{18}\text{O}$ and raise the $\Delta^{17}\text{O}$ values of the ocean as shown in path ① in Fig. 3.6A. Both the $\delta^{18}\text{O}$ and $\Delta^{17}\text{O}$ values of the seawater must change because low temperature silica-water triple oxygen isotope fractionation (such as continental weathering) follows a λ value of approximately 0.5240 (Sharp et al., 2016). The only way for the $\delta^{18}\text{O}$ value of the seawater to change while the $\Delta^{17}\text{O}$ value of the seawater remains constant is if the λ value is closer to 0.528 (see Liljestr and et al. (2020) for a λ sensitivity study regarding changing ratios of high to low temperature alteration). A λ value 0.528 is better representative of high temperature (>650 °C) alteration (Pack and Herwartz, 2014; Sharp et al., 2016) and not representative of the low temperature alteration processes required to lower the $\delta^{18}\text{O}$ value of the ocean. If the triple oxygen

isotope composition of the seawater remained constant through the Phanerozoic and the secular trend in $\delta^{18}\text{O}$ values is largely a temperature signal, then the triple oxygen isotope values of the carbonates would migrate along the modern triple oxygen isotope fractionation line. The oldest carbonates would plot around 60 °C and the youngest near 20 °C along the modern triple oxygen isotope fractionation line (path ② in Fig. 3.6A). Lastly, if the secular trend in the carbonate record is a diagenetic feature, then samples would generally plot below the modern fractionation line, assuming interaction with a

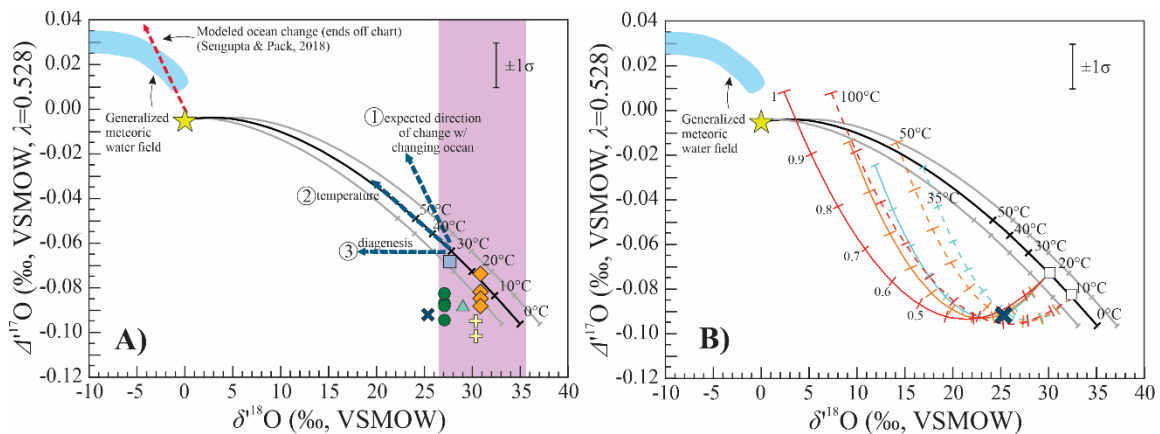


Figure 3.6 - Application of the triple oxygen isotope equilibrium curve to ancient carbonates using the calcite-water triple oxygen isotope fractionation curve (Eq. 3.10, black line), normalized to modern seawater with a $\delta^{18}\text{O}$ of 0 and $\Delta^{17}\text{O}$ of -0.005 ‰ (yellow star, Luz and Barkan, 2010). These are bracketed by fractionation curves at -2 and $+2$ ‰, representative of a larger range in tropical-temperate ocean oxygen isotopic compositions (LeGrande and Schmidt, 2006). The range of modern brachiopod $\delta^{18}\text{O}$ values is represented in the purple box (Brand et al., 2015). A) Five fossil brachiopod shells and one belemnite were analyzed for triple oxygen isotope values. Samples are: Mid Ordovician – dark blue x, Silurian – light blue square, Mid Devonian – dark green circle, Late Pennsylvanian – light green triangle, Mid Cretaceous (belemnite) – orange diamond, Mid Maastrichtian (Late Cretaceous) – yellow cross. The Silurian brachiopod and mid Cretaceous belemnite plot on the fractionation curve for modern ocean compositions. The other samples all plot to the left of the fractionation line with modern ocean isotope composition. These samples cannot be explained by different assumed temperatures of formation or changing ocean conditions that are controlled by tectonics (Sengupta and Pack, 2018; red dotted line). Calculated variations in the triple oxygen isotope composition with changing ratios of high to low temperature seafloor alteration are shown by the red dashed line. If the home-point (the marine value) moves along this vector, there is not a solution for which the measured values will intersect the equilibrium curve (blue dotted line labelled ①). If the temperature of the ocean changed over the Phanerozoic, the carbonate samples would follow the blue dotted line labelled ②. Their oxygen isotopic compositions can instead be explained by diagenesis (blue dotted line labelled ③). B) Using a fluid-rock mixing model, we are able to predict the primary carbonate composition of the altered mid Ordovician sample using two assumed diagenetic fluids of -15 (solid colored lines) and -10 (dashed colored lines) ‰ for $\delta^{18}\text{O}$ and $+0.03$ ‰ for $\Delta^{17}\text{O}$ values and different alteration temperature (100 °C, red; 50 °C, orange; 35 °C blue). Hash marks on the red, orange, and yellow lines represent the fraction of oxygen the rock exchanged with the diagenetic fluid. The mid Ordovician sample exchanged 20 – 30 % of its oxygen and initially formed in 10 – 20 °C seawater with a similar ocean oxygen isotopic composition to modern.

fluid lower in $\delta^{18}\text{O}$ value than seawater (path ③ in Fig. 3.6A). These trends can be used when analyzing well preserved (as determined by diagenetic screening) carbonates for triple oxygen isotope compositions to evaluate which of the three processes explains the carbonate record through the Phanerozoic.

3.4.3.1 Triple oxygen isotope compositions of ancient carbonates and implications on ancient seawater

Five well-preserved fossil brachiopods (Bates and Brand, 1991; Brand, 2004; Brand et al., 2012) and one belemnite from the Peedee formation were measured for their triple oxygen isotope compositions (Table 3.4). Brachiopod samples represent several periods of the Phanerozoic: Mid Ordovician, Silurian (Wenlock), Mid Devonian, Late Pennsylvanian, and Late Cretaceous (Mid Maastrichtian), and the Peedee belemnite is of Mid Cretaceous age (Table 3.1). The triple oxygen isotope compositions of each sample are plotted in Figure 3.6. There is one unique triple oxygen isotope composition per °C for a modern seawater triple oxygen isotope composition of 0 and -0.005‰ for $\delta^{18}\text{O}$ and $\Delta^{17}\text{O}$, respectively (solid black line, Fig. 3.6A). Any sample that precipitated in seawater with a similar oxygen isotope composition as modern and has not been subsequently altered must plot on the solid black curve in Figure 3.6A. Two samples, the Silurian brachiopod and Cretaceous belemnite, have triple oxygen isotope compositions that fall on our fractionation curve with a modern ocean isotope composition ($\delta^{18}\text{O} \approx -1\text{‰}$ for ice-free conditions and $\Delta^{17}\text{O} \approx -0.004\text{‰}$). The triple oxygen isotope composition of the Silurian brachiopod suggests an ocean water temperature of about 30 °C while the Cretaceous belemnite suggests an ocean water temperature of about 15 to 20 °C. These are reasonable estimates given that belemnites were nektonic, open water swimmers whereas while brachiopods are sessile organisms generally associated with carbonate

Table 3.4 - Isotopic compositions of ancient brachiopods from the Phanerozoic. Brachiopod samples are from Bates and Brand (1991), Brand (2004), and Brand et al. (2012). All samples are reported in ‰ and relative to VSMOW unless otherwise noted.

Sample	$\delta^{17}\text{O}$	$\delta^{17}\text{O}^a$	$\delta^{18}\text{O}^a$	$\delta^{18}\text{O}^a$	$\Delta^{17}\text{O}$ ($\lambda=0.528$)
Brachiopod Fragment – Mid Ordovician					
<i>Locale: Carlington, Ontario, $\delta^{18}\text{O}_{\text{calcite}} = -4.8$ ‰ (VPDB)</i>					
CM3a-1	13.546	13.455	25.991	25.659	-0.093
Avg.	13.546	13.455	25.991	25.659	-0.093
$\pm 1\sigma$					N.A.
Brachiopod Fragment – Silurian (Wenlock)					
<i>Locale: Western New York State, $\delta^{18}\text{O}_{\text{calcite}} = -2.9$ ‰ (VPDB)</i>					
IR70c-1	14.571	14.466	27.910	27.528	-0.069
Avg.	14.571	14.466	27.910	27.528	-0.069
$\pm 1\sigma$					N.A.
Athyris spiriferoides brachiopod – Mid Devonian					
<i>Locale: Eighteen Mile Cr, New York State, $\delta^{18}\text{O}_{\text{calcite}} = -3.4$ ‰ (VPDB)</i>					
NB428-1	14.308	14.206	27.456	27.086	-0.095
NB428-2	14.317	14.215	27.456	27.086	-0.086
NB428-3	14.316	14.215	27.456	27.086	-0.087
NB428-4	14.320	14.218	27.456	27.086	-0.083
Avg.	14.315	14.213	27.456	27.086	-0.088
$\pm 1\sigma$					0.005
Unidentified spiriferid brachiopod fragment – Late Pennsylvanian					
<i>Locale: Arrow Canyon, NV, $\delta^{18}\text{O}_{\text{calcite}} = -1.5$ ‰ (VPDB)</i>					
AC332-1	15.319	15.203	29.384	28.961	-0.089
Avg.	15.319	15.203	29.384	28.961	-0.089
$\pm 1\sigma$					N.A.
Pee Dee Belemnite – Mid Cretaceous					
<i>Locale: Pee Dee Formation, $\delta^{18}\text{O}_{\text{calcite}} = 0.0$ ‰ (VPDB)</i>					
PDB-1	16.117	15.989	30.920	30.442	-0.085
PDB-2	16.113	15.984	30.920	30.442	-0.089
PDB-3	16.119	15.990	30.920	30.442	-0.083
PDB-4	16.116	15.988	30.920	30.442	-0.085
PDB-5	16.119	15.990	30.920	30.442	-0.083
PDB-6	16.128	16.000	30.920	30.442	-0.074
Avg.	16.119	15.990	30.920	30.442	-0.083
$\pm 1\sigma$					0.005
Chatwinothyris sp. brachiopod – Mid Maastrichtian					
<i>Locale: Maastricht, Netherlands, $\delta^{18}\text{O}_{\text{calcite}} = -0.2$ ‰ (VPDB)</i>					
C539-1	15.989	15.863	30.683	30.222	-0.094
C539-2	15.982	15.856	30.683	30.222	-0.101
Avg.	15.986	15.859	30.683	30.222	-0.098
$\pm 1\sigma$					0.005

^a-All calcite data are corrected to the $\delta^{18}\text{O}$ value from conventional methods. The $\delta^{17}\text{O}$ value is calculated using the equation $\delta^{17}\text{O} = \Delta^{17}\text{O} + 0.528\delta^{18}\text{O}$ (Eq. 3.1). Therefore, the error is driven by the $\Delta^{17}\text{O}$ precision. See Appendices F-I for all raw data.

platforms. Therefore, the temperature and oxygen isotope composition of seawater has been similar to modern since at least the Silurian. A similar conclusion was reached by Henkes et al. (2018) using Δ_{47} values of Phanerozoic brachiopods and other mollusks where they suggest unchanged Paleozoic seawater $\delta^{18}\text{O}$ values from modern. However,

this study reports slightly cooler Silurian seawater temperature of 30 °C, compared to 35 to 40 °C reported in Henkes et al. (2018).

Seawater of the global modern ocean has a broad range of $\delta^{18}\text{O}$ values between -4 ‰ in the polar regions where very negative meltwater from land ice lowers the $\delta^{18}\text{O}$ value of the nearby seawater and $+2$ ‰ in low latitude regions where high evaporation increases the $\delta^{18}\text{O}$ values (LeGrande and Schmidt, 2006). Similarly, modern brachiopods from polar, temperate, and tropical regions exhibit a broad range in $\delta^{18}\text{O}$ values of 26.8 to 35.0 ‰ (Brand et al., 2015; Brand et al., 2019). If we consider this broad range of seawater, then brachiopod specimens from the Devonian, Pennsylvanian, and Cretaceous may also indicate calcite precipitation in seawater with a low $\delta^{18}\text{O}$ value. However, none of these specimens were found in polar regions so a more realistic modern ocean analog encompasses $\delta^{18}\text{O}$ values ranging from -2 to $+2$ ‰ (Fig. 3.6A; LeGrande and Schmidt, 2006). With this geographic consideration, the brachiopod specimens from the Ordovician, Devonian, Pennsylvanian, and Cretaceous are not preserving a triple oxygen isotope composition that formed in seawater since the samples plot to the left of the modern fractionation curve ($\delta^{18}\text{O} = 0 \pm 2$ ‰, gray curves in Fig. 3.6). Instead, they have likely undergone diagenesis (described in more detail below). It is important to note that the distinction between the oxygen isotope composition of the formation water and diagenesis could not be seen with $\delta^{18}\text{O}$ measurements alone.

3.4.3.2 Triple oxygen isotopes and carbonate diagenesis

The Ordovician, Devonian, Pennsylvanian, and Cretaceous brachiopod specimens plot to the left of the modern ocean oxygen isotope fractionation curve (Fig. 6A) and therefore are not preserving a triple oxygen isotope composition that could have formed in modern seawater. Their low $\delta^{18}\text{O}$ values are not explained by changing seawater

values because their $\Delta^{17}\text{O}$ values do not follow path ① in Figure 6A. Instead, the triple oxygen isotope values are consistent with diagenesis (path ③ in Fig. 6A). Meteoric water diagenesis will shift the oxygen isotope composition of a sample to the left of the equilibrium curve (Sengupta and Pack, 2018; Sharp et al., 2018; Liljestrand et al., 2020).

Using a simple fluid-rock mixing model adapted to the triple oxygen isotope system (cf. Herwartz et al., 2015), one can “see through” diagenesis in our sample set and back-calculate the original triple oxygen isotope composition of the carbonate (Figure 3.6B). The $\delta^{18}\text{O}$ value of the ocean is assumed to be similar to modern seawater because the triple oxygen isotope compositions of the Silurian brachiopod and Cretaceous belemnite fit such a model (Fig. 6A). The generic equation governing alteration between a rock (carbonate in this study) and the diagenetic fluid is calculated using a simple mass balance model (Taylor, 1978):

$$x(\delta_{\text{water,initial}}^y) + (1-x)(\delta_{\text{rock,initial}}^y) = \delta_{\text{bulk}}^y = x(\delta_{\text{water,final}}^y) + (1-x)(\delta_{\text{rock,final}}^y) \quad 3.13),$$

where, x is the water/rock fraction and δ^y is either $\delta^{18}\text{O}$ or $\delta^{17}\text{O}$ (two equations apply).

The final rock and water values are related to the fractionation factor (α), which varies with temperature:

$$\alpha_{\text{rock-water}} = \frac{1000 + \delta_{\text{final,rock}}^y}{1000 + \delta_{\text{final,water}}^y} \quad 3.14).$$

Eq. 3.13 and Eq. 3.14 can be combined to calculate both the $\delta^{17}\text{O}_{\text{rock,initial}}$ and $\delta^{18}\text{O}_{\text{rock,initial}}$ using:

$$x(\delta_{\text{water,initial}}^y) + (1-x)(\delta_{\text{rock,initial}}^y) = x \left(\frac{1000 + \delta_{\text{final,water}}^y}{\alpha} - 1000 \right) + (1-x)(\delta_{\text{rock,final}}^y) \quad 3.15).$$

The $\delta^{17}\text{O}$ and $\delta^{18}\text{O}$ values of the rock and water are calculated in the non-linearized δ -notation, then linearize the δ values to calculate the $\Delta^{17}\text{O}$ values. The triple oxygen isotope composition of the rock ($\delta_{\text{rock,final}}$) follows a predictable path based on the assumed diagenetic fluid ($\delta_{\text{water,initial}}$) composition. In prime notation, the fluid-rock interaction trajectories plot as curves. The oxygen isotope fractionation is calculated based on diagenetic temperatures of 35, 50, and 100 °C (Figure 3.6B, red, orange, and blue lines) and two assumed diagenetic fluids of meteoric origin with $\Delta^{17}\text{O}$ values of +0.03 ‰ and $\delta^{18}\text{O}$ values of -10 and -15 ‰. The oxygen isotope composition of the rock follows the curves in Figure 6B, starting with the original oxygen isotope composition of the rock with a fluid-rock ratio (F/R ratio is the fraction of oxygen coming from the fluid vs. the rock) of zero (no alteration) to an infinite F/R ratio in which the carbonate is in equilibrium with the initial diagenetic fluid at the temperature of alteration.

Using the fluid-rock mixing equations and the assumed range in the infiltrating meteoric water, we can construct a series of curves that pass through the measured triple oxygen isotope composition of the mid Ordovician brachiopod and extend back to the unaltered value (Fig. 6B). The Ordovician brachiopod sample appears to have exchanged ~20 – 30 % of its oxygen with the diagenetic fluid. Extrapolating back to a F/R ratio of zero gives us the original calcite composition. The initial $\delta^{18}\text{O}$ value of the mid Ordovician brachiopod was between 30.1 and 32.3 ‰. The back extrapolation to the initial $\delta^{18}\text{O}$ and $\Delta^{17}\text{O}$ values also suggest a formation temperature between 10 and 20 °C. The temperature estimate depends on the assumed initial diagenetic fluid composition and the temperature of alteration; however, changing these two variables within reasonable limits does not appreciably affect the calculated seawater temperature. Thus,

the triple oxygen isotope compositions of the studied brachiopod and belemnite calcite are consistent with cool temperature and a constant seawater $\delta^{18}\text{O}$ value over the Phanerozoic. The samples plotting with low $\delta^{18}\text{O}$ values are the result of diagenetic alteration.

3.5 Conclusions

In this work, the temperature dependence was determined for the triple oxygen isotope fractionation between calcite and water from laboratory synthesis experiments and empirically from natural marine shells and sediment. Using catalyzed synthetic calcite, uncatalyzed synthetic calcite (excluding the 5 °C experiment), marine biogenic calcite, and marine biogenic aragonite, we propose a $1000\ln\alpha^{18}\text{O}_{\text{cc-wt}}$ value of 29.0 at 25 °C, similar to the value of 29.19 suggested by Voarintsoa et al. (2020) and close to the value of 29.8 °C suggested by Coplen (2007). The calculated calcite-water θ - T relationship agrees with theoretical estimates (Hayles et al., 2018; Guo and Zhou, 2019). The θ value for aragonite-water at 25 °C is slightly less than that of calcite-water. The aragonite-water data must be viewed as preliminary because they are based on samples from a narrow temperature range.

There is a single, temperature-dependent fractionation curve for $\Delta^{17}\text{O}$ and $\delta^{18}\text{O}$ values of calcite that precipitated in modern seawater. Calcite triple oxygen isotope values that fall off this curve cannot have formed in modern seawater at any temperature. By analyzing carbonates where the water is no longer present, the robustness of triple oxygen isotope measurements is revealed. Two ancient biogenic calcite samples (Silurian brachiopod and Cretaceous belemnite) fall on the modern ocean fractionation curve. All other samples analyzed in this study plot to the left of the modern ocean fractionation

curve, even though they satisfy the criteria of minimal diagenesis. Some degree of diagenesis (interaction with meteoric water) is the most reasonable explanation for these samples. Using simple mass balance relationships, we show the alteration pathway in triple oxygen isotope space and back-calculate the original $\delta^{18}\text{O}$ value of the carbonate. The fluid-rock interaction model is sensitive enough to show diagenesis in rocks that have exchanged 20 – 30 % of their oxygen with the diagenetic fluid. Furthermore, the results suggest that $\delta^{18}\text{O}$ values and temperatures of Phanerozoic seawater were similar to that of the modern ocean.

3.6 Acknowledgements

All authors would like to thank Benjamin Passey, Andreas Pack, and an anonymous reviewer for their constructive feedback that greatly improved this manuscript. J.A.G.W and Z.S. acknowledges support from NSF GRFP grant DGE-1418062, NSF EAR 1551226, and NSF EAR 1747703. U.B acknowledges NSERC Discovery grant 2015-05282. S.J.C. acknowledges support from NSF EAR 1147537. We thank James Watkins for helpful suggestions about kinetic fractionation during calcite precipitation. Any use of trade, firm, or product names is for descriptive purposes only and does not imply endorsement by the U.S Government.

4. SEEING THROUGH DIAGENESIS IN PHANEROZOIC CARBONATE ROCKS

4.1 Introduction

The oxygen isotope composition of a carbonate is only as good as the rock it comes from. In other words, carbonate geochemistry requires careful petrographic and chemical analysis to choose the most pristine, unaltered rocks to reconstruct paleotemperatures. Minor (Sr, Na, and Mg) and trace (Fe, Mn, Zn, Cu, Cd, Pb, Ba, U) element concentrations that substitute for the Ca^+ portion of the mineral structure are useful indicators of alteration (Veizer, 1983; Swart, 2015). Besides $^{18}\text{O}/^{16}\text{O}$, other isotope ratios, such as δD , $\delta^{11}\text{B}$, $\delta^{34}\text{S}$, $\delta^{26}\text{Mg}$, $\delta^{44/40}\text{Ca}$ or $\delta^{44/42}\text{Ca}$, and $^{87}\text{Sr}/^{86}\text{Sr}$ or $^{88}\text{Sr}/^{86}\text{Sr}$ are used as indicators of alteration (see Swart, 2015 for detailed compilation of references). Correlation between $\delta^{13}\text{C}$ and $\delta^{18}\text{O}$ can indicate alteration (Allan and Matthews, 1982). Also, clumped isotope ratios (namely Δ_{47} values) are increasingly being used to suggest alteration (Dennis and Schrag, 2010). Besides chemical analysis, there are petrographic diagnostic tools to identify alteration such as the presence of micritic boring or the presence of carbonate cements (Bathurst, 1966; Golubic, 1969; Golubic et al., 1975; Perkins and Tsentas, 1976; Perkins et al., 1977; Bathurst, 1983). Additionally, a preservation index of nacre plates on shells comprised of aragonite is used as an indicator of alteration (Cochran et al., 2010). These diagnostic tests are generally performed via SEM with or without cathodoluminescence cameras and/or XRD analysis (see James and Jones (2015) for more information on identifying diagenesis in rocks and petrographic tools used for identification). An extensive review paper for more references is available in Swart (2015).

Most studies use a combination of the techniques described above to screen samples to select those that are most pristine to analyze the oxygen isotope ratios. However, it is extremely difficult to predict how much alteration occurred and whether it has affected the oxygen isotope ratios (cf. Swart, 2015). For example, the presence of secondary minerals such as brucite, low-Mg calcite (LMC), or aragonite inside voids of carbonaceous skeletal material or as recrystallization of skeletal material can make some chemical tests ambiguous (Schmalz, 1965; Weber and Kaufman, 1965; McGregor and Gagan, 2003; Buster and Holmes, 2006; Hendy et al., 2007; McGregor and Abram, 2008). Also, bores from microbes facilitate micritization and fill bore holes with fine mud and/or secondary minerals after burial, adding complexity to some of the chemical tests (Bathurst, 1966; Golubic, 1969; Golubic et al., 1975; Perkins and Tsentas, 1976; Perkins et al., 1977; Bathurst, 1983). Measuring the $\delta^{17}\text{O}$ values will add a constraint as to whether a rock has undergone any alteration as there is only one unique carbonate triple oxygen isotope composition that is in 'equilibrium' with a given water and temperature (see chapters 1 and 2 for more details). In Chapter 2, a fluid-rock mixing model was applied to an altered brachiopod fossil to see through the diagenesis and back-calculate the initial carbonate triple oxygen isotope composition. However, with only one carbonate phase (the shell) the alteration pathway is under-constrained. A range of initial triple oxygen isotope compositions of the fluid and the temperature of alteration could describe the altered sample. Here, carbonate rocks with multiple phases of calcite such as the carbonate matrix, fossils, and void filling cements are used to better constrain the alteration history of the sample and more precisely calculate the primary carbonate

oxygen isotope composition. A sample suite containing rocks from three different time periods are used: the late Cretaceous, early Triassic, and the late Ordovician.

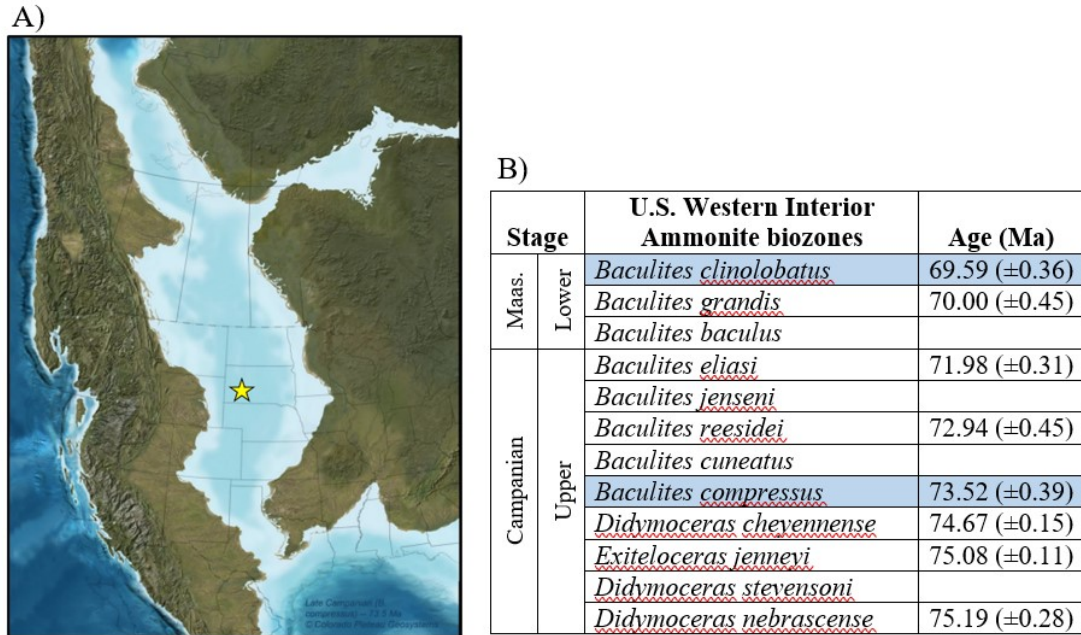


Figure 4.1 - A) Map of sample location (yellow star) and reconstruction of the Western Interior Seaway during the Late Campanian. B) Ammonite biozones of the Lower Maastrichtian and Upper Campanian Western Interior Seaway with radiometric age controls (Cobban et al., 2006). Highlighted biozones are used in this study.

4.2 Sample information

4.2.1 Carbonate concretions from the late Cretaceous Western Interior Seaway

4.2.1.1 Geologic setting

The Pierre Shale formed in the center to western portion of the epeiric Western Interior Seaway during most of the Campanian and the lower Maastrichtian and expands to cover portions of Kansas, Colorado, Wyoming, South Dakota, North Dakota, and Montana (Kauffman and Caldwell, 1993). During this time period, the Western Interior Seaway was connected to the major oceans to both the north and south (Gill and Cobban, 1966). The fossiliferous nature of the Pierre Shale Formation has allowed for excellent biostratigraphy to age control the exposure using ammonite biozones. Four carbonate concretions and one ammonite fossil found in the host shale from the Pierre Shale

Formation in South Dakota were studied. We analyzed one concretion from the *Baculites clinolobatus* biozone collected from Smith Ranch, SD and two concretions and one fossil *Placenticerias meeki* from the *Baculites compressus* biozone (Fig. 4.1; Cobban et al., 2006), collected from Patterson Ranch, SD.

Speculation still exists as to exactly how carbonate concretions form in epeiric seas. However, when they are found in the Western Interior Seaway they are generally fossil rich and found in continuous layers with friable shale as the host rock surrounding the concretion (Reeside and Cobban, 1960; Waage, 1964). They are believed to form during early diagenesis, after rapid burial (Maples, 1986; Zatoń and Marynowski, 2006; Landman and Klofak, 2012). Maples (1986) addresses four main identifying features that suggest early diagenesis: 1) the shale tends to drape over concretions, 2) fossils are not crushed so must have been lithified into the concretion before further burial, 3) fossils tend to be better preserved in the concretions as opposed to the shale, and 4) bioturbation can be preserved in the concretions but are not observed in the host rock. Some studies suggest that concretions tend to form where clusters of mollusks (such as *Inoceramid sp.*) were adhered to the sea floor (Waage, 1964, 1968). Alternatively, carbonate shells may have accumulated preferentially in depressions on the sea floor either created biologically (cf. Geraghty and Westermann, 1994), from bottom water currents (Tsujiata, 1995; Zatoń and Marynowski, 2006), or a mixture of the two (Landman and Klofak, 2012). Concretions then formed after shallow burial where carbonate concentration was highest. Landman and Klofak (2012) suggested a timeline of formation that occurs in 3 steps. First, over a period of less than 10 years, ammonites accumulate in localized areas due to

predation and/or currents. Over the next 10–100 years the concretion forms after shallow burial and calcite veins form. Finally, alteration by meteoric water during later diagenesis

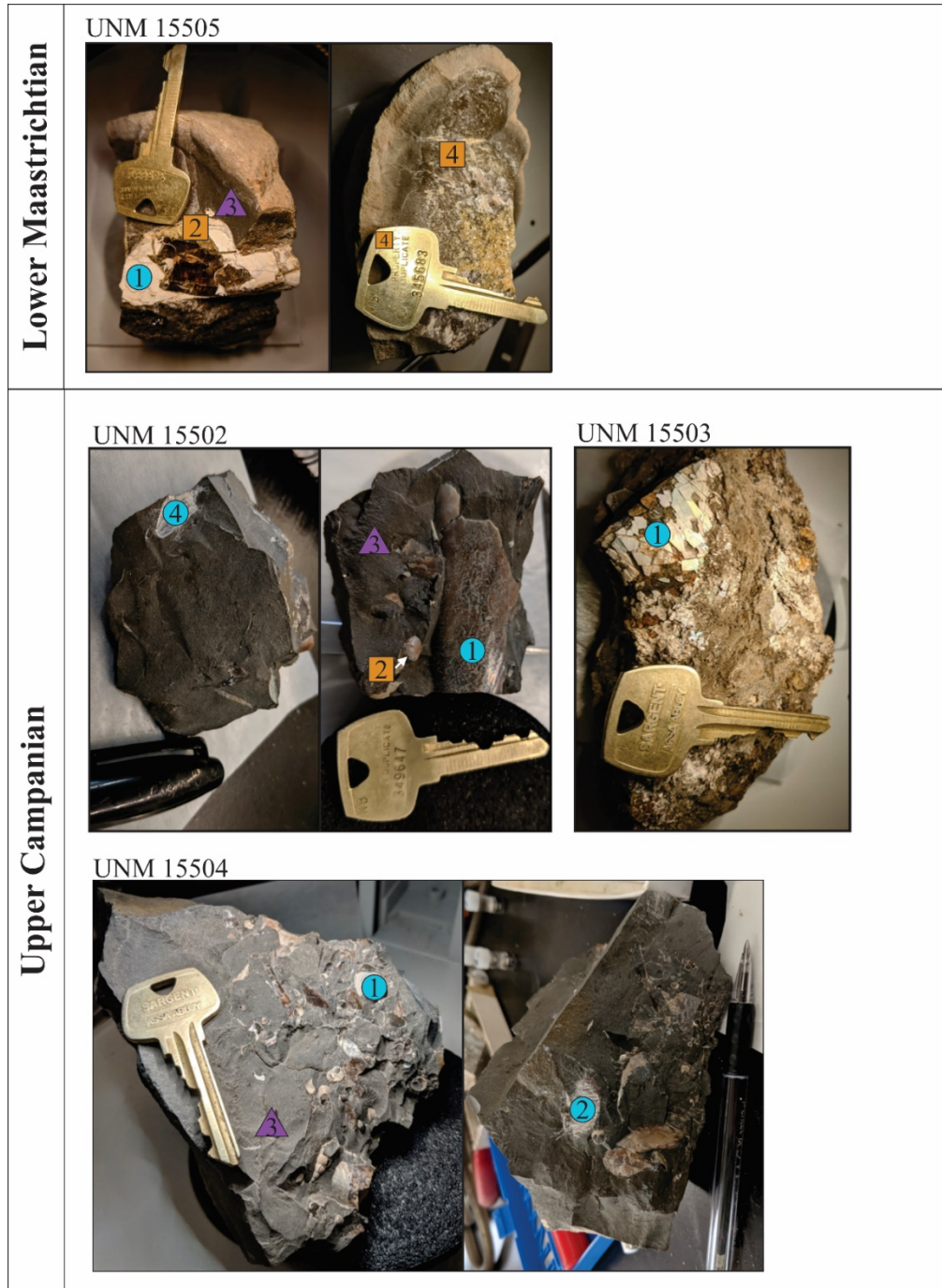


Figure 4.2 - Images of the samples from the Western Interior Seaway. Shell material (blue circle), carbonate matrix (purple triangle), and void filling calcite (orange square) were each sampled separately. Numbers correspond to the sample name in Table 1.

results in the altered shell material and infilling of ammonite chambers and voids with calcite. The dissolution and reprecipitation of carbonate in different phases make these concretions ideal samples to reconstruct the fluid that altered the concretion and calculate the pristine carbonate oxygen isotope composition.

4.2.1.2 Sample preparation

All samples were part of the University of New Mexico's Department of Earth and Planetary Sciences (UNM EPS) Collections. Calcite phases were identified in each concretion and generally falls into three categories: 1) the carbonate matrix or host, 2) fossil carbonate, and 3) calcite cement infilling cracks and voids. Not all concretions contained calcite cement. One sample (UNM 15503) was found in the host siliceous shale without a carbonate matrix. Figure 4.2 shows the different concretions and where samples were taken. Samples were removed from the concretion by manual scraping with a metal spatula or razorblade and powdered using a mortar and pestle. Organic matter was removed by adding 10 % H₂O₂ until reaction stopped. The sample was then rinsed three times with distilled water and reacted with ~5 % sodium hypochlorite until reaction stopped. The sample was rinsed with distilled water three times and dried in a 60 °C oven for 12 hours.

4.2.2 Early Triassic ammonites

4.2.2.1 Geologic setting

Two ammonite fossils spanning the Late Smithian–Early Spathian warming event were analyzed for triple oxygen isotope compositions. The Late Smithian ammonoid, *Anasibirites* sp., is from Crittenden Springs in Elko County, NV (Fig. 4.3; Jenks and Brayard, 2018). The exposure at Crittenden Springs is from the Thaynes Group and the beds containing ammonoid fossils are generally discontinuous and overturned due to a

mix of faulting and tectonic activity and/or extensive excavation in 1988 (Jenks and Brayard, 2018). The host rock in the beds of Crittenden Springs is atypical of the Thaynes Group, which is typically alternating successions of limestone and shales. At Crittenden Springs, Jenks and Brayard (2018) describes the exposure as thin, platy shaly calcareous gray-black limestone followed by yellow-brown calcareous siltstone and limestone, and a massive gray, crystalline limestone on top. The late Smithian is marked by a high-stand in sea-level when the *Anasibirites* beds were formed (Brayard et al., 2013).

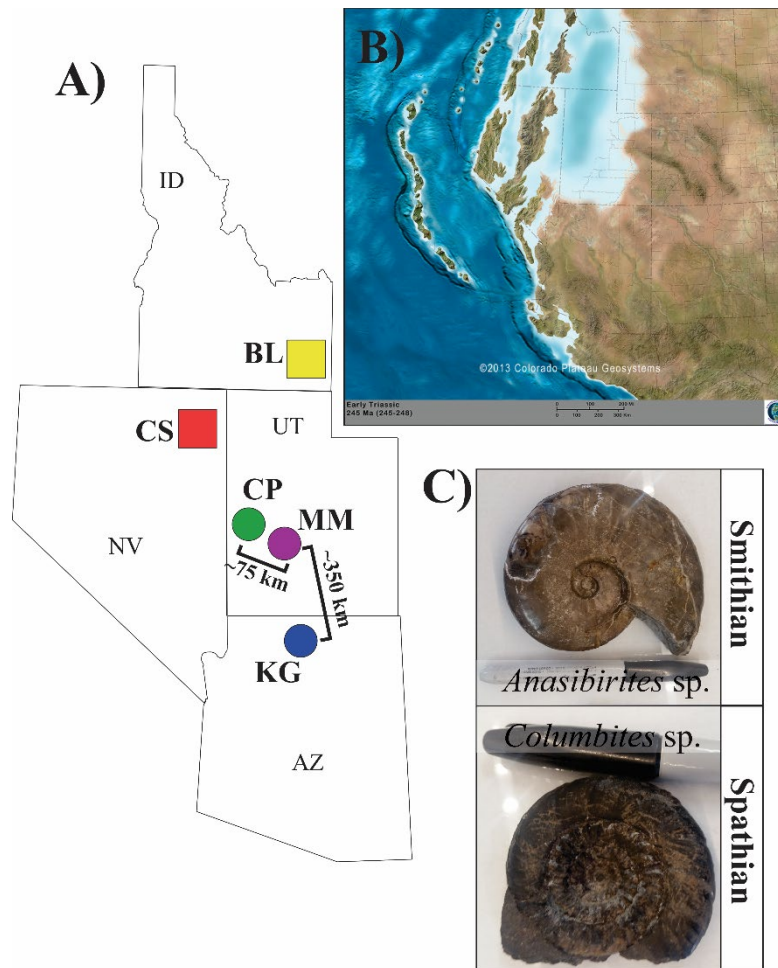


Figure 4.3 - A) Sample location map. The Smithian (red square; CS – Crittenden Springs) and Spathian (yellow square; BL – Bear Lake Hot Springs) ammonites were found in Nevada and Idaho, respectively. The bulk rock from Cowboy Pass (green circle; CP), Mineral Mountains (purple circle; MM) and Kaibab Gulch (blue circle) were found in Utah and Arizona. B) Reconstruction of the southwestern U.S from 245 to 248 Ma (Blakey, 2013). C) Pictures of ammonite fossils used in this study.

The early Spathian ammonoid, *Columbites* sp., is from the a section of the Thaynes Group in Bear Lake Hot Springs, ID (Guex et al., 2010; Jenks et al., 2013) and represents the beginning of a regressive sea-level stance. The *Columbites* bed is in the 25–40 meter thick “Middle Shale” (Jenks et al., 2013). Fossils in this bed are generally found in ellipsoidal carbonate concretions.

4.2.2.2 *Sample preparation*

Samples were provided by UNM EPS Collections through a donation from Jim Jenks. Ammonite shell material was manually removed using a metal spatula. A mortar and pestle were used to powder the material. The powdered carbonate was then cleaned using H₂O₂ and sodium hypochlorite. The sample was rinsed three times with distilled water after each cleaning step and dried in a 60 °C oven.

4.2.3 *Early Triassic bulk rock*

4.2.3.1 *Geologic setting*

The triple oxygen isotope composition of three contemporaneous, early Smithian bulk carbonate rocks from different locations (Cowboy Pass, UT; Mineral Mountain, UT; Kaibab Gulch, AZ) were measured to look at regional changes in diagenetic fluids (Figure 4.3A & Figure 4.3B). All samples were in the Sonoma Foreland Basin in eastern Panthalassa (Brayard et al., 2013). The early Triassic deposits indicate overall global sea-level rise with localized transgressive and regressive cycles (Vennin et al., 2015). The samples come from the Thaynes Group, known for its excellent preservation of ammonoid fossils (Guex et al., 2010; Brayard et al., 2013; Jenks et al., 2013; Jenks and Brayard, 2018). The Thaynes Group is generally marked by alternating layers of shale and limestone, indicative of the sea-level changes occurring in the Sonoma Foreland Basin during this time (Brayard et al., 2013; Vennin et al., 2015). Kaibab Gulch is near

the UT–AZ border and is the most onshore site of the three in this study (Figure 4.3). The sample is near a regressive–transgressive transition and is a conglomerate microbial carbonate (Jeffrey et al., 2019). The Mineral Mountains site is in east-central Utah and the sample analyzed in this paper is from Unit B described in Vennin et al. (2015). In summary, the sample is oncoid/ooid/peloid grainstone to floatstone with a notable amount of fenestral cavities filled by cements (Vennin et al., 2015). The Cowboy Pass site is in the Confusion Range of western Utah. This site is marked by longer stretches of shale formation than the Mineral Mountain site, indicating a farther offshore environment during this time period (Brayard et al., 2013).

4.2.3.2 Sample preparation

Samples were from UNM EPS Collections. The sample was broken to expose a clean face. Chips were removed from the exposed face and ground in a mortar and pestle until powdered. Samples were cleaned of any potential organic matter by exposing the sample to H₂O₂ and then sodium hypochlorite. The sample was rinsed three times with distilled water and then dried in a 60 °C oven.

4.2.4 Rugose coral from Hirnantian glaciation (late Ordovician)

4.2.4.1 Geologic setting

A near complete stratigraphic record of the Hirnantian (late Ordovician – 445.2 to 443.8 Ma) exists in a ~200 km exposure of the Ellis Bay member on Anticosti Island in eastern Canada (Fig. 4.4B; Desrochers et al., 2010; Bartlett et al., 2018; Mauviel et al., 2020). The uppermost part of the Ellis Bay member is the Laframboise member, representing a transgressive sea level during the Late Ordovician Glacial Cycle–3 (LOGC–3). The samples from this study represent time intervals before and after a large unconformity in the Laframboise member, inferred to exist due to eustatic sea level

changes during the transition of a regressive to a transgressive sea level regime (Bartlett et al., 2018).

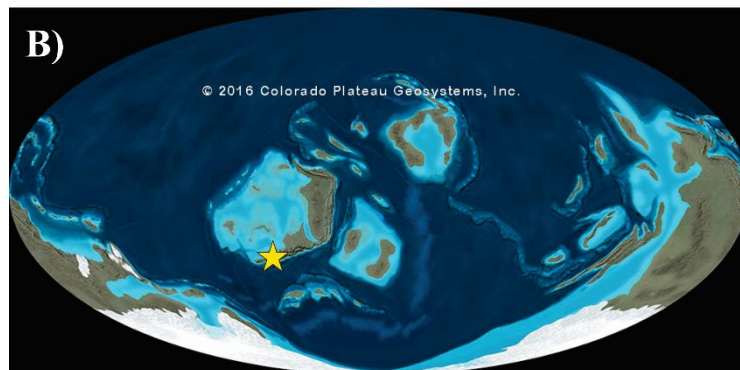
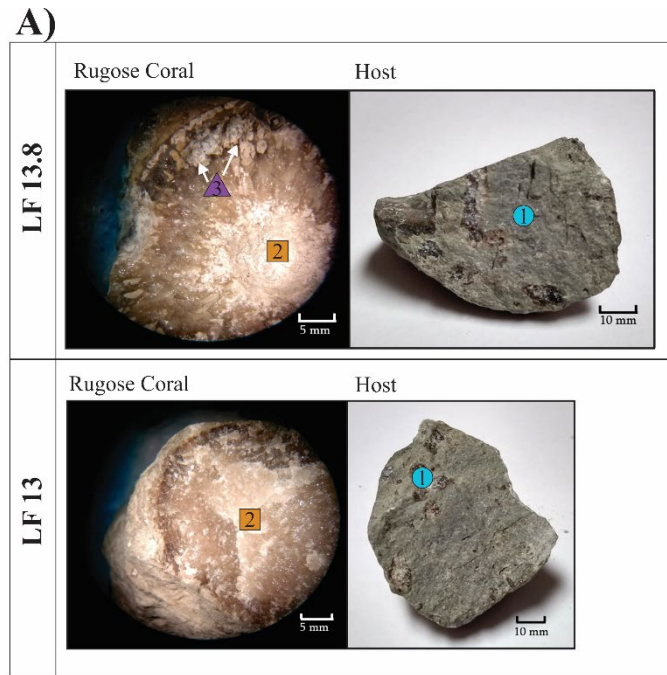


Figure 4.4 - A) Images of the samples from the Laframboise member, Anticosti Island, eastern Canada. The host rock (blue circle), inner massive calcite of the coral (orange square) and the outer void filling mud (purple triangle) were sampled. Void filling mud could not be sufficiently removed sample LF 13. Numbers corresponds to the sample name in Table 3. **B)** Reconstructed global map of 450 Ma (Blakey, 2016) with the location of the samples (yellow star)

4.2.4.2 Sample preparation

Samples were provided by the UNM EPS collections. Here, we present triple oxygen isotope values from two samples that contain multiple calcite phases (Figure 4.4). The carbonate rocks were classified as wackestone and contain large rugose coral fossils (Bartlett et al., 2018). Three phases of calcite were sampled from each rock: 1) the

carbonate matrix or host, 2) the rugose coral calcitic skeleton, and 3) the fine calcite mud infilling the voids of the rugose coral (Figure 4.4). Fine calcite mud could not be sufficiently removed from the LF 13 sample. To avoid possible contamination from the mud infill, the coral skeleton was always removed from the center of the coral. Due to the intricate pattern of the rugose coral and the size of the infilled voids, carbonate was removed from the sample using a Dremel® with a small drill bit. Organic matter was removed the same way as described for the carbonate concretion samples, using H₂O₂ and sodium hypochlorite and drying in a 60 °C oven.

4.3 Oxygen isotope systematics

An in-depth overview of triple oxygen isotope systematics is available in Chapters 1 and 2. In brief, all measurements in this study will be presented in δ -notation and expressed as per mil (‰) using the following equation (McKinney et al., 1950):

$$\delta^x\text{O} = \left(\frac{\frac{{}^x\text{O}_{sample}}{16\text{O}_{sample}}}{\frac{{}^x\text{O}_{standard}}{16\text{O}_{standard}}} - 1 \right) \times 1000 \quad 4.1)$$

where x is either mass 17 or mass 18. The standard is UNM CSI's in-house working O₂ standard gas that has been calibrated to VSMOW–SLAP (Wostbrock et al., 2020b). We express triple oxygen isotope values in terms of the deviation of $\delta^{17}\text{O}$ from a reference slope (called $\Delta^{17}\text{O}$) and is defined as (Hulston and Thode, 1965; Miller, 2002):

$$\Delta^{17}\text{O} = \delta^{17}\text{O} - \lambda \times \delta^{18}\text{O} + \gamma \quad 4.2),$$

where λ is the reference slope, γ is the y-intercept, and the δ -values are linearized (expressed as $\delta' = 1000 \ln[\delta'/1000 + 1]$). In this study we use a λ of 0.528 and γ of 0.

Linearization is necessary to compare δ -values across a large range due to a slight curve in the reference slope of terrestrial materials (Hulston and Thode, 1965; Miller, 2002).

Carbonate–water equilibrium fractionation can be expressed in terms of $\alpha_{\text{carb-water}}$ following the equation:

$$\alpha_{\text{carb-water}} = \frac{R_{\text{carb}}^x}{R_{\text{water}}^x} \quad 4.3),$$

where R is the ratio $^{x}\text{O}/^{16}\text{O}$ and x is either mass 17 or 18. In δ' -notation, $\alpha_{\text{carb-water}}$ can be re-written as:

$$1000 \ln \alpha_{\text{carb-water}}^x = \delta^{x}\text{O}_{\text{carb}} - \delta^{x}\text{O}_{\text{water}} \quad 4.4).$$

In this study, we adapt a simple fluid-rock mixing model (Taylor, 1978) for triple oxygen isotope values (c.f, Herwartz et al., 2015; Sharp et al., 2018) to see through any alteration that the carbonate experienced and back-calculate the triple oxygen isotope composition of the initial carbonate at formation. The alteration trend is calculated using the following mass balance equation (Taylor, 1978):

$$x(\delta_{\text{water,initial}}^y) + (1-x)(\delta_{\text{rock,initial}}^y) = \delta_{\text{bulk}}^y = x(\delta_{\text{water,final}}^y) + (1-x)(\delta_{\text{rock,final}}^y) \quad 4.5),$$

where x is the water-rock fraction and y is either mass 17 or 18. The final rock and water values are related to $\alpha_{\text{carb-water}}$ (Eq. 4.3), which varies with temperature. Combining equations 4.3 and 4.5 allow for the calculation of $\delta_{\text{rock,initial}}^y$ such that:

$$x(\delta_{\text{water,initial}}^y) + (1-x)(\delta_{\text{rock,initial}}^y) = x \left(\frac{1000 + \delta_{\text{final,water}}^y}{a} - 1000 \right) + (1-x)(\delta_{\text{rock,final}}^y) \quad 4.6).$$

The model is first calculated using $\delta^{17}\text{O}$ and $\delta^{18}\text{O}$ values and is linearized to calculate the $\Delta^{17}\text{O}$ values. The triple oxygen isotope composition of the rock ($\delta_{\text{rock,final}}$) follows a predictable path based on the alteration fluid and temperature. When the δ -values are

linearized, the fluid-rock interaction trajectories are curved. Wostbrock et al. (2020a) used the fluid-rock interaction model to predict the initial oxygen isotope composition of fossilized brachiopods over the Phanerozoic. However, because only one phase of calcite was analyzed, a broad range of initial oxygen isotope compositions could be assumed. Here, multiple phases of calcite are present in most samples, allowing for further constraint on the assumed alteration temperature and water oxygen isotope composition.

4.4 Oxygen isotope analysis

As described in Chapters 1 and 2, all triple oxygen isotope measurements are corrected to the $\delta^{18}\text{O}$ value of the sample analyzed using the method of phosphoric acid digestion (Wostbrock et al., 2020a; Wostbrock et al., 2020b). For determining $\delta^{18}\text{O}$ values, 0.3 and 0.4 mg of carbonate were reacted with 100 % phosphoric acid at 75 °C to release CO_2 gas. The CO_2 gas was then transferred to a Thermo-Finnigan Delta Plus XL mass spectrometer via a Thermo-Finnigan Gas Bench II autosampler. All measured values of samples are corrected to an in-house standard, Carrara marble. This standard has been calibrated to IAEA reference samples NBS 19 (28.65 ‰) and NBS 18 (7.2 ‰) (Brand et al., 2014). Average standard deviation for the $\delta^{18}\text{O}$ values is 0.2 ‰. All values are reported relative to VSMOW using the equation

$$\delta^{18}\text{O}_{\text{VSMOW}} = 1.03092 \times \delta^{18}\text{O}_{\text{VPDB}} + 30.92 \text{ (Kim et al., 2015).}$$

Triple oxygen isotope measurements were obtained using conventional fluorination in nickel reaction vessels (Sharma and Clayton, 1965; Wostbrock et al., 2020b). For this method, about 5 to 6 mg of powdered carbonate is loaded into a nickel vessel, degassed at 100 °C for 12 hours, and reacted with 30-fold stoichiometric excess BrF_5 at 750 °C for 4 days. Adding the BrF_5 reagent allows for the following reaction

$\text{BrF}_5 + \text{CaCO}_3 \rightarrow \text{CaF} + \text{CF}_4 + \frac{3}{2}\text{O}_2 + \frac{1}{2}\text{Br}_2$. The O_2 released via fluorination is purified through a series of traps. First, the O_2 is passed through two liquid nitrogen (LN_2) traps to remove any contamination gases that are condensable at LN_2 temperatures. Then, the gas is passed through a $100\text{ }^\circ\text{C}$ NaCl trap to eliminate trace F_2 gases following the reaction $\text{F}_2 + 2\text{NaCl} \rightarrow 2\text{NaF} + \text{Cl}_2$, where the Cl_2 gas is then condensed in a third LN_2 trap. The O_2 is then quantitatively adsorbed onto a 5 \AA mol sieve cooled with LN_2 . The O_2 gas is then transferred through a 5x mol sieve gas chromatographic column at 6 mL/min to separate any NF_3 or N_2 contamination gases. The now purified O_2 is collected on a second mol sieve at the inlet of the Thermo MAT 253+ mass spectrometer in the Center for Stable Isotopes at the University of New Mexico. The O_2 gas is measured in dual-inlet mode with a 26 sec integration time and 30 iterations. The sample gas is measured against the same in-house O_2 reference gas calibrated to the VSMOW–SLAP scale in Wostbrock (2020b). This fluorination procedure is used to determine the $\Delta^{17}\text{O}$ values. The average standard deviation of the $\Delta^{17}\text{O}$ value is $\pm 0.001\text{ ‰}$. The $\delta^{17}\text{O}$ value is calculated using the $\Delta^{17}\text{O}$ value measured via fluorination and the $\delta^{18}\text{O}$ value measured via phosphoric digestion using the equation $\delta^{17}\text{O} = \Delta^{17}\text{O} + 0.528 \times \delta^{18}\text{O}$. See Wostbrock et al. (2020a; 2020b) or Chapters 1 and 2 for more details.

4.5 Results and discussion

All results are listed in Tables 4.1–4.3 and Figures 4.5–4.9. The main purpose of this study was to see how triple oxygen isotope compositions can determine alteration in carbonate rocks through a suite of samples. This preliminary sample set is used to suggest potential implications on the paleo-environment in which each sample formed. Further investigation is required to produce more definitive results.

4.5.1 Carbonate concretions from the Western Interior Seaway

Multiple calcite phases from four carbonate concretions were analyzed for $\delta^{13}\text{C}$ and triple oxygen isotope values (Table 4.1). The host rock from each concretion has $\delta^{13}\text{C}$ values that suggest these concretions formed either near cold methane seep environments or from the decomposition of a large amount of organic material (Figure 4.5; e.g., Landman et al., 2018). The shell material has $\delta^{13}\text{C}$ values that are more positive than cold seep environments, but lower than typical open ocean dwelling organisms, similar to the ammonite shells presented in Landman et al. (2018). This suggests that although the ammonites may have grown some of their shell in water near cold seeps, much of their shell was grown away from cold seep water. All the calcite samples that were found infilling cracks and voids in the concretions had more negative $\delta^{13}\text{C}$ and $\delta^{18}\text{O}$ values than the shell material (Figure 4.5). The $\delta^{13}\text{C}$ and $\delta^{18}\text{O}$ values are known to be correlated in altered rocks where there is lower $\delta^{13}\text{C}$ and $\delta^{18}\text{O}$ values than the primary material (cf. Swart, 2015). The $\delta^{13}\text{C}$ and $\delta^{18}\text{O}$ values are similar to the void filling calcite oxygen and carbon isotope compositions presented in Cochran et al. (2010). No differences in $\delta^{13}\text{C}$ or $\delta^{18}\text{O}$ values were found between the two time periods (late Campanian and early Maastrichtian), not unexpected since the greenhouse climates of both time periods are similar (Ogg et al., 2012).

All calcite phases analyzed from the early Maastrichtian concretion (UNM15505) had triple oxygen isotope compositions that indicate the carbonate did not precipitate in seawater with an oxygen isotope composition similar to modern seawater. A diagenetic fluid with a $\delta^{18}\text{O}$ value of -12‰ and $\Delta^{17}\text{O}$ value of 0.03‰ was used to perform the fluid-

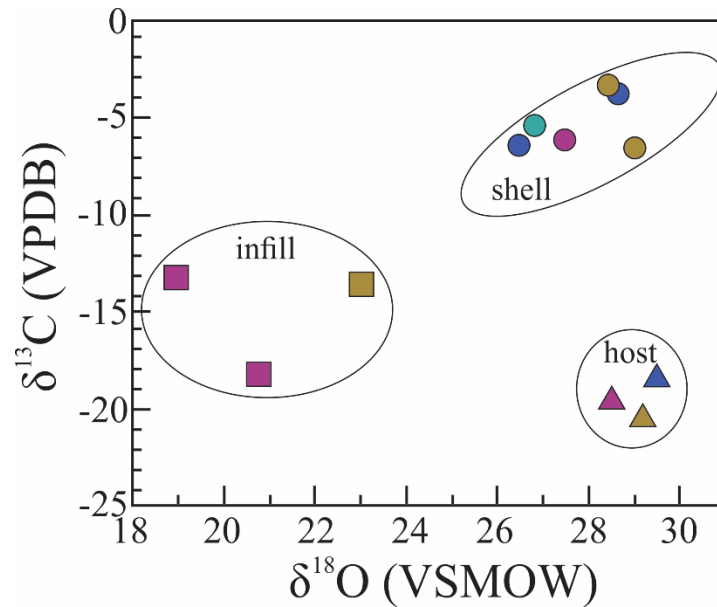


Figure 4.5 - The $\delta^{13}\text{C}$ values vs. the $\delta^{18}\text{O}$ values of the calcite phases from the carbonate concretions of the Late Cretaceous Western Interior Seaway. Each calcite phase tends to plot in similar regions (ellipses are for reference). The late Campanian concretions are UNM15502 (brown), UNM15503 (teal), UNM15504 (blue). The early Maastrichtian concretion is UNM15505 (purple).

rock mixing model. Similar to the $\delta^{13}\text{C}$ values, the crack and void filling calcite appear to be the most altered and experienced the highest fluid-rock ratio (~ 0.7 F/R). The carbonate from the shell of the *Baculites clinobatus* fossil had a higher $\Delta^{17}\text{O}$ value than the host rock (Figure 4.6A). One fluid rock mixing model does not sufficiently describe the alteration path of the carbonate samples. *Baculites clinobatus* is a nektonic organism that is expected to have spent most of its time swimming in the open ocean. As a predator, the ammonite may have spent more time in the middle water column where more species were living. Upon death, the ammonite would sink to the seafloor. In contrast, the matrix would have formed at the seafloor, expected to be about 100 m during these time periods. Therefore, it is not unreasonable to expect the primary temperature of the fossil to be warmer than the environment in which the matrix formed.

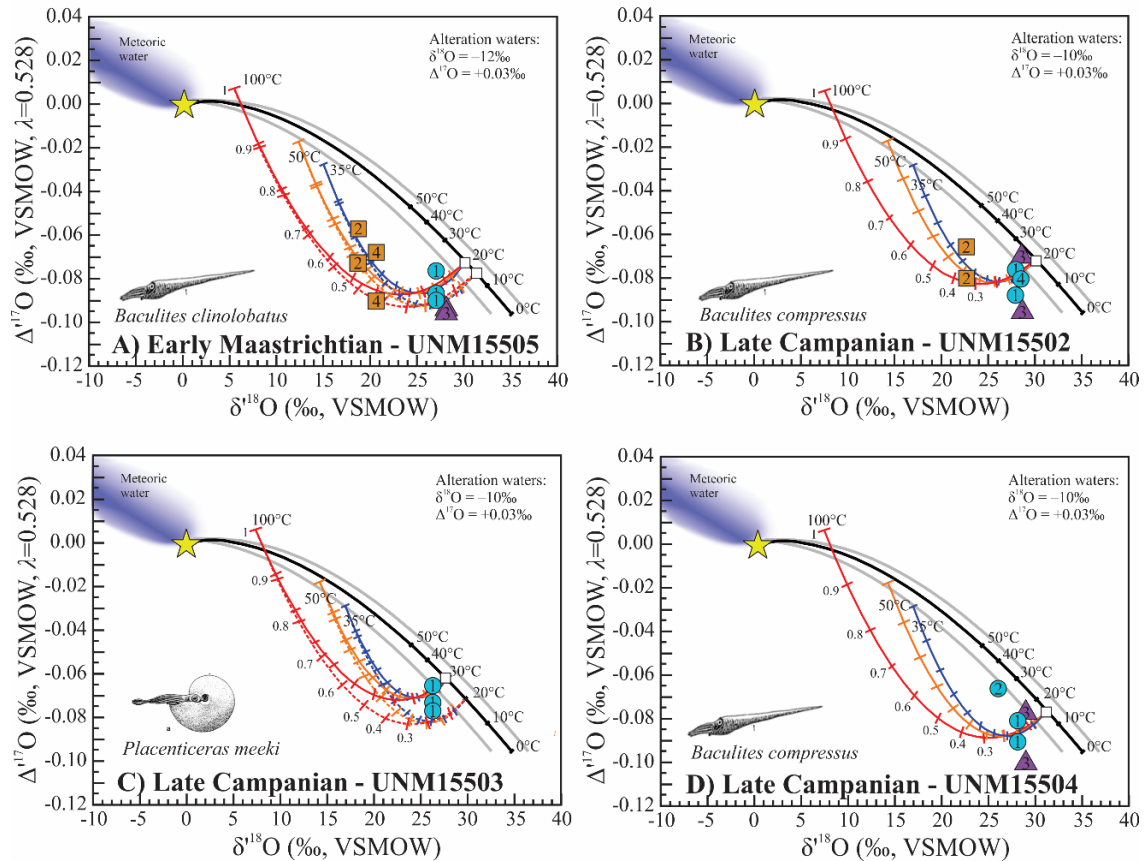


Figure 4.6 - Triple oxygen isotope values of calcite phases in carbonate concretions from the late Cretaceous Western Interior Seaway. Numbers and icons correspond to those in Fig. 2. Carbonate-seawater equilibrium fractionation curve is the black line (when $\delta^{18}\text{O}$ and $\Delta^{17}\text{O} = 0$). The grey lines represent the range of oxygen isotope composition of modern tropic and equatorial waters (-2 to +2 ‰ for $\delta^{18}\text{O}$ values). Fluid-rock interaction pathways are shown at three different temperatures, 35, 50, and 100 °C (blue, orange, red lines, respectively). Assumed alteration fluid is on each figure. A) All calcite phases in the early Maastrichtian concretion suggest alteration has occurred. Initial precipitation temperature is 15 to 20 °C (dotted and solid lines, respectively). B) The shell sample and bulk rock in the late Campanian concretion (UNM15502) are either altered with respect to an ocean with an oxygen isotope value of 0 or in equilibrium with an ocean of ~ -2 ‰. Either way, the temperature of formation is about 20 °C. C) The fossil *Placenticerias meeki* is either altered with respect to an ocean with an oxygen isotope value of 0 or in equilibrium with an ocean of ~ -2 ‰ and formed in 20-30 °C water. D) Most calcite phases in the late Campanian concretion (UNM15504) appear to be altered. The fluid-rock model suggests a primary temperature of formation of ~ 15 °C. UNM15504-2 is a juvenile *Lucinid* sp. bivalve and the triple oxygen isotope composition may preserve a slight vital effect. Alternatively, since it is a fragment, the shell may have been transported to the concretion and initially formed near the shoreline in ~ 30 °C water. (Shell – blue circle; matrix – purple triangle; infill – orange square)

The fluid rock mixing model suggest about 5 °C difference between the environment in which the *Baculites clinolobatus* shell formed and where it fell to rest in the matrix (Figure 4.6A). The calculated triple oxygen isotope composition of the ammonite shell

agrees with habitat reconstruction of *Baculites* sp. that suggest they tend to live in the middle to lower portion of water columns (Tsujiata and E.G. Westermann, 1998).

The *Placenticerias meeki* fossil (UNM15503) was the only calcite phase that could be analyzed in that sample because it was found in the host shale and not in a carbonate concretion. The triple oxygen isotope composition of the fossil suggests potential alteration or equilibrium with a seawater with $\delta^{18}\text{O}$ value of -2‰ and temperature of $\sim 29\text{°C}$ (Figure 4.6C). If the fossil is slightly altered, the fluid-rock mixing model suggests a primary temperature of formation between 20 and 30°C . This is significantly cooler water than the $37\text{--}50\text{°C}$ water previous studies that measured the $\delta^{18}\text{O}$ value of *Placenticerias meeki* shells suggested (Figure 4.7D; Tsujiata and E.G. Westermann, 1998).

Two concretions from the *Baculites compressus* ammonite biozone (late Campanian) contained at least two calcite phases and were analyzed for triple oxygen isotope compositions (UNM15502 and UNM15504). Similar to the late Maastrichtian concretion, most phases appeared to be altered. The calcite infill (UNM15502) had the highest F/R ratio of 0.4 . The matrix and the shells both experienced a very low F/R ratio (0.1 to 0.2 ; Figure 4.6B and Figure 4.6D). The calculated temperature of formation is $\sim 20\text{°C}$, similar to the habitat of the *Baculites clinolobatus* from the early Maastrichtian. Alternatively, the fossil shells and the matrix could have formed in equilibrium with seawater with a $\delta^{18}\text{O}$ value of -2‰ , not unreasonable based on the range of modern $\delta^{18}\text{O}$ values of seawater. Regardless, the habitat that the fossil formed in was about 20°C (Figure 4.6B and Figure 4.6D). The 10°C difference between the temperature of water where the *Placenticerias meeki* and the *Baculites compressus* agrees with studies

suggesting *Placenticer* sp. lived higher in the water column than *Baculites* sp. (Tsujiata and E.G. Westermann, 1998).

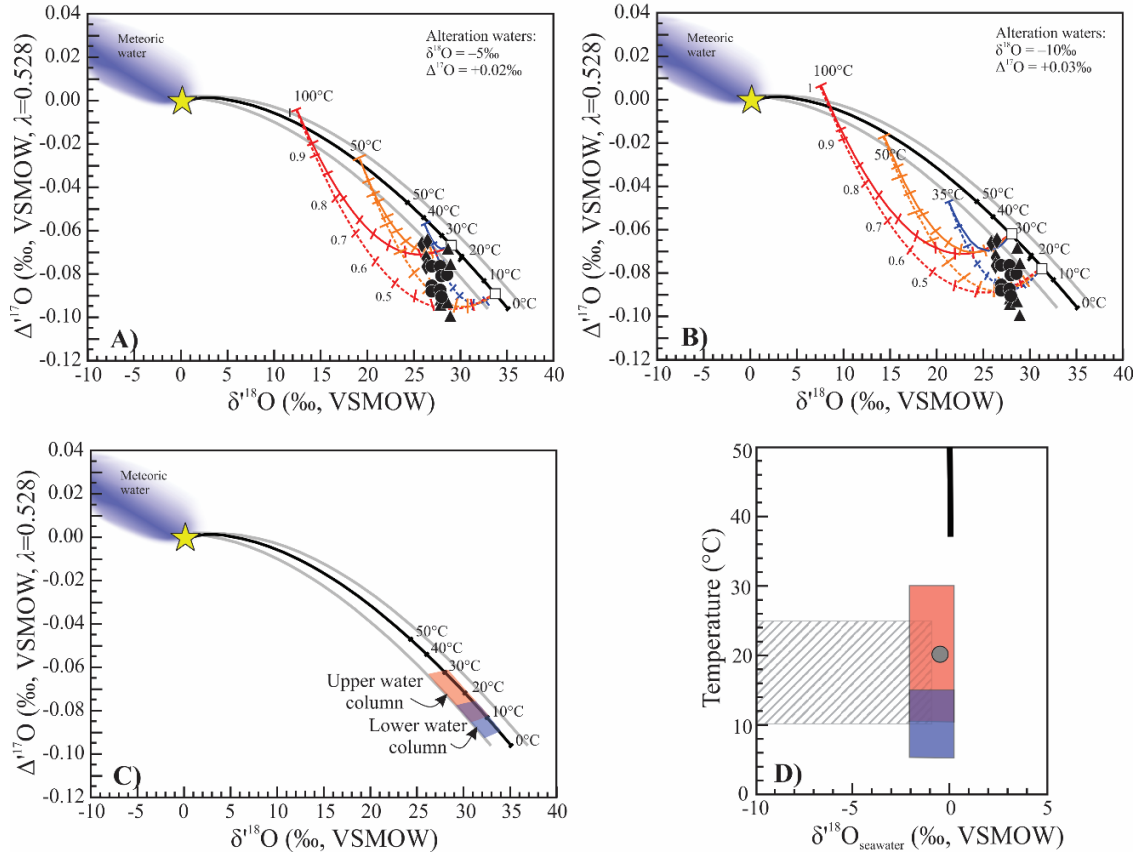


Figure 4.7 – Testing the fluid-rock mixing model sensitivity to alteration fluid oxygen isotope composition and summary of ocean temperature reconstruction. Shell and matrix data were used to test sensitivity (upper water column ammonite – diamonds; lower water column ammonite – circles; matrix – triangles). Infill calcite was omitted to see differences in fluid-rock mixing model outcomes if infill was altered at a different time than the shell and matrix. A) All samples would have to precipitate at 5 °C for the alteration fluid to be -5 ‰. If upper and lower water temperatures differ, then the upper water column’s maximum temperature is 29 °C. B) Same as figure A but with a -10 ‰ alteration fluid. Initial precipitation temperatures are slightly higher with the lower $\delta^{18}\text{O}$ value of the alteration fluid and ranges between 15 and 29 °C. C) Based on this sensitivity test, the range in temperature of the WIS is from 5 to 29 °C. D) Our results compared with the literature. Temperature estimates from this study (red and blue boxes) are larger than other studies (Petersen et al. (2016) – hashed box; Dennis et al. (2013) – gray circle). However, based on the results of our study, the $\delta^{18}\text{O}$ value of the seawater cannot be less than -2 ‰. Our temperature estimates for the upper water column disagree with that of Tsujiata and Westermann (1998) (black solid line).

Table 4.1 - Raw data from late Cretaceous Western Interior Seaway carbonate concretions. All values are reported in ‰ and relative to VSMOW–SLAP. The $\Delta^{17}\text{O}$ values are calculated using a λ of 0.528. Subscript “meas” refers to the values measured by fluorination. Subscript “corr” is the corrected values based on the $\delta^{18}\text{O}$ value obtained by conventional analysis (see methods for more details).

Sample ID ^a	Type	$\delta^{17}\text{O}_{\text{meas}}$	$\delta^{18}\text{O}_{\text{meas}}$	$\Delta^{17}\text{O}_{\text{meas}}$	$\delta^{17}\text{O}_{\text{corr}}^{\text{b}}$	$\delta^{18}\text{O}_{\text{corr}}$	$\delta^{13}\text{C}$ (PDB)
<i>Early Maastrichtian</i>							
UNM15505-1-1	shell	13.6905	26.2555	-0.086	14.33	27.48	-6.2
UNM15505-1-2	shell	13.6403	26.1400	-0.077	14.34	27.48	
UNM15505-1-3	shell	13.8392	26.5454	-0.089	14.32	27.48	
	avg.	13.7233	26.3136	-0.084			
	±1 S.D.	0.1034	0.2089	0.006			
UNM15505-2-1	infill	9.3540	17.9289	-0.072	9.90	18.97	-13.3
UNM15505-2-2	infill	8.7561	16.7587	-0.057	9.91	18.97	
	avg.	9.0551	17.3438	-0.065			
	±1 S.D.	0.4227	0.8275	0.010			
UNM15505-3-1	host	13.1308	25.1972	-0.094	14.86	28.51	-19.6
UNM15505-3-2	host	13.0929	25.1214	-0.092	14.86	28.51	
	avg.	13.1119	25.1593	-0.093			
	±1 S.D.	0.0268	0.0536	0.001			
UNM15505-4-1	infill	10.6910	20.5190	-0.090	10.83	20.78	-18.2
UNM15505-4-2	infill	10.2004	19.5385	-0.068	10.85	20.78	
	avg.	10.4457	20.0288	-0.079			
	±1 S.D.	0.3469	0.6933	0.016			
<i>Late Campanian</i>							
UNM15502-1-1	shell	13.6449	26.1482	-0.076	14.83	28.43	-3.3
UNM15502-1-2	shell	14.3142	27.4548	-0.088	14.82	28.43	
	avg.	13.9795	26.8015	-0.082			
	±1 S.D.	0.4733	0.9239	0.008			
UNM15502-2-1	infill	11.8491	22.7158	-0.080	12.01	23.03	-13.6
UNM15502-2-2	infill	11.6831	22.3700	-0.066	12.03	23.03	
	avg.	11.7661	22.5429	-0.073			
	±1 S.D.	0.1174	0.2445	0.010			
UNM15502-3-1	host	13.4027	25.7177	-0.094	15.21	29.19	-20.5
UNM15502-3-2	host	12.9738	24.8475	-0.069	15.24	29.19	
	avg.	13.1883	25.2826	-0.081			
	±1 S.D.	0.3033	0.6153	0.017			
UNM15502-4-1	shell	13.9173	26.6789	-0.081	15.13	29.01	-6.6
UNM15503-1-1	shell	12.5509	24.0298	-0.065	14.01	26.82	-5.4
UNM15503-1-2	shell	12.5557	24.0541	-0.073	14.00	26.82	
UNM15503-1-3	shell	12.5391	24.0308	-0.077	13.99	26.82	
	avg.	12.5486	24.0383	-0.072			
	±1 S.D.	0.0085	0.0138	0.006			
UNM15504-1-1	shell	12.8193	24.5465	-0.066	13.83	26.48	-6.4
UNM15504-2-1	shell	14.0769	27.0061	-0.091	14.93	28.65	-3.8
UNM15504-2-2	shell	13.3850	25.6594	-0.081	14.94	28.65	
	avg.	13.7310	26.3327	-0.086			
	±1 S.D.	0.4892	0.9522	0.007			
UNM15504-3-1	host	13.6510	26.1594	-0.076	15.40	29.51	-18.3
UNM15504-3-2	host	14.0005	26.8750	-0.099	15.37	29.51	
	avg.	13.8257	26.5172	-0.088			
	±1 S.D.	0.2471	0.5060	0.016			

^a-Sample ID is in format: sample name – number – iteration

^b- $\delta^{17}\text{O}_{\text{corr}}$ is calculated using linearized values ($\delta^{17}\text{O}=\Delta^{17}\text{O}+0.528\delta^{18}\text{O}$) and is then delinearized.

Considering that the calcite infill may have formed at a different time than the initial alteration of the matrix and shell material, we applied the fluid-rock mixing ratio to the sample set with the infill samples removed (Figure 4.7). Using two different alteration fluids (-5 and -10 ‰ for $\delta^{18}\text{O}$ values) provided a range of primary precipitation temperatures (Figure 4.7A and Figure 4.7B). Any alteration fluid with a $\delta^{18}\text{O}$ value higher than -5 ‰ or lower than -10 ‰ cannot fit all the data. Each fluid-rock mixing model was run twice for each $\delta^{18}\text{O}$ value to represent the idea that the upper water column species (*Placenticerias meeki*) may have different formation temperatures than the lower water species (*Baculites sp.*) and the matrix. In summary, the data suggest that *Placenticerias meeki* may have lived in waters with a temperature up to ~ 29 °C (Figure 4.7C and Figure 4.7D). The lower water column could not have exceeded 15 °C (Figure 4.7C and 4.7D). Additionally, the results of the dataset constrain the $\delta^{18}\text{O}$ value of the Western Interior Seaway to no lower than -2 ‰.

Two studies have presented Δ_{47} measurements of the shells of ammonites from similar sites as this study (Dennis et al., 2013; Petersen et al., 2016). In the offshore environment of the Pierre Shale formation, the studies generally agree on the temperature of the Western Interior Seaway, but disagree on the $\delta^{18}\text{O}$ value of the seawater. Petersen et al. (2016) suggests that the $\delta^{18}\text{O}$ value of the seawater is between -4 and -1 ‰, corresponding to a temperature between 10 and 25 °C. Additionally, Petersen et al. (2016) classifies a few sites in the Pierre Shale formation as “estuarine”. The Δ_{47} values of the shells from the estuarine sites suggest a $\delta^{18}\text{O}$ value of the water between -10 to -2 ‰ and a temperature of about 15 °C. Dennis et al. (2013) also classifies the Pierre Shale formation as an offshore site and suggest an average temperature of 20.7 °C and seawater

with a $\delta^{18}\text{O}$ value of -0.4‰ . The fluid-rock mixing model of this study suggests an alteration fluid with a $\delta^{18}\text{O}$ value of about -10‰ , suggesting that perhaps the estuarine sites in Petersen et al. (2016) were altered, rather than preserving estuarine conditions in the offshore site. The data suggests that the late Cretaceous Western Interior Seaway had a $\delta^{18}\text{O}$ value between -2 and 0‰ . The water column may have been potentially thermally stratified where the upper most layer had a temperature of $\sim 30^\circ\text{C}$ while the middle and bottom water had a temperature between 15 and 20°C . It is important to note, that while most studies try to find the most pristine carbonates to reconstruct the paleoenvironments, we used samples that were altered and came to similar conclusions of the paleoenvironment of the Western Interior Seaways as other studies. This means that paleoenvironmental information can still be found in altered rocks, an important conclusion for exposures with poor preservation.

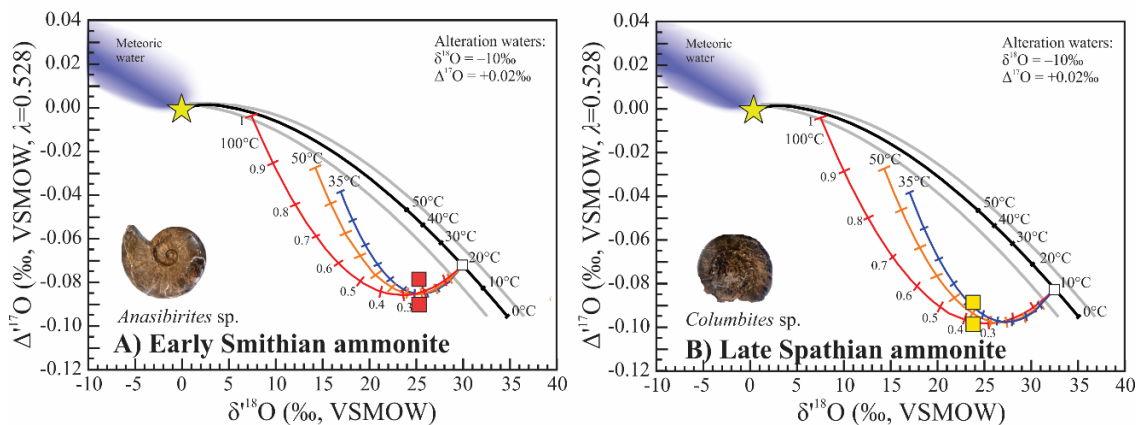


Figure 4.8 - Triple oxygen isotope values of early Smithian (A) and late Spathian (B) ammonite fossils. Both samples have triple oxygen isotope values that cannot be in equilibrium with reasonable ocean oxygen isotope compositions and suggest alteration. We back-calculated each fossil's primary triple oxygen isotope composition using the fluid-rock mixing model. If these samples represent bulk or regional ocean temperatures, it appears that Smithian ocean was about 10°C warmer than Spathian seawater.

4.5.2 Early Triassic ammonites

Two ammonites, one from the Smithian and one from the Spathian were analyzed for triple oxygen isotope values. Neither fossil preserved initial colorings and are

assumed to be altered (Figure 4.3C). The early Smithian ammonite (*Anasibirites* sp.) had $\delta^{18}\text{O}$ and $\Delta^{17}\text{O}$ values that were 1.6 and 0.010 ‰ higher than the late Spathian ammonite (*Columbites* sp.; Table 4.2). Both samples have triple oxygen isotope compositions that do not indicate equilibrium precipitation in seawater similar to modern. A fluid-rock mixing model with an alteration fluid $\delta^{18}\text{O}$ value of -10‰ and a $\Delta^{17}\text{O}$ value of 0.02‰ allows us to back-calculate the primary temperature of formation if we assume the ocean in the early Triassic was similar to modern (Figure 4.8). The temperature of formation is 20 °C for the Smithian ammonite and 10 °C for the Spathian ammonite. Using the $\delta^{18}\text{O}$ values of conodont apatite, two studies (Sun et al., 2012; Romano et al., 2013) suggest a cooling from the Smithian to the Spathian of 7.5 °C and 10 °C , respectively. However, Sun et al. (2012) suggest 20 °C warmer oceans than the triple oxygen isotope values suggest.

This would result in a 40 °C ocean during the Smithian, too hot for ammonite

Table 4.2 - Raw data from the early Triassic sample suite. All values are reported in ‰ and relative to VSMOW–SLAP. The $\Delta^{17}\text{O}$ values are calculated using a λ of 0.528. Subscript “meas” refers to the values measured by fluorination. Subscript “corr” is the corrected values based on the $\delta^{18}\text{O}$ value obtained by conventional analysis (see methods for more details).

Sample ID	$\delta^{17}\text{O}_{\text{meas}}$	$\delta^{18}\text{O}_{\text{meas}}$	$\Delta^{17}\text{O}_{\text{meas}}$	$\delta^{17}\text{O}_{\text{corr}}^{\text{a}}$	$\delta^{18}\text{O}_{\text{corr}}$
Ammonites					
Smithian 1	12.3908	23.7717	-0.090	13.43	25.77
Smithian 2	12.6328	24.2128	-0.078	13.44	25.77
avg.	12.5118	23.9922	-0.084		
±1 S.D.	0.1711	0.3119	0.008		
Spathian 1	12.3718	23.7527	-0.099	12.56	24.12
Spathian 2	11.8847	22.8006	-0.089	12.57	24.12
avg.	12.1283	23.2766	-0.094		
±1 S.D.	0.3444	0.6732	0.007		
Bulk Rock					
CowboyPass 1	10.8317	20.7354	-0.063	22.00	11.49
CowboyPass 2	11.2467	21.5384	-0.068	22.00	11.49
avg.	11.0392	21.1369	-0.065		
±1 S.D.	0.2935	0.5679	0.003		
MineralMtn 1	10.1636	19.5102	-0.090	19.53	10.17
MineralMtn 2	9.3376	17.8990	-0.073	19.53	10.19
avg.	9.7506	18.7046	-0.081		
±1 S.D.	0.5841	1.1393	0.012		
KaibabGulch 1	13.0808	25.0729	-0.079	26.60	13.87
KaibabGulch 2	13.1968	25.3149	-0.089	26.60	13.86
avg.	13.1388	25.1939	-0.084		
±1 S.D.	0.0820	0.1711	0.007		

^a- $\delta^{17}\text{O}_{\text{corr}}$ is calculated using linearized values ($\delta^{17}\text{O} = \Delta^{17}\text{O} + 0.528\delta^{18}\text{O}$) and is then delinearized.

survival. The reason for the discrepancy between temperatures calculated using carbonate triple oxygen isotope vs. apatite $\delta^{18}\text{O}$ values is unknown and beyond the scope of this study but warrant further investigation.

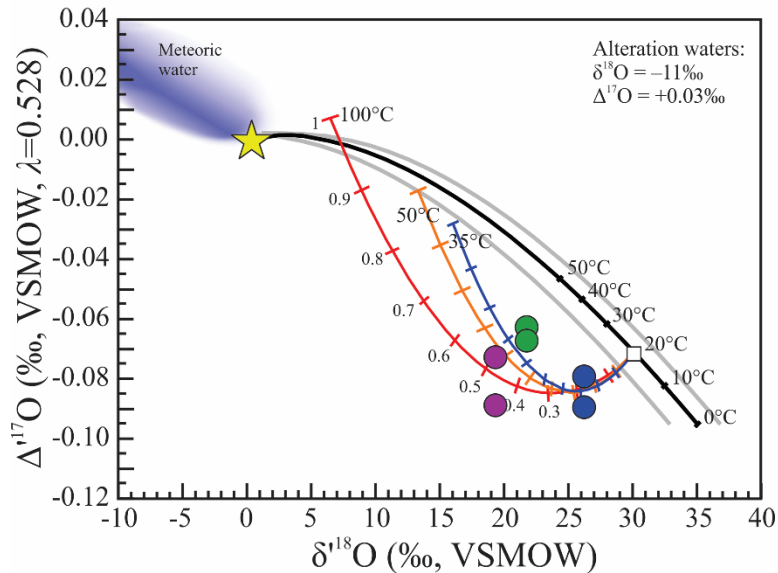


Figure 4.9 - Triple oxygen isotope values of bulk rock from the Early Triassic. Sample are from different regions but contemporaneous. All sample are altered and do not have a triple oxygen isotope composition that is in equilibrium with modern seawater (black and grey lines). A fluid-rock mixing model with similar alteration water suggests that the carbonate initially formed in 20 °C water. The Cowboy Pass sample (green circle) and the Mineral Mountain sample (purple circle) experienced different temperatures of alteration. The Kaibab Gulch sample (blue circle) plots along the alteration pathways that makes the alteration temperature ambiguous.

4.5.3 Early Triassic bulk rock

Contemporaneous (early Smithian) bulk carbonate from three different regions had triple oxygen isotope compositions that were different from one another and could not have formed in equilibrium with seawater similar to modern (Figure 4.9). Mineral Mountain and Kaibab Gulch samples had similar $\Delta^{17}\text{O}$ values (-0.081 and -0.083 ‰, respectively), about 0.015 ‰ lower than the Cowboy Pass sample (Table 4.2). The $\delta^{18}\text{O}$ values were some of the lowest measured out the entire sample suite of this study ranging from 19.5 ‰ to 26.6 ‰. The early Triassic ocean would need to have a $\delta^{18}\text{O}$ value of *at least* -6 ‰ if these samples were not altered. An ocean with a $\delta^{18}\text{O}$ value of -6 ‰ is

outside of the modern range of $\delta^{18}\text{O}$ values except at the poles where fresh water with a $\delta^{18}\text{O}$ value of about -55‰ lowers the $\delta^{18}\text{O}$ value of the immediate seawater (Schmidt et al., 1999). This is highly unlikely in the hot early Triassic climate. Instead, we suggest that meteoric water has altered most of the bulk rock in this region after deposition. An alteration fluid with a $\delta^{18}\text{O}$ value of -11‰ and $\Delta^{17}\text{O}$ value of 0.030‰ can explain all the data using the fluid-rock mixing model (Figure 4.9). The Kaibab Gulch carbonate experienced the lowest F/R ratio (0.2 to 0.3). The Cowboy Pass sample experienced the highest F/R ratio (0.7) but a low temperature of alteration (below 35 °C). Lastly, the Mineral Mountain sample experienced a F/R ratio of 0.5 and 100 °C during alteration. The Kaibab Gulch sample plots along the alteration pathway that makes the temperature of alteration ambiguous. If we assume that this bulk rock formed in similar seawater as the Smithian/Spathian ammonites from the previous section, then the bulk rock formed at about 20 °C . The extensive alteration in this region may have unknown implications on the conodont record. Although there is a preservation index for conodont isotope analyses, perhaps more consideration on the host rock is important. If carbonate that appears pristine (e.g., Phanerozoic brachiopods from Chapter 2), are in fact altered, then perhaps conodonts that appear pristine also experienced some level of alteration, resulting in anomalously high temperature estimates (e.g., Sun et al., 2012; Romano et al., 2013). This may be more evident in bulk rock that experienced high F/R ratios like the Mineral Mountain and Cowboy Pass samples.

4.5.4 Hirnantian glaciation (late Ordovician) carbonate samples

Calcite from rugose coral, the infill of rugose coral voids, and the host rock were all analyzed for triple oxygen isotope values (Table 4.3). The sample from before the

unconformity (LF13) has two phases analyzed, the host rock and the calcite of the rugose coral. The host rock has a triple oxygen isotope composition that is in equilibrium with seawater with a similar oxygen isotope composition as modern and formed in $\sim 25^\circ\text{C}$ water (Figure 4.10A). The rugose coral has a high $\delta^{18}\text{O}$ value and negative $\Delta^{17}\text{O}$ value, suggesting it formed in much colder water. The measured triple oxygen isotope composition of the rugose coral does not suggest formation in seawater similar to modern

(Figure 4.9A). Either rugose coral has a vital effect and does not form in equilibrium with

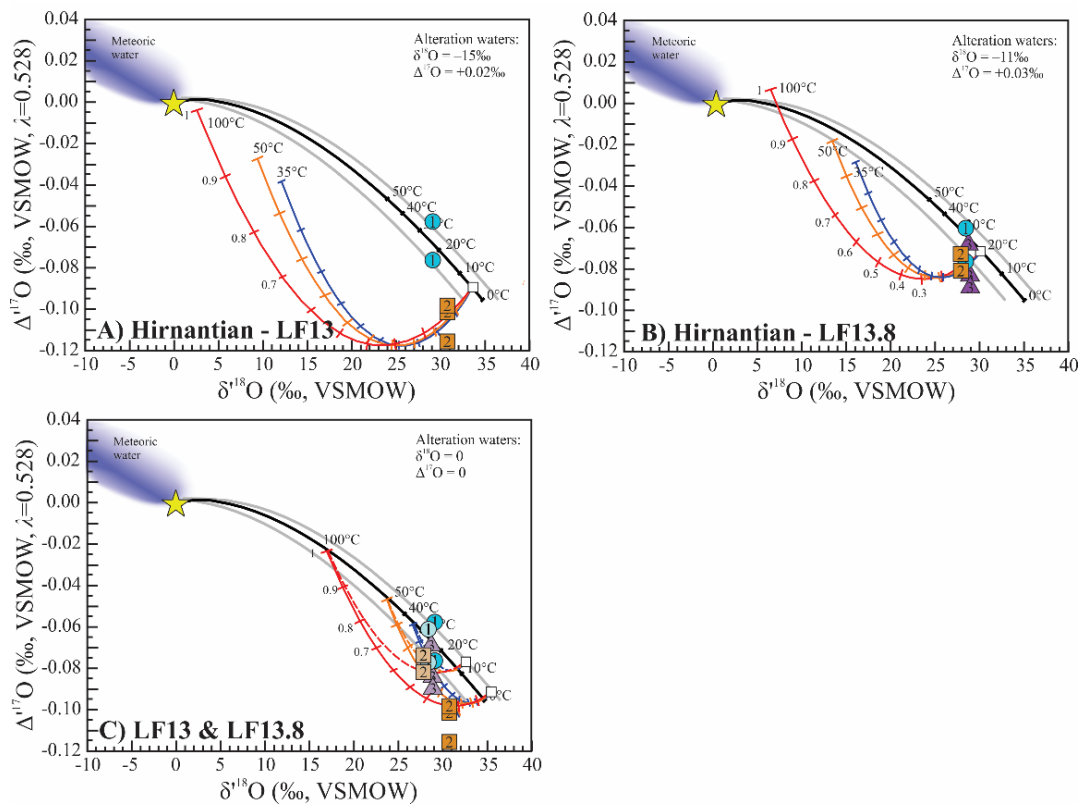


Figure 4.10 - Triple oxygen isotope values of host rock and rugose coral from the Laframboise member, Anticosti Island, Canada. Both samples formed during the Hirnantian glaciation event. Numbers correspond to sample ID in Table 3 and Figure 4. A) Sample LF13 formed below the prominent unconformity of the Laframboise member. The host rock's triple oxygen isotope composition (blue circle) suggests the seawater it formed in is similar to modern and the temperature was between 20 and 30 °C. The rugose coral appears to be altered and in initial temperature of formation is cooler than expected ($\sim 5^\circ\text{C}$). B) Sample LF13.8 formed just above the unconformity. All phases appear to preserve a triple oxygen isotope composition that suggests they formed in equilibrium with a seawater similar to modern and temperature between 20 and 30 °C. If slight alteration occurred, the temperature of formation would not change. C) Reconstructing alteration pathways with an ocean $\delta^{18}\text{O}$ value of -2‰ . Both sets of samples (LF13 – dark colors; LF13.8 – pastel colors) are plotted. An alteration fluid of 0 fits all of the data if the initial precipitation temperature was 3 °C. If the LF13 rugose coral (dark orange square) is not representative of the rest of the samples, the warmest temperature of formation is 15 °C.

the water in which it formed, or this rugose coral has experienced some level of alteration. A fluid-rock mixing model with an alteration fluid of -15‰ for $\delta^{18}\text{O}$ and 0.020‰ for $\Delta^{17}\text{O}$ provides for a calculation of the initial deposition temperature of 5°C . This is cooler than most estimates for the Hirnantian glaciation interval (Trotter et al., 2008; Finnegan et al., 2011; Bergmann et al., 2018).

Calcite from the rugose coral skeleton, the infill from the rugose coral voids, and the host rock were analyzed for triple oxygen isotope analyses from a sample just after the unconformity (LF13.8; Figure 4.10B). All samples have triple oxygen isotope values that suggest formation in equilibrium with an ocean similar to modern (-2 to 0‰) and in 20 to 30°C water. The LF13.8 sample may have preserved its original oxygen isotope composition and Hirnantian seawater was between 20 and 30°C with a $\delta^{18}\text{O}$ value of seawater between -2 and 0‰ . This is in direct contradiction to the rugose coral triple oxygen isotope values from sample LF13 (Figure 4.10). We do not know how to address the discrepancy but does warrant further investigation into the variability in the stable isotope compositions of rugose corals. The results from sample LF13.8 are in line with most literature temperature estimates of Hirnantian seawater ranging from 22 to greater than 50°C (Trotter et al., 2008; Finnegan et al., 2011; Bergmann et al., 2018).

Two studies have measured the Δ_{47} values of host rock, brachiopods, and rugose coral from the Hirnantian glaciation (Finnegan et al., 2011; Bergmann et al., 2018). Both studies suggest the temperature of Hirnantian seawater was between 30 and 50°C and the $\delta^{18}\text{O}$ of the ocean was between $+2$ and $+4\text{‰}$. However, if the samples used in their study experienced any alteration, the $\delta^{18}\text{O}$ may not have changed significantly but

Table 4.3 - Raw data from the Hirnantian glaciation (late Ordovician) sample suite. All values are reported in ‰ and relative to VSMOW–SLAP. The $\Delta^{17}\text{O}$ values are calculated using a λ of 0.528. Subscript “meas” refers to the values measured by fluorination. Subscript “corr” is the corrected values based on the $\delta^{18}\text{O}$ value obtained by conventional analysis (see methods for more details).

Sample ID ^a	Type	$\delta^{17}\text{O}_{\text{meas}}$	$\delta^{18}\text{O}_{\text{meas}}$	$\Delta^{17}\text{O}_{\text{meas}}$	$\delta^{17}\text{O}_{\text{corr}}^{\text{b}}$	$\delta^{18}\text{O}_{\text{corr}}$
LF13 1 1	host	13.2655	25.4204	-0.076	15.33	29.37
LF13 1 2	host	13.1684	25.1985	-0.057	15.34	29.37
	avg.	13.2170	25.3094	-0.067		
	±1 S.D.	0.0687	0.1569	0.013		
LF13 2 1	coral	15.1472	29.0789	-0.101	16.21	31.13
LF13 2 2	coral	14.9498	28.6966	-0.099	16.21	31.13
LF13 2 3		15.5936	29.9671	-0.117	16.20	31.13
	avg.	15.2302	29.2475	-0.106		
	±1 S.D.	0.3298	0.6518	0.010		
LF13.8 1 1	host	12.2068	23.3617	-0.060	15.07	28.86
LF13.8 1 2	host	13.0218	24.9558	-0.077	15.06	28.86
	avg.	12.6143	24.1587	-0.069		
	±1 S.D.	0.5763	1.1273	0.012		
LF13.8 2 1	coral	13.2784	25.4391	-0.073	14.74	28.24
LF13.8 2 2	coral	13.6156	26.0995	-0.080	14.73	28.24
	avg.	13.4470	25.7693	-0.076		
	±1 S.D.	0.2384	0.4670	0.005		
LF13.8 3 1	infill	14.1139	27.0701	-0.088	15.21	29.17
LF13.8 3 2	infill	14.1349	27.0721	-0.068	15.23	29.17
LF13.8 3 3	infill	14.2529	27.3251	-0.082	15.21	29.17
	avg.	14.1672	27.1558	-0.079		
	±1 S.D.	0.0749	0.1467	0.010		

^a-Sample ID is in format: sample name – number – iteration

^b- $\delta^{17}\text{O}_{\text{corr}}$ is calculated using linearized values ($\delta^{17}\text{O}=\Delta^{17}\text{O}+0.528\delta^{18}\text{O}$) and is then delinearized.

the temperature of alteration could reorder the Δ_{47} values (e.g., Henkes et al., 2014). This may result in a Δ_{47} value that is decoupled with the $\delta^{18}\text{O}$ value of the carbonate and result in a higher $\delta^{18}\text{O}$ value of the ocean calculated from the temperature and $\delta^{18}\text{O}$ value obtained from Δ_{47} measurements. If the ocean was $\sim+2\text{‰}$ during the Hirnantian glaciation, all samples would appear to have been altered based on the measured triple oxygen isotope values (Figure 4.9C). To fit all the data, the alteration fluid has to be ~ 0 and the initial temperature of formation was $\sim 3^\circ\text{C}$. If the rugose coral (LF13.2) formed under different conditions than the remaining samples, then the warmest temperature of formation that can be reconstructed using the fluid-rock mixing model is 15°C . We cannot reconcile a heavier ocean *and* a temperature $>20^\circ\text{C}$ that is suggested by Δ_{47} studies.

4.6 Conclusions

The goal of this study was to apply the fluid-rock mixing model to a suite of samples expected to have experienced diagenesis. We focused on samples that had multiple calcite phases to better constrain alteration history. We found that triple oxygen isotope values of altered rocks can be used to estimate the initial formation environments. Our temperature estimates in the Western Interior Seaway agree with most clumped isotope measurements but disagree with the $\delta^{18}\text{O}$ value of the water. We think that the clumped isotope measurements could be recording some alteration fluid in samples that experience low F/R ratios. The early Triassic exposures have experienced extensive regional level alteration that has altered the carbonate triple oxygen isotope composition of bulk rock and ammonite fossils. Conodont apatite, although thought to be more resistant to alteration than carbonate, might not be pristine and would explain the “lethally” hot temperatures suggested during the Smithian thermal excursion. Lastly, the sample suite from the Hirnantian glaciation appears to be the most pristine carbonate samples in this study. Temperature estimates for the Hirnantian glaciation are reasonable and equal to or lower than estimates based on Δ_{47} values. Our data cannot reasonably exclude a heavy ocean during the extensive glaciation, but the data does support an ocean with a similar isotopic composition as modern seawater. Overall, this study demonstrates the ability for triple oxygen isotope measurements to see through diagenesis, especially in rocks that have experience very low F/R ratios (as low as 0.2). Although the sample suite from each time interval is small, there is compelling evidence in each that warrants a more detailed study to better investigate changing ocean conditions through time.

4.7 Acknowledgements

Corrine Myers and James Witts provided the carbonate concretions from the Western Interior Seaway. Viorel Atudorei provided the early Triassic ammonites through a donation from Jim Jenks. Viorel Atudorei provided the early Triassic bulk carbonate. Maya Elrick provided the Hirnantian samples.

5. TRIPLE OXYGEN ISOTOPES IN THE SILICA–WATER AND CARBONATE–WATER SYSTEM

5.1 Introduction

The field of stable isotope geochemistry began with the recognition that the isotopic composition of ancient carbonates could be used as a paleothermometer (Urey, 1947; Urey et al., 1951). As stated by Urey (1947) “*Accurate determinations of the O^{18} content of carbonate rocks could be used to determine the temperature at which they were formed*”. This concept was based on the temperature dependence for the oxygen isotope fractionation between calcite and water. Urey realized that if a mass spectrometer with sufficient precision could be built, a method of reproducibly extracting oxygen from solid carbonate could be developed, and the isotope fractionations were quantified, then the oxygen isotope composition of ancient carbonates could be used to determine the temperature of their formation.

This idea led to the carbonate–water temperature scale (McCrea, 1950; Epstein et al., 1951; Urey et al., 1951; Epstein et al., 1953). The oxygen isotope compositions of marine carbonates increase with decreasing formation temperature, so that ancient ocean temperatures could be determined. Urey (1951) recognized the potential problems with the carbonate thermometer. These include the following: 1) the possibility that organisms form out of oxygen isotope equilibrium, a term he called the ‘*vital effect*’; 2) the possibility that shells might not preserve their oxygen isotope composition over geological time and undergo some sort of diagenesis; and 3) the uncertainty in the estimate of the oxygen isotope composition of the formation water. To this last point, the isotopic composition of the ancient ocean is estimated, not measured directly. What is the possibility that the ocean has changed its oxygen isotope composition through time? Urey

concluded that any significant changes would have occurred before the Cambrian, although he states that *'it is a conclusion based on little more than prejudice'*. In spite of these caveats, the carbonate paleothermometer has been immensely successful and applied in many thousands of studies. The concerns raised by Urey, however, remain, despite numerous efforts to ascertain diagenesis, quantify any changes in the ocean oxygen isotope composition through time, and develop additional mineral-water paleothermometers (such as silica-water paleothermometry). Recently, the rare ^{17}O isotope has been included in paleoclimate studies. With the addition of this new independent variable, we can determine if diagenesis occurred and evaluate potential variations in the oxygen isotope composition of ancient seawater.

This chapter reviews the current literature to date on the triple oxygen isotope fractionation between silica-water and carbonate-water. It starts with an overview of mineral-water thermometers. An overview of both equilibrium and disequilibrium fractionation as given through theory, empirical calibrations, and laboratory experiments is provided. Application of these different fractionation regimes to geologic samples is then addressed. A brief overview is provided of how the silica-water and calcite-water triple oxygen isotope fractionation curve can be used to reconstruct past seawater oxygen isotope values. The chapter concludes by presenting the triple oxygen isotope fractionation between silica-calcite.

5.2 Mineral–water oxygen isotope thermometers

5.2.1 $^{18}\text{O}/^{16}\text{O}$ fractionation

Oxygen isotope paleothermometers are based on the temperature dependent fractionation between authigenic minerals and their formation water. For marine sediments, we generally assume that the formation water is seawater and that the oxygen

isotope composition of the seawater has not varied through time. Obviously, this is a critical assumption that has been questioned and evaluated extensively and is discussed later in this chapter. Oxygen isotope paleothermometers have been developed for carbonates, silicates, phosphates and sulfates. This chapter addresses only the silica–water and carbonate–water paleotemperature equations. It begins with an overview of the generic $^{18}\text{O}/^{16}\text{O}$ thermometer.

The first calibration of the calcite–water oxygen isotope thermometer took the form (Epstein et al., 1951; Epstein et al., 1953)

$$t(^{\circ}\text{C}) = 16.5 - 4.3\delta + 0.14\delta^2 \quad 5.1).$$

In this equation δ is the isotopic composition of the CO_2 evolved from the carbonate relative to the δ value of CO_2 evolved from a reference carbonate (Peedee belemnite or PDB). The $\delta^{18}\text{O}$ value is defined, in per mil notation, as

$$\delta^{18}\text{O} = \left(\frac{R_{sa}}{R_{std}} - 1 \right) \times 1000 \quad 5.2)$$

where R is the $^{18}\text{O}/^{16}\text{O}$ ratio of the sample (*sa*) and standard (*std*). A similar equation can be written for the $\delta^{17}\text{O}$ value, in which case R is the $^{17}\text{O}/^{16}\text{O}$ value.

Equation 5.1 is simply a quadratic best fit equation to empirical data. It is not based on any theoretical considerations. Bigeleisen and Goepfert Mayer (1947) showed that the log of the equilibrium fractionation between diatomic molecules should be proportional to T^{-1} and T^{-2} (in Kelvin) at low and high temperatures, respectively. The system becomes more complicated with more complex phases, especially when water is considered (Criss, 1991). Empirical data are often fit to $1/T$, $1/T^2$ or a combination of these two. In mineral–water fractionation equations, a constant is often included as a

consequence of the high vibrational frequencies of water (Bottinga and Javoy, 1973). An appropriate fit to the temperature dependence of fractionation between phase i and water is given by:

$$1000 \ln \alpha_{i-H_2O} = \frac{a \times 10^6}{T^2} + c \quad (5.3).$$

Here $\alpha_{A-B} = \frac{R_A}{R_B}$ and in delta notation $\alpha_{A-B} = \frac{1000 + \delta_A}{1000 + \delta_B}$. The justification of using the

form of equation 5.3 is apparent when we consider actual data. Figure 5.1 shows experimental and empirical fractionation data for quartz–water and calcite–water as a function of $1/T^2$. The data are approximated by a linear fit and a y intercept (the c term in equation 5.3) of -3.4 ‰ (quartz) and -2.95 ‰ (calcite) (Figure 5.1A). Obviously, this relationship fails at very high temperatures, where the $1000/\ln \alpha$ must approach zero. A better fit is obtained if we use a polynomial of $1/T^2$ as predicted from theory (Clayton and Kieffer, 1991). A polynomial fit for quartz–water and calcite–water is shown in Figure 1B. The constant is 0 in these fits so that $1000/\ln \alpha$ goes to infinity at infinite temperatures. Both curves have the same general sigmoidal form, indicating that the constant in

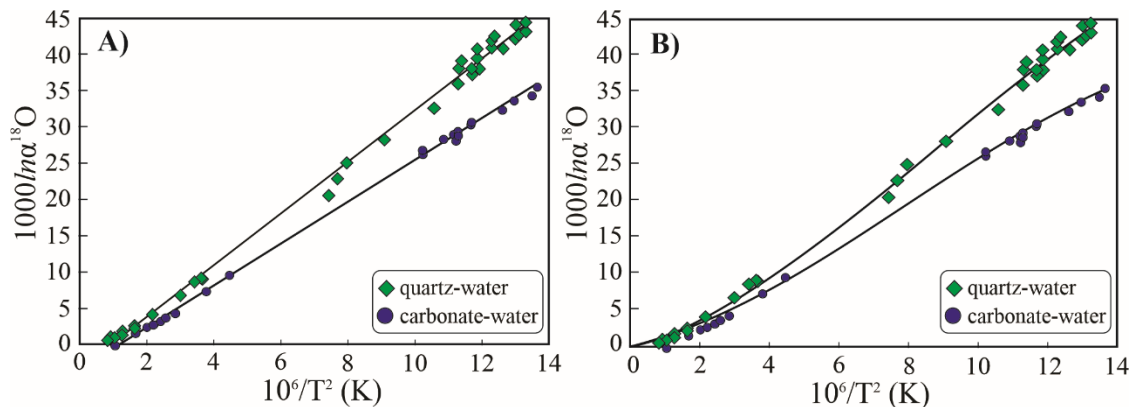


Figure 5.1 - Quartz-water (green diamond) and calcite-water (blue circle) oxygen isotope fractionation. A) Best fit using Eq. 5.3 ($a \times 10^6/T^2 + c$) with a negative y-intercept. B) Best fit using Eq. 5.5 ($a \times 10^6/T^2 + b \times 10^3/T$) and a y-intercept of zero. Based on residuals, the quartz-water data are better approximated by Eq. 5.5 (Fig. 1B), whereas the calcite-water data is better fit by Eq 5.3. Higher order polynomial fits are not warranted, as the errors in the coefficients become very large.

equation 5.3, which is likely valid at lower temperatures (e.g., Bottinga and Javoy, 1973) must decrease with increasing temperature.

An alternative form for mineral–water fractionation is to add a $1/T$ term to the equation (Zheng, 1991):

$$1000 \ln \alpha_{i-H_2O} = \frac{a \times 10^6}{T^2} + \frac{b \times 10^3}{T} + c \quad 5.4).$$

The constant in equations 5.3 and 5.4 lead to equations that are not valid at high temperatures because $1000 \ln \alpha$ approaches 0, and not c , at infinite temperatures. An alternative expression, then, is to fit the data to a polynomial of $1/T$, such as

$$1000 \ln \alpha_{i-H_2O} = \frac{a \times 10^6}{T^2} + \frac{b \times 10^3}{T} \quad 5.5).$$

The quartz–water system has been experimentally and empirically studied over a uniquely wide temperature range. Quartz–water exchange experiments have been made between 250 °C and 800 °C (see Sharp et al., 2016 for a compilation). Low temperature empirical fractionation of diatoms and abiogenic silica have been measured over the temperature range 0 to close to 100 °C. All low– and high–temperature fractionation data can be fit to equation 5 where $a = 4.28 \pm 0.07$ and $b = -3.5 \pm 0.2$ ($R^2 = 0.9978$) (Sharp et al., 2016). Eliminating the c constant (Equation 5.5) allows for the fractionation equation to be extrapolated to infinite temperature. In contrast, calcite-water experimental and empirical data are better fit to the form of equation 5.3 up to ~ 1000 K (O'Neil et al., 1969; Wostbrock et al., 2020a). This paper uses the general form of equation 5.4. Based only on fitting published fractionation data, the c term is set to zero for quartz-water, whereas for calcite-water fractionation, the b term is set equal to zero.

5.2.2 Triple oxygen isotope fractionation

The equilibrium fractionation of $^{17}\text{O}/^{16}\text{O}$ relative to $^{18}\text{O}/^{16}\text{O}$ between two phases A and B is given by the equation

$$\alpha^{17}\text{O}_{A-B} = \left(\alpha^{18}\text{O}_{A-B}\right)^{\theta} \quad 5.6).$$

In a linearized format, where $\delta' = 1000\ln(\delta/1000+1)$ (Hulston and Thode, 1965; Miller, 2002), $\delta'_A - \delta'_B = 1000\ln\alpha_{A-B}$ and equation 5.6 can be recast as

$$\delta'^{17}\text{O}_A - \delta'^{17}\text{O}_B = \theta(\delta'^{18}\text{O}_A - \delta'^{18}\text{O}_B) \quad 5.7).$$

The θ value varies with temperature ranging from 0.5305 at $T = \infty$ to 0.524 at $T = 298$ K for quartz–water (Cao and Liu, 2011; Sharp et al., 2016; Hayles et al., 2018) to as low as 0.518–0.52 for quartz–calcite at 298 K (Hayles et al., 2018 and this contribution). To a first approximation, the temperature dependence of θ for phases A and B is given by (Sharp et al., 2016)

$$\theta_{A-B} = 0.5305 - \frac{\varepsilon}{T} \quad 5.8)$$

where ε is a constant (although higher order polynomials are indicated from theory – Cao and Liu, 2011; Hayles et al., 2018; Guo and Zhou, 2019). Combining equations 5.4, 5.7 and 5.8 gives the equilibrium $\delta^{17}\text{O}$ fractionation equation between phases A and B :

$$1000\ln\alpha^{17\text{O}/^{16}\text{O}}_{A-B} = \delta'^{17}\text{O}_A - \delta'^{17}\text{O}_B = \left(\frac{a \times 10^6}{T^2} + \frac{b \times 10^3}{T} + c\right) \left(0.5305 - \frac{\varepsilon}{T}\right) \quad 5.9).$$

For all terrestrial samples not affected by mass independent fractionation processes (e.g., Thiemens, 2006), $\delta^{17}\text{O}$ varies with $\delta^{18}\text{O}$ by the empirical equation known as the *Terrestrial Fractionation Line* or TFL

$$\delta^{17}\text{O} = \lambda\delta^{18}\text{O} + \gamma \quad 5.10).$$

In equation 5.10, λ is an empirical best fit to natural data and not tied to any thermodynamic relationship and γ is the y intercept that is generally assumed to be zero. This work uses a λ value of 0.528 (Sharp et al., 2018).

Departures from the linear relationship given in equation 5.10 are extremely subtle and are expressed using the $\Delta^{17}\text{O}$ value, given by the equation

$$\Delta^{17}\text{O} = \delta^{17}\text{O} - \lambda\delta^{18}\text{O} \quad (5.11).$$

The equations governing the isotopic fractionation for the three oxygen isotopes between a mineral and water using the $^{18}\text{O}/^{16}\text{O}$ fractionation equation 5.4 as a template are the following:

$$\delta^{18}\text{O}_{\text{mineral}} = \delta^{18}\text{O}_{\text{water}} + \frac{a \times 10^6}{T^2} + \frac{b \times 10^3}{T} + c \quad (5.12),$$

$$\delta^{17}\text{O}_{\text{mineral}} = \delta^{17}\text{O}_{\text{water}} + \left(\frac{a \times 10^6}{T^2} + \frac{b \times 10^3}{T} + c \right) \left(0.5305 - \frac{\varepsilon}{T} \right) \quad (5.13),$$

$$\Delta^{17}\text{O}_{\text{mineral}} = \delta^{17}\text{O}_{\text{water}} - \lambda \cdot \delta^{18}\text{O}_{\text{water}} + \left(\frac{a \times 10^6}{T^2} + \frac{b \times 10^3}{T} + c \right) \left(0.5305 - \frac{\varepsilon}{T} - \lambda \right) \quad (5.14).$$

For minerals in equilibrium with seawater ($\delta^{17}\text{O} = \delta^{18}\text{O} = 0$), equation 5.14 reduces to

$$\Delta^{17}\text{O}_{\text{mineral}} = \left(\frac{a \times 10^6}{T^2} + \frac{b \times 10^3}{T} + c \right) \left(0.5305 - \frac{\varepsilon}{T} - \lambda \right) \quad (5.15).$$

Combining equations 5.12 and 5.14 allows us to calculate the relationship between the $\Delta^{17}\text{O}$ and $\delta^{18}\text{O}$ values of a mineral in equilibrium with water. The solution is the following:

$$\Delta^{17}\text{O} = \delta^{17}\text{O}_w + \left(\delta^{18}\text{O}_r - \delta^{18}\text{O}_w \right) \left(0.5305 + \frac{(c - \delta^{18}\text{O}_r + \delta^{18}\text{O}_w)\varepsilon}{500(b + \sqrt{b^2 - 4a(c - \delta^{18}\text{O}_r + \delta^{18}\text{O}_w)})} - \lambda \right) - \delta^{18}\text{O}_w \cdot \lambda \quad (5.16).$$

5.2.3 Equilibrium triple oxygen isotope fractionation – the $\Delta^{17}\text{O} - \delta^{18}\text{O}$ plot

The benefit of the triple oxygen isotope system is apparent when plotting the $\Delta^{17}\text{O}$ value of a mineral against the $\delta^{18}\text{O}$ value using equation 5.16 (Figure 5.2). The triple oxygen isotope plot in $\Delta^{17}\text{O} - \delta^{18}\text{O}$ space allows us to clearly distinguish equilibrium or disequilibrium in a given sample. Figure 5.2 is constructed for quartz in equilibrium with ocean water, but an equally relevant figure could be generated for calcite or any other low temperature phase for which triple oxygen isotope fractionation data are available. The curved line represents the locus of $\delta^{18}\text{O}$ and $\Delta^{17}\text{O}$ values of silica in equilibrium with seawater (yellow star). All values in triple oxygen isotope equilibrium with a water of this composition must lie on the curve. Formation temperatures (in $^{\circ}\text{C}$) decrease down and to the right along the curve.

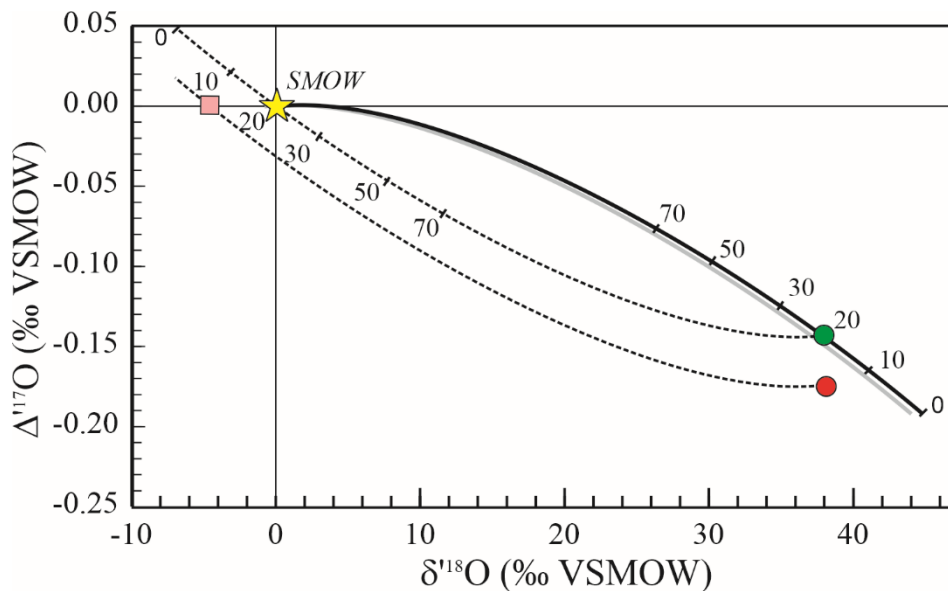


Figure 5.2 - $\Delta^{17}\text{O} - \delta^{18}\text{O}$ plot for silica-water. The curved black line shows the combined $\Delta^{17}\text{O} - \delta^{18}\text{O}$ values of silica in equilibrium with SMOW (Standard Mean Ocean Water, $\delta^{18}\text{O} = \Delta^{17}\text{O} = 0$). The position along the line indicates the temperature of equilibration. The grey line is for a seawater with a $\delta^{18}\text{O}$ value of -1 ‰ (ice free conditions). The dashed lines are the same curve only inverted. The source is now placed on the mineral. The dashed line emanating from the green circle passes through modern seawater composition. The dashed line from the red circle does not. The sample at the red circle is therefore either out of oxygen isotope equilibrium or in equilibrium with a different seawater composition, such as the pink square.

The triple oxygen isotope values of two hypothetical samples are shown in Fig. 5.2 by the red and green circles. Both have $\delta^{18}\text{O}$ values of both 37.9 ‰. With $\delta^{18}\text{O}$ values alone, the two samples are indistinguishable and correspond to a formation temperature of 20 °C. The addition of the $\Delta^{17}\text{O}$ value clearly provides more information. The green circle lies on the equilibrium curve, suggesting that the sample is indeed in equilibrium with seawater at 20 °C. The red circle does not plot on the seawater equilibrium curve. *Therefore, this sample cannot be in equilibrium with seawater ($\delta^{18}\text{O}$ and $\Delta^{17}\text{O} = 0$) at any temperature.* The third isotope of oxygen unambiguously demonstrates disequilibrium with modern seawater and/or equilibrium with a different water oxygen isotope composition. Lowering the $\delta^{18}\text{O}$ value of the ocean by ~1 ‰ during interglacial periods is shown by the grey equilibrium curve (Fig. 5.2). The $\Delta^{17}\text{O}$ value of an ice-free ocean should be close to 0, so the curve moves 1 ‰ to the left and does not explain the position of the red circle. As the following section describes, the region where a sample plots in a triple isotope diagram of the form in Figure 2 is diagnostic of the conditions of formation and disequilibrium.

The equilibrium curve of quartz in equilibrium with ocean (solid curved lines) can be inverted so that the origin of the curve is placed on the measured $\delta^{18}\text{O}$ – $\Delta^{17}\text{O}$ value of the mineral (dashed lines; Figure 5.2). In this case, the dashed line defines the water composition in equilibrium with the quartz. For the green circle, the intersection of the dashed line with SMOW occurs at 20 °C, and this is the apparent equilibrium temperature. The dashed line emanating from the red circle does not pass through SMOW, again indicating that there is no temperature at which this sample can be in equilibrium with ocean water. The red circle could be in equilibrium with a water value

having a $\delta^{18}\text{O}$ value of -5‰ and $\delta^{17}\text{O}$ value of 0‰ (pink square; Fig. 5.2) or any water with a triple oxygen isotope value along the dashed line emanating from the red circle.

5.2.4 Changing ocean composition in the past

The accuracy of oxygen isotope paleothermometry is critically dependent on the assumed $\delta^{18}\text{O}$ value of the ancient ocean. While it is generally agreed that the ocean is buffered to its present value by a complex interplay of high- to low- temperature alteration (Muehlenbachs and Clayton, 1976; Muehlenbachs, 1986), the $\delta^{18}\text{O}$ value of past seawater is still debated. Some studies (using geochemical data and/or modelling) suggest changes in the ratio high to low temperature alteration processes could have lowered the $\delta^{18}\text{O}$ value of seawater in the distant past, thereby explaining the low $\delta^{18}\text{O}$ values of Archean and early Precambrian sediments (Perry, 1967; Wallmann, 2001; Kasting et al., 2006; Jaffrés et al., 2007; Hren et al., 2009). Sengupta and Pack (2018)

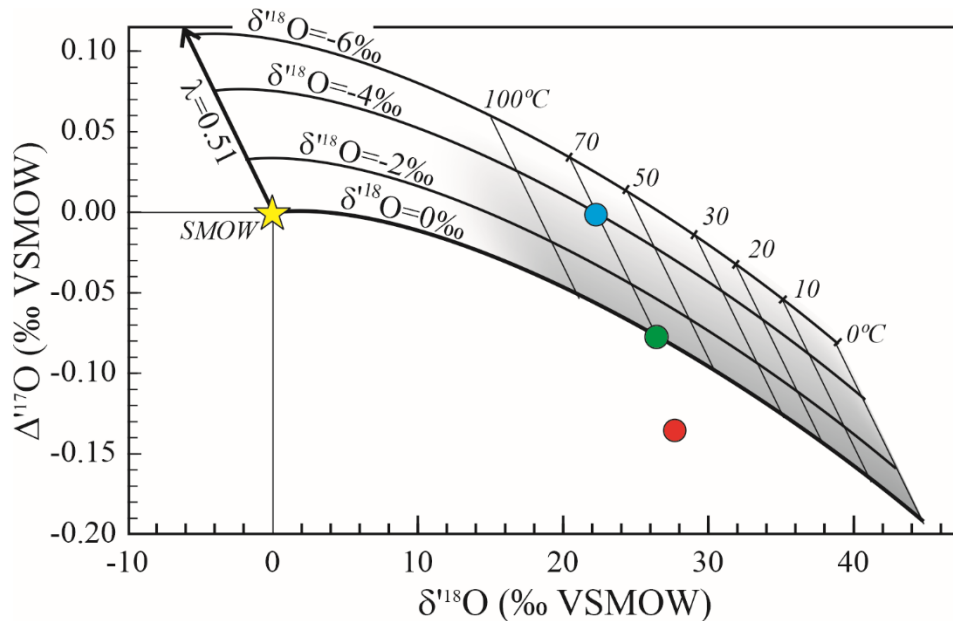


Figure 5.3 - $\Delta^{17}\text{O}$ - $\delta^{18}\text{O}$ plot of changing seawater composition in relation to changing the ratio of high to low temperature alteration (Sengupta and Pack, 2018). The line labeled $\lambda=0.51$ is the trajectory of seawater composition for changing the ratio of high to low temperature alteration. The green circle is in equilibrium with modern water at 70°C . The blue circle is the $\Delta^{17}\text{O}$ - $\delta^{18}\text{O}$ value of silica in equilibrium with $\delta^{18}\text{O}_{\text{seawater}}$ value of -4‰ at 70°C . The red circle is not in equilibrium with a lighter seawater and can only be explained by changing ocean conditions if the $\delta^{18}\text{O}$ value of the ancient ocean was heavier than today.

modeled how the $\Delta^{17}\text{O}$ and $\delta^{18}\text{O}$ values of the ocean would change in response to changing rates of continental weathering and high temperature alteration during seafloor spreading. They obtained a λ value of 0.51 for the combined effect of continental weathering and high temperature seafloor alteration. By changing the tectonic conditions in the past, namely increasing the rate of continental erosion and decreasing the rate of high temperature seafloor hydrothermal alteration, the composition of the ocean would change to lower $\delta^{18}\text{O}$ values and higher $\Delta^{17}\text{O}$ values. This trend is shown by the line in Figure 5.3 labeled $\lambda=0.51$. A similar effect was predicted by Liljestr nd et al. (2020) by using performing a sensitivity study of the λ . It is, of course, also possible that continental erosion would be less in the distant past, in which case the ocean would move to heavier $\delta^{18}\text{O}$ values and lower $\Delta^{17}\text{O}$ values (Johnson and Wing, 2020).

Sediments that formed in equilibrium with a seawater composition plotting on the $\lambda=0.51$ line will plot above the modern equilibrium curve. This region is shown in Figure 5.3 as the shaded region for a series of ocean water $\delta^{18}\text{O}$ values and temperatures. The green circle in Figure 5.3 could be in equilibrium with modern seawater. The blue circle could be in equilibrium with seawater with a $\delta^{18}\text{O}$ value of -4‰ and a $\Delta^{17}\text{O}$ value of 0.075‰ . The red circle in Figure 5.3 could only be in equilibrium with the ocean if the $\delta^{18}\text{O}$ value was significantly higher than today.

5.2.5 Diagenetic trends

The hypothetical red circle in Figure 5.3 is most likely explained as the result of diagenesis with meteoric water. Low temperature diagenesis of marine sediments generally drives the $\delta^{18}\text{O}$ values lower and $\Delta^{17}\text{O}$ higher (Sharp et al., 2018). A number of variables modify the oxygen isotope composition during diagenetic alteration, including

temperature, initial protolith and fluid compositions, and fluid/rock (F/R) ratio.

Nevertheless, the $\Delta^{17}\text{O}$ – $\delta^{18}\text{O}$ field of most diagenetically altered rock is surprisingly quite limited (Figure 5.6; Sharp et al., 2018).

The effect of low-temperature hydrothermal alteration is determined using a simple mass-balance mixing model. A fraction of water is allowed to equilibrate with a rock at a given temperature following Taylor (1978). The bulk composition is given by the equation

$$\delta^x\text{O}_{bulk} = X_{water}(\delta^x\text{O}_{water\ initial}) + (1 - X_{water})(\delta^x\text{O}_{rock\ initial}) \quad 5.17a)$$

and

$$\delta^x\text{O}_{bulk} = X_{water}(\delta^x\text{O}_{water\ final}) + (1 - X_{water})(\delta^x\text{O}_{rock\ final}) \quad 5.17b),$$

$\delta^x\text{O}$ can be either $\delta^{18}\text{O}$ or $\delta^{17}\text{O}$. The final $\delta^x\text{O}$ value of the rock is determined by the additional equation

$$\alpha^x = \frac{1000 + \delta^x\text{O}_{final,rock}}{1000 + \delta^x\text{O}_{final,water}} \quad 5.18).$$

This leads to the relationship between the initial rock and water oxygen isotope compositions, the fluid/rock ratio and the final isotopic composition of the rock:

$$\delta^x\text{O}_{rock\ final} = \frac{1000X + \alpha(X \cdot \delta^x\text{O}_{rock\ initial} - X \cdot \delta^x\text{O}_{water\ initial} - \delta^x\text{O}_{rock\ initial} - 1000X)}{\alpha X - \alpha - X} \quad 5.19).$$

A typical alteration pathway is shown in Figure 5.4. The initial protolith is silica in equilibrium with ocean water at 20 °C (red circle and δr_{init}). The meteoric water that infiltrates the rock has initial $\delta^{18}\text{O}$ and $\Delta^{17}\text{O}$ values of –6 and +0.03 ‰ (blue star and δ_{MW}). The infiltrating meteoric water always has a constant composition (δ_{MW}). The

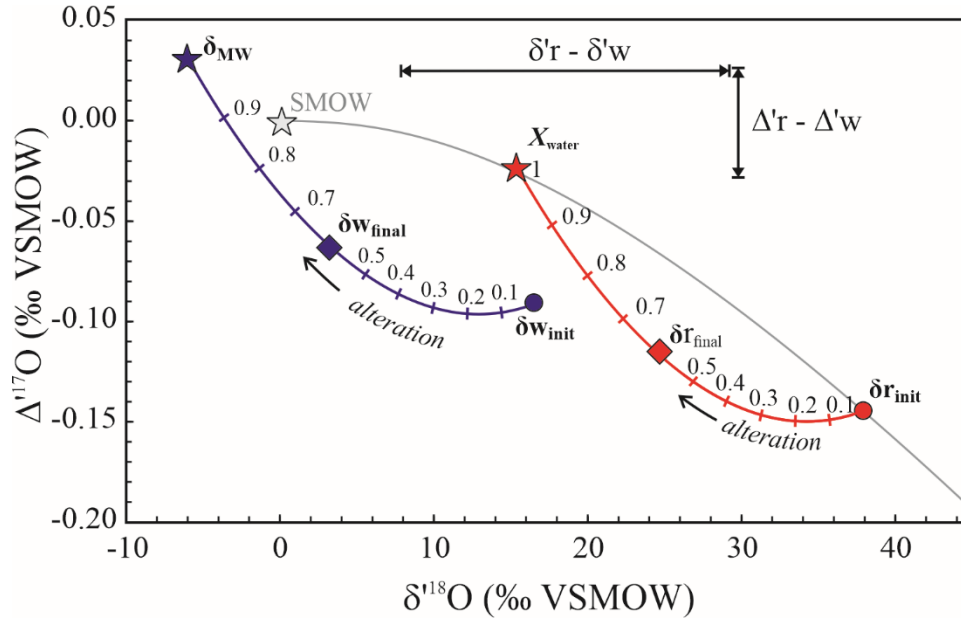


Figure 5.4 - Alteration trajectories in $\Delta^{17}\text{O} - \delta^{18}\text{O}$ space. The rock starts at $\delta_{r_{\text{init}}}$ and moves along the red curve according to the fluid/rock ratio. The infiltrating fluid has a composition at δ_{MW} (blue star). The reequilibrated water follows the blue curved path from $\delta_{w_{\text{init}}}$ towards lower $\delta^{18}\text{O}$ and higher $\Delta^{17}\text{O}$ values. The final position in this figure corresponds to an X_{water} value of 0.6. The equilibrium oxygen isotope fractionations at 100 °C are shown by the doubled arrow lines.

infiltrating meteoric water always has a constant composition (δ_{MW}) and equilibrates with the rock as it enters the system ($\delta_{w_{\text{init}}}$).

The fractionation between the water and rock at 100 °C is shown by the arrows $\delta'r - \delta'w$ and $\Delta'r - \Delta'w$. As long as temperature is held constant, these fractionations will not change. When the alteration process first begins, an infinitely small amount of water enters the system and equilibrates with the rock. The fraction of oxygen from the water relative to the total water-rock oxygen reservoir approaches 0. In the model, the water equilibrates with the overwhelmingly large oxygen reservoir of rock and has a composition given by $\delta_{w_{\text{init}}}$ shown by the blue circle. This is the isotopic composition of the equilibrated water when the fluid-rock interaction process first begins to take place.

As more fluid enters the system, the F/R ratio increases and the isotopic composition of the fluid and rock track up the curved lines. As the F/R ratio approaches

an infinite value, the composition of the system is equal to that of the water. The water ‘overwhelms’ the buffering capacity of the rock. The $\delta^{18}\text{O}$ and $\Delta^{17}\text{O}$ values of the water at an infinite F/R ratio are the same as the infiltrating water δ_{MW} (blue star; Fig. 5.4) and the rock will have an isotopic composition in equilibrium with this water, shown by the red star (Fig. 5.4). The final rock and water compositions are a function of the F/R ratio. In Figure 5.4, the red and blue diamonds illustrate an intermediate condition corresponding to an $X_{\text{water}} = 0.6$ or a fluid rock ratio of 1.5 ($X_{\text{water}}/X_{\text{rock}} = 0.6/0.4$).

Figure 5.5 shows various alteration trajectories for different water compositions (dashed lines, $\delta^{18}\text{O}_{\text{MW}} = -10\text{‰}$; solid lines, $\delta^{18}\text{O}_{\text{MW}} = -6\text{‰}$; both with a $\Delta^{17}\text{O}$ value of $+0.03\text{‰}$) and different temperatures (30, 50 and 100 °C). The variables that control the alteration pathways are the temperature of alteration, the $\delta^{18}\text{O}$ and $\Delta^{17}\text{O}$ values of the diagenetic water, and the initial isotopic composition of the sample (which is a function of its formation temperature).

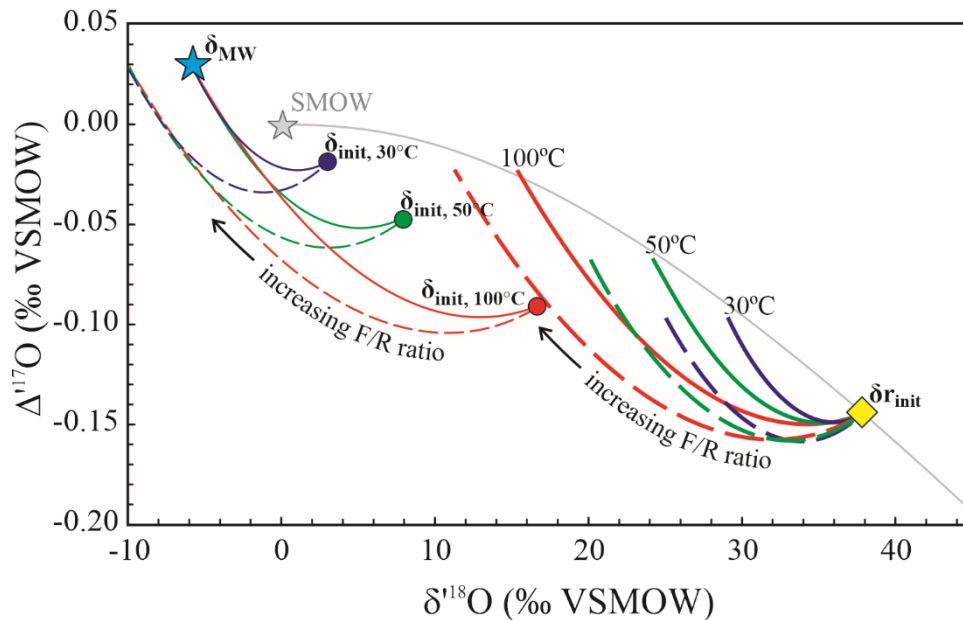


Figure 5.5 - Alteration trajectories for a rock starting with a $\delta^{18}\text{O}$ - $\Delta^{17}\text{O}$ of δ_{rinit} . Dashed and solid lines are for interaction with an infiltrating meteoric water (δ_{MW}) with $\delta^{18}\text{O}$ values of -10‰ and -6‰ , respectively, and $\Delta^{17}\text{O}$ values of 0.03‰ . The rock trajectories are thick curves, fluids are thin curves.

In general, altered rocks should lie to the left of the equilibrium curve (lavender region; Figure 5.6). This field is generated by considering a wide range of fluid compositions, temperatures of interaction, and initial rock protolith compositions (multiple curved black lines). Figure 5.6 is a schematic of expected fields, for case studies see Herwartz et al. (2015), Zakharov and Bindeman (2019), Chamberlain et al. (2020), and Herwartz (2020).

The effect of lowering the $\delta^{18}\text{O}$ value of ancient ocean lowering the ratio of high to low temperature alteration of seafloor sediments will drive the isotopic composition of marine sediments to higher $\Delta^{17}\text{O}$ values, shown by the grey region in Figure 5.6. These two fields – alteration in lavender and lowering ocean values in grey – represent the generalized regions where most sediment phases are expected to occur.

Overall, samples that lie below and to the left of the equilibrium line are explained by diagenesis. There are cases, such as fluids equilibrating with a hot rock and

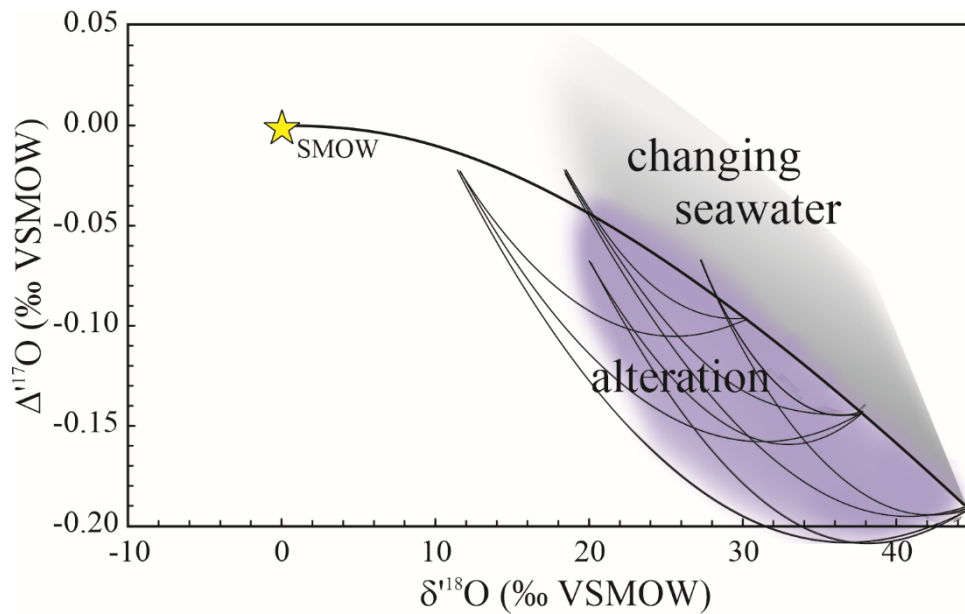


Figure 5.6 - Generalized fields for sedimentary silica. The lavender field represents the general region expected for alteration based on numerous trajectories for different conditions (black curved lines). The grey region is calculated for lower isotope compositions predicted if the ratio of high- to low-temperature alteration changed dramatically in the past.

then passing (and interacting) with a cooler rock, that would result in a positive shift for both the $\delta^{18}\text{O}$ and $\Delta^{17}\text{O}$ values. This may be seen in hot buoyant fluids that infiltrate a cooler overlying sedimentary pile (see final section of this chapter). There is an additional factor that is seen in manganese oxides. They incorporate as much as 50 % of their O from dissolved atmospheric O_2 (Sutherland et al., 2020). Because the $\Delta^{17}\text{O}$ value of air O_2 is extremely low (-0.441‰, Wostbrock et al., 2020b), manganese oxides accordingly have anomalously low $\Delta^{17}\text{O}$ values.

5.3 Silica–water fractionation

5.3.1 Calibration of the triple oxygen isotope thermometer

The $^{18}\text{O}/^{16}\text{O}$ fractionation between silica and water and its temperature dependence is extremely well studied. There are at least 7 experimental fractionation studies of quartz-water at high temperatures (see Sharp et al., 2016 for a compilation) and a number of empirical studies of naturally-formed abiogenic and biogenic amorphous hydrated silica at low to moderate temperatures (Kita et al., 1985; Leclerc and Labeyrie, 1987; Shemesh et al., 1995; Brandriss et al., 1998; Schmidt et al., 2001; Dodd and Sharp, 2010). Low temperature diatom silica initially form out of equilibrium with their host water (Brandriss et al., 1998; Dodd and Sharp, 2010), but then undergoes an early maturation phase, such that the silica reaches oxygen isotope equilibrium within the first year or two post mortem (Schmidt et al., 2001; Dodd et al., 2012; Tyler et al., 2017).

Wostbrock et al. (2018) compared the triple oxygen isotope values of abiogenic and biogenic silica and found no measurable vital effect. Therefore, both the high temperature equilibration experiments and the low temperature empirical fractionation

data from biogenic and abiogenic silica are used to derive an SiO₂ - H₂O oxygen isotope fractionation equation valid at all temperatures, given by

$$1000\ln\alpha_{\text{SiO}_2\text{-H}_2\text{O}} = \frac{4.28 \times 10^6}{T^2} - \frac{3500}{T} \quad (5.20).$$

The low temperature anchor on equation 5.20 is primarily controlled by low temperature diatom data. Shemesh et al. (1992) recommended only using low temperature Antarctic diatoms to calibrate the silica–water fractionation, thereby avoiding complications from upwelling effects seen in other regions. Equation 5.20 agrees very well with the published low temperature diatom data (Figure 5.7) suggesting that the equation is valid at both high and low temperatures.

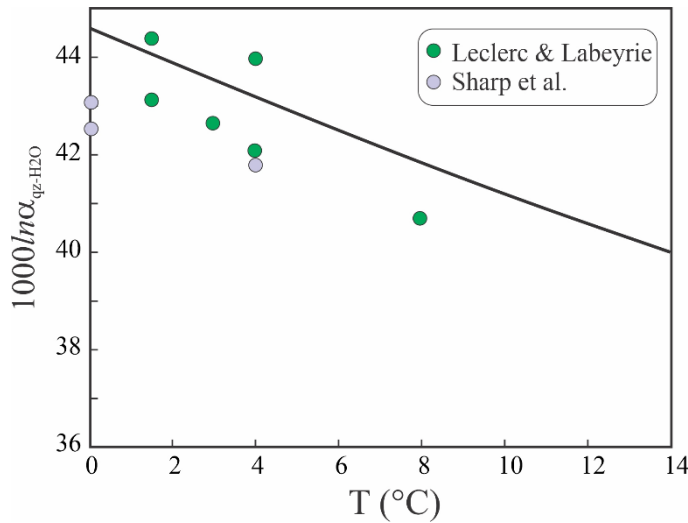


Figure 5.7 - Comparison of the quartz-water fractionation equation (solid curve) with low temperature diatom data (Leclerc and Labeyrie, 1987; Sharp et al., 2016).

The temperature dependent ¹⁷O calibration for quartz-water has been determined empirically by measuring the triple oxygen isotope compositions of abiogenic and biogenic silica (and coexisting water when possible for non-marine samples) over a temperature range of 0 to over 100°C (Sharp et al., 2016; Wostbrock et al., 2018). The θ-T relationship for silica-water can be calculated using Eq. 5.6 with the best fit given by

$$\theta_{\text{silica-water}} = 0.5305 - \frac{1.85}{T} \quad (5.21).$$

The results are shown in Figure 5.8 along with two theoretical calibrations (Cao and Liu, 2011; Hayles et al., 2018). There is generally good agreement between the empirical and theoretical estimates, with the latter having slightly higher θ values at low temperatures.

The $\Delta\Delta^{17}\text{O}$ fractionations as a function of temperature are governed by Eq. 5.14. For silica-water, the equation is

$$\Delta\Delta^{17}\text{O}_{\text{silica}} = \delta^{17}\text{O}_{\text{water}} - \lambda \cdot \delta^{18}\text{O}_{\text{water}} + \left(\frac{4.28 \times 10^6}{T^2} + \frac{3.5 \times 10^3}{T} + c \right) \left(0.5305 - \frac{1.85}{T} - \lambda \right) \quad (5.22),$$

λ is 0.528 in this manuscript. Eq. 5.22 allows us to construct the $\Delta^{17}\text{O}$ - $\delta^{18}\text{O}$ equilibrium curves (e.g., Fig. 5.2).

5.3.2 Silica in the terrestrial environment

Figure 5.9 shows the quartz-water triple oxygen isotope diagram with the equilibrium curves inverted so that the origin of the curves originates at the silica oxygen isotope

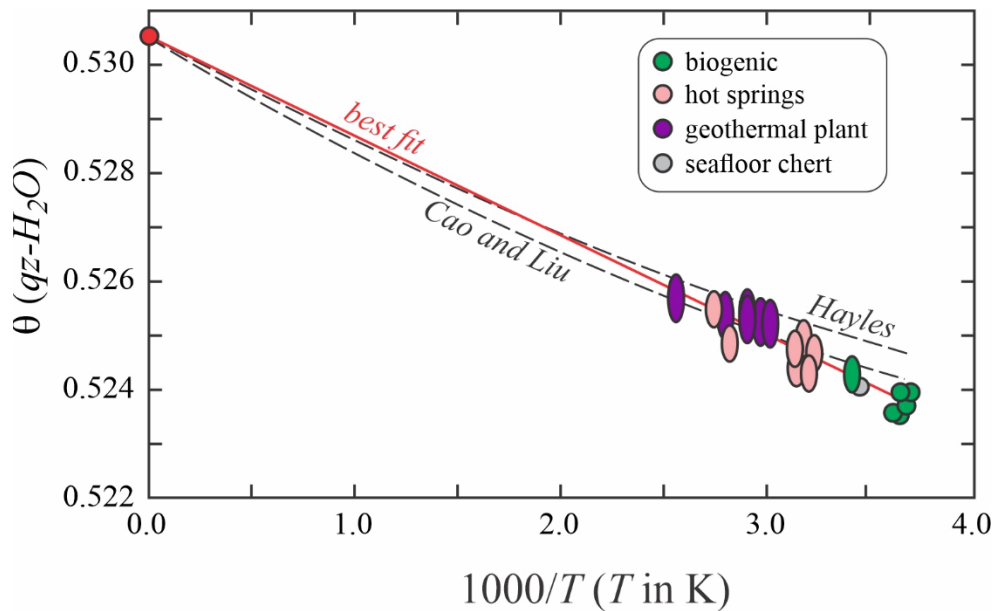


Figure 5.8 - Measured θ values for natural samples and best fit for a θ vs. $1/T$ relationship. Data from Sharp et al. (2016) and Westbrock et al. (2018). Also shown are the theoretical curves of Cao and Liu (2011) and Hayles et al. (2018).

composition. This allows us to estimate the oxygen isotope compositions of formation waters in a terrestrial (non-marine) environment in equilibrium with a silica sample. The green diamond is a modern sinter from Yellowstone National Park, Wyoming, where both the neoform silica and coexisting water (green circle) were sampled (Fig. 5.9). A water temperature of 47 °C was measured at the time of collection. The silica and water appear to be in triple oxygen isotope equilibrium. They both lie on the same equilibrium curve with a corresponding temperature of 42 °C. The measured water is ~10 ‰ higher than local meteoric water suggesting some degree of evaporation and/or hydrothermal exchange with the host rock (Sharp et al., 2016). The blue diamond is silica from a Keokuk geode that retained fossil water (blue circle; Fig. 5.9) in its core, that may or may not be representative of the water in which the geode formed. However, the triple oxygen isotope values for the quartz and the water do in fact suggest equilibrium at a temperature of ~45 °C. The final sample is a stalactitic geode from Morocco (purple diamond; Fig.

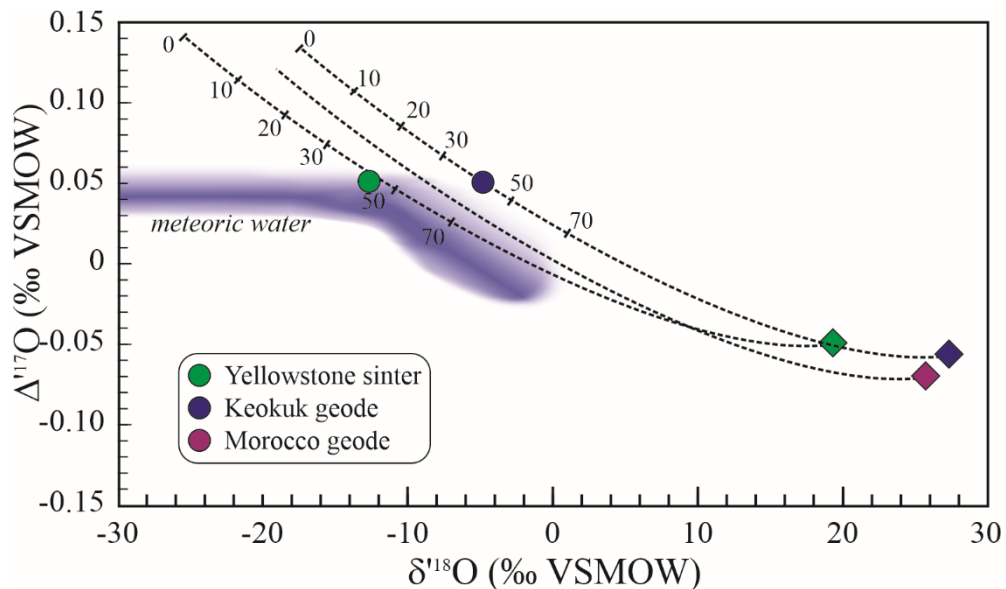


Figure 5.9 - Triple isotope compositions of low-T terrestrial silica samples. Data from Sharp et al. (2016). The Yellowstone sinter and Keokuk geode have oxygen isotope data for the coexisting waters and correspond to formation temperatures of 40-50°C. The Morocco geode has a similar oxygen isotope composition to the other two samples suggesting similar conditions of formation. Meteoric water field from Sharp et al. (2018).

5.9). Without the coexisting water, but recognizing the $\Delta^{17}\text{O}$ value of the sample is slightly lower than the other two samples, a formation temperature of $\sim 40^\circ\text{C}$ is estimated. Data from both geodes suggest that well crystalline, glassy quartz can form at temperatures as low as 40 to 50 $^\circ\text{C}$.

5.4 Triple oxygen isotope measurements of carbonates

5.4.1 Triple oxygen isotope analysis of carbonates

The standard method for determining the $\delta^{18}\text{O}$ value of carbonates was derived in 1950 (McCrea, 1950). Carbonates are reacted with $>100\%$ phosphoric acid at a constant temperature, producing CO_2 gas from the breakdown of the carbonate. Only $2/3$ of the oxygen in the carbonate is liberated to the CO_2 gas. However, if the decarbonation is performed at a constant temperature, then the fractionation ($\delta^{18}\text{O}_{\text{CO}_2(\text{ACID})} - \delta^{18}\text{O}_{\text{carbonate}}$ or $\alpha_{\text{CO}_2(\text{ACID})\text{-carbonate}}$) should be constant (although there are subtle second order effects that should be considered (Sharp, 2013)). In order to calculate the actual $\delta^{18}\text{O}$ value of the carbonate on the VSMOW–SLAP scale, it is necessary to know the $\alpha_{\text{CO}_2(\text{ACID})\text{-carbonate}}$ fractionation factor (Sharp and Wostbrock, 2020). This value is determined by liberating 100 % of the oxygen from the carbonate either through complete fluorination of the carbonate (Sharma and Clayton, 1965) or decarbonation of the carbonate as CO_2 followed by fluorination of the remaining CaO (Kim and O'Neil, 1997; Kim et al., 2007a). In these carbonate studies, CO_2 and/or a combination of CO_2 and O_2 gas were produced. The O_2 was converted to CO_2 by reaction with a heated graphite rod and all CO_2 is recombined for the measurement of the $\delta^{18}\text{O}$ value of the total carbonate. The difference between the $\delta^{18}\text{O}$ values of the CO_2 produced by reaction with phosphoric acid and total carbonate gives us the $\alpha^{18}\text{O}_{\text{CO}_2(\text{ACID})\text{-carbonate}}$ value.

These procedures are not applicable to determining the $\delta^{17}\text{O}$ value of carbonates. There is an isobaric interference at mass 45 ($^{12}\text{C}^{16}\text{O}^{17}\text{O}$) by ^{13}C ($^{13}\text{C}^{16}\text{O}^{16}\text{O}$). The $\delta^{17}\text{O}$ value must be measured on O_2 gas unless an ultra-high precision mass spectrometer is being used that can measure the O^- fragment of CO_2 (Adnew et al., 2019). The problem is that during traditional fluorination of carbonates, intermediate compounds CO and COF_2 are produced which are very difficult to fluorinate. Wostbrock et al. (2020b) modified the Sharma and Clayton (1965) method of carbonate fluorination that quantitatively produces O_2 from the fluorination of a carbonate. The method involves conventional fluorination in Ni reaction tubes heated to $750\text{ }^\circ\text{C}$ for four days. Wostbrock et al. (2020b) analyzed international standards as well as the CO_2 liberated by decarbonation and report an $\alpha^{17}\text{O}_{\text{CO}_2(\text{ACID})\text{-carbonate}}$ value of 1.00535 when using an $\alpha^{18}\text{O}_{\text{CO}_2(\text{ACID})\text{-carbonate}}$ value of 1.01025. With these data, other laboratories that measure the $\delta^{17}\text{O}$ value of CO_2 generated through phosphoric acid digestion can calculate the $\delta^{17}\text{O}$ value of the total carbonate. Techniques that measure the triple oxygen isotope values of CO_2 gas include: converting CO_2 to H_2O followed by fluorination (Passey et al., 2014); equilibrating CO_2 gas with O_2 using a hot Pt catalyst (Mahata et al., 2013; Barkan et al., 2015; Fosu et al., 2020); and analyzing the O^- fragment of CO_2 generated in the ion source using a high resolution mass spectrometer (Adnew et al., 2019). Laser spectroscopy that measured the $\delta^{17}\text{O}$ value of CO_2 is a promising new technology that has yet to be adapted to wide-scale use (Sakai et al., 2017).

The complexities in the carbonate-water system are not shared by the silica-water system. Fractionations determined from experimental, empirical, biogenic, abiogenic, amorphous silica and crystalline quartz all obey the same α -temperature ($\text{SiO}_2 - \text{H}_2\text{O}$)

relationship. The reason for the lack of complexity (and better approach towards equilibrium) may be due to the simplicity of dissolved silica species. Below a pH of 8.5, H_4SiO_4 is the predominant dissolved silica phase. If the fractionation that accompanies the crystallization of H_4SiO_4 is minimal, then the SiO_2 - H_2O system should be well behaved (Matthews and Beckinsale, 1979).

5.4.2 Triple oxygen isotope fractionation in the calcite (aragonite) – water system

The triple oxygen isotope fractionation equations for calcite have been calculated from theory (Cao and Liu, 2011; Hayles et al., 2018; Guo and Zhou, 2019) and by a combination of laboratory synthesis experiments and empirical results from natural samples (Wostbrock et al., 2020a). The synthesis experiments consisted of slowly precipitating calcite at a constant temperature following the method of O'Neil et al. (1969) either with or without carbonic anhydrase (CA) as a catalyst (Watkins et al., 2013). The natural samples included marine biogenic calcite and marine abiogenic and biogenic aragonite that had known water $\delta^{18}\text{O}$ values and growth temperatures. Data were compared to abiogenic calcite and water from Devils Hole. All samples were analyzed for their triple oxygen isotope composition by the method of total fluorination (Figure 5.10). There is a systematic increase in the $\Delta^{17}\text{O}_{\text{carbonate}} - \Delta^{17}\text{O}_{\text{water}}$ ($\Delta\Delta^{17}\text{O}_{\text{carb-wt}}$) value as a function of decreasing temperature, similar to what is seen for quartz and what is predicted from theory (Hayles et al., 2018; Guo and Zhou, 2019). There was a statistical difference between the calcite samples (blue circles and squares, Fig. 5.10) and the aragonite samples (brown circles, Fig. 5.10) where the best fit of the aragonite samples (brown line, Fig. 5.10) is lower at all temperatures, compared to the best fit of the calcite samples (Fig. 5.10). The calcite results agree well from theoretical estimates (Hayles et

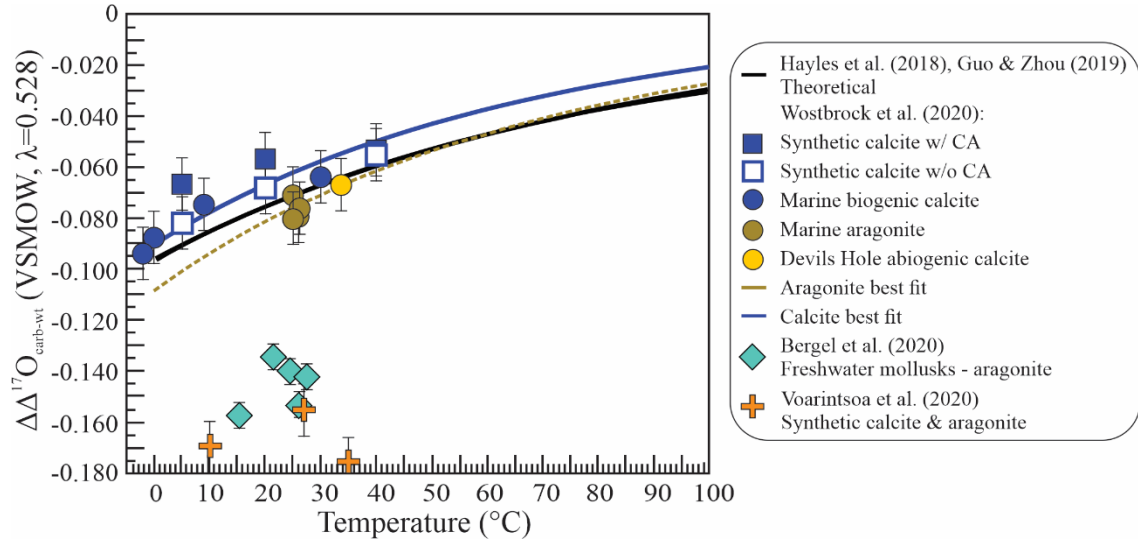


Figure 5.10 - The $\Delta\Delta^{17}\text{O}_{\text{carb-wt}}$ as a function of temperature from published studies. Icons are the average of multiple measurements of a particular sample and error bars are ± 1 s.d of average of the reported data in the study. Theoretical $\Delta\Delta^{17}\text{O}_{\text{carb-wt}}$ -Temperature relationship (thick black line) from the two theoretical studies overlap.

al., 2018; Guo and Zhou, 2019). However, theoretical calculations predict there to be little to no difference between the $\Delta^{17}\text{O}$ values of aragonite and calcite (Guo and Zhou, 2019; Schauble and Young, 2020).

Two other studies (Bergel et al., 2020; Voarintsoa et al., 2020) also derived this relationship using freshwater aragonitic mollusks (green diamonds, Fig. 5.10) and synthetic calcite/aragonite (orange crosses, Fig. 5.10), respectively using the Pt $\text{CO}_2\text{-O}_2$ equilibration method. Their data, measured on O_2 derived from CO_2 , were converted to converted to the total carbonate using the published $\alpha^{17}\text{O}_{\text{CO}_2(\text{ACID})\text{-carbonate}}$ of 1.00535 (Wostbrock et al., 2020b). Their $\Delta\Delta^{17}\text{O}_{\text{carb-wt}}$ values are significantly larger and both studies do not report a significant variation with temperature (Figure 5.10). Although the reason for the differences between the studies is unknown and warrants further investigation, one possible explanation could be a kinetic fractionation effect during the $\text{CO}_2\text{-O}_2$ equilibration method (Fosu et al., 2020; Passey and Levin, 2020) used in both the Bergel et al. (2020) and Voarintsoa et al. (2020) studies.

Debate is ongoing between which type of carbonate (synthetic, biogenic, or abiogenic) best represents equilibrium oxygen isotope fractionation is ongoing (cf. Coplen, 2007; Bajnai et al., 2018; Brand et al., 2019) or if naturally forming carbonates never reach equilibrium with the waters in which they form (Daëron et al., 2019). Wostbrock et al. (2020a) examined each category of carbonates (biogenic marine carbonate, biogenic and abiogenic marine aragonite, abiogenic Devils Hole calcite, synthesized calcite with and without carbonic anhydrase) to determine differences in triple oxygen isotope fractionation. They found no statistically significant difference in the $1000\ln\alpha^{18}\text{O}_{\text{carb-wt}}$ values between synthetic, biogenic, and abiogenic carbonates but the $1000\ln\alpha^{18}\text{O}_{\text{carb-wt}}$ values were at the higher end of that in reported literature. They used all the samples from each category, combined with the high temperature experimental data from O'Neil et al. (1969) to derive the $1000\ln\alpha^{18}\text{O}_{\text{carb-wt}}$ portion of the triple oxygen isotope fractionation given by

$$1000\ln\alpha_{\text{calcite-water}}^{18\text{O}/16\text{O}} = \frac{2.84 \times 10^6}{T^2} - 2.96 \quad (5.23).$$

A difference was seen in the $1000\ln\alpha^{17}\text{O}$ values between calcite-water and aragonite-water (Wostbrock et al., 2020a). Calcite-water has higher θ values and smaller $\Delta\Delta^{17}\text{O}_{\text{carb-wt}}$ values than aragonite-water. However, these conclusions are based on aragonite samples at only one temperature (25°C) and may change with additional data. The calcite-water triple oxygen isotope fractionation equation from Wostbrock et al. (2020a) is:

$$\Delta^{17}\text{O}_{\text{cc}} - \Delta^{17}\text{O}_{\text{wt}} = \left(\frac{2.84 \times 10^6}{T^2} - 2.96 \right) \left(\frac{-1.39}{T} + 0.5305 - \lambda \right) \quad (5.24).$$

The aragonite-water triple oxygen isotope fractionation equation from Wostbrock et al. (2020a) is:

$$\Delta^{17}\text{O}_{\text{ara}} - \Delta^{17}\text{O}_{\text{wt}} = \left(\frac{2.84 \times 10^6}{T^2} - 2.96 \right) \left(\frac{-1.53}{T} + 0.5305 - \lambda \right) \quad 5.25).$$

It is unclear whether any of the carbonates presented in Wostbrock et al. (2020a) represents true thermodynamic equilibrium. Isotopic equilibrium may not be reached in a natural setting since there are many dissolved carbonate species involved in the ultimate precipitation of carbonates, including HCO_3^- , CO_3^{2-} , CO_2 , and H_2CO_3 (Watkins et al., 2013). If one of the dissolved species is out of equilibrium with the others and water, then the precipitated carbonate may reflect that disequilibrium (Guo and Zhou, 2019). Regardless whether Eq. 5.24 represents ‘true’ thermodynamic equilibrium, it does show a correlation between $\Delta\Delta^{17}\text{O}_{\text{carb-wt}}$ and temperature that should be applicable any naturally formed carbonates.

5.4.3 Applications to natural calcite samples

Figure 5.11 shows the triple oxygen isotope compositions of marine brachiopods from different time periods over the Phanerozoic (Wostbrock et al., 2020a) and new data of ammonite from the early Triassic. Two additional triple oxygen isotope analyses of Early Triassic ammonites from the Western Interior Seaway (University of New Mexico, Earth and Planetary Sciences collections, donation by Jim Jenks) are presented. The Smithian ammonoid (*Anasibirites* sp.) comes from the Crittenden Springs (NE Nevada) locality (Jenks and Brayard, 2018). The shell preservation of the ammonoids from this locality is believed to be exceptional, as many specimens have original color patterns preserved. The Spathian ammonoids were collected from the Hot Springs locality from

SE Idaho (Guex et al., 2010) and are assigned to the *Columbites* biozone. These ammonoids are commonly found in carbonate concretions. The triple oxygen isotope values of the Smithian ammonite (rhombohedron, Fig. 5.11) are 12.624, 24.227, and -0.094 ‰ for $\delta^{17}\text{O}$, $\delta^{18}\text{O}$, and $\Delta^{17}\text{O}$, respectively. The triple oxygen isotope values of the Spathian ammonite (pentagon, Fig. 5.11) are 13.490, 25.867, and -0.084 ‰ for $\delta^{17}\text{O}$, $\delta^{18}\text{O}$, and $\Delta^{17}\text{O}$, respectively.

Of the samples shown, only two, a Silurian brachiopod (square; Fig. 5.11) and a Cretaceous belemnite from the Peedee formation (PDB, diamond; Fig. 5.11), plot close to the equilibrium curve. These samples are consistent with having precipitated in equilibrium with seawater with a $\delta^{18}\text{O}$ value of ~ 0 ‰. The PDB corresponds with a

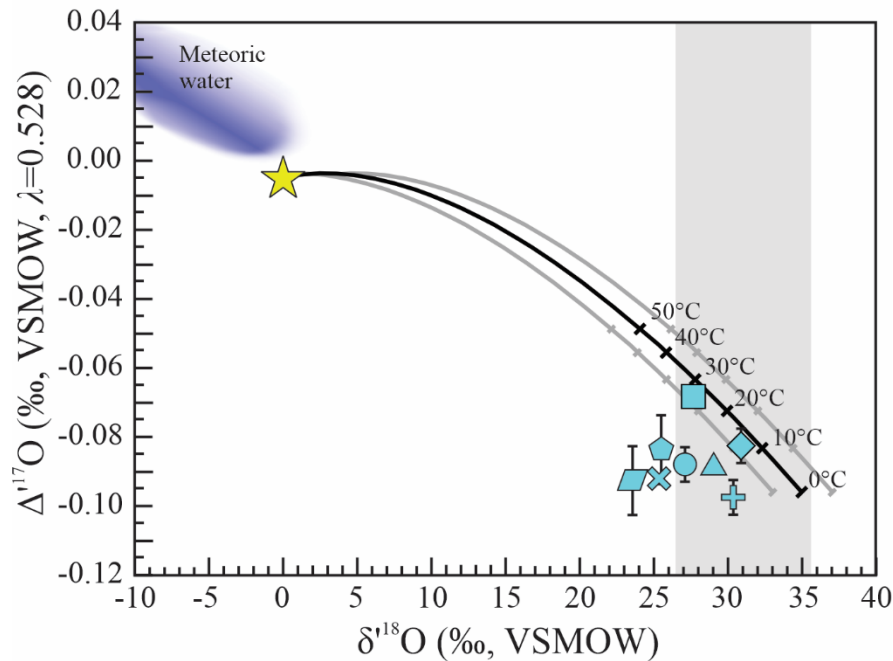


Figure 5.11 - The $\Delta^{17}\text{O}$ values vs. the $\delta^{18}\text{O}$ values of ancient carbonates in relation to the equilibrium triple oxygen isotope fractionation curve for calcite (black curve) in equilibrium with modern seawater (yellow star, $\delta^{18}\text{O}=0$ and $\Delta^{17}\text{O}=-0.005$ ‰). Temperature is marked along the black line. The seawater curve is bracketed by the modern range (-2 to $+2$ ‰) of seawater oxygen isotope compositions for equatorial and mid-latitude oceans (gray lines; Schmidt et al., 1999). The range of modern brachiopod $\delta^{18}\text{O}$ values (26.5 to 35.5‰) is represented by the light gray box (Brand et al., 2019). Samples: Cretaceous belemnite (diamond); brachiopods: Mid Ordovician, (X), Silurian (square), Mid Devonian (circle), Late Pennsylvanian (triangle), and Mid Maastrichtian (Late Cretaceous; cross); ammonites: Smithian (rhombus) and Spathian (pentagon).

formation temperature of 12 °C while the Silurian brachiopod corresponds to 28 °C. All other samples plot to the left of the equilibrium curve with modern seawater and, therefore, *cannot be in equilibrium with 0 ‰ seawater*. Assuming that the $\delta^{18}\text{O}$ value of Phanerozoic seawater was similar to today (–1 to 0 ‰), then all of these samples have Discussion of what these altered samples tell us about the ancient ocean is presented in “Ancient calcite and diagenesis”.

5.5 Application to diagenesis in silica and carbonate samples

Traditional oxygen isotope studies have looked at ancient carbonates and silicates to reconstruct the temperature of the seawater over time. There is a secular trend over time seen in the carbonate and silica (chert) record with decreasing $\delta^{18}\text{O}$ values with increasing age (Lowenstam, 1961; Degens and Epstein, 1962; Keith and Weber, 1964; Perry, 1967; Knauth and Epstein, 1976; Veizer and Hoefs, 1976; Knauth and Lowe, 1978; Perry et al., 1978; Popp et al., 1986; Veizer et al., 1986; Lohmann and Walker, 1989; Veizer et al., 1989; Veizer et al., 1997; Veizer et al., 1999; Knauth and Lowe, 2003; Brand, 2004; Knauth, 2005; Prokoph et al., 2008; Veizer and Prokoph, 2015; Ryb and Eiler, 2018). The $\delta^{18}\text{O}$ value of Archean cherts are generally 15 ‰ lower than modern (Knauth and Epstein, 1976; Knauth and Lowe, 1978; Perry et al., 1978; Winter and Knauth, 1992; Knauth and Lowe, 2003) However, the explanation for the secular trend is still debated and falls under three main hypotheses (Degens and Epstein, 1962) and a fourth, less talked about hypothesis.

- 1) The ocean was warmer in the Archean than modern (Knauth and Epstein, 1976; Knauth and Lowe, 1978; Karhu and Epstein, 1986; Winter and Knauth, 1992; Knauth and Lowe, 2003; Perry and Leticariu, 2007). This hypothesis implies the $\delta^{18}\text{O}$ value of seawater remains constant (~0 ‰) over time and the temperature of Archean seawater was 50-80 °C and cools toward the modern temperature of ~25 °C. The warm ocean theory

would also imply that the Cambrian seawater was about 40-60 °C warmer than modern seawater during the explosion of life, a direct contradiction to reasonable temperatures for most prokaryotes (Brock, 1985).

Additionally, this hypothesis complicates the faint sun paradox (Sagan and Mullen, 1972) but the faint sun paradox has been recently called into question as well (Rosing et al., 2010). Seawater modelling studies based on the oxygen isotope values of altered oceanic crust support this idea that seawater has been buffered to 0 ‰ for most of Earth's history (Muehlenbachs and Clayton, 1976; Gregory and Taylor, 1981; Muehlenbachs, 1986; Gregory, 1991; Holmden and Muehlenbachs, 1993; Muehlenbachs, 1998). Various studies using carbonate clumped isotope (Δ_{47}) values also suggest the ocean was buffered to 0 ‰, albeit with varying temperature estimates (20-70 °C), since at least the Cambrian (Eiler, 2011; Finnegan et al., 2011; Cummins et al., 2014; Ryb and Eiler, 2018; Price et al., 2020).

- 2) The $\delta^{18}\text{O}$ value of seawater was lower in the past than modern (Perry, 1967; Perry and Tan, 1972; Veizer and Hoefs, 1976; Veizer et al., 1997; Veizer et al., 1999; Hren et al., 2009; Veizer and Prokoph, 2015). This hypothesis implies the $\delta^{18}\text{O}$ value of Archean seawater was about -15 ‰ and has been shown possible by various modelling of different ratios of high to low temperature alteration flux rates (Wallmann, 2001; Kasting et al., 2006; Jaffrés et al., 2007; Kanzaki, 2020). Ocean temperatures would be similar to modern over the geologic rock record but is in contradiction to ophiolite studies suggesting a rapid ocean buffering (Muehlenbachs and Clayton, 1976; Gregory and Taylor, 1981; Muehlenbachs, 1986; Gregory, 1991; Muehlenbachs, 1998). Recent seawater oxygen isotope compositional modelling by Sengupta and Pack (2018) suggest that a 100-fold increase of continental weathering flux rate is required to lower the ocean to -8 ‰. The authors could not reconstruct a seawater with the a $\delta^{18}\text{O}$ value of -15 ‰ using any feasible changing scenario of known or estimated flux rates.
- 3) Diagenesis commonly overprints most primary depositional information (Gao and Land, 1991; Wenzel et al., 2000; Brand, 2004; Marin-Carbonne et al., 2012; Marin-Carbonne et al., 2014; Sengupta and Pack, 2018; Liljestrang et al., 2020). Diagenetic alteration generally occurs at elevated temperatures and/or in the presence of waters with a lower $\delta^{18}\text{O}$ value of seawater (Popp et al., 1986; Lohmann and Walker, 1989; Banner and Hanson, 1990; Gao and Land, 1991; Marshall, 1992; Wadleigh and Veizer, 1992; Kah, 2000; Swart, 2015; Ahm et al., 2018). However, there are rare instances where the $\delta^{18}\text{O}$ value of the diagenetic fluid may be higher than modern seawater (Grossman et al., 1991), particularly in evaporative basinal porewaters (Swart, 2015) .

- 4) Hydrothermal systems formed much of the Archean chert record (De Ronde et al., 1997; Zakharov et al., 2020; Sengupta et al., *in revision*). Hydrothermal water recycling is estimated to be ~5 times more than modern during the Archean to Proterozoic (Isley, 1995; Lowell and Keller, 2003). Some stratigraphic evidence of laterally continuous chert beds and low temperature facies preservation such as rip-up clasts suggest that at least some chert deposited in shallow, near surface settings during the Archean (Knauth, 1979; Lowe, 1983; Maliva et al., 1989; Tice et al., 2004; Maliva et al., 2005; Tice and Lowe, 2006; Perry and Lefticariu, 2007).

Of course each of these theories are in contradiction to a few studies suggesting the $\delta^{18}\text{O}$ of seawater was up to 3 ‰ higher in the past (Longinelli et al., 2002; Longinelli et al., 2003; Johnson and Wing, 2020). In summary, the $\delta^{18}\text{O}$ value of seawater over the geologic record is still an open question.

Triple oxygen isotope measurements help constrain the fluid in which the silicate or carbonate formed or can help determine if the sample is preserving primary depositional information (see Section 5.1 - Introduction for review). This is because samples must fall on a unique curve in $\Delta^{17}\text{O}$ - $\delta^{18}\text{O}$ space for a given composition of water. Departures from this line are explained by changes in the triple oxygen isotope composition of the ocean and/or diagenesis. Samples that lie to the left of the equilibrium curve have been altered by a diagenetic fluid of meteoric origin. Samples that lie above the modern seawater equilibration curve have either formed in an ocean with a lower $\delta^{18}\text{O}$ and higher $\Delta^{17}\text{O}$ value or, rarely, undergone alteration with a fluid heavier than seawater (see Fig. 5.3).

5.5.1 Ancient silica and diagenesis

Sedimentary bulk silica (broadly referred to as chert) is found throughout the rock record from 3.5 Ga through to the present day (Knauth, 2005). Chert is inherently the product of a diagenetic process where dissolved silica is reprecipitated and evolves from

Opal-A to Opal-CT to microcrystalline quartz. Generally, the term “chert” refers to microcrystalline quartz. Since the beginning of the Phanerozoic with radiolarians and siliceous sponges and more specifically diatoms appearing in the Jurassic, most SiO_2 in the ocean originates as biogenic Opal-A that transforms to microcrystalline quartz generally in an offshore environment (Maliva et al., 1989; Perry and Lefticariu, 2007). Prior to the Phanerozoic, marine silica is thought to have mostly precipitated through abiogenic (or inorganic) processes. The amount of time it takes for Opal-A to transform to microcrystalline quartz is still an active area of research (Yanchilina et al., 2020). Preservation of sedimentary features in Precambrian and earlier outcrops gives credence to the idea that some transformations can occur in the near subsurface not long after deposition (Knauth, 1973; Knauth and Lowe, 1978; Lowe, 1983; Maliva et al., 1989; Tice et al., 2004; Maliva et al., 2005; Tice and Lowe, 2006; Perry and Lefticariu, 2007). The ubiquitous presence of chert throughout geologic time and the assumed lower susceptibility to diagenesis than carbonate has enabled the oxygen isotope composition of chert to be used a paleo-indicator of ancient seawater.

Four studies have published values on the triple oxygen isotope composition of cherts from the Archean through the Phanerozoic (Levin et al., 2014; Liljestr and et al., 2020; Zakharov et al., 2020; Sengupta et al., *in revision*) and the results are presented in Figure 12. First, the vast majority of all chert samples that have been measured for triple oxygen isotope analysis plot to the left of the silica-modern seawater equilibrium fractionation line in the region generally associated with alteration. Perhaps most importantly, all chert samples from the Archean (dark blue icons in Fig. 5.12) plot to the left of the silica-modern seawater equilibrium fractionation line and not to the right which

would indicate changing seawater oxygen isotope composition (red line in Fig. 5.12), therefore the secular trend seen in the $\delta^{18}\text{O}$ values of chert is not compatible with an Archean seawater $\delta^{18}\text{O}$ value of -8 to -15 ‰.

Almost none of the chert data can be explained by equilibration with a modern seawater oxygen isotope composition. Chert samples from the Phanerozoic presented in Sengupta et al. (*in revision*), represented by the yellow diamonds in Fig. 5.12, is explained by dissolution and equilibrium re-precipitation with a meteoric-marine fluid mixture with a $\delta^{18}\text{O}$ value of -3 ‰ and a $\Delta^{17}\text{O}$ value of $+0.010$ ‰ (dashed purple line with purple star, Fig. 5.12; Sengupta et al., *in revision*). This would imply the samples are preserving a precipitation temperature between 20 and 30 °C, suggesting near-surface

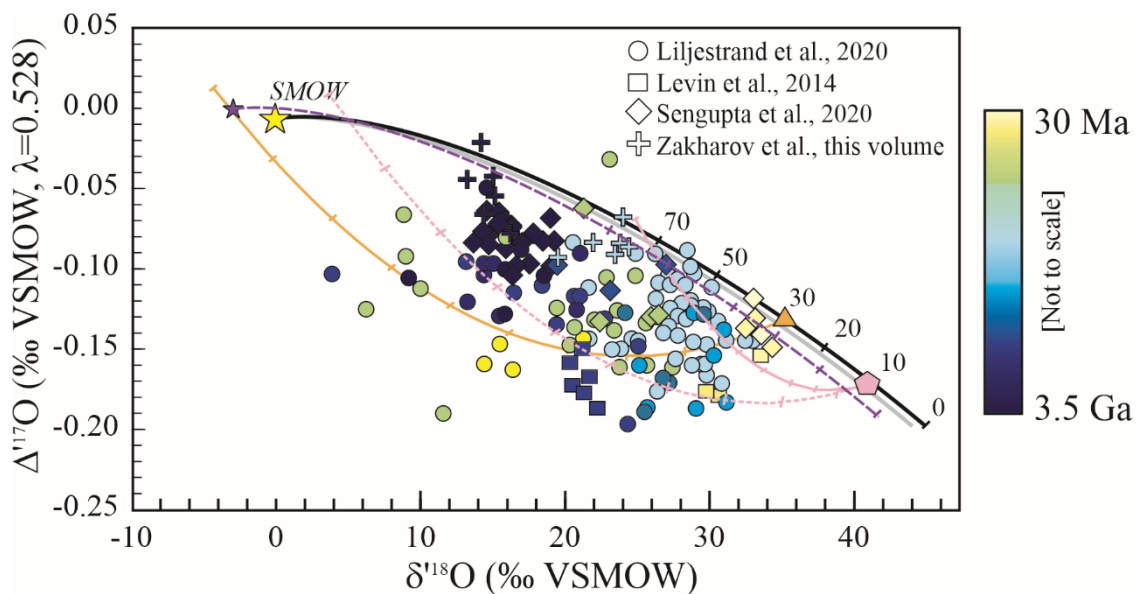


Figure 5.12 - Published $\Delta^{17}\text{O}$ and $\delta^{18}\text{O}$ values of ancient chert from the Archean through Phanerozoic from Levin et al. (2014, squares) Liljestrand et al. (2020, circles), Sengupta et al. (*in revision*, diamonds), Zakharov et al. (2020, crosses). Yellow colors are younger cherts while blue colors represent older cherts. One interpretation of the chert data suggest alteration by a fluid with a lower triple oxygen isotope value than the modern ocean (yellow star, $\delta^{18}\text{O}=0$ ‰ and $\Delta^{17}\text{O}=-0.005$ ‰). Using a fluid-rock mixing model, the precipitation temperature of the primary chert was calculated as 30 °C (Liljestrand et al, 2020; orange line and triangle) and 10 °C (Sengupta and Pack, 2018; pink lines and hexagon). Sengupta et al. (*in revision*) suggest Phanerozoic chert (yellow icons) generally form by dissolution and equilibrium re-precipitation after burial in a meteoric-marine water mixture (purple star and dashed lines), suggesting formation temperatures between 30 and 40 °C. Zakharov et al. (2020) suggests a similar precipitation scenario with pore fluid during the Proterozoic (light blue icons) and formation temperatures greater than 60 °C.

dissolution and re-precipitation. Similarly, Zakharov et al. (2020) suggest the first generation of microcrystalline quartz in a Proterozoic chert sample (light blue crosses in Fig. 5.12) formed in equilibrium with interstitial pore fluid that is similar to slightly lower than the modern seawater oxygen isotope composition at a temperature between 50 and 80 °C, representative of the temperature of early diagenesis. Three Proterozoic samples (light blue circles in Fig. 5.12) presented in Liljestr nd et al. (2020) also suggest a ~60°C temperature seawater with an oxygen isotope composition similar to modern.

All current triple oxygen isotope studies of ancient chert suggest the chert samples are either recording alteration or formed in hydrothermal fluids. Sengupta and Pack (2018) and Liljestr nd et al. (2020) suggest the initial precipitation of the silica occurred in seawater with a $\delta^{18}\text{O}$ value similar to modern seawater and at temperatures below 30 °C. Both studies used fluid-rock interaction models (see Figs. 5.4 and 5.5) to calculate primary chert compositions. Liljestr nd et al. (2020) used a Monte Carlo analysis to best constrain the alteration fluid composition and primary temperature of formation and concluded the $\delta^{18}\text{O}$ value of alteration fluid was about -16.5 ‰, the alteration occurred at about 200 °C and the initial formation temperature of the chert was about 30 °C (orange line and triangle; Fig. 5.12). Sengupta and Pack (2018) (using data from Levin et al. (2014)) used different conditions for their model: an alteration fluid with a $\delta^{18}\text{O}$ value of -6 ‰ at 50 °C for the Phanerozoic cherts and -10 ‰ at 180 °C for the Archean cherts and a chert precipitation temperature of 10 °C (pink lines and pentagon; Fig. 5.12). Sengupta et al. (*in revision*) used Bayesian model to suggest two different alteration scenarios for the Archean and Proterozoic chert measured for their study. For the Archean samples they separated samples into two groups, one with $\delta^{18}\text{O}$ values between

13 and 16 ‰ and one group with $\delta^{18}\text{O}$ values between 18.7 and 19.3 ‰. For the first Archean group, they found the initial silica precipitated in seawater with a similar oxygen isotope composition as modern seawater and was subsequently altered by a fluid with a $\delta^{18}\text{O}$ value of -16.5 ‰ at an alteration temperature of 50 °C and W/R ratio of 1. Their Bayesian model was inconclusive on initial silica precipitation temperature. For the second group of Archean chert, the Bayesian model again predicted initial precipitation in seawater with an oxygen isotope composition similar to modern at 80 °C and was subsequently altered with a fluid with a $\delta^{18}\text{O}$ value of -14 ‰ at either 50 or 150 °C. The

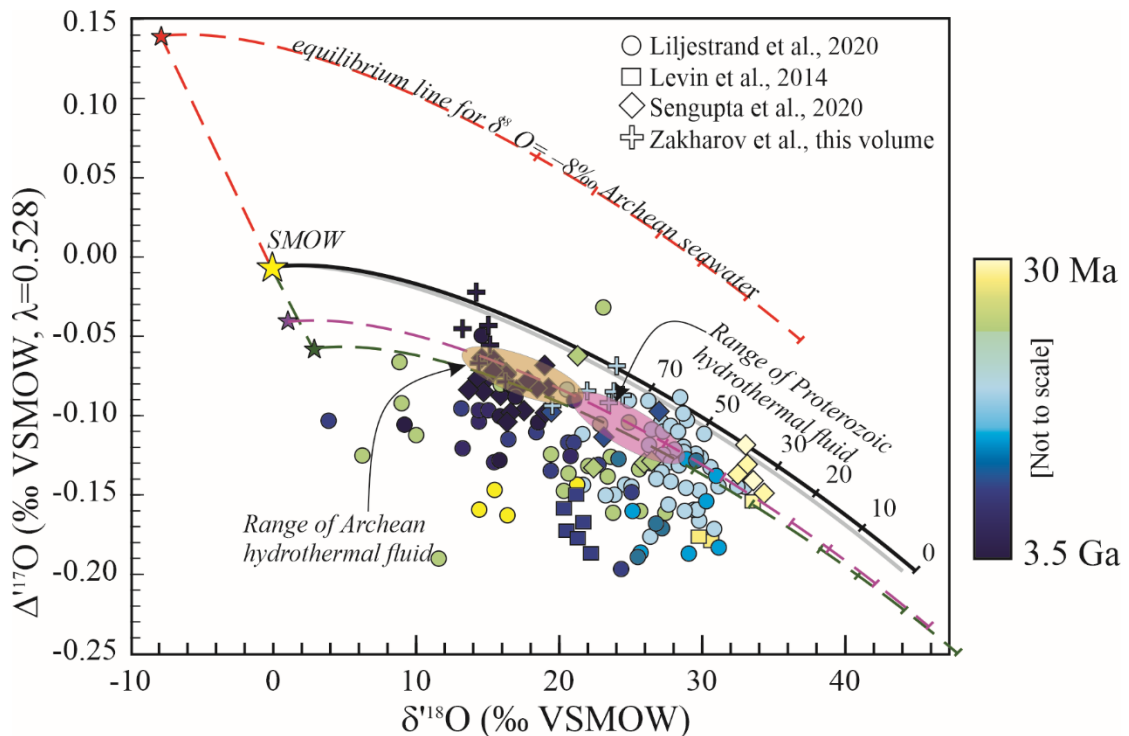


Figure 5.13 - Various seawater triple oxygen isotope compositions can describe published $\Delta^{17}\text{O}$ and $\delta^{18}\text{O}$ values of ancient chert from the Archean through Phanerozoic from Levin et al. (2014, squares) Liljestrand et al. (2020, circles), Sengupta et al. (*in revision*, diamonds), Zakharov et al. (2020, crosses). Yellow colors are younger cherts while blue colors represent older cherts. The triple oxygen isotope values of chert do not suggest the seawater had a lower $\delta^{18}\text{O}$ value in the past (red star) if corresponding change in $\delta^{18}\text{O}$ and $\Delta^{17}\text{O}$ follow the trend modelled by Sengupta and Pack (2018; dashed red line). A possible explanation is that the $\delta^{18}\text{O}$ value of seawater was higher in the Archean compared to modern or that Precambrian chert tended to form in hydrothermal fluid, resulting in a fluid with a higher $\delta^{18}\text{O}$ value than modern seawater. The heavier fluid could have a $\delta^{18}\text{O}$ value of $+1$ ‰ (purple star and dashed purple line) as proposed in Sengupta et al. (*in revision*) and Zakharov et al. (2020) or have a $\delta^{18}\text{O}$ value as high as $+3$ ‰ as proposed in Johnson and Wing (2020; green star and dashed line). Either seawater $\delta^{18}\text{O}$ scenario suggests high formation temperatures between 150 and 300 °C for Archean chert (orange circle) and 70 to 150 °C for Proterozoic chert (purple circle).

Bayesian model was ambiguous as to the W/R ratio. Proterozoic cherts fit within both Archean diagenetic models. Sensitivity in the Bayesian model suggest the initial silica for either the Archean or Proterozoic samples could have formed in temperatures as low as 10 °C (Sengupta et al., *in revision*).

Although the water-rock mixing model can explain the above data, Sengupta et al. (*in revision*) favor the hypothesis that the Archean and Proterozoic samples are retaining oxygen isotope values in which the chert interacted a higher $\delta^{18}\text{O}$ value fluid than modern seawater (Fig. 5.13), also favored in Zakharov et al. (2020). Sengupta et al. (*in revision*) acknowledge that they cannot distinguish between whether the samples formed in seawater that had higher $\delta^{18}\text{O}$ values and lower $\Delta^{17}\text{O}$ values than modern seawater (Johnson and Wing, 2020) due to higher hydrothermal water flux in the Archean (Isley, 1995; Lowell and Keller, 2003) or the samples formed in hydrothermal fluid at vents but ambient seawater was more similar to modern (Bindeman et al., 2018; Zakharov and Bindeman, 2019; Peters et al., 2020). Zakharov et al. (2020) uses a modern hydrothermal vent in Iceland as an analog to suggest that the Archean samples from their study formed in a vent-like setting in fluid with a $\delta^{18}\text{O}$ value of 0.9 to 1.6 ‰ (De Ronde et al., 1997; Farber et al., 2015) and in temperatures between 150 and 300 °C. Sengupta et al. (*in revision*) suggest a similar fluid (either vent or ambient seawater) oxygen isotope composition with a $\delta^{18}\text{O}$ value of +1‰ and $\Delta^{17}\text{O}$ value of -0.040‰ and suggest a temperature of formation for the Archean cherts of 150 to 220 °C and 75-150 °C for Proterozoic cherts (purple star and dashed line, Fig. 5.13). They explain the lower Proterozoic fluid temperatures result from a lowering of the geothermal gradient. Johnson and Wing (2020) suggest that due to the absence of continents, the Archean ocean could

have a $\delta^{18}\text{O}$ value as high as +3‰ (green star and dashed line, Fig. 5.13). Following a $\lambda \approx 0.51$ for the changing seawater trend presented in (Sengupta and Pack, 2018), an Archean seawater with a $\delta^{18}\text{O}$ value of +3‰ would have a $\Delta^{17}\text{O}$ value of about -0.05% . Seawater with a $\delta^{18}\text{O}$ value of +3‰ also fits the Archean and Proterozoic chert samples (blue icons in Fig. 5.13) at similar temperatures proposed by Sengupta et al. (*in revision*) and Zakharov et al. (2020). Interestingly, seawater with a $\delta^{18}\text{O}$ value of +3‰ does not fit the majority of the Phanerozoic chert samples. Suggesting that, if the hypothesis that most Precambrian chert formed seawater with a higher $\delta^{18}\text{O}$ value than modern is true, perhaps chert formation processes changed once silica organisms were present in seawater (Maliva et al., 1989; Maliva et al., 2005; Perry and Leticariu, 2007).

Overall, most Archean and Proterozoic chert that has currently been measured for triple oxygen isotope values could have formed or been altered by fluid that is higher in $\delta^{18}\text{O}$ than modern seawater. However, initial silica precipitation in cooler waters (less than 30 °C) in seawater with an oxygen isotope composition similar to modern which subsequently was altered by a diagenetic fluid with lower $\delta^{18}\text{O}$ values and higher $\Delta^{17}\text{O}$ values cannot be excluded (Sengupta and Pack, 2018; Liljestr and et al., 2020). Therefore, thus far, triple oxygen isotope studies of cherts have not conclusively shown the $\delta^{18}\text{O}$ value of Archean seawater. However, based on the data in published studies, the data do not suggest Archean or Proterozoic seawater had a lower $\delta^{18}\text{O}$ value than modern. Examining Archean and Proterozoic chert that preserve sedimentary facies, such as draping and rip up clast, indicating formation in a marine setting at or near the seafloor would provide additional information.

5.5.2 Ancient calcite and diagenesis

Equation 5.24 can be used to determine the temperature and/or $\delta^{18}\text{O}_{\text{water}}$ value in ancient calcite samples. Since there is only one unique triple oxygen isotope value for a given temperature and $\delta^{18}\text{O}_{\text{water}}$ value, the triple oxygen isotope composition of a carbonate for a given $\delta^{18}\text{O}_{\text{water}}$ value is limited (Fig. 5.6). Wostbrock et al. (2020a) reported the triple oxygen isotope value of five ancient brachiopods and one belemnite from the Phanerozoic. Only two samples, a Silurian brachiopod (formation temperature ~ 28 °C) and a Cretaceous belemnite (formation temperature ~ 12 °C), have triple oxygen isotope values that can be in equilibrium with seawater similar to a modern ocean oxygen isotopic composition (Fig. 5.11). The remaining brachiopods from that study and the two ammonites presented in this manuscript all have $\delta^{18}\text{O}$ and $\Delta^{17}\text{O}$ values that plot to the left of the modern ocean triple oxygen isotope fractionation curve, suggesting alteration by a meteoric water. Since the $\delta^{18}\text{O}$ values of these samples all fall within the modern range of modern brachiopod $\delta^{18}\text{O}$ values (Fig. 5.11; Brand et al., 2019), only with the addition of the $\Delta^{17}\text{O}$ value can the conclusion be stated that these ancient brachiopods could not have formed in seawater similar to modern oceans.

The fluid/rock alteration model (see Section 5.2.5 - Diagenetic trends) can be used to ‘see through’ the alteration and calculate the primary triple oxygen isotope composition before alteration (Fig. 5.14). For the Ordovician brachiopod, Wostbrock et al. (2020a) were able to fit the measured isotope data with a $\delta^{18}\text{O}$ value of the alteration fluid between -15 and -10 ‰ and a $\Delta^{17}\text{O}$ value of $+0.03$ ‰ and a diagenesis

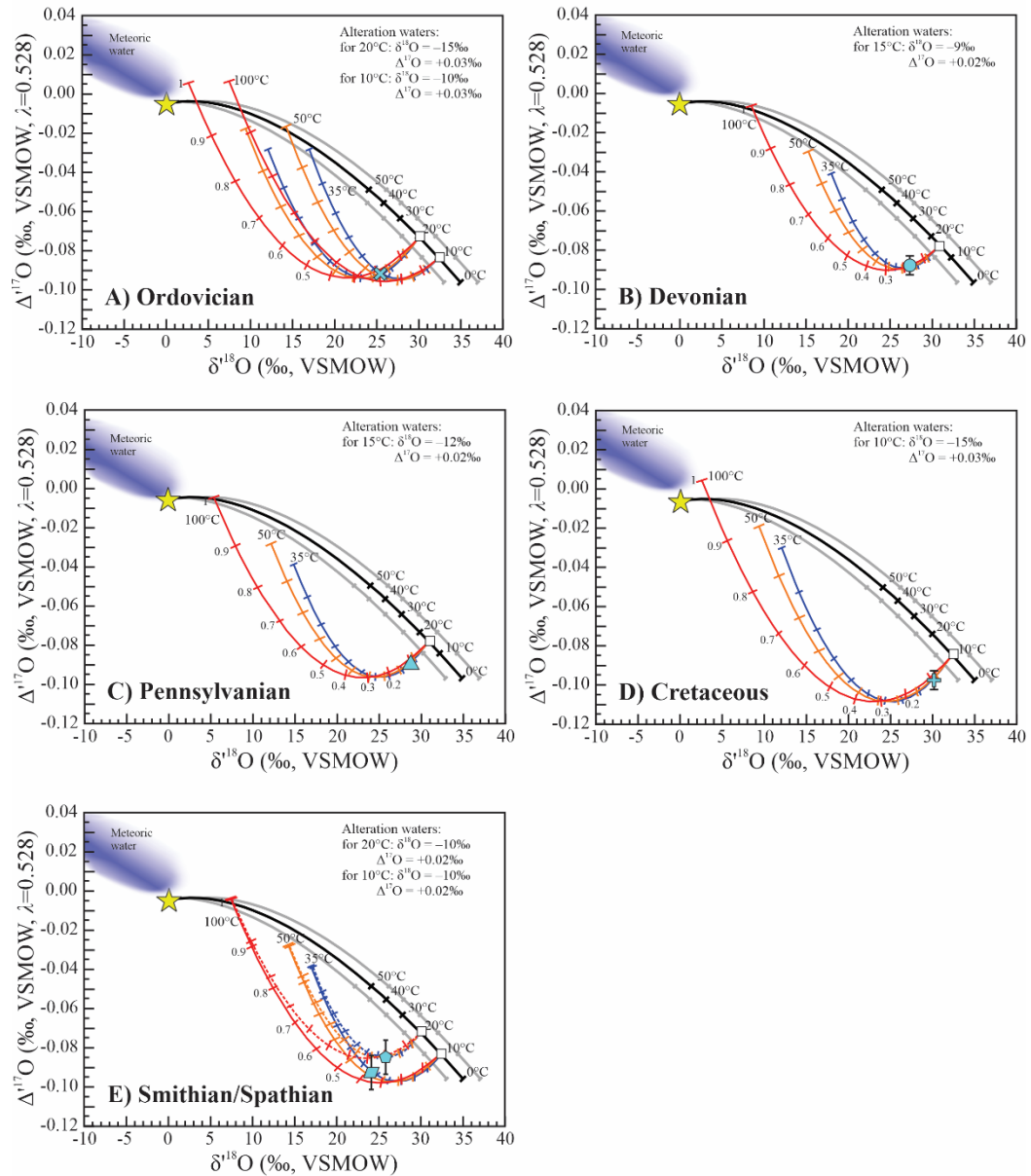


Figure 5.14 - Back-calculated initial triple oxygen isotope compositions of altered brachiopod and ammonite samples. Alteration fluid triple oxygen isotope value is written on each graph and pathways were modelled for alteration temperatures of 35 (blue lines), 50 (orange lines), and 100 (red lines) °C. A) The Mid-Ordovician brachiopod formed between 10 and 20 °C. To demonstrate the fact that the fluid-rock interaction model is under constrained, Wostbrock et al. (2020a) used two different alteration fluids to calculate two different potential primary calcite triple oxygen isotope values and show the range of results the model can produce. For B-E, we only show one potential solution for the fluid-rock mixing model for the sake of simplicity. B) The Mid Devonian brachiopod calculated primary calcite triple oxygen isotope composition suggests an initial precipitation temperature of ~18 °C. C) The Late Pennsylvanian brachiopod calculated primary calcite triple oxygen isotope composition suggests an initial precipitation temperature of ~15 °C. D) The Mid Maastrichtian (Late Cretaceous) brachiopod calculated primary calcite triple oxygen isotope composition suggests an initial precipitation temperature of ~10°C. E) The Smithian ammonite (orange diamond) calculated primary calcite triple oxygen isotope composition suggests an initial precipitation temperature of ~20°C. The Spathian ammonite (orange circle) calculated primary calcite triple oxygen isotope composition suggests an initial precipitation temperature of ~10°C.

temperature between 35 and 100 °C. Under these conditions, the back-calculated initial $\delta^{18}\text{O}$ value of the brachiopod was between 30 and 32.5 ‰, corresponding to a formation temperature of 10 to 20 °C, assuming the seawater had a similar triple oxygen isotope composition as modern oceans. Using the same fluid-rock mixing model, the primary composition of the other altered brachiopod and ammonite samples can be calculated (Fig. 5.14). All the brachiopod shells formed in water ranging between 10 and 20 °C, similar to the 0 – 30 °C water temperature range of modern brachiopods (Brand et al., 2019). For the Smithian and Spathian (early Triassic) ammonites, both were altered regardless of the visual preservation quality of the fossil shell. Nevertheless, it is possible to back-calculate the formation temperatures of 10 and 20 °C for the Spathian age and Smithian age samples, respectively. These agree well with the 10 °C difference suggested using the $\delta^{18}\text{O}$ values of conodonts (Sun et al., 2012).

5.6 Triple oxygen isotopes of quartz and coexisting calcite

The equilibrium oxygen isotope fractionation between quartz and calcite is derived by combining the $\Delta^{17}\text{O}-\delta^{18}\text{O}$ relationships for quartz–water and calcite–water (Fig. 5.15). The $\theta_{\text{qz-cc}}$ values are less than those of quartz–water or calcite–water. At 0°C, our calculated $\theta_{\text{qz-cc}}$ of 0.518 compares well with the theoretical estimate of 0.520 (Hayles et al., 2018).

Three carbonate lithologies that contain authigenic quartz are used in this study: the well-known Herkimer Diamond quartz crystals hosted in carbonate (New York, USA), doubly terminated quartz crystals in Early–Middle transition Triassic marine pelagic limestone (North Dobrogea, Romania), and chert nodules from Cretaceous limestone (Étretat, France). The Herkimer Diamond and marine pelagic limestone from

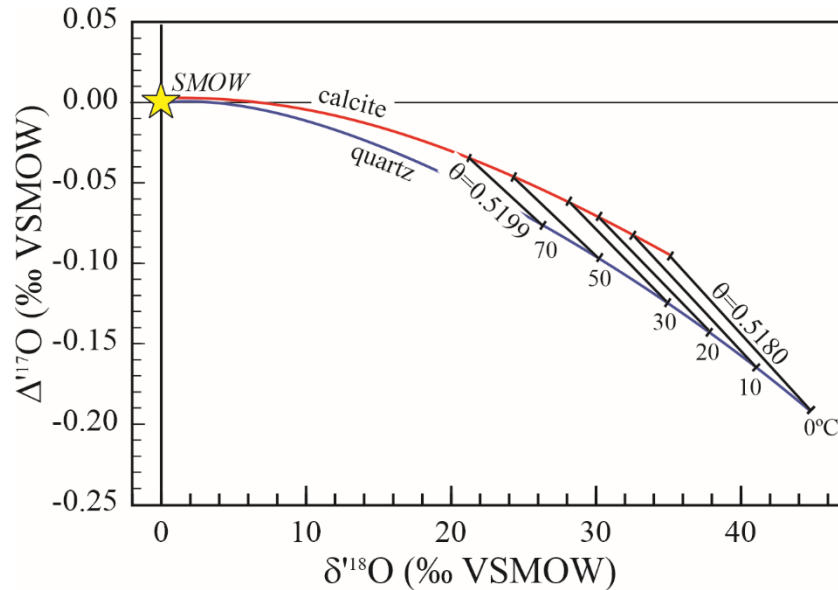


Figure 5.15 - $\Delta^{17}\text{O}$ - $\delta^{18}\text{O}$ plot for quartz and calcite and the equilibrium $\theta_{\text{qz-cc}}$ values from 0 to 70 °C.

North Dobrogea, Romania both contain glassy, optically clear quartz crystals. The Romanian samples do not contain sponge spicules, although they are found elsewhere in the section, suggesting that the quartz crystals are the product of dissolution and reprecipitation of the sponge spicules. The Étretat, France sample is chert and data are reported in Pack and Herwartz (2014). The other two samples are data from Sharp et al. (2016) and all data are normalized to the same San Carlos olivine scale (Sharp and Westbrock, 2020).

The two authigenic quartz samples can be explained by recrystallization with varying amounts of meteoric water infiltration (Fig. 5.17). If a small amount of meteoric water entered the system, it could dissolve the reactive amorphous silica and cause it to reprecipitate without appreciably affecting the isotopic composition of the host calcite. Using a simple mass balance model following equations 5.11 and 5.12, it is easy to reproduce the $\Delta^{17}\text{O}$ and $\delta^{18}\text{O}$ values for both the Romanian and New York samples with differing F/R ratios and reaction temperatures. For the Romanian samples, the $\delta^{18}\text{O}$ value

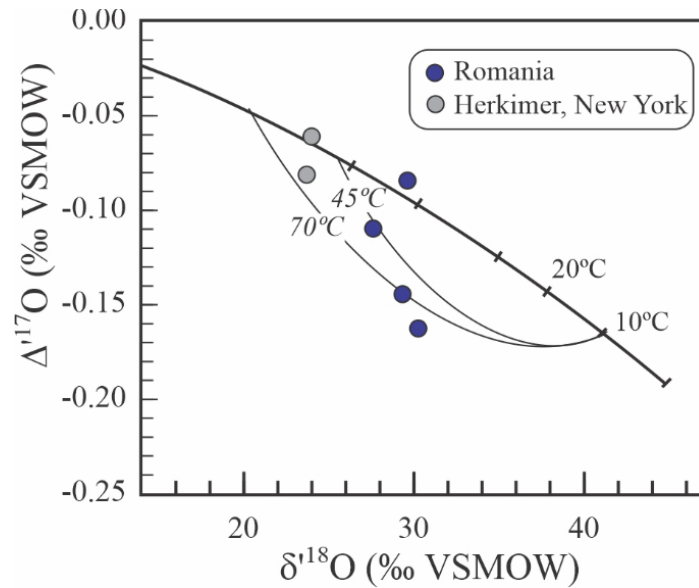


Figure 5.16 - Isotopic compositions of authigenic euhedral quartz crystals hosted in carbonates. The oxygen isotope data suggest some degree of alteration by meteoric fluids. Pathways for interaction between a sample formed at $\sim 10^\circ\text{C}$ (as evidenced by carbonate $\delta^{18}\text{O}$ values) and a meteoric fluid ($\delta^{18}\text{O} = -6\text{‰}$, $\Delta^{17}\text{O} = 0.03\text{‰}$). Alteration paths shown for temperatures of 45°C and 70°C .

of the calcite is $\sim 33.3\text{‰}$, suggesting formation temperatures of $\sim 10^\circ\text{C}$. Two reaction paths are illustrated at diagenesis temperatures of 45°C and 70°C using a starting quartz value in equilibrium with seawater at 10°C . In the case of the Herkimer diamonds, higher temperatures, approaching 100°C are expected. Calculated F/R ratios are high, but this number is the ratio of oxygen in the fluid to that in the quartz. If the calcite is relatively unreactive, then the actual amount of fluid could be very small.

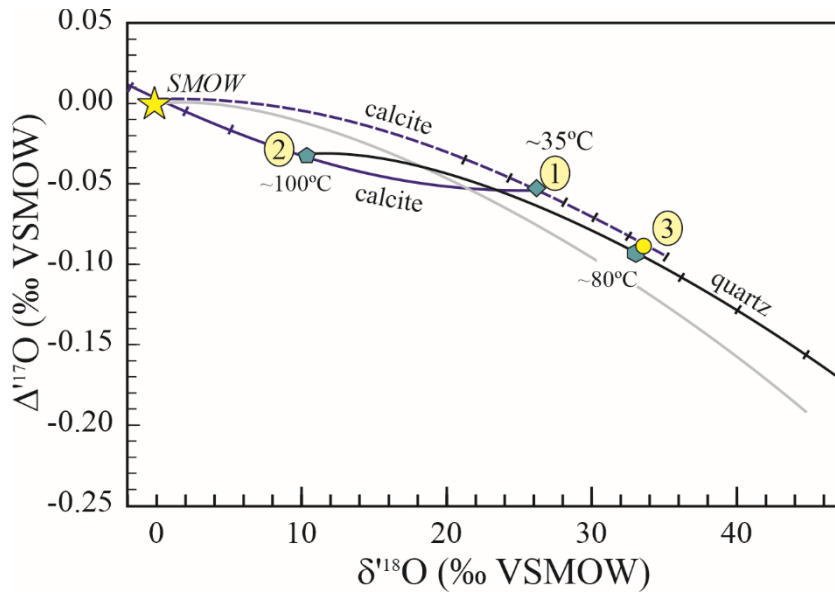


Figure 5.17 - Possible reaction sequence to explain the high $\Delta^{17}\text{O}$ value (yellow circle) of carbonate-hosted chert. 1) Carbonates form with an isotopic composition at ①. 2) The sample is heated and the fluid in equilibrium with carbonate is at ②. 3) The fluid infiltrates the overlying sediment and precipitates quartz at ③. The grey curve is the equilibrium quartz-water fractionation with seawater.

The French chert samples plot above the equilibrium curve for quartz and seawater (Fig. 5.17). It is not possible to explain this sample in terms of equilibrium with ocean water or diagenesis with meteoric water. Instead, a scenario of fluids migrating from deeper hotter sections into overlying sediments better describes this sample. The overall process shown in Figure 5.17 is the following: First, a carbonate is precipitated at composition ①. The sample is buried and heated to 100°C. Interstitial fluid in equilibrium with the heated carbonate has an oxygen isotope composition at ②. The curve between ① and ② is the oxygen isotope equilibrium curve for carbonates with the origin at the carbonate value (position ①; blue solid line). This fluid buoyantly infiltrates the overlying sediments at a lower temperature and precipitates quartz at ③. The black curve between ② and ③ is the oxygen isotope equilibrium curve for quartz with the origin at ②. It represents the process of a fluid starting at composition ② precipitating quartz at ③. The black curve between ② and ③ is the oxygen isotope equilibrium curve

for quartz with the origin at ②. It represents the process of a fluid starting at composition ② precipitating quartz at ③. The geological scenario is reasonable and provides an explanation for how samples can plot above the mineral–seawater equilibrium curve.

5.7 Conclusions

Recent studies have clearly demonstrated the usefulness in making triple oxygen isotope measurements compared to only measuring the $\delta^{18}\text{O}$ value. Triple oxygen isotope measurements serve as a unique tool that can determine equilibrium vs. non-equilibrium vs. alteration processes. The silica–water triple oxygen isotope fractionation system appears to be well constrained. Inconsistencies remain in published carbonate–water triple oxygen isotope fractionation values, probably due to the different methods used to obtain the triple oxygen isotope values. Nevertheless, application of the calcite–water or quartz–water triple isotope fractionation curves to ancient samples allows us to constrain the temperatures of formation and conditions of diagenesis. A fluid-rock mixing model can be used to see through alteration and calculate primary oxygen isotope compositions of silicate and carbonate rocks. Applying this model to ancient silicates and carbonates shows that the low $\delta^{18}\text{O}$ values of the ancient samples are not related to changing ocean oxygen isotope values. Instead, they are mostly a product of diagenesis or initially precipitated in hydrothermal fluid.

5.8 Acknowledgements

The authors express their gratitude for constructive reviews from Page Chamberlain and Weifu Guo. J.A.G.W and Z.S acknowledges support from NSF GRFP grant DGE-1418062, NSF EAR 1551226, and NSF EAR 1747703. We thank Jim Jenks, Viorel Atudorei, and UNM EPS collections for the Smithian and Spathian ammonite samples.

6. CONCLUSIONS

The work in this dissertation lays the groundwork for future studies investigating the triple oxygen isotope compositions of carbonates. All laboratories can now standardize their oxygen isotope values to the VSMOW-SLAP scale. This work aligns the traditional VPDB scale typically used for carbonates to the VSMOW-SLAP scale so that triple oxygen isotope values of carbonates can be directly compared to that of silicates and water. This should help diminish interlaboratory differences and reduce the number of studies that report triple oxygen isotope values to different scales (e.g., relative to San Carlos Olivine).

Additionally, this work developed a carbonate-water triple oxygen isotope equilibrium fractionation line using an empirical calibration of modern carbonates and associate water. Importantly, this work concludes that a difference in calcite-water fractionation does exist in most carbonates that precipitate in natural settings and laboratory precipitation experiments may not best represent natural precipitation. Also, the calcite-water triple oxygen isotope equilibrium fractionation line was demonstrated to be incredibly sensitive to samples that have undergone diagenesis. This tool can be used to see alteration in samples that have experienced F/R ratios as low as 0.2.

Lastly, the $\Delta^{17}\text{O}-\delta^{18}\text{O}$ values of carbonates change in a predictable way during diagenesis. This led to the development of a triple oxygen isotope equipped fluid-rock mixing model that can be applied to altered carbonate rocks. Using this model and few assumptions, I showed that samples that are expected to be pristine (e.g., brachiopods from Chapters 3 and 5) actually experienced slight alteration that can be seen using the triple oxygen isotope composition. With a few basic assumptions, I can see-through the

diagenesis and show that the carbonate initially formed in seawater both similar to modern and cooler than estimated using only carbonate $\delta^{18}\text{O}$ values and the assumption the $\delta^{18}\text{O}$ value of water is 0 (e.g., Figure 1.1A). This is the first study using only the oxygen isotope composition of carbonates to show that both the $\delta^{18}\text{O}$ value and temperature of seawater of the past can be similar to modern values.

The future work of triple oxygen isotope measurements on carbonates is vast and exciting. However, the required sample size (5-6 mg) and required time to analyze (~4 days of reaction) greatly constrains the number of analyses performed using the method described in this dissertation. An obvious future research direction would include new methods with higher sample throughput. Yet, with the fundamental questions about calcite-water fractionation answered, we can start to really explore the important geologic questions. I will list only a few examples of potential future studies. One example is an in-depth analysis of carbonate triple oxygen isotope values over a constrained time period to find any higher resolution changes that may be preserved. Another would be to look at lacustrine, soil, and/or cave carbonates to better constrain paleo-precipitation or $p\text{CO}_2$ values. Additionally, there are many current tools to look for diagenesis. A more in-depth analysis that correlates diagenetic features to triple oxygen isotope values may better constrain alteration histories. Finally, carbonate minerals are ubiquitous in the rock record. Any oxygen isotope analysis or study will benefit from the additional constraint of the $\delta^{17}\text{O}$ composition. Future studies can use this new tool as a way to develop a deeper understanding of geologic processes.

APPENDICES

Appendix A. Mass spec linearity and pressure effect	138
Appendix B. Residual gas analysis after carbonate fluorination.....	139
Appendix C. Published triple oxygen isotope values of silicates.....	140
Appendix D. Published triple oxygen isotope values of air	141
Appendix E. Photos of samples from Chapter 3	142
Appendix F. Raw data of marine samples from Chapter 3.....	143
Appendix G. Raw data of synthesized samples and Devils Hole from Chapter 3	144
Appendix H. Raw data of ancient calcite from Chapter 3	145
Appendix I. Fractionation associated with fluorination of carbonates in a Ni-tube	146
Appendix J. $1000 \ln \alpha^{18\text{O}}_{\text{cc-wt}}$ values used to derive calcite-water fractionation line	148
Appendix K. Literature compilation of $1000 \ln \alpha$ values for calcite–water.....	149

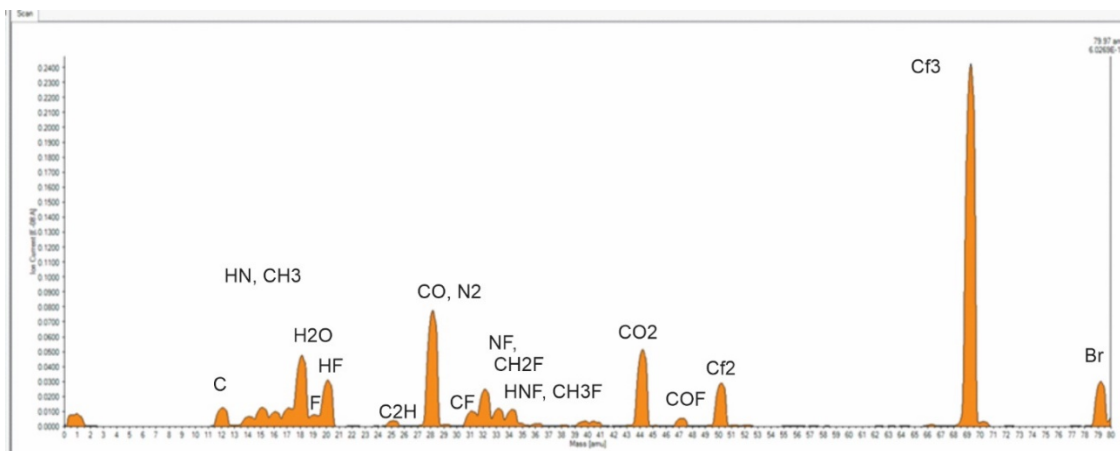
Appendix A. Mass spec linearity and pressure effect

To perform the pressure effect test two different gases were analyzed ($\Delta\delta^{18}\text{O}\approx 25\text{‰}$ and $\Delta\Delta^{17}\text{O}\approx -0.3\text{‰}$ at different pressures (3V, 5V, and 10V). The $\Delta^{17}\text{O}$ value changed by 0.002‰ and the $\delta^{18}\text{O}$ value changed by 0.04‰. Since samples are always run at 5.5V and aim to have the differences in intensity between bellows never vary by more than 200mV during a run, there is no reason to correct the data for a pressure effect as described in Yeung et al. (2018).

Voltage Trial	$\delta^{17}\text{O}$	$\delta'^{17}\text{O}$	$\delta^{18}\text{O}$	$\delta'^{18}\text{O}$	$\Delta^{17}\text{O}$
3V	14.1197	14.0209	27.6381	27.2631	-0.3739
5V	14.1328	14.0339	27.6557	27.2082	-0.3701
10V	14.1459	14.0468	27.6881	27.3049	-0.3702

Appendix B. Residual gas analysis after carbonate fluorination

Residual products were analyzed using a Pfeiffer Prism Quadrupole. Below is an example of one gas spectra of residual products still frozen in the Ni tubing after O₂ removal. Since the small amount of CO₂ and COF are within range of H₂O and CO (or N₂) these amounts must be trace compared to amount of O₂ produced. Therefore, the reaction is considered to be quantitative.



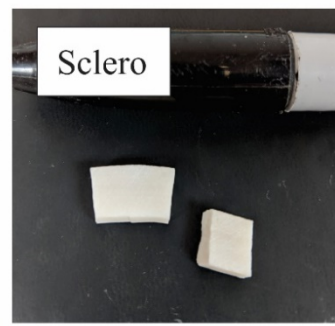
Appendix C. Published triple oxygen isotope values of silicates

Study	Mineral	$\delta^{17}\text{O}$	$\delta^{18}\text{O}$	$\delta^{17}\text{O}$	$\delta^{18}\text{O}$	$\Delta^{17}\text{O}$ ($\lambda=0.528$)
Pack et al. (2016)	SCO	2.715	5.22	2.711	5.206	-0.038
Sharp et al. (2016)	SCO	2.886	5.577	2.882	5.562	-0.055
Tanaka and Nakamura (2013)	SCO	2.7	5.28	2.696	5.266	-0.084
	UWG	2.93	5.71	2.926	5.694	-0.081
Kusakabe and Matusuhisa (2008)	NBS-28	4.96	9.56	4.948	9.515	-0.076
	NBS-28	4.76	9.04	4.749	8.999	-0.003
	UWG	2.91	5.50	2.906	5.485	0.010
	SCO	2.84	5.19	2.836	5.177	0.103
Ahn et al. (2012)	SCO	2.56	4.98	2.557	4.968	-0.066
	UWG	2.81	5.4	2.806	5.385	-0.037
	NBS-28	4.52	8.69	4.510	8.652	-0.059
Pack and Herwartz (2015)	SCO	2.69	5.28	2.686	5.266	-0.094
	NBS-28	5.06	9.75	5.047	9.703	-0.076
	UWG	3.06	5.99	3.055	5.972	-0.098
Pack et al. (2017)	NBS-28	5.04	9.65	5.027	9.604	-0.043
Franchi et al. (1999)	NBS-28	4.824	9.250	4.812	9.207	-0.049
	UWG	2.808	5.443	2.804	5.428	-0.062
	SCO	2.597	4.980	2.594	4.968	-0.029
Starkey et al. (2016)	UWG	3.011	5.779	3.006	5.762	-0.036
	NBS28	5.037	9.590	5.024	9.545	-0.016
San Carlos Olivine I (d18O = 4.88‰)		2.487	4.768	2.484	4.757	-0.028
San Carlos Olivine II (d18O = 5.23‰)		2.674	5.13	2.670	5.117	-0.031
Young et al. (2014)	SCO	2.726	5.177	2.722	5.164	-0.004
	UWG	2.972	5.678	2.968	5.662	-0.022

Appendix D. Published triple oxygen isotope values of air

Study	$\delta^{17}\text{O}$	$\delta^{18}\text{O}$	$\delta'^{17}\text{O}$	$\delta'^{18}\text{O}$	$\Delta'^{17}\text{O}$ ($\lambda=0.528$)
Barkan and Luz (2005)	12.08	23.880	12.008	23.599	-0.453
Barkan and Luz (2011)	12.026	23.881	11.954	23.600	-0.507
Pack et al. (2017)	12.270	24.150	12.195	23.863	-0.404
Young et al. (2014)	11.979	23.533	11.908	23.260	-0.374
Yeung et al. (2012)	11.932	23.424	11.861	23.154	-0.364

Appendix E. Photos of samples from Chapter 3



Appendix F. Raw data of marine samples from Chapter 3

Measured data of marine samples from fluorination in nickel reaction vessels (δ_{meas}) compared to the $\delta^{18}\text{O}$ value obtained via phosphoric acid digestion ($\delta^{18}\text{O}_{\text{conv}}$). All data are reported in ‰ and relative to VSMOW–SLAP.

Sample	$\delta^{17}\text{O}_{\text{meas}}$	$\delta^{17}\text{O}_{\text{meas}}$	$\delta^{18}\text{O}_{\text{meas}}$	$\delta^{18}\text{O}_{\text{meas}}$	$\Delta^{17}\text{O}_{\text{meas}}$	$\delta^{18}\text{O}_{\text{conv}}$	$\Delta\delta^{18}\text{O}_{\text{meas-conv}}$
Signy-1	17.256	17.109	33.112	32.576	-0.091	34.847	-1.735
Signy-2	17.704	17.549	33.997	33.432	-0.103	34.847	-0.850
Signy-3	17.274	17.127	33.155	32.617	-0.095	34.847	-1.692
Signy-4	17.072	16.928	32.791	32.265	-0.108	34.847	-2.056
Signy-5	17.061	16.917	32.749	32.224	-0.097	34.847	-2.098
Signy-6	17.090	16.946	32.800	32.273	-0.094	34.847	-2.047
Signy-7	17.252	17.104	33.116	32.580	-0.098	34.847	-1.731
Signy-8	17.194	17.048	33.010	32.477	-0.100	34.847	-1.837
Avg.	17.238	17.091	33.091	32.556	-0.098	34.847	-1.756
$\pm 1\sigma$	0.095	0.093	0.179	0.174	0.005		
Rothera-1	16.765	16.626	32.176	31.669	-0.095	34.044	-1.868
Rothera-2	16.219	16.089	31.120	30.646	-0.092	34.044	-2.924
Rothera-3	16.471	16.337	31.596	31.107	-0.087	34.044	-2.448
Rothera-4	16.643	16.506	31.933	31.433	-0.091	34.044	-2.111
Rothera-5	16.628	16.491	31.911	31.412	-0.095	34.044	-2.133
Avg.	16.545	16.410	31.747	31.253	-0.092	34.044	-2.297
$\pm 1\sigma$	0.210	0.207	0.407	0.394	0.003		
L.Ery-1	16.5087	16.374	31.6691	31.178	-0.088	32.679	-1.010
L.Ery-2	16.3862	16.253	31.416	30.933	-0.080	32.679	-1.263
L.Ery-3	16.2794	16.148	31.1912	30.715	-0.070	32.679	-1.488
Avg.	16.391	16.258	31.425	30.942	-0.079	32.679	-1.254
$\pm 1\sigma$	0.115	0.113	0.239	0.232	0.009		
Sclero-1	15.5765	15.456	29.8717	29.434	-0.085	31.136	-1.264
Sclero-2	15.6415	15.52	29.9852	29.544	-0.079	31.136	-1.151
Sclero-3	15.4557	15.337	29.6465	29.216	-0.089	31.136	-1.490
Avg.	15.558	15.438	29.834	29.398	-0.084	31.136	-1.302
$\pm 1\sigma$	0.094	0.093	0.172	0.167	0.005		
GBB-1	15.4174	15.3	29.5615	29.133	-0.082	30.904	-1.343
GBB-2	15.282	15.166	29.3003	28.879	-0.082	30.904	-1.604
GBB-3	15.1667	15.053	29.051	28.637	-0.067	30.904	-1.853
GBB-4	15.3655	15.249	29.4381	29.013	-0.070	30.904	-1.466
Avg.	15.308	15.192	29.338	28.916	-0.075	30.904	-1.566
$\pm 1\sigma$	0.109	0.108	0.219	0.213	0.008		
Ooids-1	15.4511	15.333	29.635	29.204	-0.087	30.889	-1.254
Ooids-2	15.5121	15.393	29.7436	29.31	-0.083	30.889	-1.145
Ooids-3	15.6903	15.568	30.0843	29.641	-0.082	30.889	-0.805
Avg.	15.551	15.431	29.821	29.385	-0.084	30.889	-1.068
$\pm 1\sigma$	0.124	0.122	0.234	0.228	0.002		
Reef-1	15.0011	14.89	28.7287	28.324	-0.065	29.762	-1.033
Reef-2	15.1266	15.013	29.017	28.604	-0.090	29.762	-0.745
Reef-3	15.0576	14.945	28.8565	28.448	-0.076	29.762	-0.906
Reef-4	15.2972	15.181	29.3289	28.907	-0.082	29.762	-0.433
Reef-5	15.3414	15.225	29.429	29.004	-0.089	29.762	-0.333
Avg.	15.165	15.051	29.072	28.657	-0.080	29.762	-0.690
$\pm 1\sigma$	0.149	0.146	0.300	0.292	0.010		
Palau-1	14.485	14.381	27.755	27.377	-0.074	28.724	-0.969
Palau-2	13.689	13.596	26.217	25.879	-0.068	28.724	-2.507
Palau-3	14.360	14.258	27.493	27.122	-0.062	28.724	-1.231
Avg.	14.178	14.078	27.155	26.793	-0.068	28.724	-1.569
$\pm 1\sigma$	0.428	0.422	0.823	0.801	0.006		

Appendix G. Raw data of synthesized samples and Devils Hole from Chapter 3

Raw data of synthesized calcite and Devils Hole samples from fluorination in nickel reaction vessels (δ_{meas}) compared to the $\delta^{18}\text{O}$ value obtained via phosphoric acid digestion ($\delta^{18}\text{O}_{\text{conv}}$). All data are reported in ‰ and relative to VSMOW–SLAP.

Sample	$\delta^{17}\text{O}_{\text{meas}}$	$\delta^{17}\text{O}_{\text{meas}}$	$\delta^{18}\text{O}_{\text{meas}}$	$\delta^{18}\text{O}_{\text{meas}}$	$\Delta^{17}\text{O}_{\text{meas}}$	$\delta^{18}\text{O}_{\text{conv}}$	$\Delta\delta^{18}\text{O}_{\text{meas-conv}}$
Calcite.5.1	10.793	10.735	20.662	20.452	-0.064	21.126	-0.464
Calcite.5.2	10.661	10.604	20.413	20.208	-0.065	21.126	-0.713
Calcite.5.3	10.286	10.233	19.679	19.488	-0.057	21.126	-1.447
Calcite.5.4	10.575	10.519	20.232	20.030	-0.057	21.126	-0.894
Calcite.5.5	10.093	10.042	19.327	19.143	-0.065	21.126	-1.799
Calcite.5.6	10.070	10.019	19.291	19.107	-0.069	21.126	-1.835
Avg.	10.363	10.309	19.836	19.642	-0.063	21.126	-1.290
$\pm 1\sigma$	0.306	0.303	0.582	0.571	0.005		
Calcite.20.1	8.395	8.360	16.062	15.935	-0.053	17.518	-1.456
Calcite.20.2	8.677	8.639	16.595	16.459	-0.051	17.518	-0.923
Avg.	8.645	8.607	16.522	16.387	-0.045	17.518	-0.996
$\pm 1\sigma$	0.199	0.197	0.377	0.371	0.001		
Calcite.40.1	6.607	6.586	12.616	12.538	-0.034	13.601	-0.985
Calcite.40.2	6.847	6.824	13.086	13.002	-0.041	13.601	-0.515
Calcite.40.3	6.874	6.850	13.163	13.078	-0.055	13.601	-0.438
Calcite.40.4	6.575	6.553	12.557	12.479	-0.035	13.601	-1.044
Calcite.40.5	6.480	6.459	12.360	12.284	-0.027	13.601	-1.241
Calcite.40.6	6.611	6.589	12.621	12.542	-0.033	13.601	-0.980
Calcite.40.7	6.692	6.670	12.808	12.727	-0.050	13.601	-0.793
Calcite.40.8	6.455	6.434	12.328	12.253	-0.035	13.601	-1.273
Calcite.40.9	6.747	6.724	12.892	12.810	-0.039	13.601	-0.709
Avg.	6.654	6.632	12.715	12.635	-0.039	13.601	-0.886
$\pm 1\sigma$	0.148	0.147	0.295	0.292	0.009		
Calcite.CA.5.1	10.585	10.529	20.232	20.030	-0.047	20.611	-0.379
Calcite.CA.5.2	10.386	10.332	19.875	19.680	-0.059	20.611	-0.736
Calcite.CA.5.3	10.240	10.188	19.589	19.400	-0.056	20.611	-1.022
Calcite.CA.5.4	10.452	10.398	19.989	19.792	-0.052	20.611	-0.622
Avg.	10.304	10.252	19.718	19.526	-0.058	20.611	-0.893
$\pm 1\sigma$	0.143	0.142	0.267	0.262	0.005		
Calcite.CA.20.1	8.832	8.793	16.887	16.746	-0.049	17.312	-0.425
Calcite.CA.20.2	8.743	8.705	16.719	16.581	-0.050	17.312	-0.593
Calcite.CA.20.3	8.503	8.467	16.262	16.131	-0.051	17.312	-1.050
Calcite.CA.20.4	8.912	8.872	17.043	16.899	-0.051	17.312	-0.269
Calcite.CA.20.5	8.666	8.628	16.585	16.449	-0.057	17.312	-0.727
Avg.	8.757	8.719	16.753	16.614	-0.053	17.312	-0.559
$\pm 1\sigma$	0.158	0.156	0.299	0.294	0.003		
Calcite.CA.40.1	6.739	6.717	12.889	12.807	-0.045	13.394	-0.505
Calcite.CA.40.2	6.709	6.686	12.827	12.746	-0.043	13.394	-0.567
Calcite.CA.40.3	6.790	6.767	12.988	12.904	-0.046	13.394	-0.406
Calcite.CA.40.4	6.398	6.378	12.222	12.148	-0.036	13.394	-1.172
Avg.	6.659	6.637	12.732	12.651	-0.043	13.394	-0.662
$\pm 1\sigma$	0.177	0.176	0.346	0.342	0.004		
Calcite.DH.1	7.120	7.095	13.619	13.527	-0.047	14.621	-1.002
Calcite.DH.2	7.384	7.357	14.093	13.994	-0.032	14.621	-0.528
Calcite.DH.3	7.224	7.198	13.819	13.725	-0.048	14.621	-0.802
Calcite.DH.4	7.265	7.239	13.890	13.794	-0.045	14.621	-0.731
Calcite.DH.5	7.145	7.119	13.662	13.570	-0.045	14.621	-0.959
Avg.	7.228	7.202	13.816	13.722	-0.043	14.621	-0.805
$\pm 1\sigma$	0.105	0.105	0.190	0.188	0.007		

Appendix H. Raw data of ancient calcite from Chapter 3

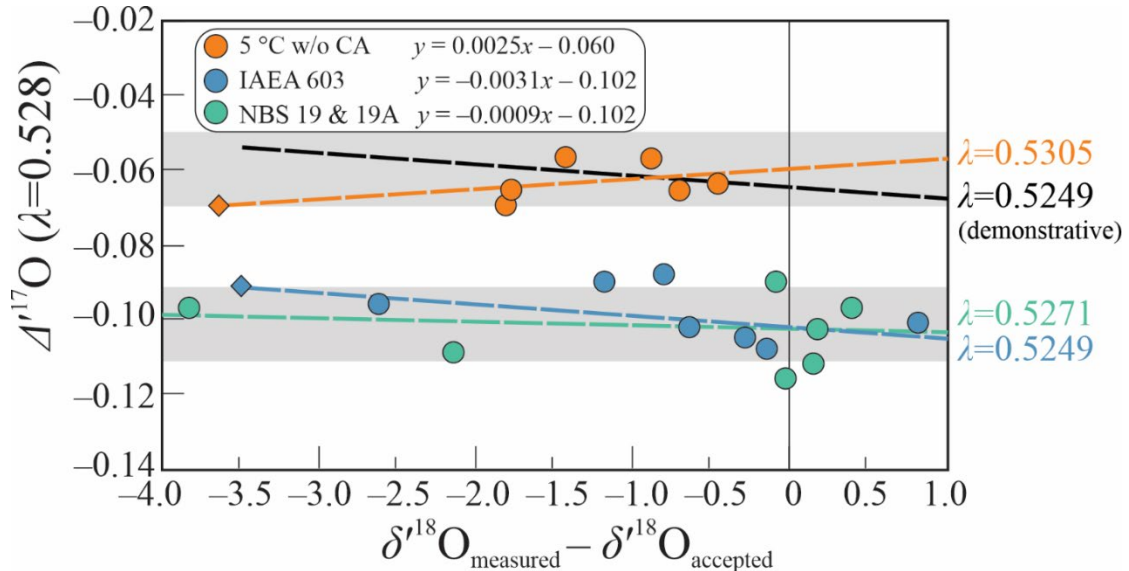
Raw data of ancient brachiopod and belemnite samples from fluorination in nickel reaction vessels (δ_{meas}) compared to the $\delta^{18}\text{O}$ value obtained via phosphoric acid digestion ($\delta^{18}\text{O}_{\text{conv}}$). All data are reported in ‰ and relative to VSMOW-SLAP.

Sample	$\delta^{17}\text{O}_{\text{meas}}$	$\delta^{17}\text{O}_{\text{meas}}$	$\delta^{18}\text{O}_{\text{meas}}$	$\delta^{18}\text{O}_{\text{meas}}$	$\Delta^{17}\text{O}_{\text{meas}}$	$\delta^{18}\text{O}_{\text{conv}}$	$\Delta\delta^{18}\text{O}_{\text{meas-conv}}$
CM3a-1	13.365	13.276	25.644	25.321	-0.093	25.991	-0.347
Avg.	13.365	13.276	25.644	25.321	-0.093	25.991	-0.347
$\pm 1\sigma$	N.A						
IR70c-1	13.408	13.319	25.679	25.355	-0.069	27.910	-2.231
Avg.	13.408	13.319	25.679	25.355	-0.069	0.000	25.679
$\pm 1\sigma$	N.A						
NB428-1	13.462	13.372	25.834	25.506	-0.095	27.456	-1.622
NB428-2	13.716	13.623	26.304	25.964	-0.086	27.456	-1.152
NB428-3	13.218	13.131	25.350	25.034	-0.087	27.456	-2.106
NB428-4	12.891	12.808	24.717	24.416	-0.083	27.456	-2.739
Avg.	13.322	13.234	25.551	25.230	-0.088	27.456	-1.905
$\pm 1\sigma$	0.352	0.347	0.679	0.662	0.005		0.679
AC332-1	15.147	15.033	29.054	28.640	-0.089	29.384	-0.330
Avg.	15.147	15.033	29.054	28.640	-0.089	29.384	-0.330
$\pm 1\sigma$	N.A						
PDB-1	15.386	15.269	29.505	29.078	-0.085	30.920	-1.415
PDB-2	15.661	15.540	30.042	29.600	-0.089	30.920	-0.878
PDB-3	15.673	15.551	30.053	29.611	-0.083	30.920	-0.867
PDB-4	15.330	15.214	29.399	28.975	-0.085	30.920	-1.521
PDB-5	15.544	15.424	29.805	29.370	-0.083	30.920	-1.115
PDB-6	15.453	15.335	29.612	29.182	-0.074	30.920	-1.308
Avg.	15.508	15.389	29.736	29.303	-0.083	30.920	-1.184
$\pm 1\sigma$	0.143	0.140	0.276	0.268	0.005		0.276
C539-1	15.112	14.999	28.998	28.586	-0.094	30.683	-1.685
C539-2	15.096	14.983	28.980	28.568	-0.101	30.683	-1.703
Avg.	15.104	14.991	28.989	28.577	-0.098	30.683	-1.694
$\pm 1\sigma$	0.011	0.011	0.013	0.012	0.005		0.013

Appendix I. Fractionation associated with fluorination of carbonates in a Ni-tube

The $\Delta^{17}\text{O}$ values measured using fluorination compared to the difference between the $\delta^{18}\text{O}$ measured ($\delta^{18}\text{O}_{\text{measured}}$) via fluorination minus the $\delta^{18}\text{O}$ measured via phosphoric acid digestion ($\delta^{18}\text{O}_{\text{accepted}}$) to examine any fractionation occurring during the fluorination reaction. Three samples were used that had a range of $\delta^{18}\text{O}_{\text{measured}} - \delta^{18}\text{O}_{\text{accepted}}$ values (5 °C without CA - orange circles, this study; IAEA 603 - blue circles, Wostbrock et al. (2020); NBS 19 - green circles, Wostbrock et al. (2020)). Most samples from this study did not have a large enough range of $\delta^{18}\text{O}_{\text{measured}} - \delta^{18}\text{O}_{\text{accepted}}$ values to produce a meaningful slope (e.g, the average standard deviation of the mean is $\sim\pm 0.3$). If the $\delta^{18}\text{O}$ value obtained via fluorination was exactly the same as that produced from the gasbench analysis, the sample would plot on 0 for the x-axis.

During fluorination, if the oxygen released from fluorination fractionates with a $\lambda=0.528$, then the best fit line to each dataset would be flat (slope of 0; best fits shown in legend). The λ between the three data sets ranges from 0.5249 to 0.5305 (average = 0.5275 (± 0.0028)), corresponding to an error of 0.0056 ‰ for $\Delta^{17}\text{O}$ values. The average $\Delta^{17}\text{O}$ standard deviation of the mean of replicated samples in this study is 0.005 ‰. Combining the errors on the analytical precision with the error during the reaction process (using root sum squares since they are not related) results in a total error of ± 0.008 ‰ for the $\Delta^{17}\text{O}$ values. A $\Delta^{17}\text{O}$ uncertainty as 0.010 ‰ (shaded gray boxes) is reported in this manuscript to account for any additional uncertainty for during the fluorination reaction. Per sample, extrapolation of the best fit where $x=0$ (also the y-intercept) for each dataset is within ± 0.002 ‰ of the average $\delta^{17}\text{O}$ of each dataset, well within analytical standard deviation ($\pm 1\sigma=0.010$).



The average $\delta^{18}\text{O}_{\text{measured}} - \delta^{18}\text{O}_{\text{accepted}}$ values of samples of all samples of this study is -1.14 ‰, meaning, on average, the measured $\delta^{18}\text{O}$ values from fluorination is 1.14 ‰ lower than the $\delta^{18}\text{O}$ values measured on the Gasbench after phosphoric acid digestion. Since the $\Delta^{17}\text{O}$ values do not have to be extrapolated very far to the ‘accepted’ values, the slopes are not as important as the analytical precision of the measurement. For

example, a slope of 0.5249 (black dashed line) can fit the 5 °C w/o CA sample (orange circles) and the y-intercept would be -0.064 ‰, only 0.001 ‰ lower than the average reported value (-0.063 ‰). In fact, it is not until the $\delta^{18}\text{O}_{\text{measured}} - \delta^{18}\text{O}_{\text{accepted}}$ is less than -3.2 ‰ that the extrapolation of the slope has a significant effect on the reported $\Delta^{17}\text{O}$ values. In this study, the lowest $\delta^{18}\text{O}_{\text{measured}} - \delta^{18}\text{O}_{\text{accepted}}$ of an individual analysis is -2.8 ‰. Therefore, the $\Delta^{17}\text{O}$ values reported are significant and reproducible within a precision of 0.010 ‰.

Appendix J. $1000\ln\alpha^{18}\text{O}_{\text{cc-wt}}$ values used to derive calcite-water fractionation line

Compilation of $1000\ln\alpha^{18}\text{O}_{\text{cc-wt}}$ values and corresponding temperatures used to calculate Eq. 6. Note that O'Neil et al. (1960) was corrected by adding 0.48 to reflect the accepted $\alpha_{\text{CO}_2\text{-wt}}$ of 1.0412 (compared to 1.0407 used in the original paper).

Temp (°C)	$1000\ln\alpha^{18}\text{O}_{\text{cc-wt}}$	Data
-2	35.459	This study
-0.4	34.345	This study
5	33.639	This study
9	32.236	This study
20	30.531	This study
20	30.748	This study
25	29.412	This study
25	28.937	This study
26	28.923	This study
26	28.228	This study
30	28.419	This study
40	26.460	This study
40	26.866	This study
201	9.89	O'Neil et al. (1969) corrected
240	7.66	O'Neil et al. (1969) corrected
320	4.75	O'Neil et al. (1969) corrected
350	4.04	O'Neil et al. (1969) corrected
370	3.58	O'Neil et al. (1969) corrected
400	3.23	O'Neil et al. (1969) corrected
430	2.81	O'Neil et al. (1969) corrected
500	1.98	O'Neil et al. (1969) corrected
700	0.36	O'Neil et al. (1969) corrected

Appendix K. Literature compilation of $1000\ln\alpha$ values for calcite–water

Literature compilation of $1000\ln\alpha^{18\text{O}}$ values and corresponding temperatures. Data are represented in the main body of the paper as the grey band in Fig. 3

Author	Type	Temp (°C)	$1000\ln\alpha^{18\text{O}}$	Notes
Coplen (2007)	Subaqueous Cave Calcite	33.7	28.09	
Kim and O'Neil (1997)	Synthetic (25 mM solution)	10	33.14	
Kim and O'Neil (1997)	Synthetic (25 mM solution)	10	33.93	
Kim and O'Neil (1997)	Synthetic (25 mM solution)	10	34.06	
Kim and O'Neil (1997)	Synthetic (25 mM solution)	10	32.77	
Kim and O'Neil (1997)	Synthetic (25 mM solution)	10	32.91	
Kim and O'Neil (1997)	Synthetic (25 mM solution)	10	33.87	
Kim and O'Neil (1997)	Synthetic (25 mM solution)	10	33.14	
Kim and O'Neil (1997)	Synthetic (25 mM solution)	25	29.59	
Kim and O'Neil (1997)	Synthetic (25 mM solution)	25	29.12	
Kim and O'Neil (1997)	Synthetic (25 mM solution)	25	29.50	
Kim and O'Neil (1997)	Synthetic (25 mM solution)	25	29.05	
Kim and O'Neil (1997)	Synthetic (25 mM solution)	25	29.19	
Kim and O'Neil (1997)	Synthetic (25 mM solution)	25	29.57	
Kim and O'Neil (1997)	Synthetic (25 mM solution)	25	29.26	
Kim and O'Neil (1997)	Synthetic (25 mM solution)	25	29.43	
Kim and O'Neil (1997)	Synthetic (25 mM solution)	40	26.00	
Kim and O'Neil (1997)	Synthetic (25 mM solution)	40	26.01	
Kim and O'Neil (1997)	Synthetic (25 mM solution)	40	26.02	
Kim and O'Neil (1997)	Synthetic (25 mM solution)	40	26.42	
Kim and O'Neil (1997)	Synthetic (25 mM solution)	40	26.20	
Kim and O'Neil (1997)	Synthetic (25 mM solution)	40	26.28	
Kim and O'Neil (1997)	Synthetic (25 mM solution)	40	26.15	
Watkins et al. (2013)	Synthetic (w/CA)	5	32.01	
Watkins et al. (2013)	Synthetic (w/CA)	5	32.40	
Watkins et al. (2013)	Synthetic (w/CA)	15	30.20	
Watkins et al. (2013)	Synthetic (w/CA)	15	30.15	
Watkins et al. (2013)	Synthetic (w/CA)	25	28.33	
Watkins et al. (2013)	Synthetic (w/CA)	25	28.10	
Tremaine et al. (2011)	Cave Calcite	19.2	30.26	
Tremaine et al. (2011)	Cave Calcite	19.7	30.68	
Tremaine et al. (2011)	Cave Calcite	19.5	29.93	
Tremaine et al. (2011)	Cave Calcite	21.5	30.12	
Tremaine et al. (2011)	Cave Calcite	21.5	30.53	
Tremaine et al. (2011)	Cave Calcite	20.5	30.60	
Tremaine et al. (2011)	Cave Calcite	19.5	29.92	
Tremaine et al. (2011)	Cave Calcite	18.5	30.58	
Tremaine et al. (2011)	Cave Calcite	18.5	30.40	
Tremaine et al. (2011)	Cave Calcite	19.2	30.36	
Tremaine et al. (2011)	Cave Calcite	16	31.29	
Tremaine et al. (2011)	Cave Calcite	21	30.31	
Tremaine et al. (2011)	Cave Calcite	20	30.23	
Tremaine et al. (2011)	Cave Calcite	20	29.79	
Tremaine et al. (2011)	Cave Calcite	18	30.69	
Tremaine et al. (2011)	Cave Calcite	18	30.62	
Tremaine et al. (2011)	Cave Calcite	21	29.72	
Tremaine et al. (2011)	Cave Calcite	19.2	30.19	
Tremaine et al. (2011)	Cave Calcite	19.2	30.32	
Tremaine et al. (2011)	Cave Calcite	19.2	30.23	

Tremaine et al. (2011)	Cave Calcite	12	31.99	Only used highest value from each temperature
Tremaine et al. (2011)	Cave Calcite	19.2	30.45	
Dietzel et al. (2009)	Synthetic	5	26.75	Only used highest value from each temperature
Dietzel et al. (2009)	Synthetic	5	28.23	
Dietzel et al. (2009)	Synthetic	5	29.49	Only used highest value from each temperature
Dietzel et al. (2009)	Synthetic	5	14.09	
Dietzel et al. (2009)	Synthetic	5	31.51	Only used highest value from each temperature
Dietzel et al. (2009)	Synthetic	5	13.07	
Dietzel et al. (2009)	Synthetic	5	31.22	Only used highest value from each temperature
Dietzel et al. (2009)	Synthetic	5	30.43	
Dietzel et al. (2009)	Synthetic	5	31.78	Only used highest value from each temperature
Dietzel et al. (2009)	Synthetic	5	30.99	
Dietzel et al. (2009)	Synthetic	25	25.01	Only used highest value from each temperature
Dietzel et al. (2009)	Synthetic	25	26.28	
Dietzel et al. (2009)	Synthetic	25	27.7	Only used highest value from each temperature
Dietzel et al. (2009)	Synthetic	25	28.26	
Dietzel et al. (2009)	Synthetic	25	29.07	Only used highest value from each temperature
Dietzel et al. (2009)	Synthetic	25	27.66	
Dietzel et al. (2009)	Synthetic	25	27.91	Only used highest value from each temperature
Dietzel et al. (2009)	Synthetic	25	28.09	
Dietzel et al. (2009)	Synthetic	25	27.21	Only used highest value from each temperature
Dietzel et al. (2009)	Synthetic	25	26.61	
Dietzel et al. (2009)	Synthetic	25	26.89	Only used highest value from each temperature
Dietzel et al. (2009)	Synthetic	25	26.85	
Dietzel et al. (2009)	Synthetic	25	27.69	Only used highest value from each temperature
Dietzel et al. (2009)	Synthetic	40	23.76	
Dietzel et al. (2009)	Synthetic	40	22.91	Only used highest value from each temperature
Dietzel et al. (2009)	Synthetic	40	24.47	
Dietzel et al. (2009)	Synthetic	40	19.81	Only used highest value from each temperature
Dietzel et al. (2009)	Synthetic	40	23.34	
Dietzel et al. (2009)	Synthetic	40	21.34	Only used highest value from each temperature
Dietzel et al. (2009)	Synthetic	40	22.4	
Dietzel et al. (2009)	Synthetic	40	21.89	Only used highest value from each temperature
Dietzel et al. (2009)	Synthetic	40	21.42	
Dietzel et al. (2009)	Synthetic	40	25.4	Only used highest value from each temperature
Dietzel et al. (2009)	Synthetic	40	25.54	
Dietzel et al. (2009)	Synthetic	40	25.38	Only used highest value from each temperature
Dietzel et al. (2009)	Synthetic	40	23.75	
Dietzel et al. (2009)	Synthetic	40	15.19	Only used highest value from each temperature
Dietzel et al. (2009)	Synthetic	40	24.68	
Dietzel et al. (2009)	Synthetic	40	24.47	Only used highest value from each temperature
Dietzel et al. (2009)	Synthetic	40	25.58	
O'Neil et al. (1969)	Synthetic	0	27.9	Only used highest value from each temperature
O'Neil et al. (1969)	Synthetic	25	28.05	
O'Neil et al. (1969)	Synthetic	25	33.94	Only used highest value from each temperature
Tartuani et al. (1969)	Synthetic	0	33.66	
Tartuani et al. (1969)	Synthetic	0	33.75	Only used highest value from each temperature
Tartuani et al. (1969)	Synthetic	25	28.1	
Jiménez-López et al. (2001)	Synthetic	25	28	Only used highest value from each temperature
Horita and Clayton (2007)	Theoretical	0	33.63	
Horita and Clayton (2007)	Theoretical	10	31.25	Only used highest value from each temperature
Horita and Clayton (2007)	Theoretical	20	29.06	
Horita and Clayton (2007)	Theoretical	30	27.03	Only used highest value from each temperature
Horita and Clayton (2007)	Theoretical	40	25.16	
Horita and Clayton (2007)	Theoretical	50	23.42	Only used highest value from each temperature
Horita and Clayton (2007)	Theoretical	60	21.81	

Horita and Clayton (2007)	Theoretical	70	20.30	
Horita and Clayton (2007)	Theoretical	80	18.89	
Horita and Clayton (2007)	Theoretical	90	17.57	
Horita and Clayton (2007)	Theoretical	100	16.34	
Horita and Clayton (2007)	Theoretical	110	15.17	
Horita and Clayton (2007)	Theoretical	120	14.08	
Horita and Clayton (2007)	Theoretical	130	13.05	
Horita and Clayton (2007)	Theoretical	140	12.07	
Horita and Clayton (2007)	Theoretical	150	11.15	
Horita and Clayton (2007)	Theoretical	160	10.27	
Horita and Clayton (2007)	Theoretical	170	9.44	
Horita and Clayton (2007)	Theoretical	180	8.65	
Horita and Clayton (2007)	Theoretical	190	7.90	
Horita and Clayton (2007)	Theoretical	200	7.19	
Desmarchelier et al. (2000)	Cave Calcite	16.8	31.56	avg. "spring chamber"
Zaarur et al. (2013)	Synthetic	5	33.61	Water calculated based on
Zaarur et al. (2013)	Synthetic	5	33.68	clumped isotopes
Zaarur et al. (2013)	Synthetic	5	33.79	
Zaarur et al. (2013)	Synthetic	8	32.60	Calcite&Vaterite
Zaarur et al. (2013)	Synthetic	8	32.70	Calcite&Vaterite
Zaarur et al. (2013)	Synthetic	8	32.65	Calcite&Vaterite
Zaarur et al. (2013)	Synthetic	15	31.59	
Zaarur et al. (2013)	Synthetic	15	31.62	
Zaarur et al. (2013)	Synthetic	15	30.95	
Zaarur et al. (2013)	Synthetic	25	28.46	
Zaarur et al. (2013)	Synthetic	25	28.40	
Zaarur et al. (2013)	Synthetic	25	28.51	
Zaarur et al. (2013)	Synthetic	35	26.78	
Zaarur et al. (2013)	Synthetic	35	26.64	
Zaarur et al. (2013)	Synthetic	35	26.66	
Zaarur et al. (2013)	Synthetic	50	25.15	Calcite&Aragonite
Zaarur et al. (2013)	Synthetic	50	24.84	Calcite&Aragonite
Zaarur et al. (2013)	Synthetic	50	25.16	Calcite&Aragonite
Zaarur et al. (2013)	Synthetic	65	22.14	Aragonite&Calcite
Zaarur et al. (2013)	Synthetic	65	22.05	Aragonite&Calcite
Zaarur et al. (2013)	Synthetic	65	22.15	Aragonite&Calcite
Voarintsoa et al. (2020)	Synthetic (25 mM solution)	10	32.55	0% Aragonite
Voarintsoa et al. (2020)	Synthetic (25 mM solution)	10	32.47	88% Aragonite
Voarintsoa et al. (2020)	Synthetic (25 mM solution)	10	32.31	99% Aragonite
Voarintsoa et al. (2020)	Synthetic (25 mM solution)	10	32.02	100% Aragonite
Voarintsoa et al. (2020)	Synthetic (25 mM solution)	27	29.05	0% Aragonite
Voarintsoa et al. (2020)	Synthetic (25 mM solution)	27	28.7	97% Aragonite
Voarintsoa et al. (2020)	Synthetic (25 mM solution)	35	27.32	0% Aragonite
Voarintsoa et al. (2020)	Synthetic (25 mM solution)	35	27.19	8% Aragonite
Voarintsoa et al. (2020)	Synthetic (25 mM solution)	35	27.2	79% Aragonite
Voarintsoa et al. (2020)	Synthetic (5 mM solution)	27	27.66	4% Aragonite
Voarintsoa et al. (2020)	Synthetic (5 mM solution)	27	28.2	37% Aragonite
Voarintsoa et al. (2020)	Synthetic (5 mM solution)	27	28.36	100% Aragonite
Demény et al. (2010)	Hot water travertines	65.2	22.70	
Demény et al. (2010)	Hot water travertines	65.2	22.40	
Demény et al. (2010)	Hot water travertines	64.8	22.69	
Demény et al. (2010)	Hot water travertines	64.8	21.81	
Demény et al. (2010)	Hot water travertines	67	22.39	
Demény et al. (2010)	Warm water travertines	36	27.14	
Demény et al. (2010)	Warm water travertines	33.8	27.74	
Demény et al. (2010)	Warm water travertines	28.5	28.82	

Demény et al. (2010)	Cave Calcite	9.8	31.81
Demény et al. (2010)	Cave Calcite	9.8	32.02
Demény et al. (2010)	Cave Calcite	9.8	31.42
Demény et al. (2010)	Cave Calcite	10.5	32.35
Demény et al. (2010)	Cave Calcite	10.5	32.16
Demény et al. (2010)	Cave Calcite	9.5	31.96
Demény et al. (2010)	Cave Calcite	9.5	31.98

REFERENCES

- Adnew, G. A., Hofmann, M. E. G., Paul, D., Laskar, A., Surma, J., Albrecht, N., Pack, A., Schwieters, J., Koren, G., Peters, W. and Röckmann, T. (2019) Determination of the triple oxygen and carbon isotopic composition of CO₂ from atomic ion fragments formed in the ion source of the 253 Ultra High-Resolution Isotope Ratio Mass Spectrometer. *Rapid Communications in Mass Spectrometry* **0**. DOI: 10.1002/rcm.8478
- Ahm, A. C., Bjerrum, C. J., Blättler, C. L., Swart, P. K. and Higgins, J. A. (2018) Quantifying early marine diagenesis in shallow-water carbonate sediments. *Geochimica et Cosmochimica Acta* **236**: 140-159. DOI: 10.1016/j.gca.2018.02.042
- Ahn, I., Lee, J. I., Kusakabe, M. and Choi, B. G. (2012) Oxygen isotope measurements of terrestrial silicates using a CO₂-laser BrF₅ fluorination technique and the slope of terrestrial fractionation line. *Geosciences Journal* **16**(1): 7-16
- Allan, J. R. and Matthews, R. K. (1982) Isotope signatures associated with early meteoric diagenesis. *Sedimentology* **29**(6): 797-817. DOI: 10.1111/j.1365-3091.1982.tb00085.x
- Bajnai, D., Fiebig, J., Tomašových, A., Milner Garcia, S., Rollion-Bard, C., Raddatz, J., Löffler, N., Primo-Ramos, C. and Brand, U. (2018) Assessing kinetic fractionation in brachiopod calcite using clumped isotopes. *Scientific Reports* **8**(1): 533. DOI: 10.1038/s41598-017-17353-7
- Baker, L., Franchi, I. A., Maynard, J., Wright, I. P. and Pillinger, C. T. (2002) A Technique for the Determination of ¹⁸O/¹⁶O and ¹⁷O/¹⁶O Isotopic Ratios in Water from Small Liquid and Solid Samples. *Analytical Chemistry* **74**(7): 1665-1673. DOI: 10.1021/ac010509s
- Banner, J. L. and Hanson, G. N. (1990) Calculation of simultaneous isotopic and trace element variations during water-rock interaction with applications to carbonate diagenesis. *Geochimica et Cosmochimica Acta* **54**(11): 3123-3137. DOI: 10.1016/0016-7037(90)90128-8
- Bao, H. and Thiemens, M. H. (2000) Generation of O₂ from BaSO₄ Using a CO₂-Laser Fluorination System for Simultaneous Analysis of δ¹⁸O and δ¹⁷O. *Analytical Chemistry* **72**(17): 4029-4032. DOI: 10.1021/ac000086e
- Bao, H. M., Thiemens, M. H., Farquhar, J., Campbell, D. A., Lee, C. C. W., Heine, K. and Loope, D. B. (2000). Anomalous O-17 compositions in massive sulphate deposits on the Earth. **406**: 176-178.

- Barkan, E. and Luz, B. (2003) High-precision measurements of $^{17}\text{O}/^{16}\text{O}$ and $^{18}\text{O}/^{16}\text{O}$ of O_2 and O_2/Ar ratio in air. *Rapid Communications in Mass Spectrometry* **17**(24): 2809-2814. DOI: 10.1002/rcm.1267
- Barkan, E. and Luz, B. (2005) High precision measurements of $^{17}\text{O}/^{16}\text{O}$ and $^{18}\text{O}/^{16}\text{O}$ ratios in H_2O . *Rapid Communications in Mass Spectrometry* **19**(24): 3737-3742. DOI: 10.1002/rcm.2250
- Barkan, E. and Luz, B. (2011) The relationships among the three stable isotopes of oxygen in air, seawater and marine photosynthesis. *Rapid Communications in Mass Spectrometry* **25**(16): 2367-2369. DOI: 10.1002/rcm.5125
- Barkan, E. and Luz, B. (2012) High-precision measurements of $^{17}\text{O}/^{16}\text{O}$ and $^{18}\text{O}/^{16}\text{O}$ ratios in CO_2 . *Rapid Communications in Mass Spectrometry* **26**(23): 2733-2738. DOI: 10.1002/rcm.6400
- Barkan, E., Musan, I. and Luz, B. (2015) High-precision measurements of $\delta^{17}\text{O}$ and ^{17}O excess of NBS19 and NBS18. *Rapid Communications in Mass Spectrometry* **29**(23): 2219-2224. DOI: 10.1002/rcm.7378
- Barkan, E., Affek, H. P., Luz, B., Bergel, S. J., Voarintsoa, N. R. G. and Musan, I. (2019) Calibration of $\delta^{17}\text{O}$ and ^{17}O excess values of three international standards: IAEA-603, NBS19 and NBS18. *Rapid Communications in Mass Spectrometry* **33**(7): 737-740. DOI: 10.1002/rcm.8391
- Bartlett, R., Elrick, M., Wheeley, J. R., Polyak, V., Desrochers, A. and Asmerom, Y. (2018) Abrupt global-ocean anoxia during the Late Ordovician–early Silurian detected using uranium isotopes of marine carbonates. *Proceedings of the National Academy of Sciences* **115**(23): 5896-5901. DOI: 10.1073/pnas.1802438115
- Bates, N. R. and Brand, U. (1991) Environmental and physiological influences on isotopic and elemental compositions of brachiopod shell calcite: Implications for the isotopic evolution of Paleozoic oceans. *Chemical Geology* **94**(1): 67-78. DOI: 10.1016/S0009-2541(10)80018-X
- Bathurst, R. G. C. (1966) Boring algae, micrite envelopes and lithification of molluscan biosparites. *Geological Journal* **5**(1): 15-32. DOI: 10.1002/gj.3350050104
- Bathurst, R. G. C. (1983). Early diagenesis of carbonate sediments. Sediment Diagenesis. A. Parker and B. W. Sellwood. Dordrecht, Springer. **115**.

- Beck, W. C., Grossman, E. L. and Morse, J. W. (2005) Experimental studies of oxygen isotope fractionation in the carbonic acid system at 15°, 25°, and 40°C. *Geochimica et Cosmochimica Acta* **69**(14): 3493-3503. DOI: 10.1016/j.gca.2005.02.003
- Bergel, S. J., Barkan, E., Stein, M. and Affek, H. P. (2020) Carbonate ¹⁷O excess as a paleo-hydrology proxy: Triple oxygen isotope fractionation between H₂O and biogenic aragonite, derived from freshwater mollusks. *Geochimica et Cosmochimica Acta* **275**: 36-47. DOI: 10.1016/j.gca.2020.02.005
- Bergmann, K. D., Finnegan, S., Creel, R., Eiler, J. M., Hughes, N. C., Popov, L. E. and Fischer, W. W. (2018) A paired apatite and calcite clumped isotope thermometry approach to estimating Cambro-Ordovician seawater temperatures and isotopic composition. *Geochimica et Cosmochimica Acta* **224**: 18-41. DOI: 10.1016/j.gca.2017.11.015
- Bigeleisen, J. and Mayer, M. G. (1947) Calculation of Equilibrium Constants for Isotopic Exchange Reactions. *The Journal of Chemical Physics* **15**(5): 261-267. DOI: 10.1063/1.1746492
- Bindeman, I. N., Zakharov, D. O., Palandri, J., Greber, N. D., Dauphas, N., Retallack, G. J., Hofmann, A., Lackey, J. S. and Bekker, A. (2018) Rapid emergence of subaerial landmasses and onset of a modern hydrologic cycle 2.5 billion years ago. *Nature* **557**(7706): 545-548. DOI: 10.1038/s41586-018-0131-1
- Blattner, P. (1973) Oxygen from liquids for isotopic analysis, and a new determination of $\alpha_{\text{CO}_2\text{-H}_2\text{O}}$ at 25°C. *Geochimica et Cosmochimica Acta* **37**(12): 2691-2693. DOI: 10.1016/0016-7037(73)90274-3
- Bottinga, Y. and Craig, H. (1969) Oxygen isotope fractionation between CO₂ and water, and the isotopic composition of marine atmospheric CO₂. *Earth and Planetary Science Letters* **5**: 285-295
- Bottinga, Y. and Javoy, M. (1973) Comments on oxygen isotope geothermometry. *Earth and Planetary Science Letters* **20**(2): 250-265. DOI: 10.1016/0012-821X(73)90165-9
- Brand, U. and Veizer, J. (1981) Chemical diagenesis of a multicomponent carbonate system -2: Stable Isotopes. *Journal of Sedimentary Petrology* **51**(3): 0987-0997
- Brand, U., Logan, A., Hiller, N. and Richardson, J. (2003) Geochemistry of modern brachiopods: applications and implications for oceanography and paleoceanography. *Chemical Geology* **198**(3): 305-334. DOI: 10.1016/S0009-2541(03)00032-9

- Brand, U. (2004) Carbon, oxygen and strontium isotopes in Paleozoic carbonate components: an evaluation of original seawater-chemistry proxies. *Chemical Geology* **204**(1): 23-44. DOI: 10.1016/j.chemgeo.2003.10.013
- Brand, U., Jiang, G., Azmy, K., Bishop, J. and Montañez, I. P. (2012) Diagenetic evaluation of a Pennsylvanian carbonate succession (Bird Spring Formation, Arrow Canyon, Nevada, U.S.A.) — 1: Brachiopod and whole rock comparison. *Chemical Geology* **308-309**: 26-39. DOI: 10.1016/j.chemgeo.2012.03.017
- Brand, U., Azmy, K., Bitner, M. A., Logan, A., Zuschin, M., Came, R. and Ruggiero, E. (2013) Oxygen isotopes and MgCO₃ in brachiopod calcite and a new paleotemperature equation. *Chemical Geology* **359**: 23-31. DOI: 10.1016/j.chemgeo.2013.09.014
- Brand, U., Azmy, K., Griesshaber, E., Bitner, M. A., Logan, A., Zuschin, M., Ruggiero, E. and Colin, P. L. (2015) Carbon isotope composition in modern brachiopod calcite: A case of equilibrium with seawater? *Chemical Geology* **411**: 81-96. DOI: 10.1016/j.chemgeo.2015.06.021
- Brand, U., Bitner, M. A., Logan, A., Azmy, K., Crippa, G., Angiolini, L., Colin, P., Griesshaber, E., Harper, E. M., Taddei Ruggiero, E. and Häussermann, V. (2019) Brachiopod-based oxygen-isotope thermometer: Update and review. *Rivista Italiana di Paleontologia e Stratigrafia* **125**: 775-787. DOI: 10.13130/2039-4942/12226
- Brand, W. A., Coplen, T. B., Vogl, J., Rosner, M. and Prohaska, T. (2014) Assessment of international reference materials for isotope-ratio analysis (IUPAC Technical Report). *Pure and Applied Chemistry* **86**(3): 425-467. DOI: 10.1515/pac-2013-1023
- Brandriss, M. E., O'Neil, J. R., Edlund, M. B. and Stoermer, E. F. (1998) Oxygen Isotope Fractionation Between Diatomaceous Silica and Water. *Geochimica et Cosmochimica Acta* **62**(7): 1119-1125. DOI: 10.1016/S0016-7037(98)00054-4
- Brayard, A., Bylund, K. G., Jenks, J. F., Stephen, D. A., Olivier, N., Escarguel, G., Fara, E. and Vennin, E. (2013) Smithian ammonoid faunas from Utah: implications for Early Triassic biostratigraphy, correlation and basinal paleogeography. *Swiss Journal of Palaeontology* **132**(2): 141-219. DOI: 10.1007/s13358-013-0058-y
- Brennkmeijer, C. A. M. and Röckmann, T. (1998) A rapid method for the preparation of O₂ from CO₂ for mass spectrometric measurement of ¹⁷O/¹⁶O ratios. *Rapid Communications in Mass Spectrometry* **12**(8): 479-483. DOI: 10.1002/(sici)1097-0231(19980430)12:8<479::Aid-rcm184>3.0.Co;2-r
- Brock, T. D. (1985) Life at High Temperatures. *Science* **230**(4722): 132-138. DOI: 10.1126/science.230.4722.132

Buster, N. and Holmes, C. (2006) Magnesium content within the skeletal architecture of the coral *Montastraea faveolata*: Locations of brucite precipitation and implications to fine-scale data fluctuations. *Coral Reefs* **25**: 243-253. DOI: 10.1007/s00338-006-0092-y

Cao, X. B. and Liu, Y. (2011) Equilibrium mass-dependent fractionation relationships for triple oxygen isotopes. *Geochimica et Cosmochimica Acta* **75**(23): 7435-7445. DOI: 10.1016/j.gca.2011.09.048

Chamberlain, C. P., Ibarra, D. E., Lloyd, M. K., Kukla, T., Sjostrom, D., Gao, Y. and Sharp, Z. D. (2020) Triple oxygen isotope systematics of meteoric hydrothermal systems and implications for paleoaltimetry. *Geochemical Perspectives Letters* **in press**.

Clayton, R. N. and Mayeda, T. K. (1963) The use of bromine pentafluoride in the extraction of oxygen from oxides and silicates for isotopic analysis. *Geochimica et Cosmochimica Acta* **27**(43-52)

Clayton, R. N. and Kieffer, S. W. (1991). Oxygen isotopic thermometer calibrations. Stable Isotope Geochemistry: A Tribute to Samuel Epstein. H. P. J. Taylor, J. R. O'Neil and I. R. Kaplan. San Antonio, Lancaster Press, Inc. **3**: 3-10.

Clayton, R. N. (1993) Oxygen isotopes in meteorites. *Annual Review of Earth and Planetary Sciences* **21**: 115-149. DOI: 10.1146/annurev.earth.21.1.115

Cobban, W. A., Walaszczyk, I., Obradovich, J. D. and McKinney, K. C. (2006) A USGS Zonal Table for the Upper Cretaceous Middle Cenomanian-Maastrichtian of the Western Interior of the United States Based on Ammonites, Inoceramids, and Radiometric Ages. *U.S Geological Survey Open-File Report* **2006-1250**: 1-45

Cochran, J. K., Kallenberg, K., Landman, N. H., Harries, P. J., Weinreb, D., Turekian, K. K., Beck, A. J. and Cobban, W. A. (2010) Effect of diagenesis on the Sr, O, and C isotope composition of late Cretaceous mollusks from the Western Interior Seaway of North America. *American Journal of Science* **310**: 69-88. DOI: 10.2475/02.2010.01

Cohn, M. and Urey, H. C. (1938) Oxygen Exchange Reactions of Organic Compounds and Water. *Journal of the American Chemical Society* **60**(3): 679-687. DOI: 10.1021/ja01270a052

Compston, W. and Epstein, S. (1958). A method for the preparation of Carbon dioxide from water vapor for oxygen isotope analysis. *Eos, Transactions American Geophysical Union*.

Coplen, T. B., Kendall, C. and Hopple, J. (1983) Comparison of stable isotope reference samples. *Nature* **302**: 236. DOI: 10.1038/302236a0

- Coplen, T. B. (2007) Calibration of the calcite–water oxygen-isotope geothermometer at Devils Hole, Nevada, a natural laboratory. *Geochimica et Cosmochimica Acta* **71**(16): 3948-3957. DOI: 10.1016/j.gca.2007.05.028
- Cowie, B. R. and Johnston, D. T. (2016) High-precision measurement and standard calibration of triple oxygen isotopic compositions ($\delta^{18}\text{O}$, $\Delta^{17}\text{O}$) of sulfate by F_2 laser fluorination. *Chemical Geology* **440**: 50-59. DOI: 10.1016/j.chemgeo.2016.07.003
- Craig, H. (1957) Isotopic standards for carbon and oxygen and correction factors for mass-spectrometric analysis of carbon dioxide. *Geochimica et Cosmochimica Acta* **12**(1): 133-149. DOI: 10.1016/0016-7037(57)90024-8
- Craig, H. (1961) Isotopic Variations in Meteoric Waters. *Science* **133**(3465): 1702. DOI: 10.1126/science.133.3465.1702
- Criss, R. E. (1991). Temperature dependence on isotopic fractionation factors. San Antonio, The Geochemical Society.
- Cummins, R. C., Finnegan, S., Fike, D. A., Eiler, J. M. and Fischer, W. W. (2014) Carbonate clumped isotope constraints on Silurian ocean temperature and seawater $\delta^{18}\text{O}$. *Geochimica et Cosmochimica Acta* **140**(Supplement C): 241-258. DOI: 10.1016/j.gca.2014.05.024
- Daëron, M., Drysdale, R. N., Peral, M., Huyghe, D., Blamart, D., Coplen, T. B., Lartaud, F. and Zanchetta, G. (2019) Most Earth-surface calcites precipitate out of isotopic equilibrium. *Nature communications* **10**(1): 429. DOI: 10.1038/s41467-019-08336-5
- Das Sharma, S., Patil, D. J. and Gopalan, K. (2002) Temperature dependence of oxygen isotope fractionation of CO_2 from magnesite-phosphoric acid reaction. *Geochimica et Cosmochimica Acta* **66**(4): 589-593. DOI: 10.1016/S0016-7037(01)00833-X
- De Ronde, C. E. J., Channer, D. M. d., Faure, K., Bray, C. J. and Spooner, E. T. C. (1997) Fluid chemistry of Archean seafloor hydrothermal vents: Implications for the composition of circa 3.2 Ga seawater. *Geochimica et Cosmochimica Acta* **61**(19): 4025-4042. DOI: 10.1016/S0016-7037(97)00205-6
- Degens, E. T. and Epstein, S. (1962) Relationship Between $\text{O}^{18}/\text{O}^{16}$ Ratios in Coexisting Carbonates, Cherts, and Diatomites I: GEOLOGICAL NOTES. *AAPG Bulletin* **46**(4): 534-542. DOI: 10.1306/bc743841-16be-11d7-8645000102c1865d
- Demény, A., Kele, S. and Siklósy, Z. (2010) Empirical equations for the temperature dependence of calcite-water oxygen isotope fractionation from 10 to 70°C. *Rapid Communications in Mass Spectrometry* **24**(24): 3521-3526. DOI: doi:10.1002/rcm.4799

- Dennis, K. J. and Schrag, D. P. (2010) Clumped isotope thermometry of carbonatites as an indicator of diagenetic alteration. *Geochimica et Cosmochimica Acta* **74**(14): 4110-4122. DOI: 10.1016/j.gca.2010.04.005
- Dennis, K. J., Cochran, J. K., Landman, N. H. and Schrag, D. P. (2013) The climate of the Late Cretaceous: New insights from the application of the carbonate clumped isotope thermometer to Western Interior Seaway macrofossil. *Earth and Planetary Science Letters* **362**: 51-65. DOI: 10.1016/j.epsl.2012.11.036
- Desmarchelier, J. M., Goede, A., Ayliffe, L. K., McCulloch, M. T. and Moriarty, K. (2000) Stable isotope record and its palaeoenvironmental interpretation for a late Middle Pleistocene speleothem from Victoria Fossil Cave, Naracoorte, South Australia. *Quaternary Science Reviews* **19**(8): 763-774. DOI: 10.1016/S0277-3791(99)00037-2
- Desrochers, A., Farley, C., Achab, A., Asselin, E. and Riva, J. F. (2010) A far-field record of the end Ordovician glaciation: The Ellis Bay Formation, Anticosti Island, Eastern Canada. *Palaeogeography, Palaeoclimatology, Palaeoecology* **296**(3): 248-263. DOI: 10.1016/j.palaeo.2010.02.017
- Dietzel, M., Tang, J., Leis, A. and Köhler, S. J. (2009) Oxygen isotopic fractionation during inorganic calcite precipitation — Effects of temperature, precipitation rate and pH. *Chemical Geology* **268**(1): 107-115. DOI: 10.1016/j.chemgeo.2009.07.015
- Dodd, J. P. and Sharp, Z. D. (2010) A laser fluorination method for oxygen isotope analysis of biogenic silica and a new oxygen isotope calibration of modern diatoms in freshwater environments. *Geochimica et Cosmochimica Acta* **74**: 1381-1390
- Dodd, J. P., Sharp, Z. D., Fawcett, P. J., Brearley, A. J. and McCubbin, F. M. (2012) Rapid post-mortem maturation of diatom silica oxygen isotope values. *Geochem. Geophys. Geosyst.* **13**: Q09014. DOI: 10.1029/2011gc004019
- Douglas, R. and Savin, S. (1971) Isotopic analysis of planktonic foraminifera from the Cenozoic of the northwest pacific, Leg 6. *Initial Reports of the Deep Sea Drilling Project* **6**. DOI: 10.2973/dsdp.proc.6.137.1971
- Douglas, R. G. and Savin, S. (1973) Oxygen and carbon isotope analyses of Cretaceous and Tertiary foraminifera from the central north pacific. *Initial Reports of the Deep Sea Drilling Project* **17**: 591-605. DOI: 10.2973/dsdp.proc.17.120.1973
- Eiler, J. M. (2007) "Clumped-isotope" geochemistry-The study of naturally-occurring, multiply-substituted isotopologues. *Earth and Planetary Science Letters* **262**(3-4): 309-327. DOI: 10.1016/j.epsl.2007.08.020

- Eiler, J. M. (2011) Paleoclimate reconstruction using carbonate clumped isotope thermometry. *Quaternary Science Reviews* **30**(25): 3575-3588. DOI: 10.1016/j.quascirev.2011.09.001
- Emiliani, C. (1955) Pleistocene Temperatures. *The Journal of Geology* **63**(6): 538-578
- Epstein, S., Buchsbaum, R., Lowenstam, H. and Urey, H. C. (1951) Carbonate-water isotopic temperature scale. *GSA Bulletin* **62**(4): 417-426. DOI: 10.1130/0016-7606(1951)62[417:CITS]2.0.CO;2
- Epstein, S., Buchsbaum, R., Lowenstam, H. A. and Urey, H. C. (1953) Revised carbonate-water isotopic temperature scale. *Geological Society of America Bulletin* **64**(11): 1315-1325. DOI: 10.1130/0016-7606(1953)64[1315:rcits]2.0.co;2
- Farber, K., Dziggel, A., Meyer, F. M., Prochaska, W., Hofmann, A. and Harris, C. (2015) Fluid inclusion analysis of silicified Palaeoarchean oceanic crust – A record of Archaean seawater? *Precambrian Research* **266**: 150-164. DOI: 10.1016/j.precamres.2015.05.020
- Finnegan, S., Bergmann, K., Eiler, J. M., Jones, D. S., Fike, D. A., Eisenman, I., Hughes, N. C., Tripathi, A. K. and Fischer, W. W. (2011) The Magnitude and Duration of Late Ordovician–Early Silurian Glaciation. *Science* **331**(6019): 903
- Fosu, B. R., Subba, R., Peethambaran, R., Bhattacharya, S. K. and Ghosh, P. (2020) Technical note: Developments and applications in triple oxygen isotope analysis of carbonates. *ACS Earth and Space Chemistry*. DOI: 10.1021/acsearthspacechem.9b00330
- Franchi, I. A., Wright, I. P., Sexton, A. S. and Pillinger, C. T. (1999) The oxygen-isotopic composition of Earth and Mars. *Meteoritics & Planetary Science* **34**(4): 657-661. DOI: 10.1111/j.1945-5100.1999.tb01371.x
- Friedman, I. and O'Neil, J. R. (1977). Compilation of stable isotope fractionation factors of geochemical interest, Washington, D.C. : U.S. G.P.O., 1977.
- Gao, G. and Land, L. S. (1991) Geochemistry of Cambro-Ordovician Arbuckle limestone, Oklahoma: Implications for diagenetic $\delta^{18}\text{O}$ alteration and secular $\delta^{13}\text{C}$ and $^{87}\text{Sr}/^{86}\text{Sr}$ variation. *Geochimica et Cosmochimica Acta* **55**(10): 2911-2920. DOI: 10.1016/0016-7037(91)90456-F
- Gázquez, F., Morellón, M., Bauska, T., Herwartz, D., Surma, J., Moreno, A., Staubwasser, M., Valero-Garcés, B., Delgado Huertas, A. and Hodell, D. (2018) Triple oxygen and hydrogen isotopes of gypsum hydration water for quantitative paleo-humidity reconstruction. *Earth and Planetary Sciences Letters* **481**: 177-188. DOI: 10.1016/j.epsl.2017.10.020

- Geraghty, M. D. and Westermann, G. E. G. (1994) Origin of jurassic ammonite concretions assemblages at Alfeld, Germany: a biogenic alternative. *Paläontologische Zeitschrift* **68**(3): 473-490. DOI: 10.1007/BF02991357
- Ghosh, P., Adkins, J., Affek, H., Balta, B., Guo, W., Schauble, E. A., Schrag, D. and Eiler, J. M. (2006) ^{13}C - ^{18}O bonds in carbonate minerals: A new kind of paleothermometer. *Geochimica et Cosmochimica Acta* **70**(6): 1439-1456. DOI: 10.1016/j.gca.2005.11.014
- Gill, J. R. and Cobban, W. A. (1966) The Red Bird section of the Upper Cretaceous Pierre Shale of Wyoming. *U.S Geological Survey Professional Paper* **393-A**: 1-73
- Golubic, S. (1969) Distribution, taxonomy and boring patterns of marine endolithic algae. *American Zoologist* **9**: 747-751
- Golubic, S., Perkins, R. D. and Lukas, K. J. (1975). Boring microorganisms and microborings in carbonate substrates. The Study of Trace Fossils. R. W. Frey. Berlin, Heidelberg, Springer.
- Gonfiantini, R. (1978) Standards for stable isotope measurements in natural compounds. *Nature* **271**(5645): 534-536. DOI: 10.1038/271534a0
- Gregory, R. T. and Taylor, H. P. (1981) An oxygen isotope profile in a section of Cretaceous oceanic crust, Samail ophiolite, Oman: Evidence for $\delta^{18}\text{O}$ buffering of the oceans by deep (>5 km) seawater-hydrothermal circulation at mid-ocean ridges. *Journal of Geophysical Research* **86**(B4): 2737-2755
- Gregory, R. T. (1991). Oxygen isotope history of seawater revisited: Timescales for boundary event changes in the oxygen isotope composition of seawater. Stable Isotope Geochemistry: A Tribute to Samuel Epstein. J. H.P Taylor, J. R. O'Neil and I. R. Kaplan. San Antonio, The Geochemical Society: 65-76.
- Grossman, E. L. and Ku, T.-L. (1986) Oxygen and carbon isotope fractionation in biogenic aragonite: Temperature effects. *Chemical Geology: Isotope Geoscience section* **59**: 59-74. DOI: 10.1016/0168-9622(86)90057-6
- Grossman, E. l., Zhang, C. and Yancey, T. E. (1991) Stable-isotope stratigraphy of brachiopods from Pennsylvanian shales in Texas. *GSA Bulletin* **103**(7): 953-965. DOI: 10.1130/0016-7606(1991)103<0953:Sisobf>2.3.Co;2
- Guex, J., Hungerbühler, A., Jenks, J. F., O'Dogherty, L., Atudorei, V., Taylor, D., Bucher, H. and Bartoloni, A. (2010) Spathian (Lower Triassic) ammonoids from western USA (Idaho, California, Utah and Nevada). *Memoires de Geologie (Lausanne)* **49**: 82

- Guo, W. and Zhou, C. (2019) Triple oxygen isotope fractionation in the DIC-H₂O-CO₂ system: A numerical framework and its implications. *Geochimica et Cosmochimica Acta* **246**: 541-564. DOI: 10.1016/j.gca.2018.11.018
- Hayles, J., Gao, C., Cao, X., Liu, Y. and Bao, H. (2018) Theoretical calibration of the triple oxygen isotope thermometer. *Geochimica et Cosmochimica Acta* **235**: 237-245. DOI: 10.1016/j.gca.2018.05.032
- Hendy, E. J., Gagan, M. K., Lough, J. M., McCulloch, M. and deMenocal, P. B. (2007) Impact of skeletal dissolution and secondary aragonite on trace element and isotopic climate proxies in Porites corals. *Paleoceanography* **22**(4). DOI: 10.1029/2007pa001462
- Henkes, G. A., Passey, B. H., Grossman, E. L., Shenton, B. J., Pérez-Huerta, A. and Yancey, T. E. (2014) Temperature limits for preservation of primary calcite clumped isotope paleotemperatures. *Geochimica et Cosmochimica Acta* **139**(Supplement C): 362-382. DOI: 10.1016/j.gca.2014.04.040
- Henkes, G. A., Passey, B. H., Grossman, E. L., Shenton, B. J., Yancey, T. E. and Pérez-Huerta, A. (2018) Temperature evolution and the oxygen isotope composition of Phanerozoic oceans from carbonate clumped isotope thermometry. *Earth and Planetary Science Letters* **490**: 40-50. DOI: 10.1016/j.epsl.2018.02.001
- Herwartz, D., Pack, A., Krylov, D., Xiao, Y. L., Muehlenbachs, K., Sengupta, S. and Di Rocco, T. (2015) Revealing the climate of snowball Earth from $\Delta^{17}\text{O}$ systematics of hydrothermal rocks. *Proceedings of the National Academy of Sciences of the United States of America* **112**(17): 5337-5341. DOI: 10.1073/pnas.1422887112
- Herwartz, D., Surma, J., Voigt, C., Assonov, S. and Staubwasser, M. (2017) Triple oxygen isotope systematics of structurally bonded water in gypsum. *Geochimica et Cosmochimica Acta* **209**: 254-266. DOI: 10.1016/j.gca.2017.04.026
- Herwartz, D. (2020) Triple oxygen isotopes in igneous, metamorphic and hydrothermally altered rocks. *Rev Mineral Geoche* **86**
- Holmden, C. and Muehlenbachs, K. (1993) The $^{18}\text{O}/^{16}\text{O}$ Ratio of 2-Billion-Year-Old Seawater Inferred from Ancient Oceanic Crust. *Science* **259**(5102): 1733-1736. DOI: 10.1126/science.259.5102.1733
- Horita, J. and Clayton, R. N. (2007) Comment on the studies of oxygen isotope fractionation between calcium carbonates and water at low temperatures by Zhou and Zheng (2003; 2005). *Geochimica et Cosmochimica Acta* **71**(12): 3131-3135. DOI: 10.1016/j.gca.2005.11.033

- Hren, M. T., Tice, M. M. and Chamberlain, C. P. (2009) Oxygen and hydrogen isotope evidence for a temperate climate 3.42 billion years ago. *Nature* **462**(7270): 205-208. DOI: 10.1038/nature08518
- Hulston, J. R. and Thode, H. G. (1965) Variations in the S³³, S³⁴, and S³⁶ contents of meteorites and their relation to chemical and nuclear effects. *Journal of Geophysical Research* **70**(14): 3475-3484. DOI: 10.1029/JZ070i014p03475
- Isley, A. E. (1995) Hydrothermal Plumes and the Delivery of Iron to Banded Iron Formation. *The Journal of Geology* **103**(2): 169-185. DOI: 10.1086/629734
- Jaffrés, J. B. D., Shields, G. A. and Wallmann, K. (2007) The oxygen isotope evolution of seawater: A critical review of a long-standing controversy and an improved geological water cycle model for the past 3.4 billion years. *Earth-Science Reviews* **83**(1-2): 83-122. DOI: 10.1016/j.earscirev.2007.04.002
- James, N. P. and Jones, B. (2015). *Origin of Carbonate Sedimentary Rocks*, Wiley - American Geophysical Union.
- Jeffrey, B. M., Elrick, M., Atudorei, V. and Lucas, S. G. (2019) Facies architecture and across-shelf variability of an extensive Lower Triassic (Smithian) microbial carbonate mound complex in the western U.S. *Palaeogeography, Palaeoclimatology, Palaeoecology* **521**: 42-56. DOI: 10.1016/j.palaeo.2019.02.007
- Jenks, J., Guex, J., Hungerbühler, A., Taylor, D. and Bucher, H. (2013) Ammonoid biostratigraphy of the Early Spathian *Columbites parisianus* Zone (Early Triassic) at Bear Lake Hot Springs Idaho, New Mexico. *N. M. Mus. Nat. Hist. Sci. Bull.* **61**. DOI: 10.5167/uzh-92203
- Jenks, J. F. and Brayard, A. (2018) Smithian Early Triassic ammonoids from Crittenden Springs, Elko County, Nevada: Taphonomy, Biostratigraphy and Biogeography. *New Mexico Museum of Natural Sciences Bulletin* **78**: 1-175
- Jiménez-López, C., Caballero, E., Huertas, F. J. and Romanek, C. S. (2001) Chemical, mineralogical and isotope behavior, and phase transformation during the precipitation of calcium carbonate minerals from intermediate ionic solution at 25°C. *Geochimica et Cosmochimica Acta* **65**(19): 3219-3231. DOI: 10.1016/S0016-7037(01)00672-X
- Johnson, B. W. and Wing, B. A. (2020) Limited Archaean continental emergence reflected in an early Archaean ¹⁸O-enriched ocean. *Nature Geoscience* **13**(3): 243-248. DOI: 10.1038/s41561-020-0538-9

- Kah, L. (2000). Depositional $\delta^{18}\text{O}$ signatures in Proterozoic dolostones: constraints on seawater chemistry and early diagenesis. *Carbonate Sedimentation and Diagenesis in the Evolving Precambrian World*. J. P. Grotzinger and N. P. James. Tulsa, OK, USA, SEPM Special Publication. **67**: 345-360.
- Kanzaki, Y. (2020) Interpretation of oxygen isotopes in Phanerozoic ophiolites and sedimentary rocks. *Geochemistry, Geophysics, Geosystems* **21**(n/a): e2020GC009000. DOI: 10.1029/2020gc009000
- Karhu, J. and Epstein, S. (1986) The implication of the oxygen isotope records in coexisting cherts and phosphates. *Geochimica et Cosmochimica Acta* **50**(8): 1745-1756. DOI: 10.1016/0016-7037(86)90136-5
- Kasting, J. F., Tazewell Howard, M., Wallmann, K., Veizer, J., Shields, G. and Jaffrés, J. (2006) Paleoclimates, ocean depth, and the oxygen isotopic composition of seawater. *Earth and Planetary Science Letters* **252**(1): 82-93. DOI: 10.1016/j.epsl.2006.09.029
- Kauffman, E. and Caldwell, W. (1993) The Western Interior Basin in space and time. *Geological Association of Canada Special Paper* **39**
- Keith, M. L. and Weber, J. N. (1964) Carbon and oxygen isotopic composition of selected limestones and fossils. *Geochimica et Cosmochimica Acta* **28**(10-11): 1787-1816
- Kercher, P. (2014). Recent terebratulide brachiopods: Do they faithfully record oceanographic conditions throughout ontogeny? *Earth and Planetary Sciences*, University of California Davis. **M.S.**
- Kim, S.-T., Mucci, A. and Taylor, B. E. (2007a) Phosphoric acid fractionation factors for calcite and aragonite between 25 and 75 °C: Revisited. *Chemical Geology* **246**(3-4): 135-146. DOI: 10.1016/j.chemgeo.2007.08.005
- Kim, S.-T., O'Neil, J. R., Hillaire-Marcel, C. and Mucci, A. (2007b) Oxygen isotope fractionation between synthetic aragonite and water: Influence of temperature and Mg^{2+} concentration. *Geochimica et Cosmochimica Acta* **71**(19): 4704-4715. DOI: 10.1016/j.gca.2007.04.019
- Kim, S.-T., Coplen, T. B. and Horita, J. (2015) Normalization of stable isotope data for carbonate minerals: Implementation of IUPAC guidelines. *Geochimica et Cosmochimica Acta* **158**: 276-289. DOI: 10.1016/j.gca.2015.02.011
- Kim, S. T. and O'Neil, J. R. (1997) Equilibrium and nonequilibrium oxygen isotope effects in synthetic carbonates. *Geochimica et Cosmochimica Acta* **61**(16): 3461-3475

- Kita, I., Taguchi, S. and Matsubaya, O. (1985) Oxygen isotope fractionation between amorphous silica and water at 34-93°C. *Nature* **314**(6006): 83-84. DOI: 10.1038/314083a0
- Kluge, T. and John, C. M. (2015) Technical Note: A simple method for vaterite precipitation for isotopic studies: implications for bulk and clumped isotope analysis. *Biogeosciences* **12**(11): 3289-3299. DOI: 10.5194/bg-12-3289-2015
- Knauth, L. P. (1973). Oxygen and hydrogen isotope ratios in cherts and related rocks. Geological and Planetary Sciences, California Institute of Technology. **PhD**.
- Knauth, L. P. and Epstein, S. (1976) Hydrogen and oxygen isotope ratios in nodular and bedded cherts. *Geochimica et Cosmochimica Acta* **40**(9): 1095-1108. DOI: 10.1016/0016-7037(76)90051-X
- Knauth, L. P. and Lowe, D. R. (1978) Oxygen isotope geochemistry of cherts from the Onverwacht Group (3.4 Ga), Transvaal, South Africa, with implication for secular variations in the isotopic composition of cherts. *Earth and Planetary Science Letters* **41**: 209-222
- Knauth, L. P. (1979) A model for the origin of chert in limestone. *Geology* **7**(6): 274-277. DOI: 10.1130/0091-7613(1979)7<274:Amftoo>2.0.Co;2
- Knauth, L. P. and Lowe, D. R. (2003) High Archean climatic temperature inferred from oxygen isotope geochemistry of cherts in the 3.5 Ga Swaziland Supergroup, South Africa. *GSA Bulletin* **115**(5): 566-580. DOI: 10.1130/0016-7606(2003)115<0566:Hactif>2.0.Co;2
- Knauth, L. P. (2005) Temperature and salinity history of the Precambrian ocean: Implications for the course of microbial evolution. *Palaeogeography, Palaeoclimatology, Palaeoecology* **219**(1-2): 53-69. DOI: 10.1016/j.palaeo.2004.10.014
- Kusakabe, M. and Matsuhisa, Y. (2008) Oxygen three-isotope ratios of silicate reference materials determined by direct comparison with VSMOW-oxygen. *Geochemical Journal* **42**(4): 309-317
- Landman, N., Cochran, J., Slovacek, M., Larson, N., Garb, M., Brezina, J. and Witts, J. (2018) Isotope sclerochronology of ammonites (*Baculites Compressus*) from methane seep and non-seep sites in the Late Cretaceous Western Interior Seaway, USA: Implications for ammonite habitat and mode of life. *American Journal of Science* **318**: 603-639. DOI: 10.2475/06.2018.01

- Landman, N. H. and Klofak, S. M. (2012) Anatomy of a concretion: Life, death, and burial in the Western Interior Seaway. *Palaios* **27**(9/10): 672-693
- Leclerc, A. J. and Labeyrie, L. (1987) Temperature dependence of the oxygen isotopic fractionation between diatom silica and water. *Earth and Planetary Science Letters* **84**(1): 69-74. DOI: 10.1016/0012-821X(87)90177-4
- Leder, J. J., Swart, P. K., Szmant, A. M. and Dodge, R. E. (1996) The origin of variations in the isotopic record of scleractinian corals: I. Oxygen. *Geochimica et Cosmochimica Acta* **60**(15): 2857-2870. DOI: 10.1016/0016-7037(96)00118-4
- LeGrande, A. N. and Schmidt, G. A. (2006) Global gridded data set of the oxygen isotopic composition in seawater. *Geophysical Research Letters* **33**(12). DOI: 10.1029/2006gl026011
- Levin, N. E., Raub, T. D., Dauphas, N. and Eiler, J. M. (2014) Triple oxygen isotope variations in sedimentary rocks. *Geochimica et Cosmochimica Acta* **139**: 173-189. DOI: 10.1016/j.gca.2014.04.034
- Liljestrand, F. L., Knoll, A. H., Tosca, N. J., Cohen, P. A., Macdonald, F. A., Peng, Y. and Johnston, D. T. (2020) The triple oxygen isotope composition of Precambrian chert. *Earth and Planetary Science Letters* **537**: 116167. DOI: 10.1016/j.epsl.2020.116167
- Lohmann, K. C. and Walker, J. C. G. (1989) The $\delta^{18}\text{O}$ record of Phanerozoic abiogenic marine calcite cements. *Geophysical Research Letters* **16**(4): 319-322. DOI: 10.1029/GL016i004p00319
- Longinelli, A., Iacumin, P. and Ramigni, M. (2002) $\delta^{18}\text{O}$ of carbonate, quartz and phosphate from belemnite guards: implications for the isotopic record of old fossils and the isotopic composition of ancient seawater. *Earth and Planetary Science Letters* **203**(1): 445-459. DOI: 10.1016/S0012-821X(02)00854-3
- Longinelli, A., Wierzbowski, H. and Di Matteo, A. (2003) $\delta^{18}\text{O}_{\text{PO}_4^{3-}}$ and $\delta^{18}\text{O}_{\text{CO}_3^{2-}}$ from belemnite guards from Eastern Europe: implications for palaeoceanographic reconstructions and for the preservation of pristine isotopic values. *Earth and Planetary Science Letters* **209**(3): 337-350. DOI: 10.1016/S0012-821X(03)00095-5
- Lowe, D. R. (1983) Restricted shallow-water sedimentation of Early Archean stromatolitic and evaporitic strata of the Strelley Pool Chert, Pilbara Block, Western Australia. *Precambrian Research* **19**(3): 239-283. DOI: 10.1016/0301-9268(83)90016-5

- Lowell, R. P. and Keller, S. M. (2003) High-temperature seafloor hydrothermal circulation over geologic time and Archean banded iron formations. *Geophysical Research Letters* **30**(7). DOI: 10.1029/2002gl016536
- Lowenstam, H. A. and Epstein, S. (1954) Paleotemperatures of the post-Aptian Cretaceous as determined by the oxygen isotope method. *The Journal of Geology* **62**(3): 207-248
- Lowenstam, H. A. (1961) Mineralogy, O^{18}/O^{16} ratios, and strontium and magnesium contents of recent and fossil brachiopods and their bearing on the history of the oceans. *The Journal of Geology* **69**(3): 241-260. DOI: 10.1086/626740
- Luz, B. and Barkan, E. (2010) Variations of $^{17}O/^{16}O$ and $^{18}O/^{16}O$ in meteoric waters. *Geochimica et Cosmochimica Acta* **74**(22): 6276-6286. DOI: 10.1016/j.gca.2010.08.016
- Mahata, S., Bhattacharya, S. K., Wang, C.-H. and Liang, M.-C. (2013) Oxygen isotope exchange between O_2 and CO_2 over hot platinum: An innovative technique for measuring $\delta^{17}O$ in CO_2 . *Analytical Chemistry* **85**(14): 6894-6901. DOI: 10.1021/ac4011777
- Majzoub, M. (1966) Une méthode d'analyse isotopique de l'oxygène sur des microquantités d'eau détermination des coefficients de partage à l'équilibre de l'oxygène 18 entre H_2O et CO_2 ; D_2O et CO_2^* . *J. Chim. Phys.* **63**: 563-568
- Maliva, R. G., Knoll, A. H. and Siever, R. (1989) Secular change in chert distribution; a reflection of evolving biological participation in the silica cycle. *Palaios* **4**(6): 519-532. DOI: 10.2307/3514743
- Maliva, R. G., Knoll, A. H. and Simonson, B. M. (2005) Secular change in the Precambrian silica cycle: Insights from chert petrology. *GSA Bulletin* **117**(7-8): 835-845. DOI: 10.1130/b25555.1
- Maples, C. G. (1986) Enhanced Paleocological and Paleoenvironmental Interpretations Result from Analysis of Early Diagenetic Concretions in Pennsylvanian Shales. *Palaios* **1**(5): 512-516. DOI: 10.2307/3514633
- Marin-Carbonne, J., Chaussidon, M. and Robert, F. (2012) Micrometer-scale chemical and isotopic criteria (O and Si) on the origin and history of Precambrian cherts: Implications for paleo-temperature reconstructions. *Geochimica et Cosmochimica Acta* **92**: 129-147. DOI: 10.1016/j.gca.2012.05.040
- Marin-Carbonne, J., Robert, F. and Chaussidon, M. (2014) The silicon and oxygen isotope compositions of Precambrian cherts: A record of oceanic paleo-temperatures? *Precambrian Research* **247**: 223-234. DOI: 10.1016/j.precamres.2014.03.016

- Marshall, J. D. (1992) Climatic and oceanographic isotopic signals from the carbonate rock record and their preservation. *Geological Magazine* **129**(2): 143-160. DOI: 10.1017/S0016756800008244
- Matsuhisa, Y., Matsubaya, O. and Sakai, H. (1971) BrF₅-technique for the oxygen isotopic analysis of silicates and water. *Journal of the Mass Spectrometry Society of Japan* **19**(2): 124-133. DOI: 10.5702/massspec1953.19.124
- Matthews, A. and Beckinsale, R. D. (1979) Oxygen isotope equilibrium systematics between quartz and water. *American Mineralogist* **64**: 232-240
- Mauviel, A., Sinnesael, M. and Desrochers, A. (2020) The stratigraphic and geochemical imprints of Late Ordovician glaciation on far-field neritic carbonates, Anticosti Island, eastern Canada. *Palaeogeography, Palaeoclimatology, Palaeoecology* **543**: 109579. DOI: 10.1016/j.palaeo.2019.109579
- McCrea, J. M. (1950) On the isotopic chemistry of carbonates and a paleotemperature scale. *The Journal of Chemical Physics* **18**(6): 849-857
- McGregor, H. V. and Gagan, M. K. (2003) Diagenesis and geochemistry of porites corals from Papua New Guinea: Implications for paleoclimate reconstruction. *Geochimica et Cosmochimica Acta* **67**(12): 2147-2156. DOI: 10.1016/S0016-7037(02)01050-5
- McGregor, H. V. and Abram, N. J. (2008) Images of diagenetic textures in Porites corals from Papua New Guinea and Indonesia. *Geochemistry, Geophysics, Geosystems* **9**(10). DOI: 10.1029/2008gc002093
- McKinney, C. R., McCrea, J. M., Epstein, S., Allen, H. A. and Urey, H. C. (1950) Improvements in mass spectrometers for the measurement of small differences in isotope abundance ratios. *Review of Scientific Instruments* **21**(8): 724-730. DOI: 10.1063/1.1745698
- Meijer, H. A. J. and Li, W. J. (1998) The use of electrolysis for accurate $\delta^{17}\text{O}$ and $\delta^{18}\text{O}$ isotope measurements in water. *Isotopes in Environmental and Health Studies* **34**(4): 349-369. DOI: 10.1080/10256019808234072
- Miller, M. F. (2002) Isotopic fractionation and the quantification of ^{17}O anomalies in the oxygen three-isotope system: an appraisal and geochemical significance. *Geochimica et Cosmochimica Acta* **66**(11): 1881-1889. DOI: 10.1016/s0016-7037(02)00832-3
- Moberly Jr., R. (1968) Composition of magnesian calcites of algae and pelecypods by electron microprobe analysis¹. *Sedimentology* **11**(1-2): 61-82. DOI: 10.1111/j.1365-3091.1968.tb00841.x

- Muehlenbachs, K. and Clayton, R. N. (1976) Oxygen isotope composition of the oceanic crust and its bearing on seawater. *Journal of Geophysical Research* **81**(23): 4365-4369
- Muehlenbachs, K. (1986). Alteration of the oceanic crust and the ^{18}O history of seawater. Stable Isotopes in High Temperature Geological Processes. J. W. Valley, H. P. Taylor Jr and J. R. O'Neil, De Gruyter: 425.
- Muehlenbachs, K. (1998) The oxygen isotopic composition of the oceans, sediments and the seafloor. *Chemical Geology* **145**(3-4): 263-273. DOI: 10.1016/S0009-2541(97)00147-2
- O'Neil, J. R. and Epstein, S. (1966) A method for oxygen isotope analysis of milligram quantities of water and some of its applications. *Journal of Geophysical Research* **71**(20): 4955-4961
- O'Neil, J. R., Clayton, R. N. and Mayeda, T. K. (1969) Oxygen isotope fractionation in divalent metal carbonates. *Journal of Chemical Physics* **51**(12): 5547-5558
- O'Neil, J. R., Adami, L. H. and Epstein, S. (1975) Revised value for the O^{18} fractionation between CO_2 and H_2O at 25°C . *Journal Research of U.S Geological Survey* **3**(5): 623-624
- Ogg, J. G., Hinnov, L. A. and Huang, C. (2012). Chapter 27 - Cretaceous. The Geologic Time Scale. F. M. Gradstein, J. G. Ogg, M. D. Schmitz and G. M. Ogg. Boston, Elsevier: 793-853.
- Pack, A. and Herwartz, D. (2014) The triple oxygen isotope composition of the Earth mantle and understanding $\Delta^{17}\text{O}$ variations in terrestrial rocks and minerals. *Earth and Planetary Science Letters* **390**: 138-145. DOI: 10.1016/j.epsl.2014.01.017
- Pack, A., Tanaka, R., Hering, M., Sengupta, S., Peters, S. and Nakamura, E. (2016) The oxygen isotope composition of San Carlos olivine on the VSMOW2-SLAP2 scale. *Rapid Communications in Mass Spectrometry* **30**(13): 1495-1504. DOI: 10.1002/rcm.7582
- Pack, A., Höweling, A., Hezel, D. C., Stefanak, M. T., Beck, A.-K., Peters, S. T. M., Sengupta, S., Herwartz, D. and Folco, L. (2017) Tracing the oxygen isotope composition of the upper Earth's atmosphere using cosmic spherules. *Nature communications* **8**: 15702-15702. DOI: 10.1038/ncomms15702
- Passey, B. H., Hu, H., Ji, H., Montanari, S., Li, S., Henkes, G. A. and Levin, N. E. (2014) Triple oxygen isotopes in biogenic and sedimentary carbonates. *Geochimica et Cosmochimica Acta* **141**: 1-25. DOI: 10.1016/j.gca.2014.06.006

Passey, B. H. and Ji, H. (2019) Triple oxygen isotope signatures of evaporation in lake waters and carbonates: A case study from the western United States. *Earth and Planetary Science Letters* **518**: 1-12. DOI: 10.1016/j.epsl.2019.04.026

Passey, B. H. and Levin, N. E. (2020) Triple oxygen isotopes in carbonates, biological apatites, and continental paleoclimate reconstruction. *Rev Mineral Geoche* **86**

Perkins, R. D. and Tsentas, C. I. (1976) Microbial infestation of carbonate substrates planted on the St. Croix shelf, West Indies. *GSA Bulletin* **87**(11): 1615-1628. DOI: 10.1130/0016-7606(1976)87<1615:Miocsp>2.0.Co;2

Perkins, R. D., Enos, P. and Perkins, R. D. (1977). Depositional Framework of Pleistocene Rocks in South Florida. Quaternary Sedimentation in South Florida, Geological Society of America. **147**: 0.

Perry, E. C. (1967) The oxygen isotope chemistry of ancient cherts. *Earth and Planetary Science Letters* **3**: 62-66. DOI: 10.1016/0012-821X(67)90012-X

Perry, E. C., Ahmad, S. N. and Swulius, T. M. (1978) The Oxygen Isotope Composition of 3,800 M.Y. Old Metamorphosed Chert and Iron Formation from Isukasia, West Greenland. *The Journal of Geology* **86**(2): 223-239

Perry, E. C. and Lefticariu, L. (2007). 7.05 - Formation and Geochemistry of Precambrian Cherts. Treatise on Geochemistry. H. D. Holland and K. K. Turekian. Oxford, Pergamon: 1-21.

Perry, E. C., Jr. and Tan, F. C. (1972) Significance of Oxygen and Carbon Isotope Variations in Early Precambrian Cherts and Carbonate Rocks of Southern Africa. *GSA Bulletin* **83**(3): 647-664. DOI: 10.1130/0016-7606(1972)83[647:Sooaci]2.0.Co;2

Peters, S. T. M., Szilas, K., Sengupta, S., Kirkland, C. L., Garbe-Schönberg, D. and Pack, A. (2020) >2.7 Ga metamorphic peridotites from southeast Greenland record the oxygen isotope composition of Archean seawater. *Earth and Planetary Science Letters* **544**: 116331. DOI: 10.1016/j.epsl.2020.116331

Petersen, S. V., Tabor, C. R., Lohmann, K. C., Poulsen, C. J., Meyer, K. W., Carpenter, S. J., Erickson, J. M., Matsunaga, K. K. S., Smith, S. Y. and Sheldon, N. D. (2016) Temperature and salinity of the Late Cretaceous Western Interior Seaway. *Geology* **44**(11): 903-906. DOI: 10.1130/g38311.1

Popp, B. N., Anderson, T. F. and Sandberg, P. A. (1986) Brachiopods as indicators of original isotopic compositions in some Paleozoic limestones. *Geological Society of*

America Bulletin **97**(10): 1262-1269. DOI: 10.1130/0016-7606(1986)97<1262:BAIOOI>2.0.CO

Price, G. D., Bajnai, D. and Fiebig, J. (2020) Carbonate clumped isotope evidence for latitudinal seawater temperature gradients and the oxygen isotope composition of Early Cretaceous seas. *Palaeogeography, Palaeoclimatology, Palaeoecology*: 109777. DOI: 10.1016/j.palaeo.2020.109777

Prokoph, A., Shields, G. A. and Veizer, J. (2008) Compilation and time-series analysis of a marine carbonate $\delta^{18}\text{O}$, $\delta^{13}\text{C}$, $^{87}\text{Sr}/^{86}\text{Sr}$ and $\delta^{34}\text{S}$ database through Earth history. *Earth-Science Reviews* **87**(3): 113-133. DOI: 10.1016/j.earscirev.2007.12.003

Reeside, J. B. and Cobban, W. A. (1960). Studies of the Mowry shale (Cretaceous) and contemporary formations in the United States and Canada. Professional Paper.

Romano, C., Goudemand, N., Vennemann, T. W., Ware, D., Schneebeli-Hermann, E., Hochuli, P. A., Brühwiler, T., Brinkmann, W. and Bucher, H. (2013) Climatic and biotic upheavals following the end-Permian mass extinction. *Nature Geoscience* **6**(1): 57-60. DOI: 10.1038/ngeo1667

Rosenheim, B. E., Swart, P. K., Thorrold, S. R., Eisenhauer, A. and Willenz, P. (2005) Salinity change in the subtropical Atlantic: Secular increase and teleconnections to the North Atlantic Oscillation. *Geophysical Research Letters* **32**(2). DOI: 10.1029/2004gl021499

Rosing, M. T., Bird, D. K., Sleep, N. H. and Bjerrum, C. J. (2010) No climate paradox under the faint early Sun. *Nature* **464**(7289): 744-747. DOI: 10.1038/nature08955

Ryb, U. and Eiler, J. M. (2018) Oxygen isotope composition of the Phanerozoic ocean and a possible solution to the dolomite problem. *Proceedings of the National Academy of Sciences* **115**(26): 6602-6607. DOI: 10.1073/pnas.1719681115

Sagan, C. and Mullen, G. (1972) Earth and Mars: Evolution of Atmospheres and Surface Temperatures. *Science* **177**(4043): 52-56. DOI: 10.1126/science.177.4043.52

Sakai, S., Matsuda, S., Hikida, T., Shimono, A., McManus, J. B., Zahniser, M., Nelson, D., Dettman, D. L., Yang, D. and Ohkouchi, N. (2017) High-Precision Simultaneous $^{18}\text{O}/^{16}\text{O}$, $^{13}\text{C}/^{12}\text{C}$, and $^{17}\text{O}/^{16}\text{O}$ Analyses for Microgram Quantities of CaCO_3 by Tunable Infrared Laser Absorption Spectroscopy. *Analytical Chemistry* **89**(21): 11846-11852. DOI: 10.1021/acs.analchem.7b03582

- Sanyal, G. and Maren, T. H. (1981) Thermodynamics of carbonic anhydrase catalysis. A comparison between human isoenzymes B and C. *Journal of Biological Chemistry* **256**(2): 608-612
- Savin, S., Douglas, R. and Stehli, F. (1975) Tertiary marine paleotemperature. *Geological Society of America Bulletin* **86**: 1499-1510. DOI: 10.1130/0016-7606(1975)86<1499:TMP>2.0.CO;2
- Savin, S. M. (1977) The history of the Earth's surface temperature during the past 100 million years. *Annual Review of Earth and Planetary Sciences* **5**(1): 319-355. DOI: 10.1146/annurev.ea.05.050177.001535
- Schauble, E. A., Ghosh, P. and Eiler, J. M. (2006) Preferential formation of ^{13}C - ^{18}O bonds in carbonate minerals, estimated using first-principles lattice dynamics. *Geochimica et Cosmochimica Acta* **70**(10): 2510-2529. DOI: 10.1016/j.gca.2006.02.011
- Schauble, E. A. and Young, E. D. (2020) Mass dependence of equilibrium oxygen isotope fractionation in carbonate, nitrate, oxide, perchlorate, phosphate, silicate, and sulfate minerals. *Rev Mineral Geoche* **86**
- Schmalz, R. F. (1965) Brucite in Carbonate Secreted by the Red Alga Goniolithon sp. *Science* **149**(3687): 993-996. DOI: 10.1126/science.149.3687.993
- Schmidt, G., Bigg, G. and Rohling, E. (1999) Global seawater oxygen-18 database. <http://data.giss.nasa.gov/o18data>
- Schmidt, M., Botz, R., Rickert, D., Bohrmann, G., Hall, S. R. and Mann, S. (2001) Oxygen isotopes of marine diatoms and relations to opal-A maturation 11 Associate editor: B. Taylor. *Geochimica et Cosmochimica Acta* **65**(2): 201-211. DOI: 10.1016/S0016-7037(00)00534-2
- Schoenemann, S. W., Schauer, A. J. and Steig, E. J. (2013) Measurement of SLAP2 and GISP $\delta^{17}\text{O}$ and proposed VSMOW-SLAP normalization for $\delta^{17}\text{O}$ and ^{17}O excess. *Rapid Communications in Mass Spectrometry* **28**(17): 1956-1956. DOI: 10.1002/rcm.6990
- Sengupta, S. and Pack, A. (2018) Triple oxygen isotope mass balance for the Earth's oceans with application to Archean cherts. *Chemical Geology* **495**: 18-26. DOI: 10.1016/j.chemgeo.2018.07.012
- Sengupta, S., Peters, S. T. M., Reitner, J., Duda, J.-P. and Pack, A. (*in revision*) Triple oxygen isotopes of cherts through time. *Chemical Geology*

Sha, L., Mahata, S., Duan, P., Luz, B., Zhang, P., Baker, J., Zong, B., Ning, Y., Brahim, Y. A., Zhang, H., Edwards, R. L. and Cheng, H. (2020) A novel application of triple oxygen isotope ratios of speleothems. *Geochimica et Cosmochimica Acta* **270**: 360-378. DOI: 10.1016/j.gca.2019.12.003

Shackleton, N. (1967) Oxygen isotope analyses and pleistocene temperatures re-assessed. *Nature* **215**(5096): 15-17. DOI: 10.1038/215015a0

Shackleton, N. J. and Kennett, J. P. (1975) Paleotemperature history of the cenozoic and the initiation of Antarctic glaciation: Oxygen and carbon isotope analyses in DSDP sites 277, 279, and 281. *DSDP Reports and Publications* **XXIX**(No. 17): 743-755. DOI: 10.2973/dsdp.proc.29.1975

Sharma, T. and Clayton, R. N. (1965) Measurement of O^{18}/O^{16} ratios of total oxygen of carbonates. *Geochimica et Cosmochimica Acta* **29**: 1347-1353

Sharp, Z. D. (1990) A laser-based microanalytical method for the in situ determination of oxygen isotope ratios of silicates and oxides. *Geochimica et Cosmochimica Acta* **54**(5): 1353-1357. DOI: 10.1016/0016-7037(90)90160-M

Sharp, Z. D. (2013). Principles of Stable Isotope Geochemistry, 2nd Edition. Albuquerque, NM, Open Educational Resources.

Sharp, Z. D., Gibbons, J. A., Maltsev, O., Atudorei, V., Pack, A., Sengupta, S., Shock, E. L. and Knauth, L. P. (2016) A calibration of the triple oxygen isotope fractionation in the SiO_2 - H_2O system and applications to natural samples. *Geochimica et Cosmochimica Acta* **186**: 105-119. DOI: 10.1016/j.gca.2016.04.047

Sharp, Z. D., Wostbrock, J. A. G. and Pack, A. (2018) Mass-dependent triple oxygen isotope variations in terrestrial materials. *Geochemical Perspectives Letters* **7**: 27-31. DOI: 10.7185/geochemlet.1815

Sharp, Z. D. and Wostbrock, J. A. G. (2020) Standardization of triple oxygen isotope compositions for water, carbonates, silicates, sulfates, and air. *Rev Mineral Geoche* **86**

Shemesh, A., Charles, C. D. and Fairbanks, R. G. (1992) Oxygen Isotopes in Biogenic Silica: Global Changes in Ocean Temperature and Isotopic Composition. *Science* **256**(5062): 1434-1436. DOI: 10.1126/science.256.5062.1434

Shemesh, A., Burckle, L. H. and Hays, J. D. (1995) Late Pleistocene oxygen isotope records of biogenic silica from the Atlantic sector of the Southern Ocean. *Paleoceanography* **10**: 179-196

Starkey, N. A., Jackson, C., Greenwood, R., Parman, S., Franchi, I., Jackson, M., Fitton, J., Stuart, F. M., Kurz, M. and Larsen, L. M. (2016) Triple oxygen isotopic composition of the high- $^3\text{He}/^4\text{He}$ mantle. *Geochimica et Cosmochimica Acta* **176**. DOI: 10.1016/j.gca.2015.12.027

Staschewski, D. (1964) Experimentelle Bestimmung der $\text{O}^{18}/\text{O}^{16}$ -Trennfaktoren in den Systemen $\text{CO}_2/\text{H}_2\text{O}$ und $\text{CO}_2/\text{D}_2\text{O}$. *Berichte der Bunsengesellschaft für physikalische Chemie* **68**(5): 454-459. DOI: 10.1002/bbpc.19640680507

Stolper, D. A., Eiler, J. M. and Higgins, J. A. (2018) Modeling the effects of diagenesis on carbonate clumped-isotope values in deep- and shallow-water settings. *Geochimica et Cosmochimica Acta* **227**: 264-291. DOI: 10.1016/j.gca.2018.01.037

Sun, Y., Joachimski, M. M., Wignall, P. B., Yan, C., Chen, Y., Jiang, H., Wang, L. and Lai, X. (2012) Lethally Hot Temperatures During the Early Triassic Greenhouse. *Science* **338**(6105): 366-370. DOI: 10.1126/science.1224126

Sutherland, K. M., Wostbrock, J. A. G., Hansel, C. M., Sharp, Z. D., Hein, J. R. and Wankel, S. D. (2020) Ferromanganese crusts as recorders of marine dissolved oxygen. *Earth and Planetary Science Letters* **533**: 116057. DOI: 10.1016/j.epsl.2019.116057

Swart, P. K., Reijmer, J. J. G. and Otto, R. (2005). A re-evaluation of facies on Great Bahama Bank II: Variations in the $\delta^{13}\text{C}$, $\delta^{18}\text{O}$ and mineralogy of surface sediments. *Perspectives in Carbonate Geology*. P. K. Swart, G. P. Eberli, J. A. McKenzie, I. Jarvis and T. Stevens: 47-59.

Swart, P. K. (2015) The geochemistry of carbonate diagenesis: The past, present and future. *Sedimentology* **62**(5): 1233-1304. DOI: 10.1111/sed.12205

Tanaka, R. and Nakamura, E. (2013) Determination of ^{17}O -excess of terrestrial silicate/oxide minerals with respect to Vienna Standard Mean Ocean Water (VSMOW). *Rapid Communications in Mass Spectrometry* **27**(2): 285-297. DOI: 10.1002/rcm.6453

Tarutani, T., Clayton, R. N. and Mayeda, T. K. (1969) The effect of polymorphism and magnesium substitution on oxygen isotope fractionation between calcium carbonate and water. *Geochimica et Cosmochimica Acta* **33**(8): 987-996. DOI: 10.1016/0016-7037(69)90108-2

Taylor, H. P. (1978) Oxygen and hydrogen isotope studies of plutonic granitic rocks. *Earth and Planetary Science Letters* **38**(1): 177-210. DOI: 10.1016/0012-821X(78)90131-0

- Thiemens, M. H. and Heidenreich, J. E. (1983) The mass-independent fractionation of oxygen: A novel isotope effect and its possible cosmochemical implications. *Science* **219**(4588): 1073-1075
- Thiemens, M. H. (2006) History and applications of mass-independent isotope effects. *Annual Review of Earth and Planetary Sciences* **34**(1): 217-262. DOI: 10.1146/annurev.earth.34.031405.125026
- Tice, M., Bostick, B. and Lowe, D. (2004) Thermal history of the 3.5-3.2 Ga Onverwacht and Fig Tree Groups, Barberton greenstone belt, South Africa, inferred by Raman microspectroscopy of carbonaceous material. *Geology* **32**. DOI: 10.1130/G19915.1
- Tice, M. M. and Lowe, D. R. (2006) The origin of carbonaceous matter in pre-3.0 Ga greenstone terrains: A review and new evidence from the 3.42 Ga Buck Reef Chert. *Earth-Science Reviews* **76**(3): 259-300. DOI: 10.1016/j.earscirev.2006.03.003
- Tremaine, D. M., Froelich, P. N. and Wang, Y. (2011) Speleothem calcite farmed in situ: Modern calibration of $\delta^{18}\text{O}$ and $\delta^{13}\text{C}$ paleoclimate proxies in a continuously-monitored natural cave system. *Geochimica et Cosmochimica Acta* **75**(17): 4929-4950. DOI: 10.1016/j.gca.2011.06.005
- Trotter, J. A., Williams, I. S., Barnes, C. R., Lécuyer, C. and Nicoll, R. S. (2008) Did Cooling Oceans Trigger Ordovician Biodiversification? Evidence from Conodont Thermometry. *Science* **321**(5888): 550-554. DOI: 10.1126/science.1155814
- Tsujita, C. J. (1995) Origin of Concretion-Hosted Shell Clusters in the Late Cretaceous Bearpaw Formation, Southern Alberta, Canada. *Palaios* **10**(5): 408-423. DOI: 10.2307/3515044
- Tsujita, C. J. and E.G. Westermann, G. (1998) Ammonoid habitats and habits in the Western Interior Seaway: a case study from the Upper Cretaceous Bearpaw Formation of southern Alberta, Canada. *Palaeogeography, Palaeoclimatology, Palaeoecology* **144**(1): 135-160. DOI: 10.1016/S0031-0182(98)00090-X
- Tyler, J. J., Sloane, H. J., Rickaby, R. E. M., Cox, E. J. and Leng, M. J. (2017) Post-mortem oxygen isotope exchange within cultured diatom silica. *Rapid communications in mass spectrometry* **31**: 1749-1760. DOI: 10.1002/rcm.7954
- Uchikawa, J. and Zeebe, R. E. (2012) The effect of carbonic anhydrase on the kinetics and equilibrium of the oxygen isotope exchange in the $\text{CO}_2\text{-H}_2\text{O}$ system: Implications for $\delta^{18}\text{O}$ vital effects in biogenic carbonates. *Geochimica et Cosmochimica Acta* **95**: 15-34. DOI: 10.1016/j.gca.2012.07.022

Urey, H. C. (1947) The thermodynamic properties of isotopic substances. *Journal of the Chemical Society*: 562-581

Urey, H. C., Lowenstam, H. A., Epstein, S. and McKinney, C. R. (1951). Measurement of paleotemperatures and temperatures of the Upper Cretaceous of England, Denmark and the southeastern United States, Geological Society of America.

Valley, J. W., Kitchen, N., Kohn, M. J., Niendorf, C. R. and Spicuzza, M. J. (1995) UWG-2, a garnet standard for oxygen isotope ratios: Strategies for high precision and accuracy with laser heating. *Geochimica et Cosmochimica Acta* **59**(24): 5223-5231. DOI: 10.1016/0016-7037(95)00386-X

Veizer, J. and Hoefs, J. (1976) The nature of O¹⁸/O¹⁶ and C¹³/C¹² secular trends in sedimentary carbonate rocks. *Geochimica et Cosmochimica Acta* **40**(11): 1387-1395

Veizer, J. (1983) Trace elements and isotopes in sedimentary carbonates. *Reviews in Mineralogy* **11**

Veizer, J., Fritz, P. and Jones, B. (1986) Geochemistry of brachiopods: Oxygen and carbon isotopic records of Paleozoic oceans. *Geochimica et Cosmochimica Acta* **50**(8): 1679-1696

Veizer, J., Hoefs, J., Lowe, D. R. and Thurston, P. C. (1989) Geochemistry of Precambrian carbonates: II. Archean greenstone belts and Archean sea water. *Geochimica et Cosmochimica Acta* **53**(4): 859-871. DOI: 10.1016/0016-7037(89)90031-8

Veizer, J., Bruckschen, P., Pawellek, F., Diener, A., Podlaha, O. G., Carden, G. A. F., Jasper, T., Korte, C., Strauss, H., Azmy, K. and Ala, D. (1997) Oxygen isotope evolution of Phanerozoic seawater. *Palaeogeography, Palaeoclimatology, Palaeoecology* **132**(1-4): 159-172. DOI: 10.1016/S0031-0182(97)00052-7

Veizer, J., Ala, D., Azmy, K., Bruckschen, P., Buhl, D., Bruhn, F., Garden, G. A. F., Diener, A., Ebner, S., Godderis, Y., Jasper, T., Korte, C., Pawellek, F., Podlaha, O. G. and Strauss, H. (1999) ⁸⁷Sr/⁸⁶Sr, δ¹³C and δ¹⁸O evolution of Phanerozoic seawater. *Chemical Geology* **161**(1): 59-88

Veizer, J. and Prokoph, A. (2015) Temperatures and oxygen isotopic composition of Phanerozoic oceans. *Earth-Science Reviews* **146**: 92-104. DOI: 10.1016/j.earscirev.2015.03.008

Vennin, E., Olivier, N., Brayard, A., Bour, I., Thomazo, C., Escarguel, G., Fara, E., Bylund, K. G., Jenks, J. F., Stephen, D. A. and Hofmann, R. (2015) Microbial deposits in

- the aftermath of the end-Permian mass extinction: A diverging case from the Mineral Mountains (Utah, USA). *Sedimentology* **62**(3): 753-792. DOI: 10.1111/sed.12166
- Voarintsoa, N. R. G., Barkan, E., Bergel, S., Vieten, R. and Affek, H. P. (2020) Triple oxygen isotope fractionation between CaCO₃ and H₂O in inorganically precipitated calcite and aragonite. *Chemical Geology* **539**: 119500. DOI: 10.1016/j.chemgeo.2020.119500
- Waage, K. M. (1964) Origin of repeated fossiliferous concretion layers in the Fox Hills Formation. *Kansas Geological Survey Bulletin* **169**: 541-563
- Waage, K. M. (1968) The Type Fox Hills Formation, Cretaceous (Maestrichtian), South Dakota, Pt. 1, stratigraphy and paleoenvironments. *Peabody Museum of Natural History Bulletin* **27**: 1-175
- Wadleigh, M. A. and Veizer, J. (1992) ¹⁸O/¹⁶O and ¹³C/¹²C in lower Paleozoic articulate brachiopods: Implications for the isotopic composition of seawater. *Geochimica et Cosmochimica Acta* **56**(1): 431-443. DOI: 10.1016/0016-7037(92)90143-7
- Walker, J. C. G. and Lohmann, K. C. (1989) Why the oxygen isotopic composition of sea water changes with time. *Geophysical Research Letters* **16**(4): 323-326. DOI: 10.1029/GL016i004p00323
- Wallmann, K. (2001) The geological water cycle and the evolution of marine δ¹⁸O values. *Geochimica et Cosmochimica Acta* **65**(15): 2469-2485. DOI: 10.1016/S0016-7037(01)00603-2
- Watkins, J. M., Nielsen, L. C., Ryerson, F. J. and DePaolo, D. J. (2013) The influence of kinetics on the oxygen isotope composition of calcium carbonate. *Earth and Planetary Science Letters* **375**: 349-360. DOI: 10.1016/j.epsl.2013.05.054
- Weber, J. N. and Kaufman, J. W. (1965) Brucite in the Calcareous Alga Goniolithon. *Science* **149**(3687): 996-997. DOI: 10.1126/science.149.3687.996
- Weber, J. N. (1974) Skeletal chemistry of scleractinian reef corals; uptake of magnesium from seawater. *American Journal of Science* **274**: 84-93. DOI: 10.2475/ajs.274.1.84
- Wenzel, B., Lécuyer, C. and Joachimski, M. M. (2000) Comparing oxygen isotope records of silurian calcite and phosphate—δ¹⁸O compositions of brachiopods and conodonts. *Geochimica et Cosmochimica Acta* **64**(11): 1859-1872. DOI: 10.1016/S0016-7037(00)00337-9

- Winkelstern, I. Z. and Lohmann, K. C. (2016) Shallow burial alteration of dolomite and limestone clumped isotope geochemistry. *Geology* **44**(6): 467-470. DOI: 10.1130/G37809.1
- Winter, B. L. and Knauth, L. P. (1992) Stable isotope geochemistry of cherts and carbonates from the 2.0 Ga gunflint iron formation: implications for the depositional setting, and the effects of diagenesis and metamorphism. *Precambrian Research* **59**(3): 283-313. DOI: 10.1016/0301-9268(92)90061-R
- Wostbrock, J. A. G., Sharp, Z. D., Sanchez-Yanez, C., Reich, M., van den Heuvel, D. B. and Benning, L. G. (2018) Calibration and application of silica-water triple oxygen isotope thermometry to geothermal systems in Iceland and Chile. *Geochimica et Cosmochimica Acta* **234**: 84-97. DOI: <https://doi.org/10.1016/j.gca.2018.05.007>
- Wostbrock, J. A. G., Brand, U., Coplen, T. B., Swart, P. K., Carlson, S. J. and Sharp, Z. D. (2020a) Calibration of carbonate-water triple oxygen isotope fractionation: seeing through diagenesis in ancient carbonates. *Geochimica et Cosmochimica Acta* **submitted**
- Wostbrock, J. A. G., Cano, E. J. and Sharp, Z. D. (2020b) An internally consistent triple oxygen isotope calibration of standards for silicates, carbonates and air relative to VSMOW2 and SLAP2. *Chemical Geology* **533**: 119432. DOI: 10.1016/j.chemgeo.2019.119432
- Yanchilina, A. G., Yam, R., Kolodny, Y. and Shemesh, A. (2020) From diatom opal-A $\delta^{18}\text{O}$ to chert $\delta^{18}\text{O}$ in deep sea sediments. *Geochimica et Cosmochimica Acta* **268**: 368-382. DOI: 10.1016/j.gca.2019.10.018
- Yeung, L. Y., Young, E. D. and Schauble, E. A. (2012) Measurements of $^{18}\text{O}^{18}\text{O}$ and $^{17}\text{O}^{18}\text{O}$ in the atmosphere and the role of isotope-exchange reactions. *Journal of Geophysical Research: Atmospheres* **117**(D18). DOI: 10.1029/2012jd017992
- Yeung, L. Y., Hayles, J. A., Hu, H., Ash, J. L. and Sun, T. (2018) Scale distortion from pressure baselines as a source of inaccuracy in triple-isotope measurements. *Rapid Communications in Mass Spectrometry* **32**(20): 1811-1821. DOI: doi:10.1002/rcm.8247
- Young, E. D., Yeung, L. Y. and Kohl, I. E. (2014) On the $\Delta^{17}\text{O}$ budget of atmospheric O_2 . *Geochimica et Cosmochimica Acta* **135**: 102-125. DOI: 10.1016/j.gca.2014.03.026
- Zaarur, S., Affek, H. P. and Brandon, M. T. (2013) A revised calibration of the clumped isotope thermometer. *Earth and Planetary Science Letters* **382**: 47-57. DOI: 10.1016/j.epsl.2013.07.026

Zachos, J. C., Stott, L. D. and Lohmann, K. C. (1994) Evolution of Early Cenozoic marine temperatures. *Paleoceanography* **9**(2): 353-387. DOI: 10.1029/93pa03266

Zakharov, D. O. and Bindeman, I. N. (2019) Triple oxygen and hydrogen isotopic study of hydrothermally altered rocks from the 2.43–2.41 Ga Vetreny belt, Russia: An insight into the early Paleoproterozoic seawater. *Geochimica et Cosmochimica Acta* **248**: 185-209. DOI: 10.1016/j.gca.2019.01.014

Zakharov, D. O., Marin-Carbonne, J., Alleon, J. and Bindeman, I. N. (2020) Temporal triple oxygen isotope trend recorded by Precambrian cherts: A perspective from combined bulk and *in situ* secondary ion probe measurements. *Rev Mineral Geoche* **86**

Zaky, A., Brand, U. and Azmy, K. (2015) A new sample processing protocol for procuring seawater REE signatures in biogenic and abiogenic carbonates. *Chemical Geology* **416**: 36-50. DOI: 10.1016/j.chemgeo.2015.10.015

Zatoń, M. and Marynowski, L. (2006) Ammonite fauna from uppermost Bajocian (Middle Jurassic) calcitic concretions from the Polish Jura—biogeographical and taphonomical implications. *Geobios* **39**(3): 426-442. DOI: 10.1016/j.geobios.2005.02.001

Zheng, Y.-F. (1991) Calculation of oxygen isotope fractionation in metal oxides. *Geochimica et Cosmochimica Acta* **55**(8): 2299-2307. DOI: 10.1016/0016-7037(91)90105-E